Thèse

Présentée pour obtenir le grade de docteur
de Télécom ParisTech
Spécialité : Informatique et Réseaux

Masood MAQBOOL

Ingénierie radio des réseaux d'accès OFDMA

Soutenue le 9 novembre 2009 devant le jury composé de

Rapporteurs	Tijani CHAHED	Télécom SudParis
	Jens ZANDER	KTH, Royal Institute of Technology, Sweden
Examinateurs	Vinod KUMAR	Alcatel-Lucent Bell Labs France
	Loutfi NUAYMI	Télécom Bretagne
Directeurs de thèse	Marceau COUPECHOUX	Télécom ParisTech
	Philippe GODLEWSKI	Télécom ParisTech
Invité	Véronique CAPDEVIELLE	Alcatel-Lucent Bell Labs France
	Thomas BONALD	Orange Labs, France

To my parents, my wife and my son.

Acknowledgments

This account of gratitudes is something special to me. For me, it is not just a formal note but more than that. It would make possible for me to express my feelings for all those who had been at my side during this important project of my life and I never found a chance to do that till now.

I was lucky to have Marceau Coupechoux as my advisor. He is a kind hearted and highly professional person. From the very start till the end, his contribution and guidance were of great value. Whenever, I needed, he was there for assistance. His precise and pertinent comments always helped me get out of difficult situations. Without his supervision, it would not have been possible for me to write this dissertation.

I am also thankful to my co-advisor Philippe Godlewski. His experience and expertise have no match. Having a highly diverse knowledge base, his suggestions were of immense value. He was of great help in getting out of many complex circumstances. His valuable foresight helped me explore multiple research ventures. I would also like to thank my industrial supervisor Véronique Capdevielle for her assistance during the coarse of thesis. It was because of her that my work found its utility in industrial domain.

I extend my compliments to all the jury members of thesis defense. I am obliged to Tijani Chahed, Jens Zander, Vinod Kumhar, Loutfi Nuaymi and Thomas Bonald for their invaluable comments.

I feel obliged to Alcatel-Lucent Bell Labs France for its financial support in carrying out the research work associated with my thesis work. At the same time, I would also like to mention the name of Higher Education Commission (HEC) of Pakistan which sponsored my Masters degree that paved a way towards my Ph.D. degree.

I was also fortunate to have many helping friends. It would not be possible for me to mention here the names of all those. But still I would like to mention the names of some of them who had been a great source of encouragement for me. It was my pleasure to have friends and colleagues like Sheraz Khan, Muhammad Usman Iftikhar, Hasham Khushk, Farhan Hyder Mirani, Federico Larroca and Paola Bermolen.

At the end, I would like to mention about my parents, siblings, wife and son who mean a lot to me. I wish my father would have been in this world to share with me the joy of this success. I miss him a lot. My mother has sacrificed much for my success and I am indebted to her. I wish one day I get a chance

to pay back a little for what my parents did for me. My brothers and sisters had always been there for me during all kind of circumstances. I am thankful for their encouragement. I pay tribute to my wife Amen for her patience and support. She had to take care of many things during my long working hours including our little angel Muhammed Shaheer. These were the innocent acts of Shaheer during evening that took away all my day long fatigue.

Abstract in English

Multi-carrier Orthogonal Frequency Division Multiple Access (OFDMA) systems promise enhanced performance as compared to preceding single carrier ones. It is imperative to analyze the performance evaluation of these systems prior to network deployment which is approaching quite fast. Therefore, in this thesis we look into dimensioning issues related to OFDMA based system.

The study of network engineering for OFDMA networks into two major components: Radio Coverage and Capacity and Traffic Analysis. While analyzing the former, we consider a static system such that users have full buffers and always have something to transmit. Traffic Analysis, on the other hand, takes into account a dynamic system in which users receive an elastic traffic during active phase and go to sleep for some duration after download is over.

In the study of Radio Coverage and Capacity, we evaluated the system performance under various frequency reuse schemes keeping in view both cell capacity and outage probability. This study is based on Monte Carlo simulations and an original analytical model. We have investigated the possibility of achieving reuse 1 and shown under which conditions it is possible while using beamforming technique. A time efficient method to acquire the spatial effective SINR distribution is also proposed.

As far as study of dynamic system is concerned, the validation and robustness study of analytical models, developed for WiMAX systems, is carried out in this thesis. The analytical models take into account different scheduling policies and different classes of traffic. The performance parameters furnished by these models could be used in the dimensioning process. We have shown that models results obtained through model have little variation with respect to those of simulations. It has also been concluded that the model provides acceptable results for different radio channels, traffic distributions and load conditions.

This thesis offers a frame work for dimensioning process of an OFDMA system. The proposed tools are based on analytical, semi-analytical and Monte Carlo simulation based approaches. In addition to its utility, the work carried out in this thesis will pave the way for future research.

Résumé court en Francais

Les systèmes cellulaires multi-porteuses OFDMA (WiMAX, LTE) offrent des gains en performances prometteurs par rapport aux systèmes des générations précédentes. Leur déploiements sont en cours ou approchent très rapidement, de telle sorte qu'il est devenu impératif de disposer d'outils d'évaluation de performances de ces réseaux. Dans cette thèse, nous abordons la problématique de l'ingénierie des réseaux OFDMA et de leur dimensionnement.

Nous avons divisé l'étude de l'ingénierie des réseaux OFDMA selon deux grands axes : l'étude de couverture et de capacité cellulaire d'une part, l'analyse du trafic d'autre part. Pour le premier axe, nous considérons un système statique composé d'utilisateurs ayant toujours des données à transmettre. De cette analyse, nous pouvons notamment déduire la capacité cellulaire et la distribution spatiale du SINR. Cette distribution est une entrée pour la seconde étape qui considère un système dynamique dans lequel les utilisateurs reçoivent un trafic élastique composé de périodes d'activité et de sommeil.

Dans le cadre de l'étude de couverture et de capacité en système statique, nous avons étudié les performances de différents schémas de réutilisation fréquentielle en comparant les débits cellulaires atteignables et les probabilités de dépassement. Cette étude est à la fois fondée sur des simulations et sur un modèle analytique original. Nous avons montré sous quelles conditions il était possible d'atteindre un facteur de réutilisation 1 en utilisant la technique des antennes intelligentes. Nous avons enfin proposé une méthode semi-analytique permettant de calculer très rapidement la distribution spatiale du SINR effectif.

En ce qui concerne l'étude du système dynamique, nous avons travaillé sur des modèles analytiques développés pour WiMAX en collaboration avec le LIP6 permettant d'obtenir les principaux paramètres de dimensionnement d'un réseau. Ces modèles sont conçus pour différents types d'ordonnancement. Nous avons validé ces modèles et nous avons étudié leur robustesse par simulation en modifiant les hypothèses de canal et de trafic.

Cette thèse fournit donc un large spectre d'outils de dimensionnement pour les systèmes OFDMA. Ces outils sont fondés sur des approches analytiques, semi-analytiques et sur des simulations de type Monte Carlo. Elle ouvre également de nouvelles perspectives de recherche.

Résumé en Francais

Introduction

Ces dernières années, la demande d'accès à large bande a augmenté de façon substantielle. En quelques années, les réseaux cellulaires ont évolué de la première génération analogique au numérique multi-service de troisième génération. Dans les normes de deuxième génération, le FDMA/TDMA a été la méthode d'accès de premier plan, tandis qu'en troisième génération, le CDMA a été à la base de toutes les normes. La prochaine génération devrait être dominée par l'OFDMA pour des raisons de simplicité et de souplesse. En conjonction avec des fonctions radio avancées, cette technique promet des débits de données très élevés et un support multi-service. WiMAX (fondé sur la norme IEEE 802.16) et LTE du 3GPP sont deux de ces technologies très attendues et qui sont basées sur l'OFDMA. Alors que le déploiement des réseaux WiMAX / LTE est en cours, les opérateurs et les fabricants ont besoin des règles d'ingénierie et de méthodes de dimensionnement. Ces règles et méthodes sont l'objet de cette thèse.

Ingénierie réseau des systèmes OFDMA

Les systèmes multi-porteuses OFDMA promettent des performances accrues par rapport aux systèmes précédents qui utilisaient une seule porteuse. Il est impératif d'évaluer les performances de ces systèmes avant le déploiement massif de ces réseaux. Quelques réseaux WiMAX sont déjà déployés, mais la plupart des opérateurs sont en phase d'essai. Dans cette thèse, nous proposons des techniques de dimensionnement pour les systèmes OFDMA. Le processus de dimensionnement permet de déterminer le nombre de BS à installer dans une certaine région en s'assurant de certains paramètres de qualité de service ou, en anglais, Quality of Service (QoS). Ces derniers incluent la couverture radio, la capacité cellulaire et les paramètres du trafic des utilisateurs.

Nous avons divisé l'étude de l'ingénierie des réseaux OFDMA selon deux grands axes (comme il est montré en Fig. 1) : l'étude de couverture et de capacité cellulaire d'une part, l'analyse du trafic d'autre part. Pour le premier axe, nous considérons un système statique composé d'utilisateurs ayant toujours des données à transmettre. De cette analyse, nous pouvons notamment déduire la capacité cellulaire et la distribution spatiale du SINR. Cette distribution est une entrée pour la seconde étape qui considère un système dynamique dans lequel

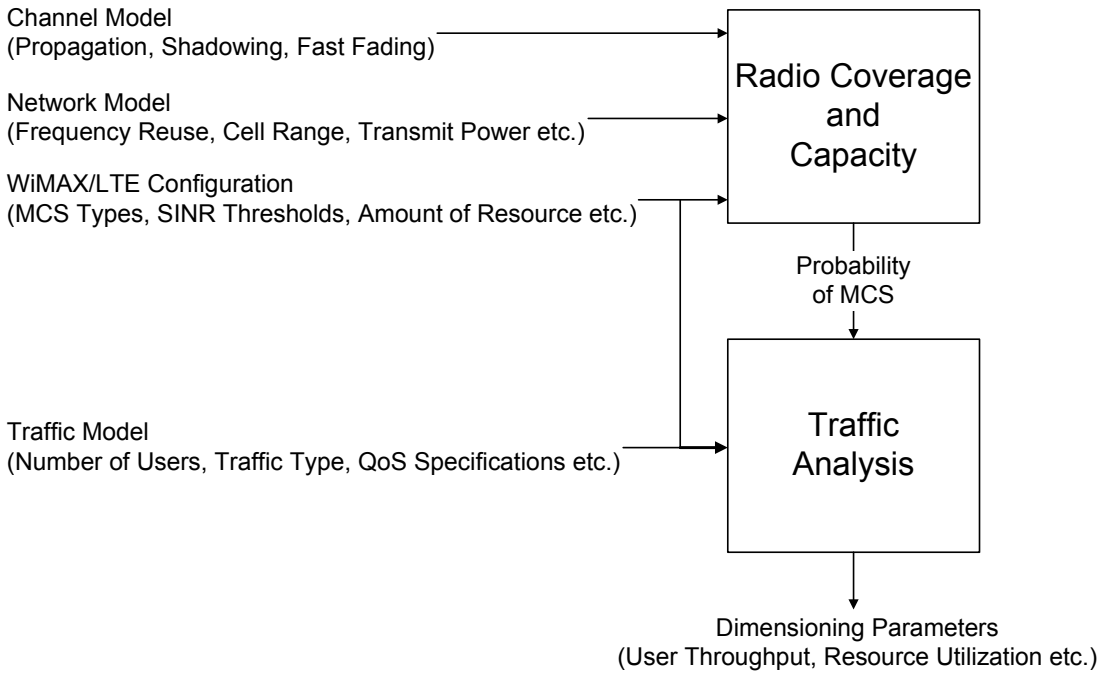

Figure 1: Le système étudié pour l'évaluation de performances.

les utilisateurs reçoivent un trafic élastique composé de périodes d'activité et de sommeil. Dans le texte qui suit, nous présentons une brève description de ces blocs.

La couverture radio et la capacité

L'étude de la couverture et la capacité est de première importance dans l'exercice de l'évaluation des performances des réseaux mobiles. Offrir une couverture radio et une certaine capacité dans une région est une question importante, mais la même chose avec une QoS déterminée représente un défi tout autre. Les paramètres de QoS considérés dans cette thèse sont : le SINR effectif moyen, le débit moyen des cellules et la probabilité de dépassement. Il faut noter que le SINR effectif est différent du SINR habituellement considéré sur une unique porteuse. La probabilité de dépassement est définie comme la probabilité qu'un utilisateur n'atteigne pas le niveau minimum de SINR effectif nécessaire pour se connecter à un service ou décoder les canaux de contrôle commun.

Il y a trois entrées du bloc *Couverture radio et capacité* : le modèle de canal, le modèle de réseau et la configuration réseau. Le premier inclut l'affaiblissement de parcours, l'effet de masque et les évanouissements rapides. Le choix des paramètres des modèles de l'affaiblissement de parcours dépend de l'environnement radio (par exemple, urbain/suburbain, LOS/NLOS). L'autre entrée est le modèle de réseau qui se compose de tous les paramètres liés au déploiement de réseau tels que la puissance de transmission des stations de base, le schéma de réutilisation fréquentielle, le rayon de cellule, le gain d'antenne, le modèle

de *beamforming*, etc. La troisième entrée est la configuration réseau qui est spécifique à la technologie déployée (par exemple, WiMAX / LTE). Des exemples de paramètres liés à une configuration du réseau sont les types de Modulation and Coding Scheme (MCS) disponibles, les seuils de SINR effectif, le nombre de ressources radio disponibles par trame, etc.

Il est important d'évaluer les performances du système à l'égard des entrées du bloc *Couverture radio et capacité*. Il est également souhaitable que certaines de ces entrées (par exemple, la réutilisation fréquentielle) soient appliquées d'une manière optimisée pour maximiser la performance du système tout en maintenant une certaine qualité de service, ce qui est l'un des sujets abordés dans cette thèse. La performance des techniques avancées telles que le *beamforming* adaptatif doit également être évaluée. En outre, il est important que les méthodes proposées permettent l'évaluation des performances du système de manière efficace, c'est-à-dire en un temps relativement court.

l'analyse du trafic

Du bloc *Analyse du trafic*, on obtient le dimensionnement de paramètres tels que le débit moyen par utilisateur, l'utilisation moyenne des ressources radio ou le nombre moyen d'utilisateurs actifs simultanément dans la cellule. Par rapport au bloc *Couverture radio et capacité*, ici nous prenons en compte un système dynamique.

Les entrées de bloc *Analyse du trafic* sont les probabilités des MCS (fournies par le bloc *Couverture radio et capacité*), la configuration du réseau et le modèle de trafic. Les principaux paramètres de configuration de réseau dans le contexte du trafic sont les suivants : la quantité de ressource radio disponible par cellule, la durée de la trame TDD et la politique d'ordonnancement. Les paramètres du modèle du trafic comprennent le nombre de mobiles présents dans la cellule, les différents types de trafic et leurs paramètres QoS associés.

La modélisation du trafic web, qui est de nature élastique, est déjà une tâche difficile. Le caractère variable des ressources radio dû au mécanisme d'adaptation rapide des MCS rend le problème plus ardu encore.

Bibliographie

Dans ce resumé, nous présentons quelques articles importants dans le domaine du dimensionnement des réseaux OFDMA. Nous commenons par la littérature sur les systèmes statiques.

Les études sur la couverture radio et la capacité des systèmes statiques sont très riches dans la littérature et l'expérience acquise dans ce domaine depuis l'époque du GSM jusqu'au HSPA+ est, sans aucun doute, très utile pour les études d'ingénierie OFDMA. La nouvelle approche de canalisation, la possibilité de déployer des schémas de réutilisation fréquentielle originales et la généralisation des fonctionnalités radio avancées font toutefois de l'OFDMA un cas très spécifique. Donc ici, nous nous concentrons sur cette technique d'accès multiple et nous

soulignons quelques articles de référence, au niveau système, qui illustrent bien les questions posées par les réseaux OFDMA.

Bien que tous ces articles étudient la capacité cellulaire (i.e., l'efficacité spectrale, le débit cellulaire, le débit utilisateur, le débit au bord de la cellule) et la couverture (par exemple, la distribution SINR, la probabilité de dépassement, la couverture des canaux de contrôle), trois thèmes principaux peuvent être soulignés : l'effet de la sous-canalisation, la comparaison de différents schémas de réutilisation fréquentielle, l'impact des caractéristiques radio avancées et en particulier des systèmes d'antennes multiples sur les performances du système. Une classification transversale de la littérature peut aussi distinguer les techniques basées sur la simulation et les approches analytiques.

La littérature sur les études au niveau système pour réseaux OFDMA peut être trouvée avant même que la première version de la norme IEEE 802.16 ait été publiée en 2004. Par exemple, [1] propose des permutations distribuées de sous-porteuses pour former des sous-canaux en mode OFDMA. Cette proposition peut être considérée comme un précurseur des permutations PUSC/FUSC dans IEEE 802.16. Cependant, ce papier ne considère que l'accès sans fil fixe et suppose donc que les équipements des utilisateurs emploient des antennes directives. Wang et al. dans [2] présentent l'évaluation de performances fondée sur la simulation d'un système WiMAX mobile. L'article couvre les aspects les plus importants des couches PHY et MAC de la norme IEEE 802.16e. En ce qui concerne la canalisation, les auteurs comparent les différents modes PUSC sur la voix montante. La capacité VoIP est également analysée par les mêmes auteurs dans [3]. La référence [2] est une étude complète, basée sur la simulation, des réseaux WiMAX mobiles au niveau du système.

Les auteurs de [4] ont mené une étude analytique sur les deux thèmes classiques en ingénierie radio des systèmes OFDMA : la canalisation et la réutilisation fréquentielle. Le premier est analysé du point de vue des collisions entre des sous-porteuses de cellules voisines. L'originalité du papier réside dans la proposition des deux nouveaux schémas de réutilisation fréquentielle et leur évaluation de performances : le FFR dynamique et le régime d'isolement partiel qui est une modification de la réutilisation 1 avec des puissances de transmission variables.

L'analyse des systèmes dynamiques sur la voie descendante pour les réseaux OFDMA avec un trafic de type élastique est très similaire à celle effectuée pour les réseaux GPRS, E-GPRS ou HSDPA. La raison réside dans le fait que toutes ces technologies mettent en œuvre sur la voie descendante un canal partagé avec des MCS adaptatifs et un ordonnancement rapide tenant compte des conditions radio. Dans cette thèse, nous avons mis l'accent sur les spécificités des réseaux WiMAX, mais nous présentons ci-dessous quelques travaux importants qui concernent plusieurs technologies.

Dans [5], les auteurs présentent un modèle analytique permettant de calculer des paramètres de performance tels que le débit d'utilisateur, la probabilité de blocage, le délai de transfert et la probabilité stationnaire des utilisateurs actifs (dans l'état téléchargement) dans la cellule pour un trafic de type élastique. Ils considèrent un système HDR-CDMA mettant l'accent sur la voie descendante.

Comme dans les réseaux OFDMA, la consommation des ressources dépend de la localisation de l'utilisateur et de ses conditions radio. Par conséquent, il est mentionné dans cet article que le trafic n'est pas seulement caractérisé par son intensité, mais a aussi une composante spatiale. Borst dans [6] étudie le système dynamique comportant une population fixe d'utilisateurs générant le trafic élastique pour un système CDMA 1xEV-DO. Une stratégie équitable proportionnelle est prise comme hypothèse. Les utilisateurs entrent et sortent selon des temps contrôlées par l'arrivée et l'achèvement des demandes de services. Les auteurs de [7] dérivent les formules du débit utilisateur pour deux modèles de trafic, OCOF et OCMF, et pour deux régimes, Quasi Stationary (QS) et FL. OCOF est à la base un modèle ON/OFF, où les flux actifs sont séparés par des périodes de lecture. OCMF suppose au contraire que chaque utilisateur est une source Poisson.

Après avoir brièvement présenté quelques articles de référence, nous allons maintenant présenter les contributions principales de cette thèse.

Les contribution de la thèse

La contribution de cette thèse couvre à la fois les systèmes statiques et dynamiques. Nous commençons par le premier point.

Dans le contexte de l'analyse de la couverture radio et de la capacité, nous étudions les performances du système en considérant des schémas de réutilisation fréquentielle différents, la faisabilité de la réutilisation 1 et nous proposons des outils semi-analytiques et analytiques efficaces pour le dimensionnement du réseau. Ci-après, nous présentons les différents domaines de ce sujet pour lesquels cette thèse a contribué.

Nous réalisons d'abord une analyse exhaustive des six schémas de réutilisation fréquentielle classiques proposés dans [8]. Ainsi nous prolongeons le travail effectué dans la littérature existante (e.g., [2]) avec une vue systématique, en considérant des cellules sectorisées/non sectorisées, la puissance de transmission des BS et le rayon des cellules. Nous réalisons des simulations Monte Carlo en voie descendante. Nous analysons soigneusement la distribution du SINR effectif et soulignons le compromis entre la capacité de la cellule et la probabilité de dépassement. Nous concluons que la réutilisation 1 n'est pas possible sans les fonctions radio avancées. Ces travaux ont été publiés dans [9, 10].

Nous avons ensuite considéré le *beamforming* adaptatif comme un moyen efficace de parvenir à la réutilisation 1. Le *beamforming* adaptatif en WiMAX est essentiellement étudié avec le mode AMC dans la littérature existante. La permutation distribuée des sous-porteuses est pourtant une caractéristique importante des systèmes basés sur IEEE 802.16 qui offre la diversité de fréquences. Dans cette thèse, nous étudions la performance du *beamforming* adaptatif en utilisant à la fois les permutations de sous-porteuses distribuées et adjacentes dans les réseaux cellulaires WiMAX. La comparaison des systèmes de réutilisation fréquentielle est répétée avec le *beamforming* adaptatif. Il est montré comment le *beamforming* affecte les résultats de cette comparaison et comment la réutilisation 1 peut

être atteinte. Ces résultats ont été présentés dans [10, 11, 12, 13].

Des méthodes efficaces en temps pour obtenir les statistiques SINR peuvent être trouvées dans la littérature. Cependant, ces méthodes ne peuvent être employées pour les réseaux OFDMA. Du fait de la nature multi-porteuse du système, c'est le SINR effectif (plutôt que le SINR) qui doit être étudié. À cet égard, nous proposons une méthode semi-analytique pour acquérir la distribution spatiale du SINR effectif en considérant l'effet de masque, les évanouissements rapides et en supposant que les utilisateurs sont attachés au meilleur serveur. Nous montrons comment la distribution spatiale du SINR effectif peut être approchée par une distribution GEV. Les statistiques de SINR effectif obtenues par le bloc *Couverture radio et capacité* sert également comme une entrée pour l'analyse du trafic. La méthode semi-analytique a été publiée en [14, 15, 16].

Poursuivant avec les méthodes efficaces en temps pour le dimensionnement de réseau et en contraste avec les travaux existants sur les schémas de réutilisation fréquentielle, nous présentons dans la thèse des modèles analytiques approximatifs pour les schémas IFR, FFR et TLPC. TLPC est une planification des fréquences avec un mécanisme de contrôle de puissance. Nous obtenons des expressions pour le calcul du SIR à une distance donnée de la BS et nous calculons l'efficacité spectrale en utilisant la formule classique de Shannon. On détermine aussi le débit global de la cellule tout en considérant trois politiques d'ordonnancement différentes : l'équité en débit, l'équité en ressources et opportuniste. Cette étude analytique a été publiée dans [17, 18].

L'étude des trois types d'ordonnancement montre la nécessité de considérer le système dynamique. Cela pourra en effet nous permettre d'obtenir des paramètres de performance plus précis concernant le trafic et l'expérience de l'utilisateur.

Pendant cette thèse, le travail dans le domaine de la modélisation du trafic a été réalisée en collaboration avec le LIP6. Notre contribution majeure est la validation et l'étude de la robustesse des modèles analytiques pour le trafic BE de WiMAX présentés dans [19, 20, 21, 22]. Contrairement aux travaux existants basés sur la file d'attente PS, nous présentons une approche différente basée sur une modèle de type Engset et sa chaîne de Markov linéaire liée. En outre, nous intégrons dans notre étude des caractéristiques spécifiques du système WiMAX et nous proposons une meilleure modélisation du canal radio variant, qui prend en compte entre autres la possibilité pour un utilisateur d'être en dépassement. Enfin, nous comparons trois politiques d'ordonnancement traditionnelles (l'équité en débit, l'équité en ressource et l'opportuniste) à une politique dite d'étranglement. Cette politique suppose que le débit utilisateur est limité par MSTR, un paramètre prévu par la norme pour la classe BE. Notre travail se caractérise aussi par une étude de robustesse approfondie, où les principales hypothèses de ces modèles sont assouplies.

Nous présentons maintenant un bref exposé sur les grandes parties de cette thèse, suivi par une conclusion et quelques perspectives pour l'avenir.

Sur la réutilisation fréquentielle

La réutilisation fréquentielle est une technique importante dans les réseaux cellulaires. Dans cette thèse, nous évaluons la performance d'un réseau WiMAX dans des scénarios variés de réutilisation fréquentielle. La qualité radio en termes de SINR et la probabilité de dépassement d'une part, le débit d'autre part, sont les paramètres pris en considération pour cette analyse. Des simulations Monte Carlo, basées sur le calcul du SINR effectif en utilisant le modèle d'abstraction MIC, ont été effectuées sur la voie descendante. Les résultats de simulations montrent que certains schémas de réutilisation fréquentielle ayant une très bonne performance en termes de débit global peuvent cependant avoir une probabilité de dépassement importante. Les schémas de réutilisation fréquentielle satisfaisant les deux paramètres (le dépassement et le débit) de la meilleure manière possible, sont suggérés pour les réseaux WiMAX. L'influence du rayon de cellule et de la puissance par sous-porteuse est également étudiée pour des schémas de réutilisation fréquentielle différents.

On va maintenant présenter les détails sur le modèle de SINR et quelques points importants de simulation suivis par les résultats clés.

Le SINR d'une sous-porteuse n est calculé selon la formule suivante :

$$SINR_n = \frac{P_{n,Tx} a_{n,Sh}^{(0)} a_{n,FF}^{(0)} \frac{K}{d^{(0)\alpha}}}{N_0 W_{Sc} + \sum_{b=1}^{B} P_{n,Tx} a_{n,Sh}^{(b)} a_{n,FF}^{(b)} \frac{K}{d^{(b)\alpha}} \delta_n^{(b)}},$$

où $P_{n,tx}$ est la puissance par sous-porteuse, $a_{n,Sh}^{(0)}$ et $a_{n,FF}^{(0)}$ représentent les facteurs du masque (log-normal) et de l'évanouissement rapide (Rician/Rayleigh) respectivement sur le signal reçu de la BS serveuse, B est le nombre de BS interféreuses, K et α sont les constantes du modèle d'affaiblissement de parcours et $d^{(0)}$ est la distance entre le MS et la BS serveuse. Les termes en exposant b sont liés à toutes les BS interféreuses. W_{Sc} est la bande passante d'une sous-porteuse, N_0 est la densité de bruit thermique et $\delta_N^{(b)}$ est égal à 1 si la BS interféreuse transmet sur la sous-porteuse n et à 0 sinon.

Une fois le SINR d'une sous-porteuse déterminé, le $SINR_{eff}$ est calculé sur les sous-porteuses d'un slot qui est l'unité de base de la ressource dans le système IEEE 802.16. Il y a certaines considérations à propos du masque et de l'évanouissement rapide qui sont comptabilisées pendant le calcul du $SINR_{eff}$. Le masque est tiré au hasard pour un slot et est le même pour toutes les sous-porteuses d'un slot. En supposant que la distribution des sous-porteuses en sous-canaux est uniforme et aléatoire, l'évanouissement rapide est tiré indépendamment pour chaque sous-porteuse d'un slot (Fig. 2). D'autre part, les sous-porteuses, pour une canalisation AMC, sont contigues et, partant, leurs évanouissements rapides ne peuvent plus être considérés comme indépendants. Afin de trouver les valeurs de corrélation d'un évanouissement rapide, nous avons à calculer la bande de cohérence B_C (la bande passante sur laquelle le gain de canal peut être considéré constant).

Les simulations Monte Carlo sont effectuées dans le sens descendant. Le MS

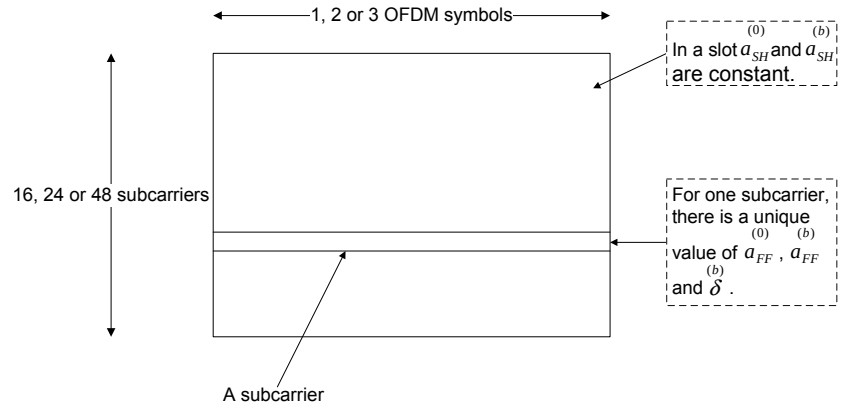

Figure 2: Le masque et l'évanouissement rapide sur un slot PUSC/FUSC/AMC.

est placé dans l'espace cellulaire en utilisant une distribution aléatoire uniforme. Pour accélérer les simulations et pour inclure l'effet de réseau infini, la technique *wraparound* a été utilisée. Le MS s'attache à une BS selon le meilleur lien. Pour chaque MS, le signal reçu de toutes les cellules/secteurs dans le réseau est mesuré. Le MS sélectionne la cellule ou le secteur dont il reçoit le signal maximum. Les autres cellules/secteurs sont alors des interféreurs (en fonction du motif de réutilisation). L'effet du masque est pris en compte au cours de cette procédure. Toutefois, les évanouissements rapides ne sont pas considérés lors du choix de la BS serveuse. Afin de trouver le gain de l'antenne, la diagramme de rayonnement d'antenne définie par le 3GPP2 [8] est pris en compte.

Les paramètres de sortie obtenus par les simulations sont les suivants : les valeurs moyennes de $SINR_{eff}$, le débit moyen de la cellule et la probabilité de dépassement. Les résultats des simulations montrent que, même si certains schémas de réutilisation fonctionnent très bien en termes de débit moyen des cellules, seule la réutilisation 3x3x3 a une valeur acceptable de la probabilité de dépassement (par exemple, $< 5\%$). Tous les autres types ont des probabilités de dépassement de plus de 5%.

Nous continuons l'analyse de performances en faisant varier le rayon de cellule et la puissance d'émission afin d'observer l'effet du bruit. Il a été constaté que les paramètres de performance n'ont pas changé de manière significative avec des valeurs différentes du rayon de cellule et de la puissance d'émission. Il y a un peu de dégradation de performance pour des rayons de cellule grands et des puissances d'émission faibles. On a aussi vérifié que, pour la réutilisation 3x3x3, le rayon de cellule pourrait être étendu à 2000 m en diminuant légèrement le débit moyen et sans augmenter la probabilité de dépassement.

Notre étude des motifs de réutilisation fréquentielle montre que les schémas de réutilisation qui offrent une bonne performance du débit posent des problèmes de couverture radio. La probabilité de dépassement devient alors un facteur déterminant et seule la réutilisation 3x3x3 a une valeur acceptable de celle-ci même si elle a le débit le plus faible entre tous les schémas de réutilisation. Il est également démontré que les paramètres de performance ne changent pas de

manière significative avec des valeurs différentes du rayon de cellule et de la puissance d'émission.

Il ressort clairement de la conclusion ci-dessus qu'une réutilisation agressive n'est pas possible sans des fonctionnalités avancées du système. Par conséquent, à l'étape suivante, nous examinons les performances du système en présence de *beamforming* adaptatif.

Évaluation de performances avec beamforming adaptatif

L'étude de la réutilisation fréquentielle a amené à la conclusion que seulement la réutilisation 3x3x3 (sans les options avancées) était acceptable pour les réseaux WiMAX en raison des limitations causées par la probabilité de dépassement. Toutefois, il a également été remarqué que, à cause du facteur de réutilisation faible, le débit cellulaire est moindre pour la réutilisation 3x3x3 par rapport à d'autres schémas de réutilisation. Par conséquent, dans cette thèse, nous exploront comment les autres schémas de réutilisation peuvent être rendus possibles par la réduction de leur probabilité de dépassement. Les MS au bord de la cellule sont relativement plus enclins au dépassement à cause de puissance du signal reçu faible et de l'interférence co-canal forte. Par conséquent, il est important de chercher des techniques qui peuvent réduire l'interférence et/ou augmenter la puissance du signal en même temps. Une de ces techniques dans le système WiMAX est le *beamforming* adaptatif.

Le type ou même la possibilité du *beamforming* adaptif dépend de l'organisation des sous-porteuses pilotes. Cela permet également de déterminer la façon dont l'interférence est modélisée. En fait, les sous-porteuses pilotes sont requises pour l'estimation de canal. En cas de *beamforming*, des pilotes dédiés sont nécessaires pour chaque faisceau dans la cellule. Donc, il est important d'avoir une idée de la distribution des sous-porteuses pilotes dans les différents schémas de canalisation des réseaux OFDMA. Par exemple, dans les réseaux WiMAX, il existe trois types de canalisation : PUSC, FUSC et AMC. Pour PUSC et FUSC, il existe un ensemble de sous-porteuses pilotes communs pour un certain nombre de sous-canaux, alors qu'en mode AMC, chaque sous-canal a ses propres sous-porteuses pilotes. Par conséquent, le nombre de faisceaux orthogonaux possibles dans une cellule (du réseau cellulaire) dépend de la distribution de sous-porteuses pilotes et, donc du type de permutation des sous-porteuses.

En PUSC, les sous-canaux sont regroupés en six groupes. Chaque groupe a son ensemble de sous-porteuses pilotes et donc le *beamforming* peut être fait par groupe PUSC. On considère que les sous-porteuses d'un sous-canal sont choisies au hasard. Dans ce cas, chaque sous-porteuse de la cellule serveuse peut subir l'interférence des différents faisceaux d'une cellule interféreuse donnée. De cette façon, les sous-porteuses d'un sous-canal ne subissent pas forcément la même interférence. La puissance de l'interférence dépend alors du gain de réseau

d'antennes associé à la sous-porteuse en collision qui appartient à l'un des six faisceaux interférents de la cellule voisine.

Les sous-porteuses pilotes dans FUSC sont communes à tous les sous-canaux, donc un seul faisceau est possible dans chaque cellule. Contrairement à PUSC, toutes les sous-porteuses d'un sous-canal expérimentent la même interférence. Cela est dû au fait que chaque sous-porteuse en collision aura le même gain de réseau d'antenne puisqu'il n'y a qu'un seul faisceau par cellule interféreuse.

Quand on considère l'AMC pour le *beamforming*, il peut y avoir autant de faisceaux orthogonaux que de sous-canaux puisque chaque sous-canal a ses sous-porteuses pilotes dédiées. On considère le cas où il n'y a aucune coordination entre BS pour l'attribution des sous-canaux au MS. En raison de l'affectation similaire de sous-porteuses aux sous-canaux dans les cellules voisines, toutes les sous-porteuses subissent la même interférence à cause des faisceaux interféreurs dans la cellule voisine. Les sous-porteuses en collision dans un faisceau auront le même gain de réseau d'antenne. En outre, contrairement à PUSC et FUSC, puisque les sous-porteuses d'un sous-canal sont contigues dans AMC, le gain diversité de fréquence n'est pas obtenu.

On répète la comparaison des six schémas de réutilisation fréquentielle mais cette fois en considérant le *beamforming*. Le $SINR_{eff}$, le débit moyen de cellule et la probabilité de dépassement de l'ensemble des six types de réutilisation avec et sans *beamforming* sont analysés. Il a été remarqué que la technique de *beamforming* a amélioré les trois paramètres pour les six schémas de réutilisation. Malgré une amélioration importante, la réutilisation 1x3x1 et 1x1x1 ont encore une probabilité de dépassement trop grande. Quant aux quatre autres types, les réutilisations 1x3x3 et 3x3x1 ont non seulement une probabilité de dépassement faible mais aussi un débit moyen plus élevé que les autres. En outre, ces deux types de réutilisation ont des performances comparables et pourraient être considérés comme un bon choix pour les réseaux WiMAX avec *beamforming*.

Même si le *beamforming* adaptatif a considérablement amélioré la performance du système, le schéma de réutilisation 1x3x1 (ou réutilisation 1) a toujours une probabilité de dépassement importante (i.e., 9%). Dans cette thèse, nous avons proposé deux méthodes pour réaliser la réutilisation 1.

La première méthode est la charge partielle des sous-canaux. Les simulations sont effectuées avec 80% et 60% de charge des sous-canaux. Il est observé à partir des résultats de simulation que 80% de la charge de sous-canaux apporte une probabilité de dépassement pour la réutilisation 1x3x1 bien contrôlée (moins de 5%), mais il est également important de voir son effet sur le débit moyen disponible. Le débit moyen de cette réutilisation est évalué à 80% de la charge des sous-canaux et se trouve à 39.5 Mbps. Cette valeur de débit moyen est supérieure à celles de tous les autres types de réutilisation dans des conditions de pleine charge.

La deuxième méthode proposée est de faire le *beamforming* par PUSC group. Les simulations sont effectuées avec six, trois et un faisceau par secteur. On trouve à partir des résultats de simulation que la probabilité de dépassement diminue de façon significative lorsque on profite de la diversité offerte par PUSC.

L'augmentation du nombre de faisceaux diminue la probabilité de dépassement d'une valeur inacceptable de 9% (avec un faisceau) à un raisonnable 2% (avec six faisceaux). Il est intéressant de noter que le débit moyen et le $SINR_{eff}$ moyen ne sont pas touchés par le gain obtenu en termes de probabilité de dépassement. Ainsi, en employant le *beamforming* par PUSC *Major group*, nous avons atteint la réutilisation 1 sans charge partielle des sous-canaux ni coordination entre stations de base.

Nous avons également effectué une comparaison des trois types de canalisation en présence de *beamforming*. La comparaison de la valeur moyenne du débit cellulaire (par rapport à la distance à la BS) montre que dans la région proche de la BS, PUSC est un peu moins performant que FUSC et AMC. Ce résultat peut être justifié quand on analyse les probabilités de MCS, on remarque alors que la probabilité stationnaire du meilleur MCS (64QAM-3/4) est plus élevée avec FUSC et AMC. En raison du signal fort dans la région proche de station de base, la probabilité pour un MS d'atteindre un meilleur MCS est plus importante. À environ 350 m et au-delà (de la station de base), le débit moyen avec PUSC est environ 1 Mbps inférieure à celui de FUSC et AMC même si PUSC a la meilleure performance en termes de qualité radio. Cela est dû au fait que, avec PUSC, le nombre de slots disponibles est moindre.

Lors de l'étude des motifs de réutilisation fréquentielle avec le *beamforming*, nous avons remarqué que la performance, en termes de qualité de radio et de débit, est améliorée par rapport au cas sans *beamforming*. Seule la probabilité de dépassement des motifs 1x3x1 et 1x1x1 est restée supérieure au seuil de 5%. Pour réduire encore la probabilité de dépassement du motif de réutilisation 1 avec *beamforming*, deux méthodes (charge partielle des sous-canaux et *beamforming* par groupe PUSC) sont proposées.

L'analyse des motifs de réutilisation fréquentielle nous montrent que la distribution du $SINR_{eff}$ est une mesure cruciale et peut être obtenue précisément par des simulations. Mais l'inconvénient de la simulation réside dans son temps de calcul. C'est pourquoi, au cours de la prochaine étape de la thèse, nous recherchons une méthode efficace en temps pour obtenir les statistiques du SINR dans un système cellulaire WiMAX.

Méthode semi-analytique pour modéliser la distribution de SINR effectif

Dans cette thèse, on introduit une approche semi-analytique (présentée en Fig. 3) pour trouver les probabilités stationnaires des MCS pour un réseau WiMAX en voie descendante en supposant les utilisateurs desservis par la meilleure BS. En utilisant des simulations Monte Carlo, on trouve les distributions spatiales de $SINR_{eff}$ pour différentes valeurs d'écart-type du masque (σ_{SH}). À l'aide d'une méthode d'ajustement de distribution, on montre que la distribution GEV fournit un bon ajustement pour les différents schémas de réutilisation de fréquences. En

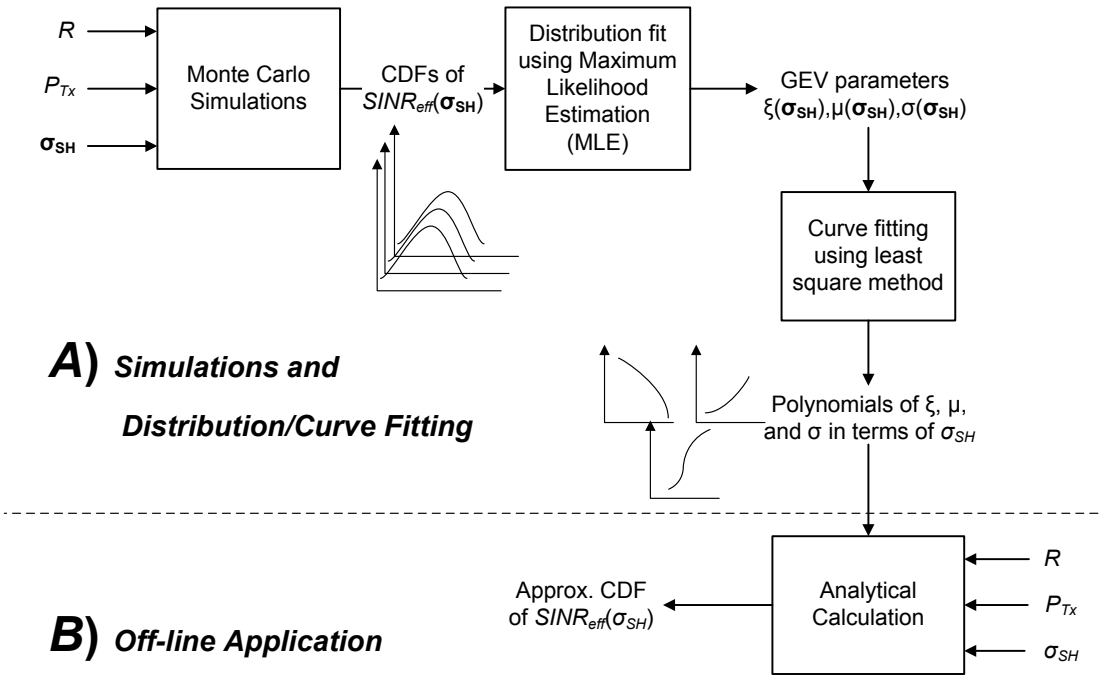

Figure 3: Vue d'ensemble de la méthode semi-analytique proposée.

outre, en utilisant l'ajustement de courbe, nous démontrons que les paramètres des distributions GEV, en fonction de σ_{SH}, peuvent être exprimés en termes des polynômes. Ces polynômes peuvent ensuite être utilisées hors ligne (au lieu des simulations longues) pour obtenir la distribution GEV, et donc les probabilités stationnaires des MCS, pour toute valeur désirée de σ_{SH}. Nous montrons également que ces polynômes peuvent être utilisés pour d'autres configurations de cellules avec un écart acceptable et un gain de temps significatif.

Afin de valider la méthode semi-analytique, des simulations Monte Carlo sont réalisées pour un ensemble de $\sigma_{SH} = 4, 5, ..., 12$ dB. Les autres paramètres d'entrée sont le rayon de cellule $R = 1500$ m et la puissance d'émission $P_{Tx} = 43$ dBm. La distribution du $SINR_{eff}$ est obtenue pour chaque valeur de σ_{SH}. En utilisant l'ajustement de distribution, les paramètres de la GEV sont déterminés pour chacune de ces distributions. Ces paramètres de GEV, sont ensuite séparément tracés en fonction de σ_{SH}. À l'aide de l'ajustement de courbe, les polynômes des courbes approximatives sont trouvées.

En guise d'exemple, la PDF du $SINR_{eff}$ (obtenue par la simulation) et la PDF GEV pour $\sigma_{SH} = 9$ dB sont comparées. Les deux distributions ont une dissimilitude de seulement 0,052 ce qui représente 2,6% de l'erreur maximale possible. Cette comparaison d'une valeur intégrale de σ_{SH} est destinée à démontrer le fait que la PDF GEV est une bonne approximation de la PDF du $SINR_{eff}$. En revanche, pour la validation de notre méthode semi-analytique, nous prennons des valeurs non-intégrales de σ_{SH}.

Pour valider l'application hors ligne, on choisit une valeur non-intégrale arbitraire $\sigma_{SH} = 7,5$ dB. Nous calculons les paramètres GEV grâce aux polynômes

et on obtient la PDF, les probabilités des MCS et le débit cellulaire. Pour la même valeur de σ_{SH} et pour des valeurs $R = 1500$ m et $P_{Tx} = 43$ dBm, on trouve la PDF, les probabilités des MCS et le débit cellulaire par simulations. En outre, nous vérifions l'applicabilité des résultats obtenus avec les paramètres de la GEV, avec $\sigma_{SH} = 7,5$ dB, pour plusieurs configurations cellulaires. À cette fin, on fixe $\sigma_{SH} = 7,5$ dB et on réalise les simulations pour différentes valeurs de R et P_{Tx}. La valeur maximale de R considérée est 2000 m car au-delà la probabilité de dépassement est inacceptable. Les PDFs, les probabilités des MCS et les débits moyens de cellule, obtenues par des simulations avec des configurations différentes, sont comparés avec ceux obtenus avec les paramètres GEV et la méthode semi-analytique.

Nous avons montré que la distribution de $SINR_{eff}$, obtenue par les simulations Monte Carlo au niveau système, peut être approchée avec succès par une distribution GEV. En outre, il est montré que les paramètres de la distribution GEV peuvent être exprimés en utilisant des polynômes simples en fonction de σ_{SH}. Ces polynômes peuvent être utilisés pour calculer les paramètres GEV pour toute valeur de σ_{SH} désirée. Ces paramètres peuvent être utilisés pour estimer la distribution de $SINR_{eff}$, et par conséquent les probabilités stationnaires des MCS. Les résultats peuvent être utilisés pour un certain nombre de configurations de réseau avec une précision suffisante. En conséquence, nous n'avons plus besoin des simulations coûteuses en temps pour obtenir la distribution du $SINR_{eff}$.

Revenant à l'étude de la réutilisation fréquentielle dans la prochaine étape, on envisage des schémas de réutilisation plus complexes. Nous introduisons des modèles analytiques pour l'évaluation des performances d'un système OFDMA en prenant en compte trois systèmes de réutilisation fréquentielle. Pour chaque motif, trois types d'ordonnancement différents sont aussi considérés dans cette étude. Les résultats obtenus analytiquement sont validés par des simulations Monte Carlo. Les expressions analytiques sont ensuite utilisées pour comparer les performances des trois schémas de réutilisation en tenant compte des types d'ordonnancement et des conditions radio.

Approche analytique pour l'évaluation des performances de divers schémas de réutilisation fréquentielle et d'ordonnancement

Les modèles analytiques pour l'évaluation des performances dans les réseaux cellulaires sont bien connus pour fournir des résultats avec une efficacité en un temps suffisant. Dans cette thèse, nous présentons une solution analytique pour effectuer l'analyse des performances de différents motifs de réutilisation fréquentielle dans un réseau cellulaire OFDMA. On étudie les performances dans le sens descendant en termes de SIR et de débit total de la cellule. Le débit total est analysé en prenant en compte trois types d'ordonnancement différents : l'équité en débit, l'équité en bande passante et l'opportuniste. Les modèles analytiques sont pro-

posés pour les motifs IFR, FFR et TLPC. Ces modèles sont basés sur un modèle fluide qui a été initialement proposé pour les réseaux CDMA. La clé de la modélisation de cette approche est de considérer des entités discrètes que sont les BS comme un continuum. Pour valider notre approche, des simulations Monte Carlo sont effectuées. La validation de l'étude montre que les résultats obtenus par notre méthode analytique sont conformes à ceux obtenus par des simulations. Une comparaison entre les motifs de réutilisation fréquentielle mentionnées ci-dessus et les politiques d'ordonnancement est également présentée. Nous proposons également une optimisation des paramètres en jeu (rayon interne de cellule et rapport des puissances).

Dans ce resumé et en guise d'exemple, nous étudions IFR1 (IFR avec réutilisation 1) en présence d'un ordonnancement équitable en débit. En utilisant le modèle fluide, l'expression du SINR d'un utilisateur à la distance normalisée x est donnée par l'équation suivante :

$$\gamma_{IFR1}(x) = \frac{\sqrt{3}}{\pi}(\eta - 2)(2 - x)^{-2}(2/x - 1)^{\eta}, \tag{1}$$

où $x = r/R_c$, r désigne la distance du MS à sa BS et R_c est le rayon de la cellule.

Les valeurs de SINR obtenues par le modèle fluide sont comparées aux résultats de simulation Monte Carlo. Cette comparaison montre une harmonie entre les deux pour différentes valeurs de l'exposant d'affaiblissement de parcours η. On utilise maintenant cette expression de SINR pour trouver l'efficacité spectrale (en bits/s/Hz) en fonction de la variable x en utilisant la formule de Shannon :

$$C_{IFR1}(x) = \log_2[1 + \gamma_{IFR1}(x)]. \tag{2}$$

En considérant l'équité en débit, les utilisateurs se voient alloués une bande passante permettant d'atteindre le même débit D_u pour chaque utilisateur. Comme le SINR et l'efficacité spectrale dépendent de r, plus la distance d'un utilisateur à sa BS est grande, moins l'efficacité spectrale est importante et donc plus grande doit être la bande passante (ou le nombre de sous-porteuses) allouée à cet utilisateur. Soit $W_u(r)$ la bande passante allouée par l'ordonnanceur à un utilisateur situé à la distance r de la BS. Son débit utilisateur D_u peut maintenant être écrit de la manière suivante :

$$D_u = W_u(r)C(r), \tag{3}$$

sous la contrainte que la bande passante totale par cellule W ne peut pas être dépassée. La bande passante totale utilisée dans une cellule (calculée en intégrant sur la surface de cellule) est donc donnée par l'expression :

$$W = 12 \int_0^{\pi/6} \int_0^{R_c/\cos\theta} W_u(r)\rho_u \, r \, dr \, d\theta. \tag{4}$$

Si N_u est le nombre d'utilisateurs dans une cellule, la densité d'utilisateurs est $\rho_u = N_u/(2\sqrt{3}R_c^2)$. En utilisant les équations ci-dessus, la valeur de ρ_u et la

transformation de la variable r en x, le débit utilisateur est donné par :

$$D_u = \frac{\sqrt{3}W/6}{N_u \int_0^{\pi/6} \int_0^{1/\cos\theta} \frac{x}{C_{IFR1}(x)}\, dx\, d\theta}.$$

Comme tous les utilisateurs reçoivent le même débit et puisqu'il y a N_u utilisateurs dans la cellule, le débit total de la cellule est $D_{T,IFR1} = N_u D_u$ et peut être écrit en utilisant résultat précédent :

$$D_{T,IFR1} = \frac{\sqrt{3}W/6}{\int_0^{\pi/6} \int_0^{1/\cos\theta} \frac{x}{C_{IFR1}(x)}\, dx\, d\theta}. \tag{5}$$

On peut remarquer dans l'expression ci-dessus que le débit total de cellule ne dépend ni du nombre d'utilisateurs dans la cellule, ni de la valeur de R_c.

Ensuite, on compare les résultats du modèle (avec équité en débit) avec ceux des simulations. La bande passante disponible dans le réseau est $W = 10$ MHz et le nombre d'utilisateurs par cellule est $N_u = 30$. Le débit total de cellule $D_{T,IFR1}$ avec le modèle fluide et les simulations, pour différentes valeurs de η, est analysé. Le meilleur accord est obtenu pour $\eta = 2,7$, mais la différence reste inférieure à 10% pour η entre $2,6$ et $3,2$. Le débit utilisateur (D_u) peut être facilement obtenu en divisant le débit total de la cellule ($D_{T,IFR1}$ dans ce cas) par le nombre d'utilisateurs (N_u) dans la cellule.

Après la validation de l'approche analytique (basée sur le modèle fluide), on l'utilise pour comparer les motifs IFR, FFR et TLPC tout en considérant trois types d'ordonnancement différents : l'équité en débit, l'équité en bande passante et l'opportuniste.

De cette étude comparative, on en déduit que IFR3 fournit la meilleure performance en termes de valeurs de SINR. IFR1 est beaucoup plus faible que IFR3 en termes de qualité radio. FFR suit exactement la courbe IFR1 jusqu'à R_0 et IFR3 après. Par rapport à l'IFR1, TLPC améliore le SINR dans la région extérieure au détriment d'une qualité radio dégradée dans la région intérieure.

On compare maintenant le débit total de la cellule pour tous les motifs de réutilisation fréquentielle en présence des trois algorithmes d'ordonnancement. Le débit total de la cellule avec FFR dépend des valeurs de R_0 et W_1. De la même manière, TLPC dépend des paramètres R_0 et δ. Pour ces deux motifs, la valeur maximale possible du débit total de la cellule, fondée sur des valeurs optimales de leurs paramètres, a été prise en compte dans la comparaison. La valeur de la bande passante du réseau est de 10 MHz. Le nombre d'utilisateurs par cellule N_u est considéré égal à trente dans tous les cas. L'exposant d'affaiblissement de parcours η est égal à trois.

Avec l'équité en débit, IFR3 fournit la plus faible performance bien que les valeurs du SINR soient plus importantes. Cela est dû au fait que l'utilisation de la bande passante du réseau par cellule est inférieure à celle des autres motifs. TLPC a la valeur maximale avec $\delta = 13,2$ et a une performance comparable à celle de FFR (avec $R_0 = 757$ m). Par conséquent, en appliquant les motifs TLPC

et FFR, on peut résoudre le problème de la mauvaise qualité radio (SINR) en bord de cellule présent dans le cas IFR1. En même temps, la bande passante est utilisée plus efficacement qu'avec IFR3. En raison de sa simplicité, la FFR pourrait être préféré à TLPC avec l'ordonnancement équitable en débit.

L'équité en bande passante vise à améliorer l'utilisation des ressources (par rapport à l'équité en débit) tout en veillant à la répartition équitable des ressources entre les utilisateurs (contrairement à l'ordonnancement opportuniste). Donc, pour tous les motifs de réutilisation, le débit total cellulaire obtenu se situe entre ceux obtenus avec les deux autres types d'ordonnancement. Avec l'équité en bande passante, IFR1 fournit la plus grande capacité cellulaire, car il bénéficie de l'utilisation de la bande passante totale du réseau dans chaque cellule. Bien que les valeurs SINR soient plus élevées avec IFR3, ce système alloue seulement un tiers de la bande passante totale du réseau à chaque cellule, ce qui explique la faible performance atteinte. FFR et TLPC ne peuvent pas faire mieux que IFR1 et atteignent leur valeur maximale pour un jeu de paramètres qui les rend très proches de IFR1. Avec FFR et en supposant $R_0 = R_c$ (valeur optimale), la plus grande partie de la bande passante est utilisée avec une réutilisation 1. Une meilleure qualité radio en bord de la cellule est obtenue au prix d'une légère réduction du débit total de la cellule par rapport à IFR1. Avec TLPC, la valeur $\delta = 1$ (valeur optimale) réduit presque ce motif à IFR1.

Le débit total de la cellule obtenu avec l'ordonnancement opportuniste fournit une borne supérieure (pour un nombre donné d'utilisateurs) sur la performance cellulaire mais cette performance est obtenue au prix de l'équité. Sauf avec le motif TLPC, seul le meilleur utilisateur est servi et obtient toute la bande passante. IFR1 réalise encore le meilleur débit cellulaire. FFR approche IFR1, avec une bande passante très faible attribuée à la région externe. Le choix d'ordonnancer deux utilisateurs (un dans la région interne, l'un à l'extérieur) réduit la performance de TLPC par rapport à IFR1 car une partie de la bande passante est attribuée à un utilisateur un peu éloigné de la BS.

On étudie aussi le débit total de la cellule en fonction de l'exposant d'affaiblissement de parcours pour les trois motifs de réutilisation fréquentielle et les trois politiques d'ordonnancement. On remarque que la hiérarchie entre les motifs de réutilisation fréquentielle observée avec $\eta = 3$ reste valable pour η entre $2,6$ et $3,6$. Pour l'ordonnancement équitable en débit, l'avantage de TLPC sur FFR est un peu plus prononcé lorsque η augmente. Le résultat principal dans tous les cas est que le débit total de la cellule augmente linéairement en fonction de l'exposant de l'affaiblissement de parcours.

On conclut maintenant cette étude analytique en en soulignant les points clés. La méthode analytique proposée est très souple. Nous avons été capables de l'appliquer à différents types de réutilisation fréquentielle et de politiques d'ordonnancement. La méthode est très efficace en temps car les résultats sont obtenues instantanément contrairement aux simulations qui sont relativement longues.

Après avoir abordé l'analyse statique de la couverture radio et l"étude de capacité, dans la dernière partie de la thèse, nous prenons en compte le système

dynamique et abordons la question de la modélisation du trafic. Dans cette partie, des modèles analytiques pour le trafic BE dans un système WiMAX (prenant en compte différentes politiques d'ordonnancement) sont présentés et sont validées par des simulations Monte Carlo.

La validation de modèles de trafic au mieux pour les réseaux WiMAX

Les travaux présentés jusqu'à présent considérent un système statique. Mais l'analyse de la dynamique d'un système est impérative pour compléter le portrait global du dimensionnement. Donc, dans cette partie, nous prenons en compte le système dynamique qui admet en entrée les probabilités stationnaires des MCS fournis par le système statique. Cette analyse prend en compte la nature du trafic et différentes classes de trafic WiMAX (associées à différentes QoS).

L'étude du système dynamique a été réalisée en collaboration avec le Laboratoire d'informatique de Paris 6 (LIP6). Notre contribution majeure a été la validation et l'étude de la robustesse des modèles analytiques, pour le trafic BE de WiMAX, présentées dans [19, 20, 21, 22]. Donc, dans cette thèse, nous expliquons l'analyse de la validation et de la robustesse de ces modèles pour lesquels un simulateur a été développé pour effectuer des simulations Monte Carlo. Les modèles analytiques prennent en compte le trafic BE mono/multi-profil où un profil est un ensemble de paramètres qui représentent une classe de trafic BE. Ces paramètres sont : le volume de données ON (taille du téléchargement) et la durée de la période OFF (temps de lecture). Quatre politiques d'ordonnancement différents sont également considérés lors de la formulation de modèles analytiques.

Parmi les quatre types d'ordonnancement considérés, trois sont conventionnels : l'équité en ressource, l'équité en débit et l'opportuniste. Le quatrième type d'ordonnancement est le régime d'étranglement qui est proposé pour modéliser une métrique de performance de la norme IEEE 802.16e appelé MSTR. Cette métrique spécifie une limite supérieure pour le débit maximal qui pourrait être offert à un utilisateur.

Il y a trois paramètres de performance obtenus à partir du modèle analytique markovien. Ces paramètres sont les suivants : le débit moyen, l'utilisation moyenne de la ressource et le nombre moyen d'utilisateurs actifs.

L'étude de validation et de robustesse

Dans le but de valider les modèles, un simulateur a été développé qui implémente un générateur de trafic ON/OFF, un canal sans fil pour chaque utilisateur et un ordonnanceur central qui alloue les ressources radio, i.e., les slots, aux utilisateurs actifs sur chaque trame. On montre aussi la robustesse du modèle lorsque le trafic et le modèle de canal sont supposés plus complexes.

La comparaison entre la simulation et le modèle est réalisée en fonction des trois paramètres de performance mentionnés ci-dessus.

L'étude de validation

Dans une première phase, on valide le modèle analytique par simulations. Le simulateur prend en compte les mêmes hypothèses de trafic et de canal que celles du modèle analytique. Donc, dans les simulations, nous supposons que les paramètres du trafic, volume de données ON et période OFF, sont distribués de façon exponentielle. En outre, le modèle de canal est supposé être sans mémoire, c'est-à-dire que les MCS sont tirés indépendamment à chaque trame pour chaque utilisateur avec les probabilités discrètes des différents types de MCS. Il est à noter que dans le simulateur les MCS d'utilisateurs sont déterminés trame par trame et l'ordonnancement est réalisé en temps réel (basé sur le MCS à cet instant). Le modèle analytique, d'autre part, considère seulement les probabilités stationnaires des MCS.

Les résultats de l'étude de validation montrent que la différence maximale entre la simulation et le modèle analytique pour tous les types d'ordonnancement (pour le trafic mono/multi-profils) ne dépasse pas 6%. Cette phase montre que décrire le système par le nombre d'utilisateurs actifs est une approximation suffisante pour obtenir les paramètres de dimensionnement.

L'étude de robustesse

Dans la deuxième phase, l'étude de robustesse, on relâche les hypothèses retenues pour le modèle analytique en considérant des modèles plus réalistes de trafic et de canal radio. La comparaison avec les résultats de simulation nous montre à quel point le modèle analytique est robuste à ces assouplissements.

Même s'il est bien adapté à la période OFF, la propriété *sans mémoire* ne correspond pas toujours à la réalité du trafic de données. C'est la raison pour laquelle, pour l'étude de robustesse, le volume de données ON est caractérisé par une distribution de Pareto tronquée.

En ce qui concerne le type de canal, deux canaux avec mémoire sont introduits dans l'étude de la robustesse. Entre ces deux types de canaux, l'un suppose que toutes les stations mobiles dans une cellule sont dans les mêmes conditions radio tandis que l'autre suppose que la moitié des stations mobiles sont dans de mauvaises conditions radio et la moitié dans de bonnes conditions radio.

Les résultats de l'étude de robustesse prouvent que même quand on s'éloigne des hypothèses du modèle analytique la conclusion ne change pas beaucoup par rapport à celle de l'étude de validation. Bien que l'accord entre la simulation et les résultats du modèle est quelque peu dégradée, l'écart maximal reste inférieur à 10% dans tous les cas.

Conclusion et perpectives

Les performances cibles fixées pour le système OFDMA sont très prometteuses. Cependant, pour atteindre ces objectifs, des outils d'ingénierie sont indispensables. Dans cette thèse, nous avons présenté un certain nombre de méthodes

pour l'ingénierie des systèmes OFDMA. Ces méthodes concernent à la fois les systèmes statiques et dynamiques. Dans ce qui suit, on décrit brièvement ces méthodes.

On a d'abord développé une technique de simulation qui nous a permis de comparer les différents schémas de réutilisation fréquentielle en considérant certains paramètres de QoS. Il est montré que certains schémas de réutilisation fréquentielle offrant un débit élevé sont aussi confrontés à une probabilité de dépassement élevée. Donc, un compromis entre les deux est demandé. On est capable de montrer que sans les fonctionnalités avancées, les systèmes OFDMA ne peuvent pas employer une réutilisation des fréquences agressive en raison d'une probabilité de dépassement considérable. Seule la réutilisation 3x3x3, caractérisée par 2% probabilité de dépassement, est faisable dans un tel cas. On a aussi étudié l'impact sur les performances de différents paramètres de la cellule (par exemple, le rayon et la puissance d'émission) et nous avons noté que les conclusions ne variaient pas beaucoup.

En incluant le *beamforming* adaptatif dans la comparaison des motifs fréquentiels, on a conclu que des schémas de réutilisation des fréquences plus agressifs (à l'exception de la réutilisation 1) que 3x3x3 fournissaient plus de débit avec une probabilité de dépassement acceptable. Ensuite, on a examiné la possibilité de parvenir à la réutilisation 1. Nous avons pu montrer que la réutilisation 1 pouvait être possible soit par le chargement partiel des sous-canaux (par exemple, en utilisant 80% des sous-canaux) ou en exploitant la structure des groupes PUSC. En outre, on a présenté une comparaison des trois systèmes de permutation de sous-porteuses (PUSC, FUSC et AMC) avec réutilisation 1, et il a été constaté que seul le *beamforming* par groupe PUSC pouvait fournir une probabilité de dépassement acceptable. L'AMC, sans coordination de BS, donne une probabilité de dépassement supérieure à 5%.

Il a été souligné dans cette thèse que les statistiques de $SINR_{eff}$ sont très importantes et que des méthodes sont souhaitées pour acquérir ces statistiques de manière efficace. Pour cela, une méthode semi-analytique est proposée. Par rapport aux méthodes reposant exclusivement sur des simulations Monte Carlo, cette méthode permet d'obtenir des résultats de manière instantanée et avec une erreur sur les résultats acceptable.

Les schémas plus complexes de réutilisation fréquentielle, telles que FFR, promettent d'améliorer les SINR pour les utilisateurs en bord de cellule en appliquant la réutilisation 3 dans la région cellulaire externe et de bénéficier d'une réutilisation agressive en planifiant la réutilisation 1 dans la région intérieure. Ils offrent un compromis entre la réutilisation 1 complète et la réutilisation 3 complète et exploitent les avantages des deux. On a proposé une méthode analytique pour calculer le SINR pour différents types de réutilisation, IFR, FFR et TLPC. On a également fourni des expressions pour le débit total de la cellule en prenant en compte les trois politiques d'ordonnancement suivantes : l'équité en débit, l'équité en bande passante et l'opportuniste. Il est démontré que la taille optimale des régions intérieures et extérieures, pour les motifs FFR et TLPC, dépend de la politique d'ordonnancement. La conclusion reste vraie pour le rap-

port des puissances des régions interne/externe pour TLPC et la division de la bande passante entre les régions interne/externe pour FFR. On a également donné une comparaison entre trois schémas de réutilisation fréquentielle en termes de valeurs SINR et de débits. On a aussi étudié l'effet de différentes valeurs de l'exposant de l'affaiblissement de parcours sur nos résultats.

En ce qui concerne l'étude du système dynamique, on a fait une étude de validation et de robustesse des modèles analytiques développés pour les systèmes WiMAX. Ces modèles fournissent les paramètres de performance qui sont utilisés dans le processus de dimensionnement. Les modèles prennent en compte différentes politiques d'ordonnancement et classes de trafic. On a montré que les résultats obtenus par les modèles sont proches de ceux obtenus avec les simulations. Nous avons également conclu que le modèle fournit des résultats acceptables pour différents canaux radio, distributions de trafic et conditions de charge.

Après avoir présenté une brève conclusion de nos travaux, on propose maintenant des extensions possibles.

Dans le cas des systèmes statiques, on a étudié la performance du *beamforming* adaptatif pour six schémas de réutilisation fréquentielle. On suggère de faire la même analyse avec les réseaux MIMO et de comparer les deux. Les techniques de coordination de BS sont importantes dans le contexte de la permutation de sous-porteuse AMC et doit être analysée. Alors que l'on a proposé une méthode semi-analytique pour modéliser les statistiques de $SINR_{eff}$, une méthode complètement analytique (qui peut fournir des résultats rapidement) est plus souhaitable et devrait être recherchée. Dans l'étude analytique de IFR, FFR et TLPC, on n'a pas tenu compte de l'effet de masque et du phénomène d'évanouissement rapide, une étude plus précise est donc nécessaire.

Notre étude des systèmes dynamiques considére uniquement le trafic élastique. Il serait utile d'inclure le trafic temps réel dans les modèles analytiques et de le mixer avec du trafic non temps-réel. Cela permettrait de donner une image complète de la dynamique du système et devrait prendre en compte le type d'affectation des ressources aux deux types de trafic. Retard et de gigue ne sont pas pris en compte dans les travaux présentés et doivent donc être étudiés. L'adaptation des modèles à LTE serait aussi une tâche importante. Dans les systèmes dynamiques, on a considéré une cellule dans le réseau multicellulaire, il serait utile d'étudier l'effet de l'interaction entre les cellules du réseau.

Contents

List of Figures

List of Tables

List of Acronyms

1xEV-DO	1xEvolution-Data Optimized
3GPP	3rd Generation Partnership Project
AMC	Adaptive Modulation and Coding
AWGN	Additive White Gaussian Noise
BE	Best Effort
BLER	Block Error Rate
BS	Base Station
BW	Bandwidth
CCI	Co-channel Interference
CDF	Cumulative Distribution Function
CDMA	Code Division Multiple Access
CTMC	Continuous Time Markov Chain
DBR	Delivered Bit Rate
DL	downlink
EESM	Exponential Effective SINR Mapping
ESM	Effective SINR Mapping
FDMA	Frequency Division Multiple Access
FEC	Forward Error Correction
FFR	Fractional Frequency Reuse
FL	Flow Level
FTFR	Fractional Time and Frequency Reuse
FTR	Fractional Time Reuse
FUSC	Full Usage of Subchannels
GEV	Generalized Extreme Value
HARQ	Hybrid Automatic Repeat Request
HDR-CDMA	High Data Rate CDMA

HSPA	High Speed Packet Access
IFR	Integer Frequency Reuse
IFR1	Integer Frequency Reuse 1
IS	Infinite Server
LIP6	Laboratoire d'informatique de Paris 6
LLS	Link Level Simulation
LOS	Line of Sight
LTE	Long Term Evolution
MCS	Modulation and Coding Scheme
MIC	Mean Instantaneous Capacity
MIMO	Multiple-input and Multiple-output
MLE	Maximum Likelihood Estimation
MS	Mobile Station
MSTR	Maximum Sustained Traffic Rate
NLOS	Non-line of Sight
OCMF	One Customer Multiple Flows
OCOF	One Customer One Flow
OFDM	Orthogonal Frequency Division Multiplex
OFDMA	Orthogonal Frequency Division Multiple Access
PARC	Per-Antenna-Rate Control
PDF	Probability Density Function
PS	Processor Sharing
PUSC	Partial Usage of Subchannels
QoS	Quality of Service
QS	Quasi Stationary
RF	Radio Frequency
RTG	Receive/Transmit Transition Gap

SC-FDMA	Single Carrier Frequency Division Multiple Access
SDMA	Space Division Multiple Access
SINR	Signal to Noise-plus-Interference Ratio
$SINR_{eff}$	Effective Signal to Noise-plus-Interference Ratio
SIR	Signal to Interference Ratio
SLS	System Level Simulation
SOFDMA	Scalable OFDMA
TDD	Time Division Duplex
TDMA	Time Division Multiple Access
TLPC	Two Level Power Control
TTG	Transmit/Receive Transition Gap
UL	uplink
ULA	Uniform Linear Array
VoIP	Voice over IP
WCDMA	Wideband CDMA
WiMAX	Worldwide Interoperability for Microwave Access
WPF	Weighted Proportional Fair

Chapter 1

Introduction

In recent years, the demand for broadband access has increased substantially. In few years, cellular networks have evolved from analog first generation to digital multi-service third generation. In the second generation, Frequency Division Multiple Access (FDMA)/Time Division Multiple Access (TDMA) has been the leading access method, while in the third one, Code Division Multiple Access (CDMA) was the basis of all standards. Next generation is expected to be dominated by Orthogonal Frequency Division Multiple Access (OFDMA) because its simplicity and flexibility, in conjunction with advanced radio features, promises very high data rates and multi-service support. Worldwide Interoperability for Microwave Access (WiMAX), based on IEEE 802.16 standard, and 3GPP Long Term Evolution (LTE) are two of such highly anticipated technologies based on OFDMA. As deployment of WiMAX/LTE networks is underway, need arises for operators and manufacturers to develop engineering rules and dimensioning methodologies. These rules and methods are the subject of this thesis.

In this chapter, we present a brief introduction of these two technologies and we explain the resource organization in an OFDMA system with the help of examples. The context of the thesis is also discussed followed by synopses of the related work in the literature. At the end, the contribution of thesis alongwith outline of proceeding chapters is provided.

1.1 OFDMA Networks

Physical layers of both WiMAX and LTE are characterized by OFDMA. The underlying technology for OFDMA based systems is Orthogonal Frequency Division Multiplex (OFDM). With OFDM, available spectrum is split into a number of parallel orthogonal narrowband subcarriers. These subcarriers can be independently assigned to different users in a cell. Resources of an OFDMA system occupy place both in time (OFDM symbols) and frequency (subcarriers) domains thus introducing both the time and frequency multiple access [23]. Hereafter, we present an introduction of two OFDMA technologies, LTE and WiMAX.

1.1.1 LTE

The Long Term Evolution (LTE), defined and proposed by 3rd Generation Partnership Project (3GPP), is a potential candidate for 4th generation mobile networks. At physical layer, it uses OFDMA in downlink (DL) while in uplink (UL) it employs Single Carrier Frequency Division Multiple Access (SC-FDMA). A LTE system enjoys the flexibility of choosing the spectrum between 1.4 MHz and 20 MHz. Using a bandwidth of 20 MHz and 2×2 Multiple-input and Multiple-output (MIMO), LTE system promises 150 Mbps of user data rate in DL. By extending the MIMO system to 4×4, this data rate could reach 300 Mbps [24]. Other important performance targets set for LTE as given in [24] are: two to four times higher spectral efficiency than that of High Speed Packet Access (HSPA) Release 6, minimum data rates of 100 Mbps in DL and 50 Mbps in UL, radio-network round trip time less than 10 ms, an optimized terminal power efficiency and high level of mobility and security.

1.1.2 WiMAX

WiMAX, as mentioned earlier, is based on IEEE standard 802.16. The first operative version of IEEE 802.16 is 802.16-2004 (fixed/nomadic WiMAX) [25]. It was followed by a ratification of amendment IEEE 802.16e (mobile WiMAX) in 2005 [26]. A new standard, 802.16m, is currently under definition for providing higher efficiency. On the other hand, consortium WiMAX Forum was founded to specify profiles (technology options are chosen among those proposed by the IEEE standard), define an end-to-end architecture (IEEE does not go beyond physical and MAC layer), and certify products (through inter-operability tests).

Like LTE, mobile WiMAX has also a scalable structure for system bandwidth. It can choose a bandwidth between 1.25 MHz and 20 MHz. However, unlike LTE, physical layers of both the DL and UL in WiMAX are OFDMA based. DL and UL share the radio resource through time division duplexing. The peak data rates in DL and UL are 46 Mbps and 14 Mbps respectively (assuming 10 MHz of bandwidth,2×2 MIMO and DL/UL ratio of 3:1) [27]. The other key features of mobile WiMAX mentioned in [28] are: Scalable OFDMA (SOFDMA), MIMO and adaptive beamforming support, Hybrid Automatic Repeat Request (HARQ), possibility of Fractional Frequency Reuse (FFR), Quality of Service (QoS) support and adaptive modulation and coding.

The two systems (WiMAX and LTE) have closely related functionalities and hence methods of their engineering will be similar. In this thesis, we focus on WiMAX. But before we look into engineering issues, it is essential to understand how radio resources are organized in OFDMA systems.

1.2 Radio Resource in OFDMA

In dimensioning process of a wireless network, we are interested in system level performance. However, system level performance has close ties with physical layer

characteristics. Physical layer features of an OFDMA based system are different from those of preceding single carrier technologies. On the physical layer level, an OFDMA based system may profit from the frequency diversity of the multi-path channel by transmitting the interleaved coded information across the sub-carriers. Hence, before we start with carrying out the performance analysis, it is important to study different interleaving techniques. Furthermore, the resource structure at cellular level has also a pronounced effect on system performance. Therefore, in this section, we discuss the organization of resource of an OFDMA system both on physical/MAC layer and cellular levels. These details would help us in our study of dimensioning process.

Both LTE and WiMAX have similar resource structures. For reference purposes, we focus on WiMAX and explain its organization of resource. We start with an introduction to Time Division Duplex (TDD) frame. We then discuss the channelization process and explain how modulation and coding are adapted to the channel. In the end, we present the possibilities offered by OFDMA in terms of frequency reuse schemes.

1.2.1 TDD Frame

IEEE 802.16e (mobile WiMAX) has specified TDD as the duplexing technique. Different values of DL/UL ratios are given in [29]. DL and UL sub-frames are separated by Receive/Transmit Transition Gap (RTG) and the interval between successive frames is called Transmit/Receive Transition Gap (TTG). WiMAX Forum has specified a TDD frame of 5 ms duration. An example of a WiMAX TDD frame is shown in Fig. 1.1. It has a two dimensional structure with horizontal and vertical axes showing the time and frequency domain respectively. In the DL sub-frame, the first part contains Preamble, Frame Control Header (FCH), UL_MAP and DL_MAP. Preamble is used for synchronization. FCH provides length and encoding of two MAP messages and information about usable subchannels. The MAP messages furnish the data mapping for users. The second part of DL sub-frame is made of data bursts. Each of these bursts is further composed of slots encoded with same Modulation and Coding Scheme (MCS). A slot is the smallest unit of resource in a frame which occupies space both in time (OFDM time symbol) and frequency domain (subchannel). A subchannel is composed of a certain subset of subcarriers. The assignment of subcarrier to a subchannel is determined by the subcarrier permutation types which are discussed in the following section. We shall keep downlink (DL) part in consideration which is the area of focus in this thesis.

1.2.2 Subcarrier Permutation Types

There are two types of subcarrier permutation in WiMAX: distributed subcarrier permutation and adjacent subcarrier permutation. The former one has further two subtypes, namely Partial Usage of Subchannels (PUSC) and Full Usage of Subchannels (FUSC). Both PUSC and FUSC have additional optional subtypes

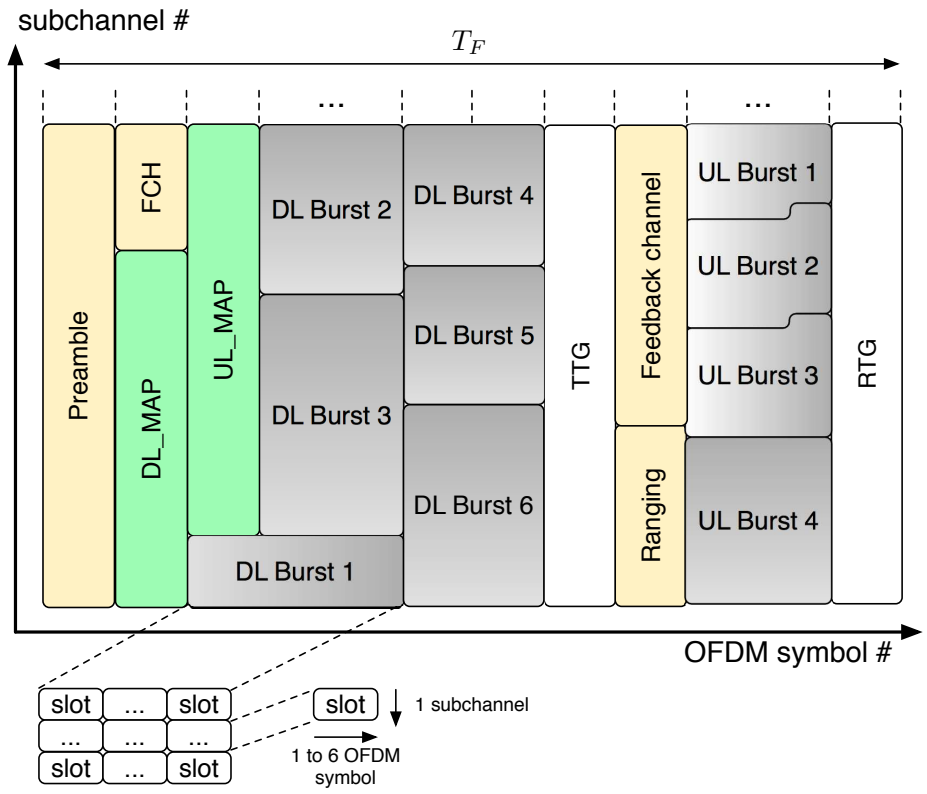

Figure 1.1: TDD frame structure.

but only primary subtypes are described here. The process of subcarrier distribution is different for PUSC DL, FUSC DL and PUSC uplink (UL). As far as adjacent subcarrier permutation type is concerned, out of two types, Adaptive Modulation and Coding (AMC) or regular AMC is discussed. We start our discussion with distributed subcarrier permutations.

1.2.2.1 Distributed Subcarrier Permutation

PUSC and FUSC are the two types to be discussed under distributed subcarrier permutation. PUSC can be employed to both DL and UL, while FUSC can be used in DL only [26, 25]. The process of permutation for PUSC DL and UL is not the same. Since in this thesis, our focus is on DL, only DL related points are discussed.

In PUSC and FUSC, subcarriers are grouped into subchannels using special permutation formulas. These subcarriers are distributed to subchannels in such a way that each subchannel is formed of subcarriers spread throughout the available bandwidth and hence resulting into frequency diversity. The difference in FUSC and PUSC lies in terms of segmentation option. In FUSC mode, all subchannels are transmitted together and cannot be segmented. On the other hand, a number of subchannels in PUSC can be grouped together into a segment. There can be three segments in all and each segment can be assigned to one sector. The process

of permutation has been explained with the help of examples in appendix A.

If we look into details of FUSC and PUSC permutation methods, it will be evident that including these methods in a system level simulator will be a laborious job. However, an alternative way to handle this issue exists in the literature.

In appendix A, we show that, in PUSC and FUSC, the allocation of subcarriers to subchannels (through permutation process) in a cell/sector is controlled by an integer called DL_PermBase. It implies that same subchannel in two different cells/sectors, using the same frequency band but different DL_PermBase, will comprise of different subcarriers and result in interference diversity. In this case, it has been shown in [8, 30] that the above process is equivalent to choosing subcarriers using uniform random distribution on the entire bandwidth in every cell/sector.

1.2.2.2 Adjacent Subcarrier Permutation

In this type of subcarrier permutation, subchannels are composed of contiguous subcarriers. Because of a frequency selective channel, a MS may experience variable link quality on different subchannels. Therefore, this permutation scheme may benefit from opportunist scheduling. The permutation method is same for UL and DL.

We have considered *regular AMC* or simply AMC in this thesis. The explanation of subcarrier permutations in AMC mode can be found in appendix A.

1.2.3 Modulation and Coding Schemes (MCS)

Whatever be the type of subcarrier permutation, a slot always carries 48 subcarriers. Hence, a slot has fixed quantity of radio resource. However, the weight of this radio resource could be changed by using different types of MCS. WiMAX networks can support a number of different MCS types in DL [8]. We have considered six different MCS types in this thesis which are: QPSK-1/2 (the most robust), QPSK-3/4, 16QAM-1/2, 64QAM-2/3 and 64QAM-3/4 (for the best radio conditions). Effective Signal to Noise-plus-Interference Ratio (SINR) threshold values for MCS types are given in Tab. 1.1 and have been referred from [31]. If effective SINR of a user is less than the threshold of the most robust MCS (i.e., less than 2.9 dB), it can neither receive nor transmit anything and is said to be in outage.

After explaining the composition of WiMAX radio resource on physical and MAC layer level, the distribution of this resource on a cellular level is presented.

1.2.4 Frequency Reuse Schemes

The frequency reuse schemes are the methods of spectral resource allocation on cellular level. In [8], the frequency reuse pattern has been defined by the expression: N_c x N_t x N_f. Where N_c is the number of cells in the network cluster.

Table 1.1: Threshold of effective SINR values for six MCS types [31].

Index	**MCS**	**bits per slot m_k**	**SINR$_{\text{eff}}$ [dB]**
0	Outage	0	< 2.9
1	QPSK 1/2	48	2.9
2	QPSK 3/4	72	6.3
3	16QAM 1/2	96	8.6
4	16QAM 3/4	144	12.7
5	64QAM 2/3	192	16.9
6	64QAM 3/4	216	18

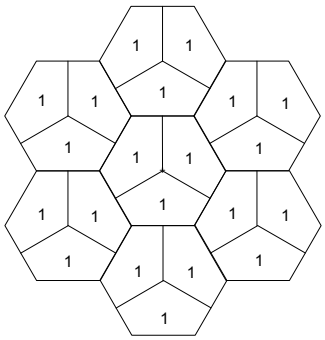

Figure 1.2: Frequency reuse pattern 1x3x1.

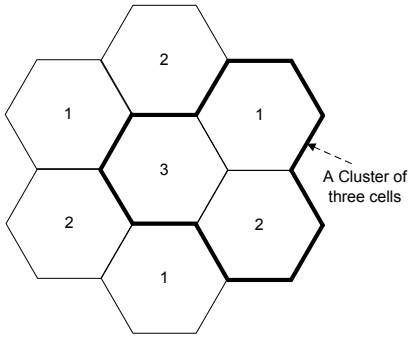

Figure 1.3: Frequency reuse pattern 3x1x1.

It determines the inter-cellular frequency reuse. N_t represents the number of sectors in a cell and N_f demonstrates intra-cellular frequency reuse. The example of the highest frequency reuse case 1x3x1 is depicted in Fig. 1.2. As can be seen in the figure, same frequency bandwidth (available network bandwidth) is used in every sector of a cell specifying an intra-cellular frequency reuse of one (i.e., $N_f = 1$). Three sectors in every cell are represented by $N_t = 3$. Since all the cells are using the same frequency bandwidth, inter-cellular frequency reuse is also one (i.e., $N_c = 1$).

A case of non-sectored cell, reuse type 3x1x1, is explained in Fig. 1.3. Available network bandwidth is divided into three distinct but unique parts. Three different digits are present in different cells. Each digit corresponds to one of these distinct bandwidth parts.

In this thesis (particularly in chapter 5), we also use a synonym Integer Frequency Reuse (IFR) for reuse type N_cx1x1. For example, IFR1 is used in place of reuse 1x1x1. It is done for harmony of acronyms while comparing reuse N_cx1x1 with FFR (introduced hereafter).

The users in the outer region of cell suffer from low SINR values specially for reuse patterns 1x1x1, 1x3x1 and 1x3x3. To resolve this issue, Fractional Frequency Reuse (FFR) has been suggested in [27]. In this frequency reuse scheme, available bandwidth is divided among inner and outer regions in such

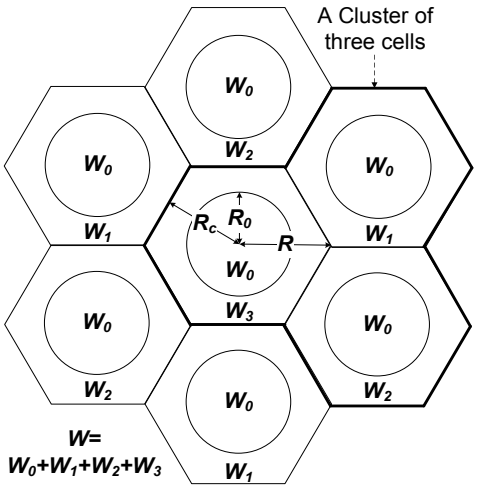

Figure 1.4: Fractional Frequency Reuse (FFR) case. Bandwidth W_0 is deployed with reuse 1 in the inner regions, while W_1, W_2 and W_3 are deployed with reuse 3 in outer regions.

a way that former employs reuse 1 while the latter applies frequency reuse 3. Further details on FFR could be referred from chapter 5.

The above explanation about radio resource in WiMAX system has helped us to have an idea about radio resource structure of an OFDMA system which is quite different from preceding single carrier systems. These theoretical details will be useful in the study of network engineering which is the topic of this thesis.

1.3 Network Engineering of OFDMA Systems

The multi-carrier OFDMA systems promise enhanced performance as compared to preceding single carrier ones. It is imperative to analyze the performance evaluation of these systems prior to network deployment which is approaching quite fast. Some WiMAX networks are already deployed but most of the operators are in trial phases. In this thesis, we look into dimensioning issues of an OFDMA based system. The dimensioning process determines the number of Base Station (BS) to be deployed in a certain area while keeping in consideration certain Quality of Service (QoS) parameters. These QoS parameters pertain to radio coverage, capacity and user traffic.

The study of network engineering for OFDMA networks can be divided into two major components. As shown in Fig. 1.5, we classify it into two components: *Radio Coverage and Capacity* and *Traffic Analysis*. While analyzing the former, we consider a static system such that users have full buffers and always have something to transmit. *Traffic Analysis*, however, takes into account a dynamic system in which users receive an elastic traffic during active phase and go to sleep for some duration after download is over. In the following text, we present a brief description of these blocks.

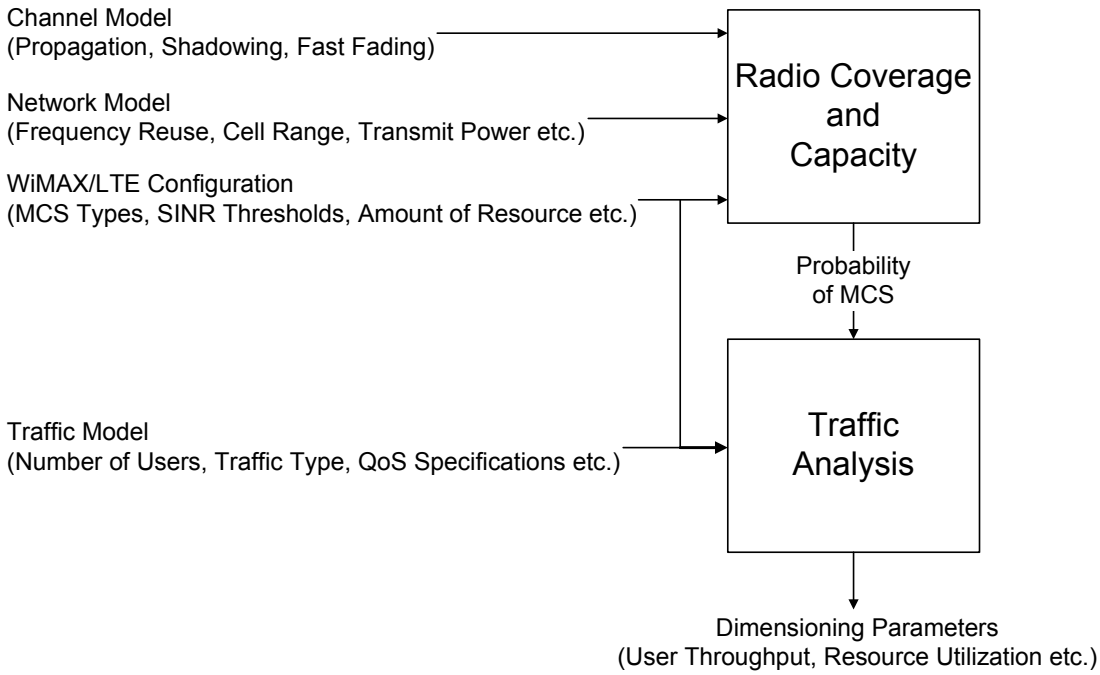

Figure 1.5: Studied system for performance evaluation.

1.3.1 Radio Coverage and Capacity

The study of radio coverage and capacity is of prime importance while carrying out performance evaluation of mobile networks. Providing radio coverage and capacity in an area is one issue but rendering the same with a certain Quality of Service (QoS) is another challenge. The QoS parameters considered in this thesis are: average effective SINR, average cell throughput and outage probability. It should be noted that this effective SINR is different from SINR of single carrier. Its description can be found in chapter 2. The outage probability is defined as the probability that a user does not reach the minimum effective SINR level required to connect to a service or to decode common control channel.

There are three inputs to *Radio Coverage and Capacity*: channel model, network model and network configuration. The first one includes the path-loss, shadowing and fast fading models. The choice of the models' parameters depends upon radio environment (e.g., urban/sub-urban, Line of Sight (LOS)/Non-line of Sight (NLOS)). The other input is the network model which consists of all parameters related to the network deployment such as Base Station (BS) transmit power, the frequency reuse scheme, cell range, antenna gain, beamforming model, etc. The third input is network configuration which is specific to deployed technology (e.g., WiMAX/LTE). The examples of the parameters associated with network configuration are available Modulation and Coding Scheme (MCS) types, the effective SINR thresholds, the number of available radio resources per frame, etc.

It is important to evaluate the system performance with respect to these in-

puts. It is also desired that some of these inputs (e.g., frequency reuse) are applied in an optimized way to maximize the system performance while maintaining a certain QoS which is one of the topics covered in this thesis. The performance of advanced techniques such as adaptive beamforming has also to be evaluated. In addition, methods are sought to carry out the system performance evaluation in a time efficient manner.

1.3.2 Traffic Analysis

From the *Traffic Analysis*, we are able to obtain dimensioning parameters such as the average throughput per user, the average radio resource utilization or the average number of simultaneous active users in the cell. As compared to *Radio Coverage and Capacity* study, here we take into account a dynamic system.

Traffic Analysis block takes as inputs the MCS probabilities from *Radio Coverage and Capacity* block, network configuration and the traffic model. Key network configuration parameters in context of traffic are: the amount of available radio resource per cell, duration of Time Division Duplex (TDD) frame and scheduling policy. Traffic model parameters include, the number of mobiles present in the cell, different types of traffic and their associated QoS parameters.

The analytical modeling of elastic web traffic is a challenging task. The variable amount of available resource, owing to possibility of adaptive MCS in OFDMA networks, makes this task even harder.

1.4 Related Work

In this section, we present the work carried out for both the static and dynamic systems. The work cited in this section comprises some prominent articles in the related areas. This is not an exhaustive account of bibliographical work and some notable areas have been presented. However, with respect to various aspects covered in this thesis, the specific references are cited therein. We discuss first the literature on static system.

Radio coverage and capacity studies of static systems are very rich in the literature and experience gained in this domain since the early times of GSM to the last improvements of HSPA+ is, without any doubt, highly useful for OFDMA engineering studies. The new channelization approach, the possibility to deploy original frequency reuse schemes and the generalization of advanced radio features make however the OFDMA case very specific. In this section, we thus focus on this multiple access technique and highlight few reference papers at system level that well illustrate the issues raised by OFDMA.

Although all these papers study cellular capacity (i.e., spectral efficiency, cell throughput, user throughput, throughput at cell edge) and coverage (i.e., SINR distribution, outage probability, common control channels coverage), three main themes can be highlighted: the effect of sub-channelization, the comparison of various frequency reuse schemes and the impact of advanced radio features, and

in particular of multiple antenna systems, on system performance. A transverse classification of the literature could also distinguish simulation based and analytical approaches.

The literature on system level study of an OFDMA system can be found even before the first operative version of IEEE 802.16 was released in 2004. For example, [1] addresses the issue of sub-channelization by proposing distributed subcarrier permutations to form subchannels in OFDMA mode. This proposal can be seen as a precursor of PUSC/FUSC permutations in IEEE 802.16. This paper however deals only with fixed wireless access and so assumes that user equipments employ directive antennas. Reuse scheme 1x1x1 is proved to be efficient in this case but the question remains open for mobile access. OFDMA is also compared to Time Division Multiple Access (TDMA) and Code Division Multiple Access (CDMA). With TDMA, reuse 1 is said to be impossible because of the lack of diversity and with CDMA, capacity is limited by intra-cell interference. OFDMA advantages are thus well emphasized.

Wang et al. in [2] present a simulation based performance evaluation of a mobile WiMAX system. The article covers key aspects of PHY and MAC layer of IEEE 802.16e standard. As far as channelization is concerned, authors compare different PUSC schemes on the uplink. Frequency reuse schemes 1x3x1, 1x3x3 and FFR are studied and it is exhibited that FFR combines the advantage of reuse 1 (more bandwidth) and reuse 3 (interference reduction). Various multiple antenna features are compared such as MIMO, beamforming or receive diversity. The Cumulative Distribution Function (CDF) of the control channel coverage is provided and includes the effect of the number of HARQ retransmissions. Voice over IP (VoIP) capacity is also analyzed by the same authors in [3]. Reference [2] is thus a very complete simulation based system level study for mobile WiMAX.

The authors of [4] study two of the classical three themes in OFDMA radio engineering: channelization and frequency reuse. The former is analyzed from the point of view of the collisions between subcarriers of nearby cells. But the originality of paper lies in the proposal and the performance evaluation of two new frequency reuse schemes: on one hand, a dynamic FFR, whose subcarrier allocation algorithm depends both on path-loss and traffic load; on the other hand, a so called partial isolation scheme, which is a modified reuse 1 with variable transmit powers. The result of the comparison shows that the DL partial isolation scheme offers the greatest system throughput and the lowest blocking rate as compared to dynamic FFR. As fas as user throughput in UL is concerned, FFR outperforms other schemes. A dynamic study based on Markov chains also captures the interactions between cells through a fixed point algorithm.

In [32], authors propose a very complete and detailed framework for future wireless networks, where OFDMA is considered for the DL. System level simulations focuses on advanced radio features like beamforming and receive diversity. A spatial multiplexing 4×4 MIMO system is particularly highlighted: it is based on a per-antenna-rate control (PARC), in which user receives parallel chunks of data from multiple antennas.

An important reference on LTE is [33]. It presents a simulation based perfor-

mance analysis in a static system and compares a 2×2 MIMO LTE system with Wideband CDMA (WCDMA) on one hand and an advanced WCDMA system on the other hand. Advanced WCDMA includes 2×2 MIMO on the DL and 16QAM modulation on the UL. In DL, the simulation results show that LTE outperforms basic WCDMA and is somewhat better than advanced WCDMA. However, the difference between LTE and advanced WCDMA is not that significant.

Before showing how this thesis is positioned in this context, we review now some reference papers in the traffic analysis field.

The analysis of dynamic systems on the DL for OFDMA networks with elastic Best Effort (BE) traffic is very similar to the one performed for GPRS, E-GPRS or HSDPA-like networks. The reason lies in the fact that all these technologies implement focus on a shared DL channel while considering adaptive modulation and coding and channel aware fast scheduling. In this thesis, we have focused on the specificities of WiMAX networks but we present hereafter some significant work that span several technologies.

In [5], authors present an analytical model to compute performance parameters such as user throughput, blocking probability, transfer delay and steady state probability of active (in download state) users in the cell for elastic traffic type. They consider a High Data Rate CDMA (HDR-CDMA) system with focus on DL. Like in OFDMA networks, the resource consumption depends upon user location and its channel conditions. Therefore, it is mentioned in the article that traffic is not only characterized by its intensity but has also a spatial component. The proposed model takes into account this two aspects. Two scheduling schemes considered in the paper are: resource fairness and data rate fairness. With resource fairness, the number of active users evolves like the number of customers in a processor-sharing queue with Poisson arrivals and i.i.d. service times. For data rate fairness scheduling, the number of active users evolves like the number of customers in a discriminatory processor-sharing queue. The user throughput comparison for two scheduling exhibits that resource fairness scheduling performs better than data rate fairness in the region close to BS, while in the outer region the inverse conclusion holds. The authors then compare blocking probabilities for two admission control schemes based on the number of active users and minimum data rate and show the two schemes do not differ significantly.

Borst in [6] studies the dynamic system comprising a fixed population of elastic traffic users for a channel-aware CDMA 1xEvolution-Data Optimized (1xEV-DO) system. A proportional fair strategy is assumed. The users come and go with the passage of time as controlled by arrival and completion of service demand. They are grouped into classes characterized by their respective load and time average rate. In a first model, statistics of the fluctuations around the average rate are the same for all classes. In this case, the analyzed system is a multi-class Processor Sharing (PS) system with class dependent arrival rates. In a second model, fluctuations statistics are different from one class to another and class differentiation is assumed. In this case, PS approach could not be employed and author focuses on stochastic majorization properties and stability issues. The last part of the article presents a validation study of the proposed mode by comparing

with simulation results. For different distributions of SINR, mean transfer delay and mean number of active users are the studied parameters in this validation study .

The authors of [7] derive user throughput formulae for two traffic models, One Customer One Flow (OCOF) and One Customer Multiple Flows (OCMF), and for two regimes, Quasi Stationary (QS) and Flow Level (FL). OCOF is basically a ON/OFF model, where active flows are separated by thinking times. On the contrary, OCMF assumes that each user is a Poisson source of flows. In QS regime, users are static; in FL regime, all users move indefinitely fast and have thus the same channel capacity. Whereas previous work is for infinite population, [7] provides results for finite population. OCOF is analyzed thanks to a two-node BCMP [34] closed network for single (FL) and multi-class (QS) users. OCMF is analyzed with a M/G/1-PS queue for both regimes.

In light of these reference papers, we now detail the contribution of the thesis and its outline.

1.5 Contribution of Thesis

The contribution of this thesis spans both the static and dynamic systems. We start with an account for static system.

While carrying out Radio Coverage and Capacity analysis, we study the system performance under various frequency reuse schemes, analyze the feasibility of reuse 1 and propose efficient analytical and semi-analytical tools for network dimensioning. Hereafter, we present different areas in which this thesis has contributed.

We first perform an exhaustive analysis of the six classical frequency reuse schemes proposed in [8]. We thus extend the work done in [2] and in the literature with a systematic view, which considers sectorized and non-sectorized cells, BS output power and cell range. We carefully analyze the effective SINR distribution and highlight the trade-off between cell capacity and outage probability. We conclude that reuse 1 is not possible without advanced radio features. The details of physical abstraction models to compute effective SINR, the details of the Monte Carlo simulator, and simulation results are presented in chapter 2. This work has been published in [9, 10].

We then consider adaptive beamforming as an efficient way of achieving frequency reuse 1. Adaptive beamforming in WiMAX is primarily studied with AMC mode in existing work. Distributed subcarrier permutation is an important feature of IEEE 802.16 based systems that offers frequency diversity. In chapter 3, we investigate the performance of adaptive beamforming while using both distributed and adjacent subcarrier permutations in WiMAX cellular networks. The comparison of frequency reuse schemes is repeated by introducing adaptive beamforming in the picture. It is shown how beamforming affects the results of this comparison and how frequency reuse 1 can be achieved. These results have been presented in [10, 11, 12, 13].

Time efficient methods to obtain SINR statistics could be found in literature. However, these methods could not be employed for OFDMA networks. Because of multi-carrier nature, it is the effective SINR (rather than the SINR) which is to be worked with. In this regard, we propose in chapter 4 a semi-analytical method to acquire spatial distribution of effective SINR in presence of shadowing and fast fading and while assuming that users are attached to the best server. We show how the spatial distribution of the effective SINR can be approximated by Generalized Extreme Value (GEV) distribution. Effective SINR statistics obtained through *Radio Coverage and Capacity* also serve as input to Traffic Analysis. In this way, the former one complements the latter. The semi-analytical method has been published in [14, 15, 16].

Continuing with time efficient methods for network dimensioning, and in contrast with existing work on frequency reuse schemes, we present in chapter 5, the approximate analytical models for Integer Frequency Reuse (IFR), Fractional Frequency Reuse (FFR) and Two Level Power Control (TLPC) schemes. TLPC is a power controlled allocation mechanism described in details in chapter 5. We derive expressions to calculate Signal to Interference Ratio (SIR) at a given distance from BS and compute spectral efficiency using Shannon's classical formula. We also determine total cell data rate while considering three different scheduling schemes: equal data rate, equal bandwidth and opportunist. This analytical study has been published in [17, 18].

The study of the three scheduling schemes highlights the necessity to consider dynamic systems. This will indeed allow us to obtain more precise performance parameters concerning traffic and user experience.

During this thesis, the work in the area of traffic modeling was carried out in collaboration with Laboratoire d'informatique de Paris 6 (LIP6). Our major contribution is the validation and robustness study of analytical models for WiMAX Best Effort (BE) traffic presented in [19, 20, 21, 22]. In contrast to existing work based on PS queue, we present in chapter 6 a different approach based on a Engset-like model and its related linear Markov chain. Moreover, we incorporate in our study the specific characteristics of WiMAX systems and we better model channel variations, including the possibility for a user to be in outage. At last, we compare three traditional scheduling policies (throughput fairness, resource fairness and opportunist) to a throttling policy. This algorithm assumes that user throughput is caped by Maximum Sustained Traffic Rate (MSTR), a parameter foreseen by the standard for BE class. Our work is also characterized by a deep validation and robustness (in which main assumptions of the models are relaxed) study.

The last chapter (chapter 7) details out the major results of this thesis and concludes this thesis report with some propositions for future work.

Chapter 2

On Frequency Reuse

In this chapter, we evaluate the performance of a WiMAX network in different frequency reuse scenarios. Radio quality in terms of SINR and outage probability on one hand, and throughput on the other hand, are the parameters considered for this analysis. Extensive Monte Carlo simulations, based on effective SINR computation using abstraction model MIC, have been performed in downlink. The simulation results show that some frequency reuse schemes with a very good global throughput performance result however into significant user outage. The frequency reuse patterns, satisfying the two parameters (outage and throughput) in the best possible way, are being suggested for WiMAX networks. Effect of variable cell range and subcarrier power is also investigated for different reuse patterns.

2.1 Introduction

Since WiMAX is intended to offer broadband services, cell throughput will be an important issue in a WiMAX cellular network. To achieve high cell throughput, frequency reuse has to be well planned to maximize both the bandwidth utilization and Signal to Noise-plus-Interference Ratio (SINR). From the point of view of operator, it would be valuable to increase the cell throughput through complete usage of bandwidth in each sector of the cellular network. However, it is not desired to achieve high throughput at the cost of increased outage probability. Hence, a frequency reuse satisfying the radio quality and offering a high throughput is sought. WiMAX networks are going through their initial phase and our work could substantiate the trial phase of WiMAX network deployment.

Reference [35] analyzes the effect of using a frequency repartitioning scheme and only focuses on non-sectorized cells. In [36], aside from dynamic frequency reuse, case of sectored cells has been taken into account. Authors have compared two different reuse patterns with emphasize on the effect of Perm_Base (cf. section 1.2.2.1 for details). It is shown that even with dynamic frequency reuse different Perm_Base scheme results into significant outage probability. Authors of [37] have compared two frequency reuse types (1x3x1 and 1x3x3) using MIMO

(Multiple Input Multiple Output). The authors of [38, 39, 40] also discuss the capacity and interference for the same two reuse types of an OFDM WiMAX system. In addition, [39] gives results for different cell ranges as well.

In this chapter, we have investigated six different reuse patterns for a WiMAX network. This work is mainly based on [9, 10]. Radio coverage and throughput performance for each frequency reuse type would enable an operator to choose any of them depending upon service type and Quality of Service (QoS) to be provided. The results of this comparison are equally applicable to distributed subcarrier permutations PUSC and FUSC since both enjoy similar diversity of subcarriers per subchannel. However, PUSC has been kept as a reference in simulations. On the other hand, AMC is discussed in the next chapter when adaptive beamforming appears in the picture. We start with details of network and interference model which is followed by simulation details and discussion of results.

2.2 Network and Interference Model

2.2.1 Frequency Reuse

The six reuse patterns (cf. section 1.2.4 for description of a reuse pattern) compared in this chapter are: 1x1x1, 1x3x1, 1x3x3, 3x1x1, 3x3x1 and 3x3x3. These are the frequency reuse patterns being proposed for WiMAX networks in [8] and are shown in Fig. 2.1.

2.2.2 Antenna Pattern

According to [8], all BS antenna elements have the beam pattern defined by 3GPP2. The gain of single antenna is given by Eq. 2.1 [8].

$$G(\psi) = G_{max} + \max\left[-12\left(\frac{\psi}{\psi_{3dB}}\right)^2, -G_{FB}\right], \tag{2.1}$$

where G_{max} is the maximum antenna gain in boresight direction, ψ is the angle MS subtends with sector boresight such that $|\psi| \leq 180°$, ψ_{3dB} is the angle associated with half power beamwidth and G_{FB} is the front-to-back power ratio. For omni-directional antennas $G_{FB} = 0$.

2.2.3 Effective SINR

An important feature of WiMAX network is assignment of MCS type to a user depending upon its channel conditions. This decision is taken by BS based on channel quality information received from a user. BS may either send a request to the user which returns the channel quality metric or it can allocate the user a channel (CQICH) in UL subframe for periodic reporting of channel quality parameter. Effective SINR ($SINR_{eff}$) is one of the metrics used for channel

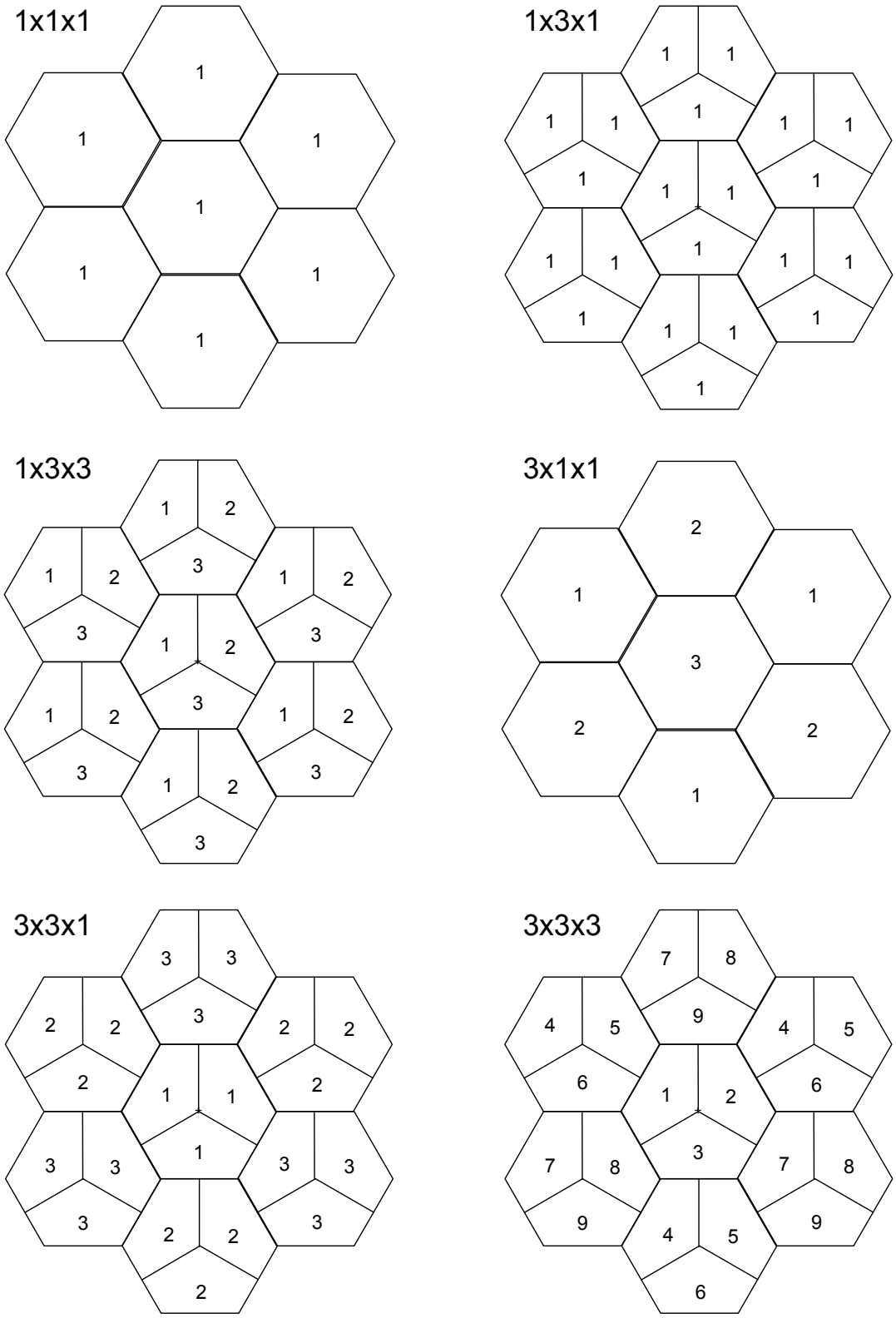

Figure 2.1: Six different reuse patterns.

quality indications. In order to find $SINR_{eff}$, SINR of individual subcarriers is required.

2.2.3.1 Subcarrier SINR

SINR of a subcarrier n is computed by the following formula:

$$SINR_n = \frac{P_{n,Tx} a^{(0)}_{n,Sh} a^{(0)}_{n,FF} \frac{K}{d^{(0)\alpha}}}{N_0 W_{Sc} + \sum_{b=1}^{B} P_{n,Tx} a^{(b)}_{n,Sh} a^{(b)}_{n,FF} \frac{K}{d^{(b)\alpha}} \delta^{(b)}_n}, \tag{2.2}$$

where $P_{n,Tx}$ is the per subcarrier power, $a^{(0)}_{n,Sh}$ and $a^{(0)}_{n,FF}$ represent the shadowing (log-normal) and fast fading (Rician/Rayleigh) factors for the signal received from serving BS respectively, B is the number of interfering BS, K is the path loss constant, α is the path loss exponent and $d^{(0)}$ is the distance between MS and serving BS. The terms with superscript b are related to interfering BS. W_{Sc} is the subcarrier frequency spacing, N_0 is the thermal noise density and $\delta^{(b)}_n$ is equal to 1 if interfering BS transmits on n^{th} subcarrier and 0 otherwise.

2.2.3.2 Effective SINR Modeling

In System Level Simulation (SLS), we come across with time and frequency selective channels. In multi-carrier OFDMA systems, channel gain on each subcarrier may not be the same because of frequency selective fading. Hence the subcarrier SINR values at receiver end are non-uniform. The data to be sent to a user is transmitted in the form of coded block and data symbols inside these blocks are transmitted over multiple sub-carriers. Since these subcarriers may suffer from different SINR, the error rates on these subcarriers may not be the same and hence Block Error Rate (BLER) over coded block cannot be obtained through direct averaging of these error rates.

The role of PHY abstraction methodology is to predict the BLER at the receiver end for a transmitted code block based on SINR values of different subcarriers obtained (over which code block is transmitted) through SLS. It acts as a mapping function and finds out a single effective value of SINR ($SINR_{eff}$) that could be accurately mapped to link level SNR versus BLER curves. These link level SNR versus Block Error Rate (BLER) curves are obtained through Link Level Simulation (LLS) assuming a flat fading channel i.e., under Additive White Gaussian Noise (AWGN) conditions. It is important that this mapping function, termed as Effective SINR Mapping (ESM) in [41], should not involve heavy computations. This ESM PHY abstraction has been defined in [41] as compressing the vector of received subcarrier SINR values of SLS to a single effective SINR value, which can then be further mapped to a link level SNR versus BLER curve. The PHY abstraction methodology has been depicted in Fig. 2.2.

Few possible PHY abstraction models for WiMAX system evaluation are given in [8] and [41]. Two of these models are: Exponential Effective SINR Mapping (EESM) and Mean Instantaneous Capacity (MIC). A brief introduction of these two models is presented in the following sections.

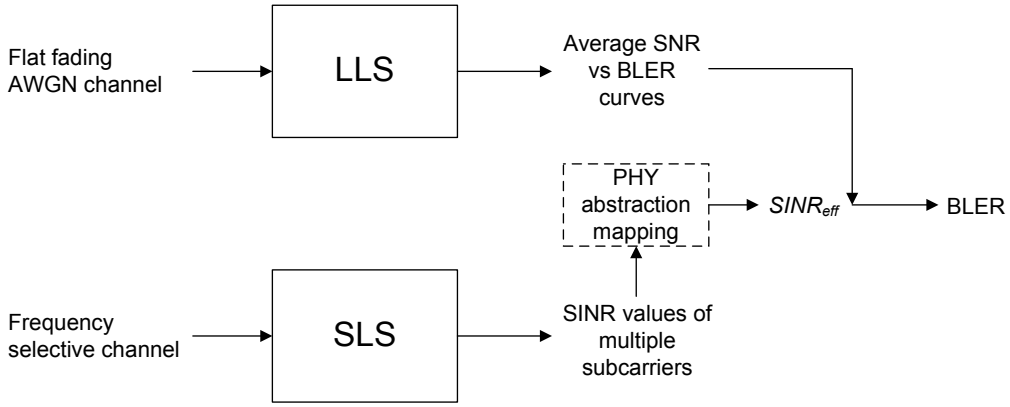

Figure 2.2: PHY abstraction methodology.

2.2.3.2.1 Exponential Effective SINR Mapping (EESM)

This model computes $SINR_{eff}$ using Eq. 2.3 [8].

$$SINR_{eff} = -\beta \cdot \ln\left(\frac{1}{N'}\sum_{n=1}^{N'} e^{-\frac{SINR_n}{\beta}}\right), \tag{2.3}$$

where $SINR_n$ is the SINR value of the n^{th} subcarrier and N' is the number of subcarriers over which $SINR_{eff}$ is computed. The variable β is an optimization/adjustment factor that depends on the Forward Error Correction (FEC) type, MCS and receiver implementation. It is obtained through LLS.

2.2.3.2.2 Mean Instantaneous Capacity (MIC)

The first step in this method is to compute capacity for n^{th} subcarrier using Shannon's formula:

$$C_n = \log_2(1 + SINR_n) \qquad [bps/Hz].$$

Next using the values of capacity, MIC is computed by averaging capacities of N' subcarriers:

$$MIC = \frac{1}{N'}\sum_{n=1}^{N'} C_n \qquad [bps/Hz].$$

$SINR_{eff}$ is obtained from MIC value using following equation:

$$SINR_{eff} = 2^{MIC} - 1. \tag{2.4}$$

Both MIC and EESM provide acceptable mapping of effective SINR [3]. However, due to simpler implementation of MIC [3], we apply it in our analysis.

Table 2.1: Path powers and delays of six paths of vehicular-A profile with v=60Km/h (Table A.1.1 at page 117 of [8]).

Index (k)	**1**	**2**	**3**	**4**	**5**	**6**
Power of path (p_k)[dB]	0	-1	-9	-10	-15	-20
Path Delay (τ_k) [μs]	0	0.3	0.7	1.1	1.7	2.5

2.2.3.3 Effective SINR over a Slot

As slot is the basic resource unit in an IEEE 802.16 based system, we compute $SINR_{eff}$ over the subcarriers of a slot. Shadowing is drawn randomly for a slot and is same for all subcarriers of a slot. Assuming the uniform random distribution of subcarriers in subchannels (cf. section 1.2.2.1), fast fading is drawn independently (using uniform random distribution) for every subcarrier of a slot (Fig. 2.3). On the other hand, the subcarriers in an AMC slot are contiguous and hence their fast fading factor can no longer be considered independent. In order to find the correlated values of fast fading, we have to calculate the coherence bandwidth B_c (the bandwidth over which flat channel response could be assumed). For a correlation factor of 0.5, the coherence bandwidth is given as [42]:

$$B_c = \frac{1}{5\sigma_\tau},$$

where σ_τ is the RMS delay spread and is equal to $\sqrt{\bar{\tau^2} - (\bar{\tau})^2}$. The variables $\bar{\tau}$ and $\bar{\tau^2}$ are the average and square average path delays respectively. These can be calculated as follows:

$$\bar{\tau} = \frac{\sum p_k^2 \tau_k}{\sum p_k^2},$$

and

$$\bar{\tau^2} = \frac{\sum p_k^2 \tau_k^2}{\sum p_k^2},$$

such that p_k is the power (in watts) of a received path and τ_k is the delay (in seconds) of each path. In Tab. 2.1, parameters required to compute coherence bandwidth are listed.

With the values given in Tab. 2.1, the value of B_c is found to be 1.12 MHz that spans approximately 102 subcarriers.

2.3 Simulation Details

The simulations are carried out in DL. Full loading of subchannels has been considered hence all subcarriers in a slot will experience interference from all interfering cells. A significant number of snapshots is being carried out for Monte Carlo simulations. A hexagonal cellular network is considered with length of one side of

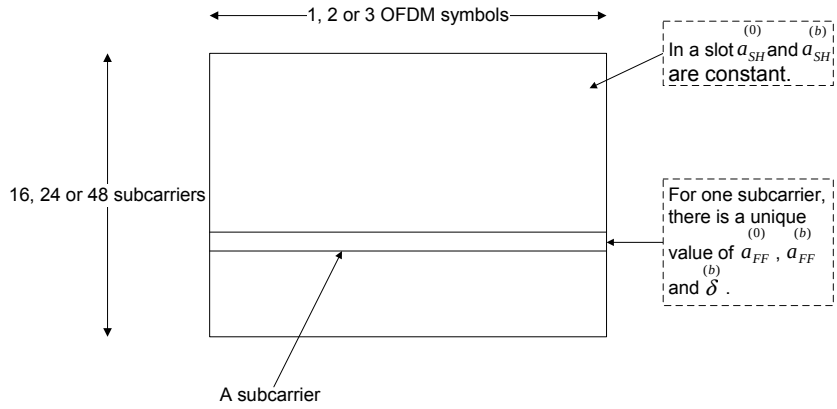

Figure 2.3: Shadowing and fast fading over a PUSC/FUSC/AMC slot.

the hexagon equal to R. To include the effect of an infinite network, wraparound technique has been employed. The details about wraparound technique, referred from [43] and [44], are given in the following section.

2.3.1 Wraparound Technique [43, 44]

The symmetry in a hexagonal network means that one would not notice the difference when standing in the middle of the hexagon, while the hexagon is rotated or reflected. In a two tier network, with finite number of nodes, only the central cell enjoys such symmetry. In such a network only the data collected in the central cell will have statistical characteristics equivalent to a network consisting of infinite number of cells. Also to collect a large amount of data, it is desired to drop the SS in the cells other than the central one. To address this issue, idea of wraparound is introduced.

Using wraparound method, the network is extended to a cluster of networks consisting of eight copies of the original hexagonal network. With the original hexagonal network in the middle, eight copies are attached to it symmetrically as shown in the Fig. 2.4. This cell layout is wrapped around to form a toroidal surface. In order to be able to perform this mapping, the number of cells in a cluster has to be a rhombic number. There is a one-to-one mapping between cells/sectors of the center hexagon and cells/sectors of each copy. In this way, every cell in the extended network is identified with one of the cells in the central original network. Those corresponding cells have thus the same antenna configuration, traffic, fading, etc, except the location. This correspondence is shown in Fig. 2.4 through shaded sectors of the same cell in all the networks.

Let us consider a two tier wraparound model. The distance from any MS to any BS is obtained as follows. A coordinate system is defined with center cell of original network at $(0, 0)$. The path distance and angle used to compute the path loss and antenna gain of a MS at (x, y) to a BS at (a, b) is the minimum of the following:

Distance1 = Distance between (x, y) and (a, b)

$$\text{Distance2} = \text{Distance between } (x, y) \text{ and } (a + 2.5\sqrt{3}D, b + D/2)$$

$$\text{Distance3} = \text{Distance between } (x, y) \text{ and } (a + \sqrt{3}D, b + 4D)$$

$$\text{Distance4} = \text{Distance between } (x, y) \text{ and } (a - \sqrt{3}D/2, b + 7.5D)$$

$$\text{Distance5} = \text{Distance between } (x, y) \text{ and } (a - 1.5\sqrt{3}D, b + 3.5D)$$

$$\text{Distance6} = \text{Distance between } (x, y) \text{ and } (a - 2.5\sqrt{3}D, b - D/2)$$

$$\text{Distance7} = \text{Distance between } (x, y) \text{ and } (a - \sqrt{3}D, b - 4D)$$

$$\text{Distance8} = \text{Distance between } (x, y) \text{ and } (a + \sqrt{3}D/2, b - 7.5D)$$

$$\text{Distance9} = \text{Distance between } (x, y) \text{ and } (a + 1.5\sqrt{3}D, b - 3.5D)$$

where D is the distance between two neighboring BS.

2.3.2 MS Spatial Distribution and Selection of Serving BS

MS is dropped into the cell using uniform random distribution. If the cell is sectorized, three MS are dropped into a cell during every snapshot such that each sector has exactly one MS. Since we are using wraparound technique, three MS are dropped into every cell of the network. In case of non-sectorized cell, one MS is dropped per cell during one snapshot.

There are two ways by which a MS can attach itself to a BS: minimum path-loss or best link. Since best link is closer to practical scenario, it is being employed in the simulations. For each MS, signal strength is measured from all the cells/sectors in the network. The MS selects the cell/sector from which it receives the maximum signal strength. The rest of the cells/sectors are the interfering ones (depending on the reuse pattern). Shadowing effect is taken into account during this procedure. However, fast fading is not considered during serving BS selection. The reason being that MS measures the signal from BS over sufficient interval of time to average out the fading effect.

2.3.3 Simulation Parameters

Simulation parameters are listed in Tab. 2.2. These values are mainly based on [8]. It is to be noted that value of BW_T used in simulations does not correspond to any FFT size. However, this bandwidth is divided into three equal parts (each of 5 MHz which corresponds to 512-FFT). It is done to gain flexibility in allocating a bandwidth to a cell/sector for every reuse pattern and it corresponds to a practical/real deployment scenario. If 10 MHz is assigned to a cell, it does not mean that 1024-FFT is employed, rather two unique parts (of 5 MHz each) with 512-FFT are assigned to the cell. P_{TX} of Tab. 2.2 is the power transmitted

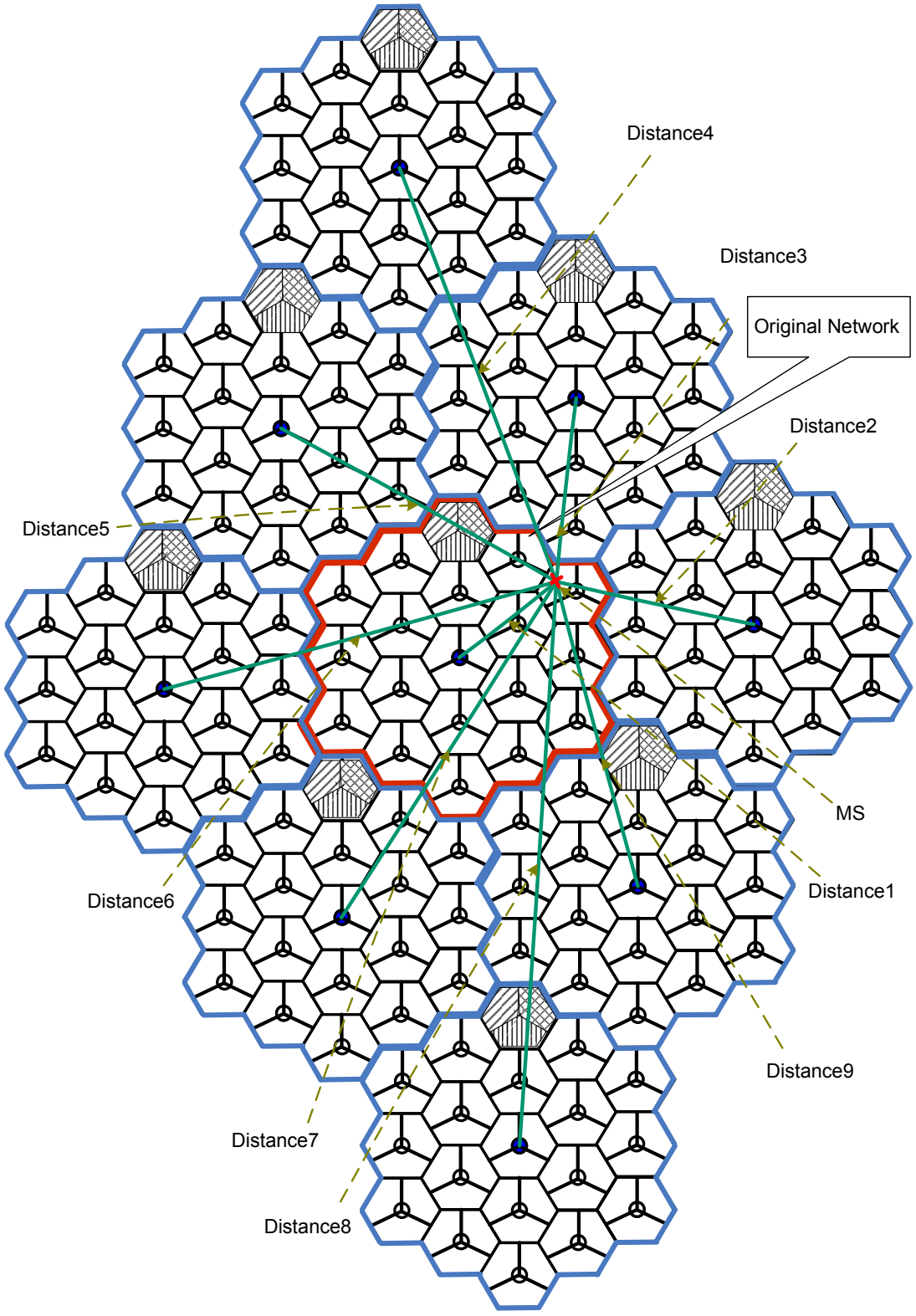

Figure 2.4: An example of wraparound network.

by BS on all used subcarriers (data+pilot) in a cell. Power transmitted on one subcarrier is given by following expression:

$$P_{n,Tx} = \begin{cases} \frac{P_{Tx}N_f}{N_t N_{Sc}} & \text{for sectorized cells;} \\ \\ \frac{P_{Tx}N_c}{N_t N_{Sc}} & \text{for non-sectorized cells,} \end{cases} \tag{2.5}$$

where N_{Sc} is the total number of subcarriers (data+pilot) present w.r.t. total network bandwidth BW_T and N_c, N_t ,N_f characterize a reuse pattern (cf. section 1.2.4). It is clear from the above expression that subcarrier power may be different for all reuse patterns. However, BS power budget is constant.

In order to give a clear view of relationship between available bandwidth and reuse factor, let us divide the BW_T of Tab. 2.2 into three equal but distinct parts of 5 MHz each such that $BW_1 = BW_2 = BW_3 = 5$ MHz. For different reuse patterns, these bandwidth parts are allocated in different ways. For frequency reuse pattern 3x3x3, FUSC is not possible as it cannot be segmented. Fig. 2.5 gives detail about bandwidth allocation for six reuse factors.

2.3.4 Throughput Calculation

Global average DL throughput of a WiMAX cell X [bps] in DL is given as:

$$X = \frac{N_S}{T_F} \sum_{k=1}^{K} m_k p_k, \tag{2.6}$$

where K represents the total number of considered MCS types. The other two variables, p_k and m_k, are respectively the probability and bits per slot for MCS type k and T_F is the duration of Time Division Duplex (TDD) frame. N_S is the number of slots in DL sub-frame of a cell and its value depends on frequency reuse pattern (N_cxN_txN_f), network bandwidth, subcarrier permutation type and number of OFDM symbols in DL sub-frame. For a given subcarrier permutation type and number of OFDM symbols in DL sub-frame, N_S is given as:

$$N_S = N_S^{111} \times \frac{N_t}{N_f N_c},$$

where N_S^{111} is the number of slots in DL sub-frame for reuse 1x1x1.

2.4 Comparison of Frequency Reuse Patterns

In this section, we present the simulation results. We look for a compromise between cell throughput and outage probability.

Average $SINR_{eff}$ has been plotted versus distance for all six reuse patterns in Fig. 2.6 and 2.7. It can be noticed that reuse type 3x3x3 has the best performance with respect to average $SINR_{eff}$ while reuse type 1x1x1 has the lowest values of average $SINR_{eff}$.

Table 2.2: Description and values of parameters used in simulations.

Parameter	Description	Value
f	Carrier frequency	2.5 GHz
P_{TX}	Total rms transmit power of a cell	43 dBm
$\frac{K}{d^{\alpha}}$	Pathloss model	COST-HATA-231, $\alpha = 3.5$, $K = 1.4 \times 10^4$
N_F	Number of OFDMA symbol in a frame	47
N_{DL}	Number of DL data OFDMA symbols	30
R_{DLUL}	DL to UL OFDMA symbols' ratio	2:1
BW_T	System bandwidth	15 MHz
FFT Size	Total number of available subcarriers with Bandwidth (BW)=5MHz	512
N_{Sc}	Total number of used subcarriers (data+pilot) corresponding to BW_T	1260
N_{Sch}	Total number of used subchannels corresponding to BW_T	45
σ_{SH}	Log normal shadowing standard deviation	9 dB
$\triangle f$	Subcarrier spacing	10.9375 KHz
T_S	OFDMA useful symbol duration	91.43 μs
T_F	Frame Duration	5 ms
N_0	Thermal noise density	-174 dBm/Hz
R	One side of hexagonal cell	1.5 Km
h_{BS}	Height of BS	32 m
h_{MS}	Height of MS	1.5 m
θ_{3dB}	3dB antenna beam width	70°
G_{FB}	Front-to-back antenna power ratio	25 dBi
G_{max}	Antenna Gain (boresight)	16 dBi

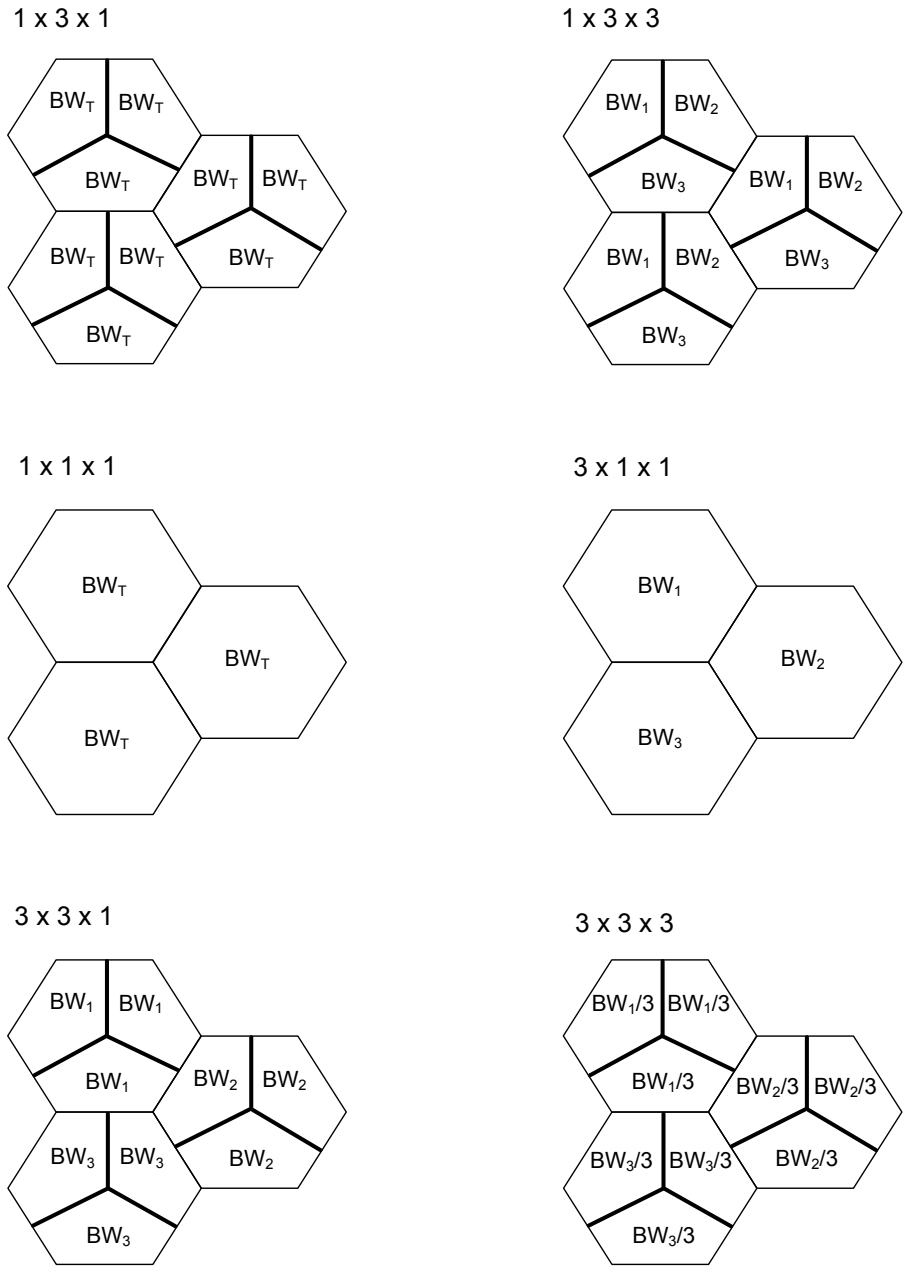

Figure 2.5: An example of bandwidth allocation for six different reuse factors.

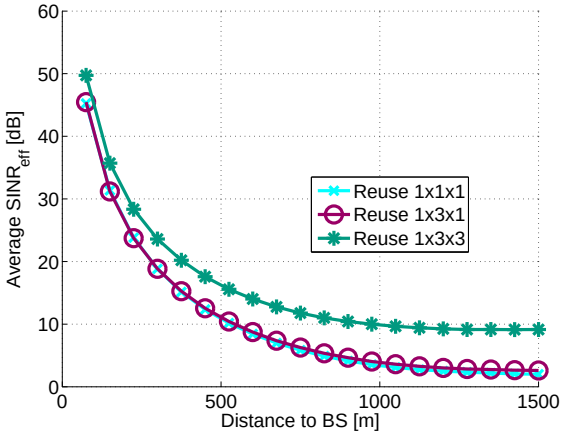

Figure 2.6: Avg. $SINR_{eff}$ (DL) vs distance for reuse 1x1x1, 1x3x1 and 1x3x3.

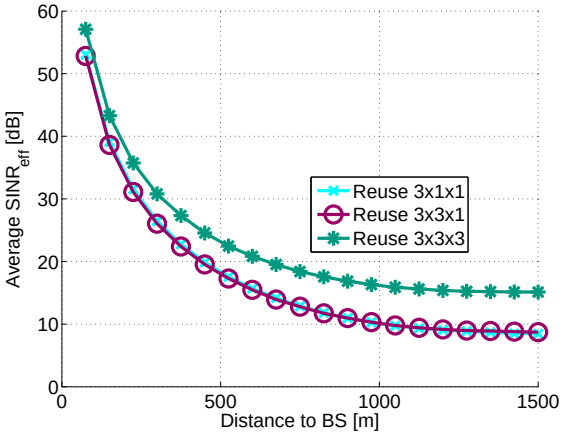

Figure 2.7: Avg. $SINR_{eff}$ (DL) vs distance for reuse 3x1x1, 3x3x1 and 3x3x3.

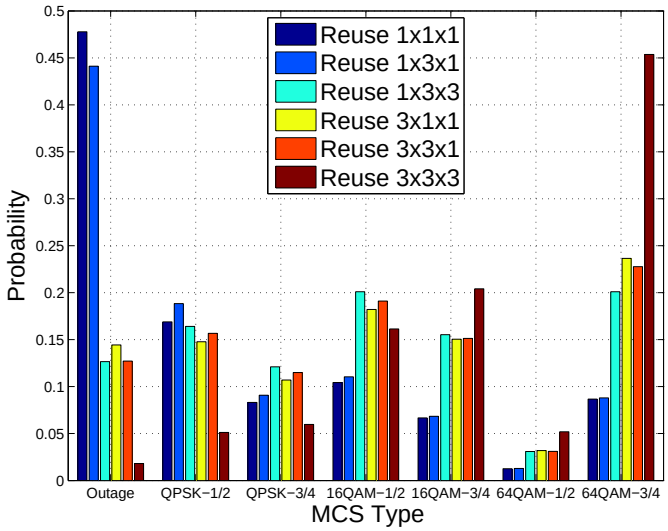

Figure 2.8: MCS probabilities with full loading of subchannels.

However, even with good values of average $SINR_{eff}$ at a particular distance, some MS may attain very low $SINR_{eff}$. To verify this fact, it is necessary to measure the probability of outage. For all six reuse patterns, MCS probabilities are presented in Fig. 2.8. Once again reuse type 3x3x3 shows the best performance and has an acceptable value of outage probability ($< 5\%$). All the remaining types have outage probabilities greater than 5% and even 55% in the worst case.

The other important aspect of network performance evaluation is cell throughput. In Fig. 2.9 and 2.10, average cell throughput has been plotted versus distance for all six reuse patterns. The average values of cell throughput show a totally different picture. Reuse factor 3x3x3, which had the best results for $SINR_{eff}$ analysis, is now placed very low in the list. On the other hand, reuse 1x3x1 has the highest value of average throughput but it lagged performance in case of $SINR_{eff}$ analysis.

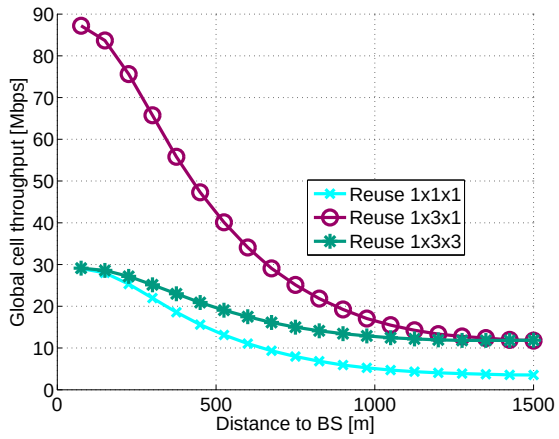

Figure 2.9: Avg. cell throughput vs distance for reuse 1x1x1, 1x3x1 and 1x3x3.

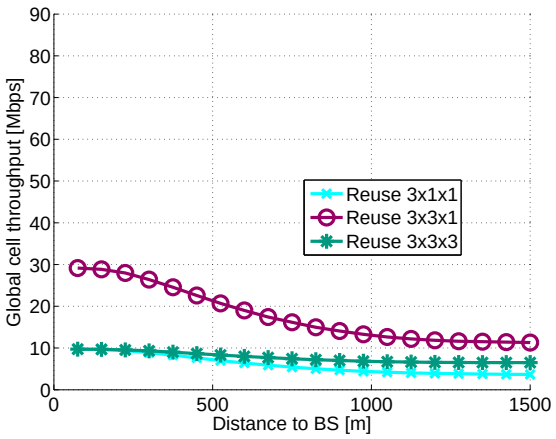

Figure 2.10: Avg. cell throughput vs distance for reuse 3x1x1, 3x3x1 and 3x3x3.

Table 2.3: Frequency reuse comparison table.

Reuse Type	**Average $SINR_{eff}$ [dB]**	**Outage Probability**	**Average Throughput (Mbps)**
1 x 1 x 1	5.6	0.48	7.4
1 x 3 x 1	6.0	0.44	23.3
1 x 3 x 3	11.8	0.13	14.5
3 x 1 x 1	12.43	0.14	5
3 x 3 x 1	12.4	0.13	15
3 x 3 x 3	18.3	0.02	7.2

To get an overall picture, average values of $SINR_{eff}$ and cell throughput alongwith outage probabilities for all six reuse patterns are put together in Tab. 2.3. It can be made out that even though some reuse patterns perform very well in terms of average cell throughput, only reuse 3x3x3 has an acceptable value of outage probability (i.e., $< 5\%$). All the remaining types have outage probabilities greater than 5%.

In the above comparison, we have fixed the value of cell range and transmission power. In the following section, we try to investigate the effect of change in the values of cell range and subcarrier power on system performance for all six reuse patterns.

2.5 Cell Range and Power Study

In this section, we try to investigate the effect noise by varying the cell range and power. The observed output parameters are: average $SINR_{eff}$, outage probability and average throughput.

We start with examining the effect of cell range R which was fixed as 1500 meters in section 2.4. Here we shall see the influence of changing the cell range

Table 2.4: Average $SINR_{eff}$ values for different cell ranges.

Reuse Type	**Cell Range R [Km]**										
	0.5	**0.75**	**1**	**1.25**	**1.5**	**1.75**	**2**	**2.25**	**2.5**	**2.75**	**3**
	Average $SINR_{eff}$ [dB]										
1x1x1	5.6	5.6	5.6	5.6	5.6	5.6	5.5	5.4	5.3	5.2	5.1
1x3x1	6.3	6.3	6.3	6.2	6.0	5.8	5.5	5.1	4.7	4.3	3.8
1x3x3	12.4	12.4	12.3	12.1	11.8	11.5	11.1	10.6	10	9.5	8.9
3x1x1	12.5	12.5	12.5	12.5	12.4	12.4	12.3	12.2	12	11.8	11.7
3x3x1	13	13	12.9	12.7	12.4	12	11.6	11.1	10.5	9.9	9.3
3x3x3	19.3	19.2	19	18.7	18.3	17.8	17.1	16.5	15.8	15.1	14.3

Table 2.5: Average throughput values for different cell ranges.

Reuse Type	**Cell Range R [Km]**										
	0.5	**0.75**	**1**	**1.25**	**1.5**	**1.75**	**2**	**2.25**	**2.5**	**2.75**	**3**
	Average Throughput [Mbps]										
1x1x1	7.4	7.4	7.4	7.4	7.4	7.4	7.3	7.2	7.2	7.1	7.0
1x3x1	24.2	24.2	24.0	23.7	23.3	22.7	21.9	21	20	18.9	17.8
1x3x3	15.2	15.2	15.0	14.8	14.5	14.1	13.6	13.1	12.4	11.8	11.1
3x1x1	5	5	5	5	5	5	4.9	4.9	4.9	4.8	4.7
3x3x1	15.6	15.6	15.5	15.3	15	14.6	14.1	13.5	12.9	12.2	11.5
3x3x3	7.4	7.4	7.4	7.3	7.2	7	6.8	6.6	6.4	6.1	5.8

from 500 m to 3000 m. Rest of the parameters remain the same.

The results of variable cell range simulations are presented in Tab. 2.4, 2.5 and 2.6. As far as average $SINR_{eff}$ and throughput are concerned, the values decrement (though very slowly) when cell range goes from 500 m to 3000 m. This is because of the fact that with increasing cell range, the noise becomes more significant. Apart from reuse 3x3x3, the outage probabilities of all reuse patterns are still unacceptable for different cell ranges (lower than or higher than 1500 m). Even with cell range of 500 m, situation is not better enough. For reuse 3x3x3, the outage probability is almost constant from cell range of 500 m to 2000 m and starts increasing further on. We can observe that for reuse 3x3x3, compromising marginally on average throughput, cell range could be extended to 2000 m (beyond which outage probability starts to rise).

Now we see the effect of various values of transmission power per cell. These values range from 37 to 51 dBm. All other parameters, including cell range, are the same as given in section 2.3.3.

The results of simulations with variable cell power are listed in Tab. 2.7, 2.8 and 2.9. As can be noticed, in general, there is a slight improvement in average $SINR_{eff}$, average throughput and outage probabilities for all reuse cases. We can therefore conclude that increase or decrease in cell power with respect to

Table 2.6: Outage probabilities for different cell ranges.

Reuse Type	Cell Range R [Km]										
	0.5	**0.75**	**1**	**1.25**	**1.5**	**1.75**	**2**	**2.25**	**2.5**	**2.75**	**3**
	Outage Probabilities										
1x1x1	0.48	0.48	0.48	0.48	0.48	0.48	0.48	0.49	0.49	0.5	0.5
1x3x1	0.42	0.42	0.43	0.43	0.44	0.45	0.47	0.49	0.51	0.53	0.56
1x3x3	0.11	0.11	0.11	0.12	0.13	0.14	0.15	0.17	0.19	0.22	0.25
3x1x1	0.14	0.14	0.14	0.14	0.14	0.14	0.15	0.15	0.15	0.16	0.16
3x3x1	0.11	0.12	0.12	0.12	0.13	0.14	0.15	0.17	0.19	0.21	0.24
3x3x3	0.02	0.02	0.02	0.02	0.02	0.02	0.02	0.03	0.03	0.04	0.05

Table 2.7: Average $SINR_{eff}$ values for different cell powers.

Reuse Type	Cell Power [dBm]							
	37	**39**	**41**	**43**	**45**	**47**	**49**	**51**
	Average $SINR_{eff}$ [dB]							
1x1x1	5.4	5.5	5.5	5.6	5.6	5.6	5.6	5.6
1x3x1	5.2	5.5	5.8	6.0	6.1	6.2	6.2	6.3
1x3x3	10.6	11.2	11.6	11.8	12.0	12.2	12.3	12.3
3x1x1	12.2	12.3	12.4	12.4	12.4	12.5	12.5	12.5
3x3x1	11.1	11.6	12.1	12.4	12.6	12.8	12.9	12.9
3x3x3	16.6	17.3	17.8	18.3	18.6	18.8	19	19

43 dBm considered in section 2.3.3 does not significantly improve the system performance in terms of radio coverage and throughput. However, the effect of noise somewhat decrements the performance at lower transmission powers.

2.6 Conclusion

Frequency reuse is an important issue in cellular networks. In this chapter, we have evaluated the performance of WiMAX networks while taking into account six different frequency reuse patterns. It is shown that the reuse patterns which offer a good throughput performance lack the radio coverage performance. Outage probabilities act as a deciding factor and only reuse 3x3x3 has an acceptable value of it even though it has the least throughput among all reuse patterns. We further analyzed performance by varying cell range and power to observe the effect of noise. It was found that performance parameters did not change significantly with different values of cell range and power. Performance degraded a bit for higher cell range and low transmission power. We also examined that for reuse 3x3x3, cell range could be extended to 2000 m by slightly decreasing the average throughput and without increasing the outage probability.

Table 2.8: Average throughput values for different cell powers.

Reuse Type	Cell Power [dBm]							
	37	**39**	**41**	**43**	**45**	**47**	**49**	**51**
	Average Throughput [Mbps]							
1x1x1	7.3	7.3	7.4	7.4	7.4	7.4	7.4	7.4
1x3x1	21.0	22.0	22.7	23.3	23.6	23.9	24.0	24.1
1x3x3	13.1	13.7	14.2	14.5	14.8	14.9	15.0	15.1
3x1x1	4.9	5	5	5	5	5	5	5
3x3x1	13.6	14.2	14.7	15	15.2	15.4	15.5	15.6
3x3x3	6.6	6.9	7	7.2	7.3	7.3	7.4	7.4

Table 2.9: Outage probabilities for different cell powers.

Reuse Type	Cell Power [dBm]							
	37	**39**	**41**	**43**	**45**	**47**	**49**	**51**
	Outage Probabilities							
1x1x1	0.49	0.48	0.48	0.48	0.48	0.48	0.48	0.48
1x3x1	0.49	0.47	0.45	0.44	0.43	0.43	0.43	0.42
1x3x3	0.17	0.15	0.13	0.13	0.12	0.12	0.11	0.11
3x1x1	0.15	0.15	0.14	0.14	0.14	0.14	0.14	0.14
3x3x1	0.16	0.15	0.13	0.13	0.12	0.12	0.12	0.12
3x3x3	0.03	0.02	0.02	0.02	0.02	0.02	0.02	0.02

It is clear from the above conclusion that aggressive reuse is not possible without including advanced features in the system. Therefore, in next chapter, we discuss the system performance in presence of adaptive beamforming.

Chapter 3

Adaptive Beamforming in OFDMA Networks

It was concluded in previous chapter that only reuse 3x3x3 (without advanced features) is acceptable for WiMAX networks because of limitations caused by outage probability. However, it was also noticed that owing to low reuse factor, cell throughput was lesser for reuse 3x3x3 as compared to other reuse patterns. Hence, in this chapter we explore how other reuse patterns could be made possible by reducing their outage probabilities. The MS at cell border are relatively more prone to outage because of strong co-channel interference and reduced signal strength. Therefore, it is important to look for techniques that may reduce the interference and/or increase the signal strength at the same time. One of such techniques in WiMAX system is adaptive beamforming.

3.1 Introduction

Adaptive beamforming technique is a key feature of mobile WiMAX. It does not only enhance the desired directional signal but also its narrow beamwidth reduces interference caused to the users in neighboring cells. Resultant increase in Signal to Noise-plus-Interference Ratio (SINR) offers higher capacity and lower outage probability. Adaptive beamforming can be used with PUSC, FUSC and AMC (refer Tab. 278 of [26]).

Authors of [45] study the power gain, because of adaptive beamforming, for a IEEE 802.16e based system. Results presented by authors are based on measurements carried out in one sector of a cell with no consideration of interference. Measurements are carried out using an experimental adaptive beamforming system. Reference [46] discusses the performance of WiMAX network using beamforming in conjunction with Space Division Multiple Access (SDMA). The simulations are carried out for OFDM (not OFDMA). Hence frequency diversity, because of distributed subcarrier permutations, is not taken into account. Authors of [37] have also compared two frequency reuse types using MIMO (Multiple Input Multiple Output) without considering beamforming. References [47, 48]

analyze the performance of beamforming capable WiMAX systems for non line-of-sight (NLOS). Physical abstraction model for SINR computation is not taken into account. Only AMC mode has been studied. Author investigates the possibility of reuse 1. Suggested interference coordination technique gives higher values of SINR at the cost of lower resource utilization.

In this chapter, we repeat the comparison of six frequency reuse patterns for WiMAX networks in presence of adaptive beamforming and see if higher frequency reuse than 3x3x3 is possible. We also look into the possibility of achieving reuse one (i.e., 1x3x1) through beamforming with partial loading of subchannels and beamforming per PUSC group. Furthermore, we compare the system performance of a beamforming WiMAX network for three subcarrier permutation types: PUSC, FUSC and AMC. Hence four different cases are considered in the study with adaptive beamforming: frequency reuse comparison, beamforming with partial loading of subchannels, beamforming per PUSC group and comparison of PUSC/FUSC/AMC. In addition, we study ways of reducing computational load of beamforming simulations. The comparison of uniform spatial distribution of users and uniform angular distribution of radiation beams is carried out. The work presented in this chapter is based on [10, 11, 12, 13].

3.2 Subcarrier Permutation and Beamforming

The mode or even possibility of adaptive beamforming depends upon organization of pilot subcarriers. This will also determine the way interference is modeled. In fact, pilot subcarriers are required for channel estimation. In case of beamforming, dedicated pilots are required for each beam in the cell. For PUSC and FUSC, there is a common set of pilot subcarriers for a number of subchannels while in AMC mode, each subchannel has its own pilot subcarriers. Hence, the number of possible orthogonal beams in a cell (of cellular network) depends upon distribution of pilot subcarriers and hence the subcarrier permutation type.

3.2.1 PUSC

In PUSC, subchannels are put together in six groups. Each group has its own set of pilot subcarriers and hence, beamforming can be done per PUSC group. As subcarriers of a subchannel are chosen randomly (cf. section 2.2.3.3), each subcarrier of the serving cell may experience the interference from different beams of a given interfering cell. In this way, subcarriers of a subchannel may not experience the same interference. The value of interference will dependent upon array-plus-antenna gain associated with the colliding subcarrier that may belong to any of six interfering beams in the neighboring cell.

3.2.2 FUSC

Pilot subcarriers in FUSC are common to all subchannels hence a single beam is possible in every cell. In contrast to PUSC, all subcarriers of a subchannel experience the same interference. This is due to the fact that every colliding subcarrier will have the same array-plus-antenna gain since there is only one beam per interfering cell.

3.2.3 AMC

When we consider AMC for beamforming, there can be as many orthogonal beams as the number of subchannels since every subchannel has its own pilot subcarriers. We consider the case when there is no coordination among BS for allocation of subchannels. Due to similar assignment of subcarriers to subchannels in neighboring cells, all subcarriers will experience same amount of interference because of an interfering beam in the neighbouring cell. Colliding subcarriers in a beam will have same array-plus-antenna gain. In addition, unlike PUSC and FUSC, since subcarriers of a subchannel are contiguous in AMC, no frequency diversity gain is achieved.

3.3 Simulation Details

The simulation details are almost the same as were discussed in section 2.3 except for few additions and changes because of adaptive beamforming coming into picture.

3.3.1 Path-loss Model

Previously, a NLOS path-loss model was considered in simulations. In study of beamforming, we assume that we have exact knowledge of MS location in the cell. For this purpose, Line of Sight (LOS) environment has been considered in simulations and LOS path loss (PL) model for suburban macro (scenario C1) has been referred from [49]. It is a three slope model described by the following expressions:

$$PL(d) = \begin{cases} 32.44 + 20log_{10}(f_c/10^9) & \text{if } d \leq 20\ m; \\ +20log_{10}(d) & \\ (\textit{free-space model}) & \\ \\ C(f_c) + 23.8log_{10}(d) & \text{if } 20\ m < d \leq d_{BP}; \\ \\ C(f_c) + 40log_{10}(d/d_{BP}) & \text{if } d > d_{BP}, \\ +23.8log_{10}(d_{BP}) & \end{cases}$$

where f_c is the carrier frequency in Hz, $C(f_c)$ is the frequency factor given as: $33.2 + 20log_{10}(f_c/2 \cdot 10^9)$, d_{BP} is the breakpoint distance and σ_{Sh} is the stan-

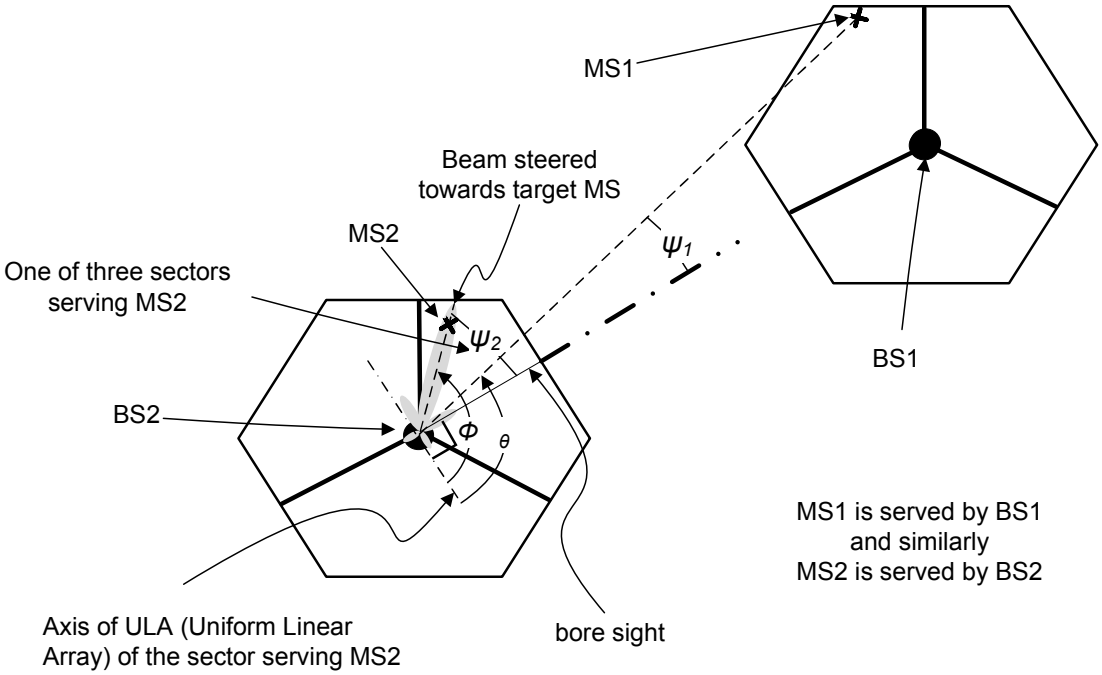

Figure 3.1: Example showing beamforming scenario

dard deviation of log-normal shadowing. The breakpoint distance is computed as: $d_{BP} = 4h_{BS}h_{MS}/\lambda_c$, with h_{BS} and h_{MS} being the heights of BS and MS respectively. All heights and distances are in meters. The value of σ_{Sh} associated with above model is 4 dB for $d \leq d_{BP}$ and is equal to 6 dB beyond d_{BP}.

3.3.2 Beamforming Array Factor

The beamforming model considered in our simulations is the delay and sum beamformer (or conventional beamformer) with Uniform Linear Array (ULA). The power radiation pattern for a conventional beamformer is a product of array factor and radiation pattern of a single antenna. The array factor for this power radiation pattern is given as [50]:

$$AF(\theta) = \frac{1}{n_t}\left|\frac{\sin(\frac{n_t\pi}{2}(\cos(\theta)-\cos(\phi)))}{\sin(\frac{\pi}{2}(\cos(\theta)-\cos(\phi)))}\right|^2, \tag{3.1}$$

where n_t is the number of transmit antennas at BS (with inter-antenna spacing equal to half wavelength), ϕ is the look direction (towards which the beam is steered) and θ is any arbitrary direction. Both these angles are measured with respect to array axis at BS (see Fig. 3.1).

The array factor is multiplied by gain of single antenna (cf. Eq. 2.1) to give the resultant beamforming gain.

3.3.3 Distribution of Beams

The number of beams in a cell/sector is specific to subcarrier permutation type (cf. section 3.2). We noticed that with FUSC we can have only one beam per cell/sector. On the other hand, AMC mode can have as many number of beams as possible. In the current study, for AMC mode, we do not consider BS coordination and take into account a generic slot. Hence, only one beam will be simulated in every snapshot.

To find the direction of adaptive beams, equivalent number of MS are drawn in a cell using spatial uniform distribution. Hereafter, we discuss how beams are drawn for PUSC, FUSC and AMC and how distribution of beams affects interference. Since FUSC and AMC have both one beam per sector/cell, we treat them together.

3.3.3.1 FUSC and AMC

For both FUSC and AMC, one MS is drawn per cell/sector and all subcarriers of a slot experience the same interfering beam pattern from a neighboring cell/sector.

3.3.3.2 PUSC

With PUSC, there can be up to six beams per sector i.e., one beam per group. There can be three different scenarios for PUSC given that there are 1, 3 or 6 adaptive beams per sector/cell. These scenarios are presented hereafter:

- For the first scenario, all six PUSC groups are used by one beam. One MS is drawn per sector and all subcarriers of a slot experience the same interfering beam pattern from a neighboring sector.
- In the second scenario, each beam uses one odd and one even group and hence there are three beams per sector. Three MS are dropped in a sector for three beams per sector. For each subcarrier used by a MS, the interfering beam is chosen with equal probability.
- As for third scenario, each beam uses a distinct group and there are six beams per sector. It is to be noted that number of channels per even and odd group are different (see Tab. 3.1). Hence, when there are six beams in a sector, the selection of interfering beam per subcarrier is no more equally probable. The reason being that beams are associated to even or odd groups and thus have different number of subchannels. Hence, for a subcarrier, the probability of interfering with an even beam is given as:

$$p_e = \frac{N_e}{N_{Sch}},$$

and with an odd beam it is:

$$p_o = \frac{N_o}{N_{Sch}}.$$

Considering a subcarrier, six MS are drawn per interfering sector. Respective beams are steered, three of them are odd and the other three are even. In a given interfering sector, the chosen beam is drawn according to the above discrete distribution. As mentioned earlier, beamforming not only increases the signal strength but also reduces the interference. To verify this fact, a scenario assuming beamforming only in the serving cell is also considered in simulations of beamforming per PUSC group case.

It is mentioned that to find the direction of a beam towards a MS, we first drop the MS in cell space using uniform random distribution and then steer the beam towards it. In section 3.6, we show how computational load of beamforming simulations could be reduced by using uniform angular distribution of radiation beams instead of uniform spatial distribution of users.

3.3.4 Simulation Parameters

Simulation parameters are also the same as in section 2.3 except for few changes. The number of transmit antennas n_t was equal to one in section 2.3 but for adaptive beamforming it is taken equal to four. Network bandwidth for case of frequency reuse comparison is still 15 MHz (considered in section 2.3) as it is exclusively required for gaining flexibility in assigning bandwidth per cell in six different reuse patterns. However, for the rest of three cases, the network bandwidth is taken as 10 MHz. The associated PUSC, FUSC and AMC parameters with this bandwidth are given in Tab. 3.1.

3.4 Frequency Reuse Comparison

In this section, we present the comparison of six frequency reuse patterns in presence of adaptive beamforming. We have considered first scenario of PUSC for all reuse types. We show how beamforming improves the system performance in terms of radio quality and cell throughput. It is also exhibited how beamforming technique enables us to use certain reuse patterns that were previously not feasible because of high outage probability. Average $SINR_{eff}$ has been plotted versus distance for all six reuse patterns in Fig. 3.2 and 3.3. For each type of reuse, two curves have been presented: one without beamforming and the other with beamforming. A remarkable difference can be seen between the two for all reuse patterns.

Outage probabilities of all reuse patterns with/without beamforming are presented in Fig. 3.4. All reuse types show an improvement, i.e., the diminution of the outage probability. Owing to beamforming, all reuse patterns, except 1x1x1 and 1x3x1, have now acceptable outage probabilities (i.e., $< 5\%$). Based on radio quality, four reuse patterns (i.e., 1x3x3, 3x1x1, 3x3x1 and 3x3x3) could be considered for WiMAX networks which employ adaptive beamforming. To narrow down the choice and select the best one among these four reuse patterns, their average cell throughput has to be compared.

Table 3.1: PUSC/FUSC/AMC parameters for 1024 FFT [26].

Subcarrier Permutation	**Parameter**	**Value**
PUSC	No. of subchannels N_{Sch}	30
	No. of subchannels per even group N_e	6
	No. of subchannels per odd group N_o	4
	No. of PUSC groups	6
	No. of total data subcarriers	720
	No. of total pilot subcarriers	120
	No. of available slots in DL (considering 30 OFDM symbols in DL)	450
FUSC	No. of subchannels N_{Sch}	16
	No. of total data subcarriers	768
	No. of total pilot subcarriers	82
	No. of available slots in DL (considering 30 OFDM symbols in DL)	480
AMC	No. of subchannels N_{Sch}	48
	No. of total data subcarriers	768
	No. of total pilot subcarriers	96
	No. of available slots in DL (considering 30 OFDM symbols in DL)	480

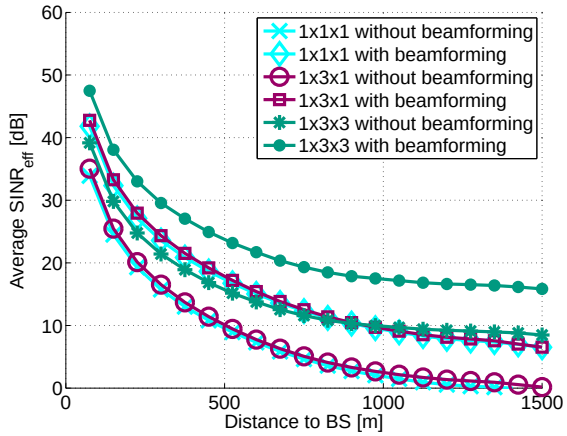

Figure 3.2: Average $SINR_{eff}$ (DL) vs distance for reuse 1x1x1, 1x3x1 and 1x3x3 with beamfomorming.

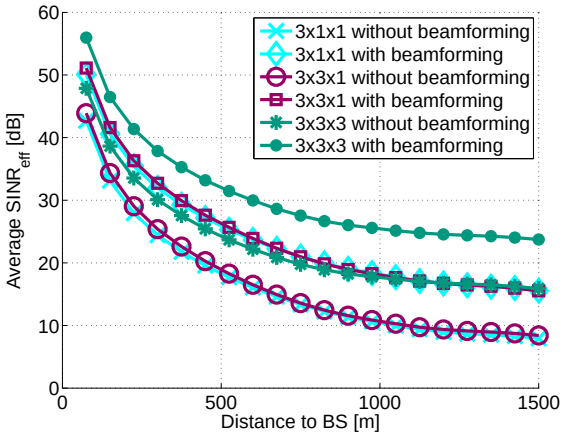

Figure 3.3: Average $SINR_{eff}$ (DL) vs distance for reuse 3x1x1, 3x3x1 and 3x3x3 with beamfomorming.

Table 3.2: Frequency reuse comparison with full loading of subchannels with/without beamforming.

Reuse Type	**Average $SINR_{eff}$ [dB]**		**Outage Probability**		**Average Throughput [Mbps]**	
	without beamforming	with beamforming	without beamforming	with beamforming	without beamforming	with beamforming
1 x 1 x 1	3.8	11.3	0.55	0.09	5.3	14.3
1 x 3 x 1	4.4	11.5	0.51	0.08	17.8	43.5
1 x 3 x 3	11.5	19.1	0.06	0.004	14.7	23.5
3 x 1 x 1	12.3	20	0.06	0.006	5.2	8.1
3 x 3 x 1	12.7	20.1	0.06	0.005	16	24
3 x 3 x 3	19.4	27.2	0.002	0.0002	8	9.4

Average $SINR_{eff}$, average cell throughput and outage probabilities of all six reuse types with and without beamforming are given in Tab. 3.2. It can be noticed that beamforming phenomenon has improved all the three parameters for all six reuse patterns. Despite sufficient improvement, reuse 1x3x1 and 1x1x1 still have significant outage probabilities. Out of the rest four, reuse types 1x3x3 and 3x3x1 have not only lower outage probabilities but also greater throughput than the others. Furthermore, these two reuse types have comparable performance and could be considered as a good choice for beamforming capable WiMAX networks.

Albeit, adaptive beamforming has considerably improved the system performance, the reuse pattern 1x3x1 (or reuse 1) is still down played by 9% of outage probability. In the following section, we see how could we futher reduce the outage probability of reuse 1x3x1 so as to bring it in acceptable range (i.e., $< 5\%$).

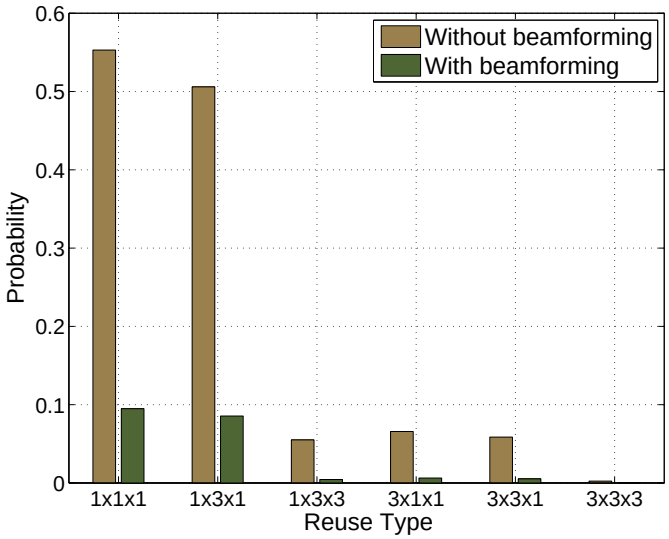

Figure 3.4: Outage probabilities for six reuse types with/without beamforming with full loading of subchannels.

3.5 Achieving Frequency Reuse 1

Network bandwidth is a precious resource in wireless systems. As a consequence, reuse 1 is always cherished by wireless network operators. The advantage of reuse 1, availability of more bandwidth per cell, is jeopardized by increased interference because of extensive reutilization of spectrum. We have already observed in previous sections that this increased interference results in increased outage probability. Adaptive beamforming ameliorated the situation and reduced its outage probability from 55% to 9% which is still significant to question the QoS.

Existing solutions are BS coordination techniques resulting in partial usage of resources (see e.g., [47]). In this thesis, we propose two solutions to further decrease the outage probability of reuse 1: beamforming with partial loading of subchannels and beamforming per PUSC group. Both of the proposed solutions do not implicate BS coordination.

3.5.1 Beamforming with Partial Loading of Subchannels

In frequency reuse comparison full loading of subchannels is considered. All subcarriers of a slot experience the same interfering beam pattern from a neighboring cell/sector causing interference. However, when partial loading of subchannels is assumed, not all subchannels are used in every cell. Since we have assumed independent uniform random distribution of subcarriers to subchannels in every cell, assuming partial loading of subchannels, some subcarriers used in a cell might not be reused in the neighboring cell. Hence MS in a cell will not receive interference on all subcarriers of a subchannel.

We have done simulations with eighty and sixty percent of total subchannels and consider first scenario of PUSC.The outage probabilities with partial loading

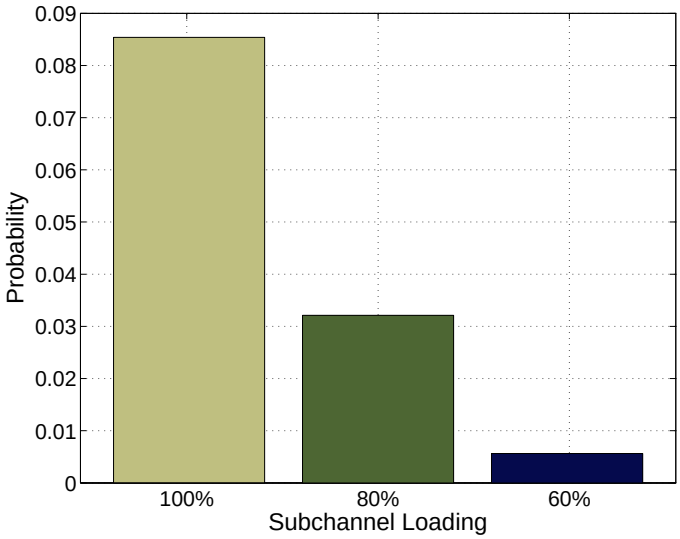

Figure 3.5: Outage probabilities for reuse 1x3x1 with partial loading of subchannels and beamforming.

of subchannels in presence of adaptive beamforming are presented in Fig. 3.5. It is clear from this figure that eighty percent of subchannel loading brings the outage probability of reuse type 1x3x1 well under control (less than five percent) but it is also important to see its effect on available average throughput. The average throughput of this reuse is computed at eighty percent of subchannel loading and is found to be 39.5 Mbps. Even this value of average throughput is greater than those of all other reuse types under full load conditions.

However, this solution does not offer a true reuse 1 since we are unable to use 100% subchannels. The other solution presented in this thesis is based on exploiting the group structure and frequency diversity of subcarrier permutation PUSC and is explained in the next section.

3.5.2 Beamforming per PUSC Group

In this section, we consider three different scenarios of PUSC for reuse 1x3x1. An additional beamforming scenario "beamforming in the serving cell only" has also been simulated in which first scenario of PUSC is modified in such a way that array-plus-antenna gain of beamforming is only taken into account for signal. For interfering BS, only single antenna gain is considered. The interest in simulating this case is to observe interference reduction because of beamforming.

Average $SINR_{eff}$ and average global throughput with respect to distance from BS for four scenarios of beamforming and without beamforming case are presented in Fig. 3.6 and 3.7 respectively. A clear difference can be observed between beamforming and without beamforming cases. We can notice about 7 to 8 dB gain. The gain for "beamforming in the serving cell only" scenario is about 2 dB less. The difference shows the effect of beamforming on interference

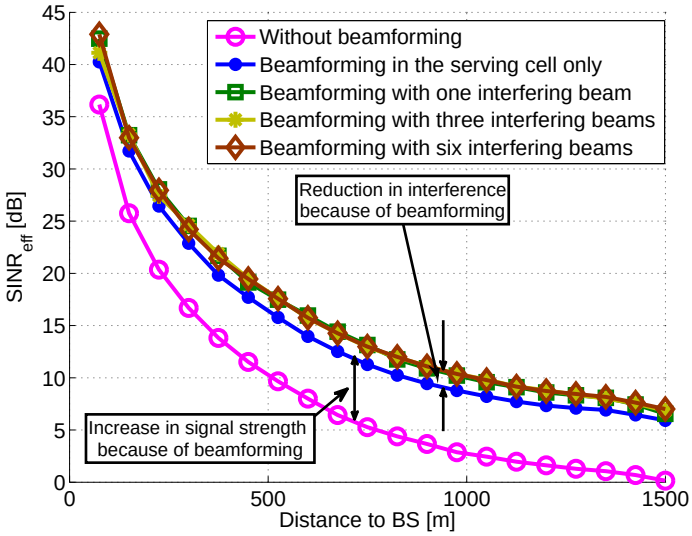

Figure 3.6: Average $SINR_{eff}$ vs distance to base station for PUSC.

reduction. The difference in terms of $SINR_{eff}$ and global throughput is not much with varying number of interfering beams (i.e., for three different cases of PUSC).

However, it can be clearly seen in Fig. 3.8 that outage probability significantly decreases when we take full advantage of diversity offered by PUSC. Increasing the number of beams, outage probability decreases from an unacceptable 9% (with one beam) to a reasonable 2% (with six beams). It is interesting to note that average throughput and $SINR_{eff}$ are not affected by the gain in outage probability. Hence, by employing the beamforming per PUSC major group, we have achieved reuse 1 without partial loading of subchannels or base station coordination.

It can also be noticed that outage probability of "beamforming in the serving cell only" scenario is quite small. The reason being signal strength in the serving cell is increased because of beamforming while absence of beamforming in interfering cells keeps the interference strength unchanged (see Fig. 3.8).

We have seen that group structure of PUSC used with adaptive beamforming could be exploited to achieve reuse 1. However, it would be interesting to compare the performance of PUSC with other two subcarrier permutation types (i.e., FUSC and AMC) in presence of beamforming for reuse 1x3x1.

3.5.3 Comparison of PUSC, FUSC and AMC

In Fig. 5.16, average values of effective SINR ($SINR_{eff}$) are plotted as a function of distance from base station (BS) for three subcarrier permutation types considering reuse 1. As can be noticed, there is almost no difference between values of $SINR_{eff}$ with PUSC, FUSC and AMC. On the other hand, when we look at MCS probabilities in Fig. 3.11, PUSC outclasses the other two (FUSC

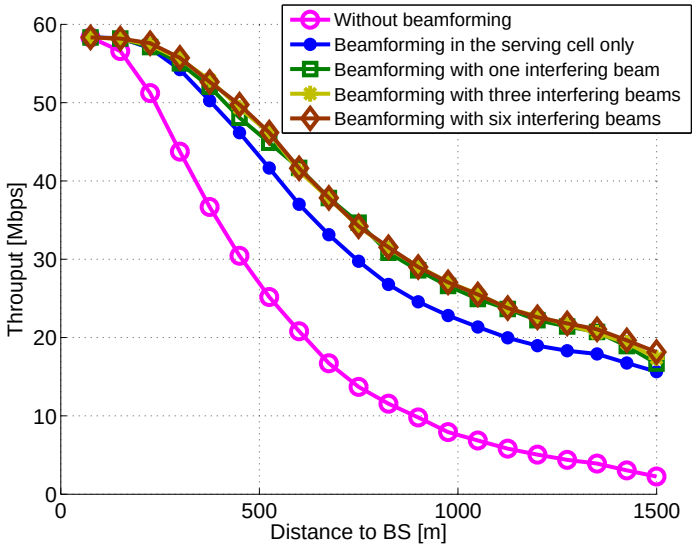

Figure 3.7: Average cell throughput vs distance to base station for PUSC.

and AMC) in terms of outage probabilities. Though average $SINR_{eff}$ are same for all, only PUSC offers an outage probability in the acceptable range (less than 5%). Since subcarriers in a PUSC subchannel experience variable interference gains, it average outs the possibility of all subcarriers suffering from same and high interference. That is why outage probability is reduced. At the same time, it also reduces the probability that all colliding subcarriers have low power. This effect can be noticed while looking at probabilities of high rate MCS. For example, with PUSC, probability to transmit with 64QAM-3/4 for PUSC is less as compared to FUSC and AMC.

If we look at average values of cell throughput (w.r.t. distance from BS) in Fig. 3.10, it can be noticed that in the region close to BS, PUSC is somewhat less performing than FUSC and AMC. This result can be justified in light of probabilities of MCS in Fig. 3.11 where stationary probabilities of the best MCS (64QAM-3/4) are higher with FUSC and AMC. Owing to strong signal strength in the region close to base station, probability for a MS to achieve better MCS is more. At about 350 m and onward (from base station), throughput with PUSC is around 1 Mbps less than that of FUSC and AMC even if PUSC has better performance in terms of radio quality. This is because of the fact that with PUSC, number of available slots are lesser (see Tab. 3.1).

3.6 Uniform Angular Distribution of Beams

In this section, we investigate the way of reducing the computational load of beamforming simulations. For this purpose, instead of considering spatial distribution of MS in the interfering sectors, uniform angular distribution of beams is considered.

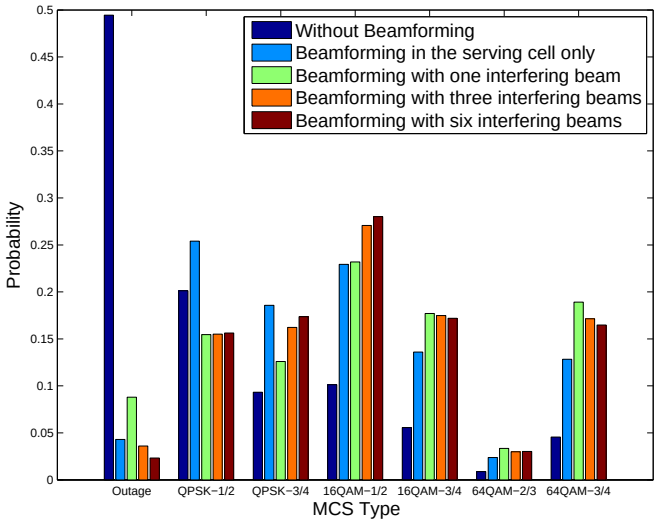

Figure 3.8: MCS distribution for PUSC.

To calculate array-plus-antenna gain because of an interfering beam, we only require the angle that beam subtends at ULA and boresight of the serving sector. For this, we need a two step procedure. In the first step, MS are uniformly distributed in the interfering sector and then, during second step, angles are calculated to find out their beam patterns. If we draw these angles in a sector using uniform angular distribution, first step can be avoided and simulation time can be saved. However, since the shape of cell is hexagonal (not circular), spatial distribution is not exactly equal to angular distribution.

The comparison of uniform spatial distribution of MS and uniform angular distribution of beams is depicted in Fig. 3.12. The results of two are almost the same. Though average throughput and MCS probabilites are not presented here, they were also in agreement with the results of average $SINR_{eff}$ *vs distance from BS* curve presented here.

3.7 Conclusion

Adaptive beamforming is a promising technique in future wireless systems. In this chapter, we have shown how beamforming improved the system performance for six different frequency reuse patterns. Without beamforming, only reuse 3x3x3 offered an acceptable outage probability. After employing beamforming, we noticed that outage probabilities of reuse patterns 1x3x3, 3x1x1, 3x3x1 and 3x3x3 became acceptable. Among these four reuse patterns, reuse 1x3x3 and 3x3x1 exhibited the best and comparable performance in terms of radio quality and cell throughput. The reuse 1 (i.e., 1x3x1) is still characterized by a significant value of outage probability (i.e., 9%). To decrease this value further, two solutions have been proposed: beamforming with partial loading of subchannels and beamforming per PUSC group. Though reuse 1x3x1 employing beamforming with partial

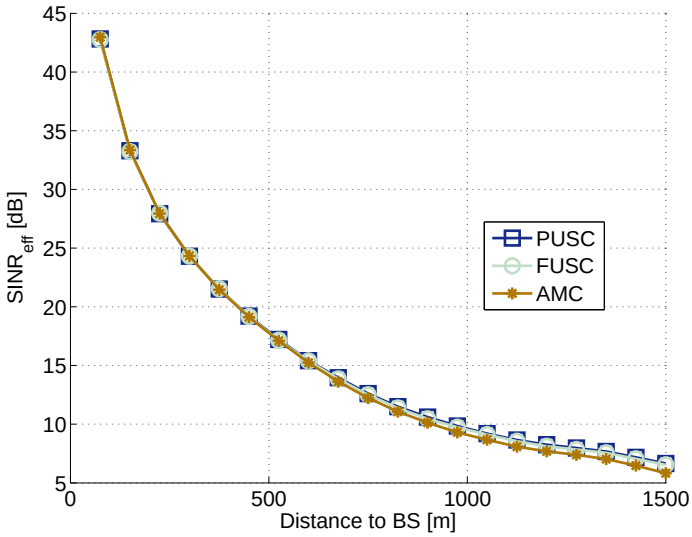

Figure 3.9: Average $SINR_{eff}$ vs distance to base station for PUSC/FUSC/AMC with beamforming.

loading of subchannels provided the best performance but true sense of reuse 1 was possible with the latter solution. At the end, we also presented a brief comparison of three subcarrier permutation schemes in presence of beamforming.

During study of frequency reuse, we noticed that distribution of $SINR_{eff}$ is a crucial measure and can be obtained precisely through simulations. But the drawback of simulations is extensive time consumption. Hence, during next stage of the thesis, we look for a time efficient method to model SINR statistics in a cellular WiMAX system.

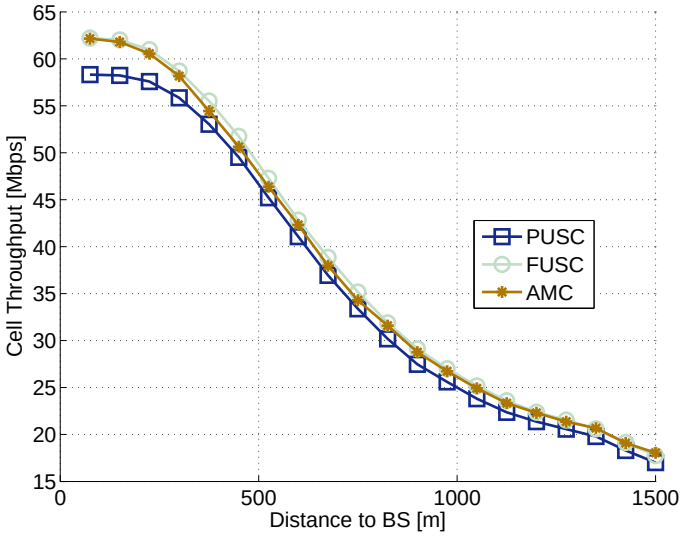

Figure 3.10: Average cell throughput vs distance to base station for PUSC/FUSC/AMC with beamforming.

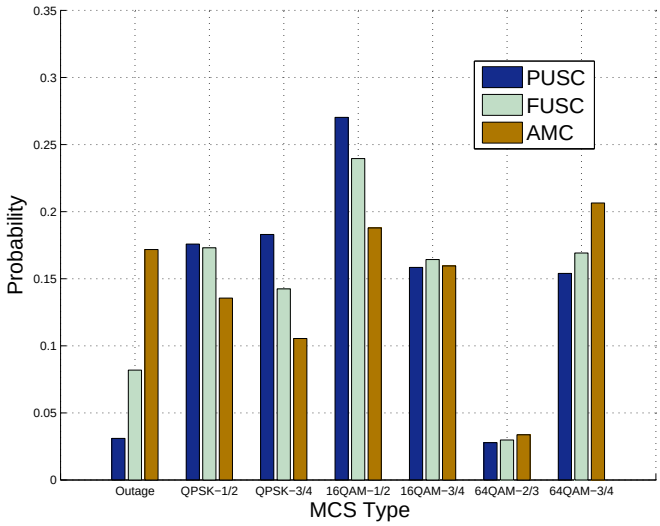

Figure 3.11: MCS distribution for PUSC/FUSC/AMC with beamforming.

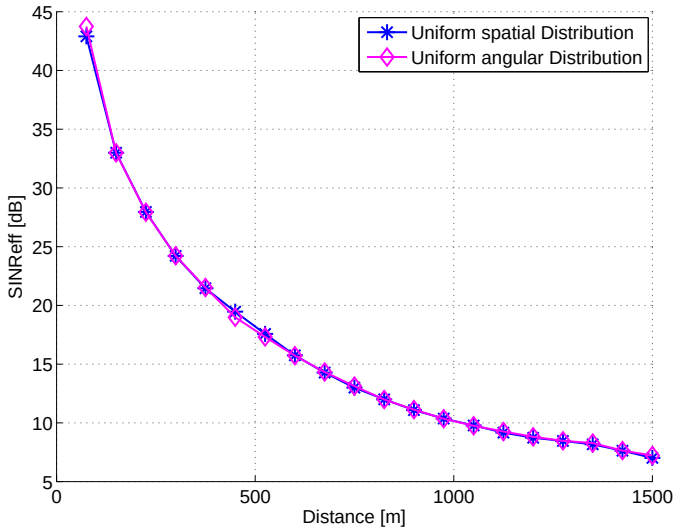

Figure 3.12: Average $SINR_{eff}$ versus distance with beamforming and reuse 1x3x1.

Chapter 4

Semi-analytical Method to model Effective SINR Distribution

In this chapter, we introduce a semi-analytical approach, based on [14, 15, 16], to find out the stationary probabilities of MCS for a WiMAX network in DL with users served by the best BS. Using Monte Carlo simulations, we find the spatial distributions of Effective Signal to Noise-plus-Interference Ratio ($SINR_{eff}$) for different values of shadowing standard deviation (σ_{SH}). With the help of distribution fit, we show that Generalized Extreme Value (GEV) distribution provides a good fit for different frequency reuse patterns. Furthermore, by applying curve fitting, we demonstrate that the parameters of GEV distributions, as a function of σ_{SH} values, can be expressed using polynomials. These polynomials can then be used off-line (in place of time consuming simulations) to find out GEV Cumulative Distribution Function (CDF), and hence the stationary probabilities of MCS, for any desired value of σ_{SH}. We further show that these polynomials can be used for other cell configurations with acceptable deviation and significant time saving.

4.1 Introduction

The number of subcarriers possessed by a slot (the basic resource unit of WiMAX) is fixed (i.e., forty eight). It is independent of the subcarrier permutation scheme. However, the number of bits it can transfer depends upon the MCS type used by the MS. Therefore, cell throughput depends upon the probabilities of the possible MCS types. These MCS probabilities can be used in traffic analysis to obtain network dimensioning parameters (cf. section 1.3). Since each MCS type is characterized by a $SINR_{eff}$ threshold value (cf. section 1.2.3), we require CDF of $SINR_{eff}$ spatial distribution. Therefore an efficient way to obtain this CDF is always desired.

The study of SINR statistics in cellular environment is not recent. For examples, analytical/semi-analytical modeling of interference for mobile radio networks employing code division multiple access (CDMA) is given in [51, 52, 53]. How-

ever, the analysis carried out with single carrier in the physical layer can not be applied to multi carrier OFDMA based networks since the latter offers frequency diversity. System level simulations (SLS) have been used in [38, 54, 36, 55, 56, 57] (and chapters 2 and 3 of this thesis) to find out percentage of MCS for an IEEE 802.16 based networks. The drawback of purely simulation based methods is the excessive time consumption. In [58], an analytical method to calculate MCS probabilities and hence throughput in AMC mode of WiMAX has been proposed. However, the analysis does not take into account the shadowing effect. The authors of [59] present a semi-analytical method to calculate outage probabilities in OFDMA network (with no consideration of WiMAX specifications). In [60], an analytical calculation of symbol error rate for different MCS types is presented. To calculate symbol error, authors have not taken $SINR_{eff}$ into account. In short, a method is required by which modeling of $SINR_{eff}$ statistics in WiMAX networks can be carried out more efficiently.

In this thesis, we propose a semi-analytical method to find out stationary probabilities of different MCS types for a mobile WiMAX network that can substitute a number of simulations. We start with Monte Carlo simulations and find out spatial distributions of $SINR_{eff}$ for some integral values of σ_{SH}. It is shown that the Probability Density Function (PDF) of $SINR_{eff}$ can be approximated by GEV distributions [61]. We exhibit that GEV distributions' parameters can be expressed in terms of σ_{SH} using polynomials. Instead of simulations, these polynomials can then be used to find out GEV distribution, and hence MCS probabilities, for any desired value of σ_{SH} in the above range. Furthermore, we demonstrate the applicability of these polynomials for different values of cell range R and BS transmission power P_{Tx} and discuss the time efficiency offered.

We choose the GEV PDF to approximate the $SINR_{eff}$ distribution. The reason for this choice is detailed hereafter. According to extreme value theory, the distribution of maximum of a number of i.i.d random variables can be approximated by GEV distribution. In our simulations, we have considered that MS are attached to the best server (i.e., the BS from which the highest signal strength is received). Since the signal strength from different BS in the network is an i.i.d random variable, an analogy exists between the extreme value theory and our simulation scenario. This analogy is the motivation behind choosing GEV distribution. To verify this fact, we tried the distribution fit with some other distributions (e.g., normal). It was found that GEV distribution provided the best fit.

For explanation of semi-analytical method, only one frequency reuse type (3x3x3) has been considered. However, method is equally applicable to five other possible reuse types: 1x1x1, 1x3x1, 1x3x3, 3x1x1 and 3x3x1. The results pertaining to these five reuse types are listed down in appendix B of this thesis report. Also included in the appendix are the results for reuse type 1x3x1 when beamforming is also considered.

Before semi-analytical method is presented, a brief introduction of GEV distribution is given in the next section.

4.2 Generalized Extreme Value (GEV) Distribution

The details of GEV distribution have been referred from [61]. The PDF of this distribution is given by following equation:

$$f(x;\mu,\sigma,\xi) = \frac{1}{\sigma}\left[1+\xi\left(\frac{x-\mu}{\sigma}\right)\right]^{-1-\frac{1}{\xi}} \exp\left\{-\left[1+\xi\left(\frac{x-\mu}{\sigma}\right)\right]^{-\frac{1}{\xi}}\right\},$$

with the condition that $1+\xi\left(\frac{x-\mu}{\sigma}\right) > 1$. The variables ξ, σ and μ are the shape, scale and location parameters respectively. The CDF of GEV distribution is:

$$F(x;\mu,\sigma,\xi) = \exp\left\{-\left[1+\xi\left(\frac{x-\mu}{\sigma}\right)\right]^{-\frac{1}{\xi}}\right\},$$

and once again given that $1+\xi\left(\frac{x-\mu}{\sigma}\right) > 1$.

4.3 Semi-analytical Method

A systematic overview of the proposed semi-analytical method is depicted in Fig. 4.1. The method is divided into two steps: A) Simulations and Distribution/Curve Fitting and B) Off-line Application. In the following text, these steps are explained in detail.

4.3.1 Simulations and Distribution/Curve Fitting

During this step, spatial distributions of $SINR_{eff}$ is obtained using Monte Carlo simulations for a given value of R, P_{Tx} and a specified range of σ_{SH} integral values inside vector $\boldsymbol{\sigma_{SH}}$.

Each distribution of $SINR_{eff}$ is specific to a value of σ_{SH}. With the help of distribution fit, based on Maximum Likelihood Estimation (MLE), the parameters of GEV distribution (ξ, σ and μ), approximating the simulation PDFs, are acquired for each value of σ_{SH}.

In order to evaluate the distribution fit, the dissimilarity or error Ξ between GEV and simulation PDFs, φ_{GEV} and φ_{sim}, is quantified as follows [62]:

$$\Xi \triangleq \int_{-\infty}^{\infty} |\varphi_{GEV}(t) - \varphi_{sim}(t)|\, dt. \tag{4.1}$$

Since the area under a PDF is 1, the maximum value of error can be 2. Hence the value of error can be between 0 and 2 i.e., $0 \leq \Xi \leq 2$.

Once it is verified that simulation PDFs of $SINR_{eff}$ can be approximated by GEV PDFs, three GEV parameters are then separately plotted against the integral values of σ_{SH}. With the help of curve fitting (using least square method), distinct polynomials, expressing each parameter in terms of σ_{SH}, are found.

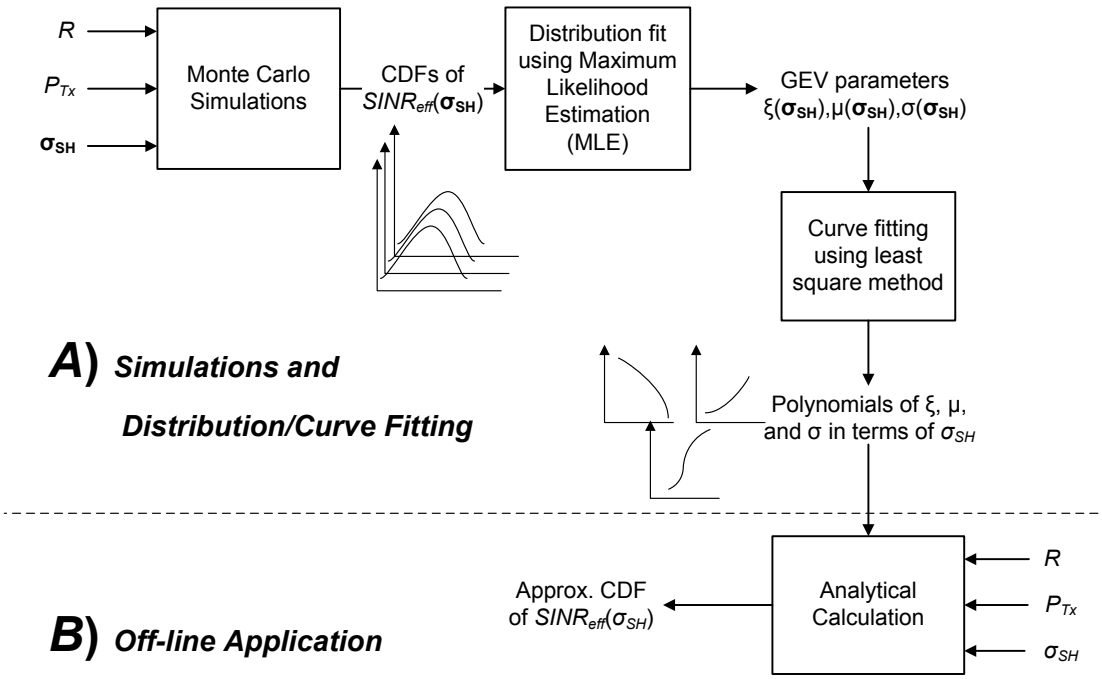

Figure 4.1: Overview of proposed semi-analytical method.

4.3.2 Off-line Application

To calculate $SINR_{eff}$ distribution for any desired value (integral/non-integral) of σ_{SH} in the range specified in section 4.3.1, we no longer require to carry out time consuming Monte Carlo simulations. It is sufficient to find out GEV parameters through polynomials for that value of σ_{SH}. Then using GEV CDF and thresholds values of $SINR_{eff}$ for different MCS types of Tab. 1.1, probabilities of these MCS can be obtained. These MCS probabilities are used to calculate sector/cell throughput by applying Eq. 2.6. In section 4.4, we also show that results obtained through this method are applicable for various values of R and P_{Tx}.

4.4 Numerical Results

In this section, we present the numerical results. Simulation details are the same as were given in section 2.3 for all cases without beamforming. However, for beamforming case, simulation details of section 3.3 can be referred. For Monte Carlo simulations, range of σ_{SH} is considered to be $4, 5, ..., 12$ dB. Other input parameters are $R = 1500$ m and $P_{Tx} = 43$ dBm. The $SINR_{eff}$ distribution is obtained for each value of σ_{SH}. Using distribution fitting, GEV parameters are determined for each of these distributions. As an example, in Fig. 4.2, approximation of $SINR_{eff}$ PDF (obtained through simulation) by a GEV PDF for $\sigma_{SH} = 9$ dB is shown. As can be noticed, the two distributions only have a dissimilarity error of 0.052 which is 2.6% of the maximum possible error. This comparison for an integral value of σ_{SH} is aimed at demonstrating the fact that

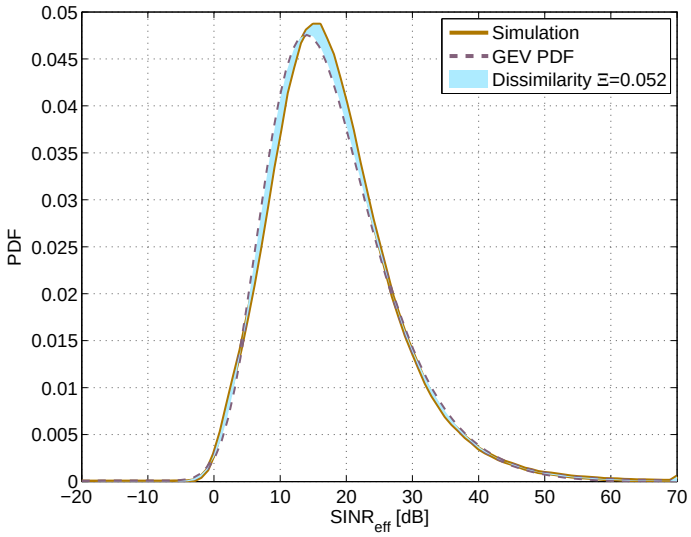

Figure 4.2: $SINR_{eff}$ distribution through simulation and GEV parameters for $\sigma_{SH} = 9$ dB, $R = 1500$ m, $P_{Tx} = 43$ dBm and reuse 3x3x3.

GEV PDF is a good approxiamtion of $SINR_{eff}$ PDF. However, for the validation of our semi-analytical method, we shall take non-integral value of σ_{SH}.

GEV parameters, obtained though distribution fitting, are separately plotted against σ_{SH} values in Fig. 4.3, 4.4 and 4.5. With the help of curve fitting, polynomials of the curves approximating these plots are found and are also given in the figures.

To validate off-line application (cf. section 4.3.2), we choose an arbitrary non-integral value $\sigma_{SH} = 7.5$ dB. We calculate the GEV parameters through polynomials and get PDF, MCS probabilities and cell throughput. For the same value of σ_{SH} and assuming the values of $R = 1500$ m, $P_{Tx} = 43$ dBm, we find the PDFs, MCS probabilities and cell throughput through simulations. Furthermore, we also check the applicability of results obtained through GEV parameters, with $\sigma_{SH} = 7.5$ dB, for various cell configurations. For this purpose, we fix $\sigma_{SH} = 7.5$ dB and carry out simulations for different values of R and P_{Tx}. The maximum value of R is considered to be 2000 m beyond which outage probability is unacceptable (cf. section 2.5). PDFs, MCS probabilities and average cell throughput, obtained through simulations with different configurations, are compared with those obtained through GEV parameters.

The results of validation and applicability for various cell configurations are given in Fig. 4.6 and Tab. 4.1. For MCS probabilities, maximum difference was found to be 0.06 (for MCS 64QAM-3/4) with simulation configuration of $R = 1000$ m, $P_{Tx} = 43$ dBm, which is 13% of the value of MCS 64QAM-3/4 probability. As far as cell throughput and PDF error are concerned, the percentage error w.r.t maximum possible error never exceeds 5% and cell throughput does not differ more than 5.47% for all cell configurations.

For explanation, results of reuse 3x3x3 are discussed in this section. The

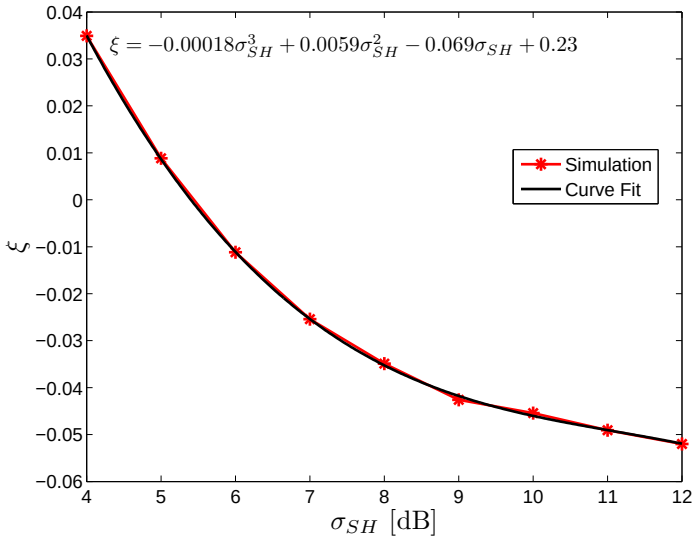

Figure 4.3: Shape parameter ξ of GEV distribution vs σ_{SH} for $R = 1500$ m, $P_{Tx} = 43$ dBm and reuse 3x3x3.

Table 4.1: Comparison of results obtained through simulation and GEV parameters for $\sigma_{SH} = 7.5$ dB for reuse 3x3x3.

Simulation Configuration		**Dissimilarity Ξ**	**Percentage w.r.t max error**	**Throughput X [Mbps]**		**Percentage difference**
$\mathbf{P_{Tx}}$ [dBm]	**R** [m]			**Sim**	**GEV**	
43	1000	0.095	4.73	5	4.73	5.47
43	1250	0.073	3.65	4.96	4.73	4.57
43	1500	0.056	2.83	4.88	4.73	3.17
43	1750	0.058	2.92	4.78	4.73	1.18
43	2000	0.1	5	4.66	4.73	1.35
40	1500	0.065	3.27	4.75	4.73	0.49
46	1500	0.075	3.77	4.96	4.73	4.72

results for other five reuse patterns without beamforming and for reuse 1x3x1 with beamforming are presented in appendix B. These results also show similar behavior.

The simulations were run on a computer with following specifications: 3 GHz Intel Core 2 Duo processor, 2 GB RAM and 4 MB shared L2 cache. Time taken by one Monte Carlo simulation was about 5 hours. Time required for semi-analytical method is around $N_{SH} \times 5$ hours, where N_{SH} is the length of vector $\sigma_{\mathbf{SH}}$. If MCS distributions are required for N different scenarios (each defined by specific values of σ_{SH}, R and P_{Tx}), our proposed method always requires fixed duration which is equal to $N_{SH} \times 5$ hours while the same task carried out by Monte Carlo simulations will require $N \times 5$ hours.

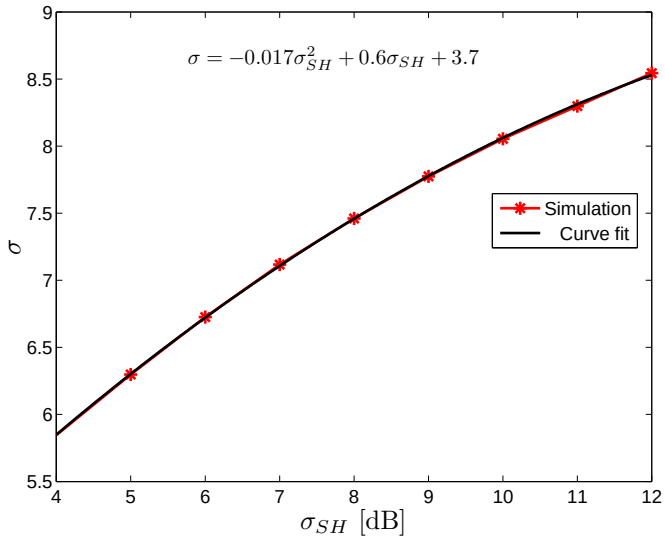

Figure 4.4: Scale parameter σ of GEV distribution vs σ_{SH} for $R = 1500$ m, $P_{Tx} = 43$ dBm and reuse 3x3x3.

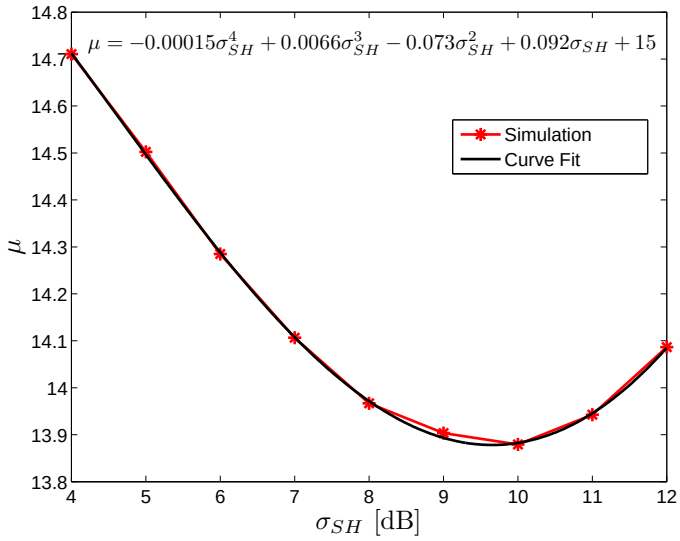

Figure 4.5: Location parameter μ of GEV distribution vs σ_{SH} for $R = 1500$ m, $P_{Tx} = 43$ dBm and reuse 3x3x3.

4.5 Conclusion

In this chapter, we have proposed a semi-analytical method to model SINR statistics in mobile WiMAX cellular networks. We have shown that $SINR_{eff}$ distribution, obtained through system level Monte Carlo simulations, can be successfully approximated by a GEV distribution. It is further illustrated that the parameters of GEV distribution can be expressed using simple polynomials in terms of σ_{SH}. These polynomials can be used to calculate the GEV parameters for any desired value of σ_{SH}. These parameters can be used to estimate $SINR_{eff}$ distribution

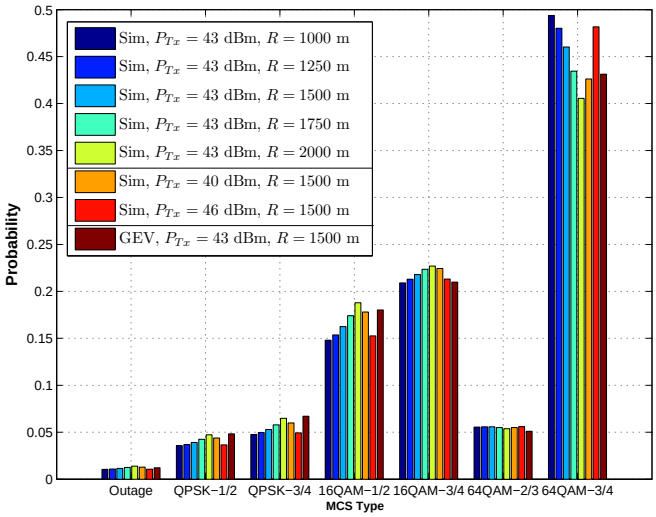

Figure 4.6: MCS probabilities for $\sigma_{SH} = 7.5$ dB and reuse 3x3x3.

and hence the MCS stationary probabilities. The results can be used for a number of network configurations with sufficient accuracy. As a result, we no longer require exhaustive simulations to derive distribution of $SINR_{eff}$.

Moving on with the study of frequency reuse, in next chapter we consider more complex frequency reuse schemes. We introduce analytical models for performance evaluation of an OFDMA system keeping in view three different frequency reuse schemes. For each reuse scheme, three different scheduling schemes are also considered in this study. Results obtained analytically are validated with the help of Monte Carlo simulations. The analytical expressions are then used to compare performance of the three reuse schemes keeping in view different scheduling and channel conditions.

Chapter 5

Analytical Performance Evaluation of Various Frequency Reuse and Scheduling Schemes in Cellular OFDMA Networks

Analytical models for performance evaluation in cellular networks are well-known for providing results with sufficient time efficiency. In this chapter (based on [17, 18]), we present an analytical solution to carry out performance analysis of various frequency reuse schemes in an OFDMA based cellular network. We study the performance in downlink in terms of Signal to Interference Ratio (SIR) and total cell data rate. The latter is analyzed while keeping in view three different scheduling schemes: equal data rate, equal bandwidth and opportunist. Analytical models are proposed for Integer Frequency Reuse (IFR), Fractional Frequency Reuse (FFR) and Two Level Power Control (TLPC) schemes. These models are based on a fluid model that was originally being proposed for CDMA networks. The modeling key of this approach is to consider the discrete base station entities as a continuum. To validate our approach, Monte Carlo simulations are carried out. Validation study shows that results obtained through our analytical method are in conformity with those obtained through simulations. A comparison between the above mentioned frequency reuse schemes and scheduling policies is also presented. We also propose an optimal tuning of involved parameters (inner cell radius and power ratios).

5.1 Introduction

Co-channel Interference (CCI) limits the spectral efficiency of an Integer Frequency Reuse 1 (IFR1) cellular network. The CCI becomes more critical for the users present in the border area of a cell. To combat this problem, in an OFDMA based system, Fractional Frequency Reuse (FFR) has been proposed in [27]. In FFR, cell is divided into inner (close to base station) and outer (border area)

regions. Available bandwidth is divided among inner and outer regions in such a way that former employs reuse 1 while the latter applies frequency reuse 3. Hence, users located in border area of the cell mitigate CCI owing to frequency reuse 3. By properly adjusting the sizes of inner and outer regions, spectral efficiency can be improved.

Authors of [63] studied the performance of FFR for 3GPP/ 3GPP2 OFDMA systems and term it soft frequency reuse. Authors have used System Level Simulation (SLS) in their analysis. In [64] and [48], author has studied the FFR in a IEEE 802.16 based system. Author has proposed an interference coordination system, which focuses on the scheduling of users. Proposed algorithm is implemented in SLS to present results. Two new algorithms, Fractional Time Reuse (FTR) and Fractional Time and Frequency Reuse (FTFR), are proposed in [65] to cater for reduced capacity in the border area of cell because of FFR. In [66], authors have studied the capacity of a WiMAX system in the presence of FFR. In [36] also, performance of a FFR system is analyzed through simulations.

In contrast to the existing work, in this chapter we present approximate analytical models for IFR, FFR and TLPC schemes of an OFDMA based cellular network. We derive expressions to calculate SIR at a given distance from BS and compute spectral efficiency using Shannon's classical formula. We also determine total cell data rate while considering three different scheduling schemes: equal data rate, equal bandwidth and opportunist.

The work presented in this chapter extends the framework, based on a fluid model, proposed in [67] and [68]. The model provides a simple closed-form formula for the other-cell interference factor f in downlink of CDMA networks as a function of distance to BS, path-loss exponent, distance between two BS and network size. The modeling key of this approach is to consider the discrete BS entities of a cellular network as a continuum.

Rest of the chapter is organized as follows: section 5.2 introduces notations used throughout the chapter and recalls the main result of the fluid model. Section 5.3 focuses on IFR and derives SIR and spectral efficiency expressions for both reuse 1 and reuse K. The case of FFR is studied in section 5.4. A two level power control scheme is considered in section 5.5. In section 5.6, three frequency reuse schemes (IFR, FFR and TLPC) are compared in terms of SINR and total cell data rate. Finally, section 6.4 discusses the conclusion of this analysis.

5.2 Fluid Model and Notations

In this section, we explain the application of fluid model to an OFDMA system. We focus on downlink and consider a single subcarrier. BS have omni-directional antennas, such that one BS covers a single cell. If a user u is attached to a station b (or serving BS), we write $b = \psi(u)$.

The propagation path-gain $g_{b,u}$ designates the inverse of the path-loss pl between station b and user u, $g_{b,u} = 1/pl_{b,u}$. In the rest of this chapter, we assume that $g_{b,u} = Ar_{b,u}^{-\eta}$, where A is a constant, $r_{b,u}$ is the distance between BS b and

user u and η (> 2) is the path-loss exponent.

Before presenting the expression of fluid model, we establish the following terms:

- P_{Tx} is the transmitted power per subcarrier. We assume that the output power per subcarrier is constant. Only in section 5.5, we consider two possible values of output power per subcarrier: P_i for the inner region of the cell and P_o for the outer region. In this thesis, we do not consider dynamic power allocation per subcarrier since in current OFDMA systems (WiMAX, Long Term Evolution), output power per subcarrier is constant;
- $S_{b,u} = P_{Tx}\, g_{b,u}$ is the useful power received by user u from station b;
- W is the total system bandwidth and W_u is the bandwidth dedicated to user u;
- R, R_c and R_{nw} are respectively the cell radius, half distance between neighboring base stations and network range (see Fig. 5.1);
- R_e is the radius of a circular region whose area is equal to that of the hexagon with length of each side equal to R. Based on definitions of R_e, R and R_c, it can be deduced that $R_e = aR_c = a\frac{\sqrt{3}}{2}R$, where $a = \sqrt{\frac{2\sqrt{3}}{\pi}}$.
- ρ_u, ρ_{BS} and N_u are respectively the user density, BS density and number of users per cell;
- D_u is the data rate allocated to a user and D_T is the total cell data rate;
- N_{BS} represents the total number of base stations in the network.

The total amount of power received by a user u in a cellular system can always be split up into three parts: useful signal ($S_{b,u}$), interference and noise (N_{th}). It is common to split the system power into two parts: $I_u = I_{int,u} + I_{ext,u}$, where $I_{int,u}$ is the *internal* (or own-cell) received power and $I_{ext,u}$ is the *external* (or other-cell) interference. We consider that useful signal $S_{b,u}$ is included in $I_{int,u}$. It should be noted that this useful signal power has to be distinguished from the commonly considered own-cell interference. In a CDMA network, the lack of orthogonality induces own-cell interference. In a OFDMA network, there is a perfect orthogonality between users and thus $I_{int,u} = S_{b,u}$.

With the above notations, the Signal to Noise-plus-Interference Ratio (SINR) is given by:

$$\gamma_u = \frac{P_{Tx} g_{b,u}}{\sum_{j \neq b} P_{Tx} g_{j,u} + N_{th}}, \tag{5.1}$$

where $g_{j,u}$ is the path-gain between BS j and user u.

Reference [67] has defined the interference factor for user u as the ratio of total power received from other BS to the total power received from the serving BS $\psi(u)$: $f_u = I_{ext,u}/I_{int,u}$. The quantities f_u, $I_{ext,u}$, and $I_{int,u}$ are location dependent

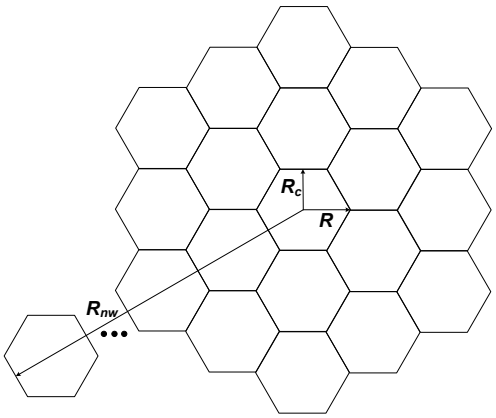

Figure 5.1: Hexagonal network and main parameters of the study.

and can thus be defined for any location x as long as the serving BS is known. In an OFDMA network, $I_{ext,u}$ is the total interference, and thus f_u is the inverse of the SIR per subcarrier. Throughout this chapter, we shall neglect noise in our analytical calculations. This is a common assumption for macro-cells in dense urban areas. In this case, the SINR, γ_u can be approximated by the SIR:

$$\gamma_u \approx \frac{S_{b,u}}{I_{ext,u}} = 1/f_u.$$

As a consequence, it is clear that the approach developed in [67] can be adapted to OFDMA networks, given that the orthogonality factor α considered in CDMA networks is zero (details on fluid model are given in appendix C). In this case, SIR per subcarrier is simply the inverse of the interference factor considered in [67].

$$\gamma_u = \frac{r_u^{-\eta}(\eta - 2)}{2\pi\rho_{BS}(2R_c - r_u)^{2-\eta}}. \tag{5.2}$$

Note that the shadowing effect is neglected in formulation of the model. An extension of the fluid model has been proposed in [69] to take into account the shadowing factor. The results presented in this thesis can thus be extended accordingly. However, we have not verified it in this thesis and set it to be a task for future.

We now compare the results obtained with Eq. 5.2 with those obtained numerically through Monte Carlo simulations. The simulator assumes a homogeneous hexagonal network made of several rings around a central cell. Fig. 5.1 shows an example of such a network with the main parameters involved in this study.

Fig. 5.2 shows the simulated SINR (using Monte Carlo simulations) as a function of the distance from the base station. Following are the simulation parameters: $R = 1$ Km, η between 2.7 and 4, $\rho_{BS} = (3\sqrt{3}R^2/2)^{-1}$, the number of rings around central BS is 15, and the number of snapshots is 3000. To include the effect of path-loss, Erceg model [70] is used: $g_{b,u} = Ar_{b,u}^{-\eta}$, such that $A = \left(\frac{4\pi d_0 f}{c d_0^{\eta/2}}\right)^2$, $d_0 = 100$ m, $f = 2.5$ GHz and c is the speed of light. Thermal

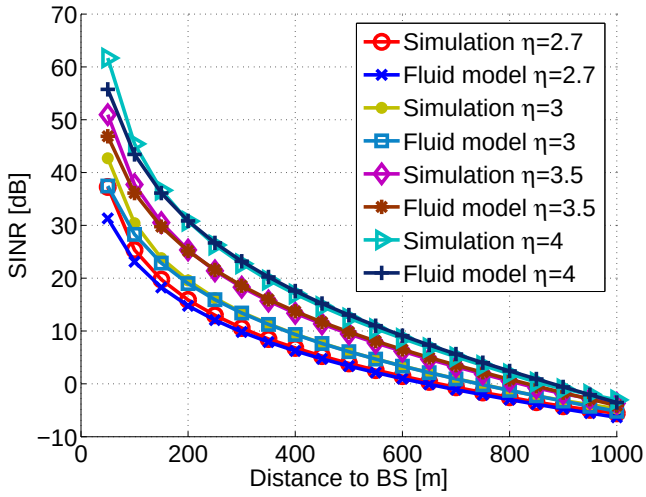

Figure 5.2: SINR vs distance to the BS; comparison of the fluid model with simulations on a hexagonal network with $\eta = 2.7$, 3, 3.5, and 4 (reuse 1).

noise density has been taken as -174 dBm/Hz and a subcarrier spacing of 11 KHz is considered [8]. Eq. 5.2 is also plotted for comparison.

In all cases, the fluid model matches very well the simulation results in a hexagonal network for various values of path-loss exponent. Only in a short area around the BS, the fluid model is a little bit pessimistic, but this is not a region of prime interest for operators. It is to be noted that thermal noise was not considered in the fluid model while simulator does include its effect. However, the results of the two (fluid model and simulator) still match. It indicates that value of interference is much more pronounced as compared to that of thermal noise. Hence, neglecting thermal noise in the fluid model is a reasonable assumption.

For the rest of the chapter, all the above parameters are used for simulations. However, instead of different values of η, a fixed value of 3 is used in the rest of simulations, except mentioned otherwise. The closed-form formula 5.2 will allow us to quickly compute performance parameters of an OFDMA network and in particular to compare different frequency reuse schemes with different scheduling algorithms.

5.3 Integer Frequency Reuse (IFR)

In this section, we consider the application of fluid model to IFR scheme. In integer frequency reuse, all subcarriers allocated to a cell can be used anywhere in the cell without any specification of user's location. However, reutilization of subcarriers in network cells may be one or greater. An example of IFR with frequency reuse 1 (denoted by IFR1) is shown in Fig. 5.3, where W represents the available network bandwidth. For frequency reuse 1, cell bandwidth equals network bandwidth. However, in this chapter, we do not consider sectored cells and hence use a simplified notation (i.e., IFR).

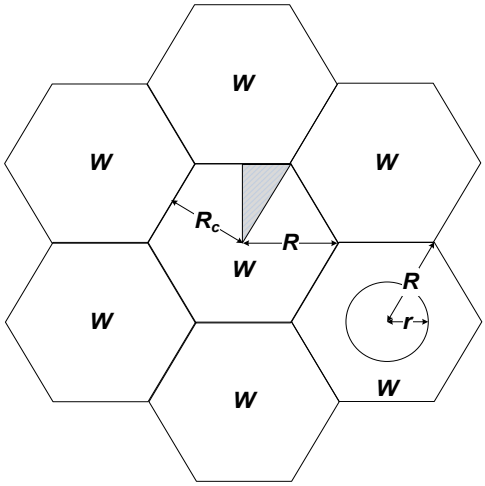

Figure 5.3: Integer Frequency Reuse (IFR) case (reuse 1). Shaded triangular region shows the basic integration area.

Two cases, frequency reuse 1 and K, have been considered in this study. We first derive SINR and spectral efficiency expressions as functions of the distance from the BS using the fluid model. Next we take into account the three scheduling schemes (equal data rate, equal bandwidth and opportunist) and derive the total cell data rate expression for each of them. Results of analytical expressions are also compared with those of Monte Carlo simulations.

5.3.1 IFR with Reuse 1

Consider Eq. 5.2 that gives expression for SINR of a subcarrier for a user at distance r_u. A user at distance r from BS has a specific value of SINR and spectral efficiency. Hence, in rest of the sections, subscript u is omitted for r, SINR and spectral efficiency. With $\rho_{BS} = 1/(2\sqrt{3}R_c^2)$ and introducing the normalized distance x such that $x = r/R_c$, the expression for SINR can be rewritten as:

$$\gamma_{IFR1}(x) = \frac{\sqrt{3}}{\pi}(\eta - 2)(2 - x)^{-2}(2/x - 1)^{\eta}. \tag{5.3}$$

For comparison between simulation and fluid model, Fig. 5.2 can be consulted in which all curves for fluid model have been drawn using Eq. 5.3.

By using Shannon's formula, spectral efficiency (in bps/Hz) as a function of variable x is given as:

$$C_{IFR1}(x) = \log_2[1 + \gamma_{IFR1}(x)], \tag{5.4}$$

where $\gamma_{IFR1}(x)$ is furnished by Eq. 5.3.

In the following sections, we use this expression of spectral efficiency to calculate total cell data rate for the three scheduling schemes.

5.3.1.1 Equal Data Rate

While considering equal data rate, users are assigned the bandwidth in a way that resultant data rate for every user, D_u, is the same. As SINR and spectral efficiency depend on r, higher the distance of a user from BS, lower is the available spectral efficiency and thus higher is the bandwidth (or number of subcarriers) allocated to it. Let $W_u(r)$ be the bandwidth allocated by the scheduler to a user at distance r from the BS. User data rate, D_u, can now be written for any r as:

$$D_u = W_u(r)C(r), \tag{5.5}$$

under the constraint that total cell bandwidth W cannot be exceeded. Total bandwidth used in a cell is now given as:

$$W = 12 \int_0^{\pi/6} \int_0^{R_c/\cos\theta} W_u(r)\rho_u \, r \, dr \, d\theta. \tag{5.6}$$

Integration is done over the shaded triangular region in Fig. 5.3 and multiplied by twelve to obtain the result over the entire hexagonal cell.

If N_u is the number of users in a cell, user density is $\rho_u = N_u/(2\sqrt{3}R_c^2)$. Using Eq. 5.6 and 5.5, value of ρ_u and variable transformation r to x, user data rate is given as:

$$D_u = \frac{\sqrt{3}W/6}{N_u \int_0^{\pi/6} \int_0^{1/\cos\theta} \frac{x}{C_{IFR1}(x)} \, dx \, d\theta},$$

where $C_{IFR1}(x)$ is given by Eq. 5.4.

Since all users receive same data rate and there are N_u users in the cell, total cell data rate is $D_{T,IFR1} = N_u D_u$ and can be written using previous result as:

$$D_{T,IFR1} = \frac{\sqrt{3}W/6}{\int_0^{\pi/6} \int_0^{1/\cos\theta} \frac{x}{C_{IFR1}(x)} \, dx \, d\theta}. \tag{5.7}$$

A worth noting observation regarding Eq. 5.7 is that the total cell data rate neither depends upon the number of users in the cell nor upon the value of R_c.

The change of variables $\theta = z$ and $x = \frac{y}{\cos z}$, whose Jacobian is $\left|\frac{\partial(\theta,x)}{\partial(z,y)}\right| = \left|\frac{1}{\cos z}\right|$, provides the equivalent equation:

$$D_{T,IFR1} = \frac{\sqrt{3}W/6}{\int_0^{\pi/6} \int_0^{1} \frac{y/\cos z}{\cos z C_{IFR1}(y/\cos z)} \, dy \, dz}.$$

To compare the above results with those of simulations, parameters of section 5.2 are used. We set the available network bandwidth to $W = 10$ MHz and the number of users per cell to $N_u = 30$ in simulations. In Tab. 5.1, total cell data rate $D_{T,IFR1}$ with both the fluid model (Eq. 5.7) and simulations, for various values of η, are given. The best agreement is for $\eta = 2.7$, while the difference remains below 10% for η between 2.6 and 3.2. The user data rate (D_u) can be

Table 5.1: Total cell data rate ($D_{T,IFR1}$) vs η (IFR reuse 1, bandwidth=10 MHz, equal data rate).

η	$D_{T,IFR1}$ [Mbps]		Difference
	Fluid model	Simulation	
2.5	6.62	7.43	10.9%
2.6	7.83	8.26	5.21%
2.7	9.01	9.08	0.77%
2.8	10.16	9.89	2.73%
3	12.4	11.6	6.9%
3.2	14.5	13.2	9.85%
3.3	15.5	13.9	11.51%

easily obtained by dividing the total cell data rate (i.e., $D_{T,IFR1}$ in this case) by number of users (N_u) in the cell. To avoid the complexity of calculating double integral, it is also possible to integrate $W_u(r)$ over a disk, whose area equals the hexagon area. Such a disk has a radius $R_e = aR_c$, where $a = \frac{\sqrt{2\sqrt{3}}}{\pi}$. Using this approach, total cell data rate can be approximated as:

$$D_{T,IFR1} \approx \frac{\sqrt{3}W/\pi}{\int_0^a \frac{x}{C(x)}\,dx}. \tag{5.8}$$

For value of $\eta = 3$ and $W = 10$ MHz, data rates obtained with Eq. 5.7 and 5.8 are found to be 12.4 Mbps and 12.6 Mbps respectively with a difference of only 1.6%.

5.3.1.2 Equal Bandwidth

Equal bandwidth means that all users are assigned the same bandwidth whatever the spectral efficiency is available to them. Since users close to BS benefit from higher spectral efficiency, they will attain a higher data rate as compared to users at cell edge. Let W_u denote the bandwidth allocated to each user such that $W = N_u W_u$. Data rate of a user at a distance r is then given as:

$$D_u(r) = W_u C(r), \tag{5.9}$$

total data rate can then be obtained by integrating the user data rates over cell surface:

$$D_{T,IFR1} = 12 \int_0^{\pi/6} \int_0^{R_c/\cos\theta} D_u(r)\rho_u\, r\, dr\, d\theta, \tag{5.10}$$

using Eq. 5.9, user density $\rho_u = N_u/(2\sqrt{3}R_c^2)$, user bandwidth $W_u = N_u/W$ and transformation of variable r to x, we get:

$$D_{T,IFR1} = \frac{6W}{\sqrt{3}} \int_0^{\pi/6} \int_0^{1/\cos\theta} xC_{IFR1}(x)\, dx\, d\theta. \tag{5.11}$$

The simulation and fluid model results are compared in Tab. 5.2.

Table 5.2: Total cell data rate ($D_{T,IFR1}$) vs η (IFR reuse 1, bandwidth=10 MHz, equal bandwidth).

η	$D_{T,IFR1}$ [Mbps]		Difference
	Fluid model	Simulation	
2.5	12.2	13	5.92%
2.6	14.2	14.3	0.76%
2.7	16.1	15.8	1.86%
2.8	18	17.3	4.28%
3	21.6	20.1	7.3 %
3.2	25.1	22.7	10.33%
3.3	26.8	24.5	9.43%

5.3.1.3 Opportunist

In opportunist scheduling, user experiencing the greatest SINR is assigned all the resources and the rest of the users receive no resources at all. In light of assumptions considered in this study, user nearest to the BS will have the maximum SINR value. To calculate the total cell data rate for opportunist scheduling, we require Probability Density Function (PDF) of the distance, X, of the user nearest to the BS. For N_u users in the cell, the Cumulative Distribution Function (CDF) of X is given by:

$$F_X(r) = p[X \leq r] = 1 - p[X > r] = 1 - (1 - \pi r^2/2\sqrt{3}R_c^2)^{N_u},$$

and its PDF can be obtained by differentiating the CDF:

$$p_{X,IFR}(r) = \frac{\pi N_u r}{\sqrt{3}R_c^2}\left(1 - \frac{\pi r^2}{2\sqrt{3}R_c^2}\right)^{N_u-1},$$

with change of variable r to x, the PDF for IFR over small distance dx can be rewritten as:

$$p_{X,IFR}(x)dx = \frac{\pi N_u x}{\sqrt{3}}\left(1 - \frac{\pi x^2}{2\sqrt{3}}\right)^{N_u-1} dx, \tag{5.12}$$

taking into account the circular disk of radius $R_e = aR_c$ with $a = \frac{\sqrt{2\sqrt{3}}}{\pi}$ (refer section 5.2) the average cellular spectral efficiency for opportunist scheduling can be calculated using the following equation:

$$\bar{C}_{IFR1} = \int_0^a C_{IFR1}(x)p_{X,IFR}(x)\,dx.$$

Finally total cell data rate is written as:

$$D_{T,IFR1} = W\bar{C}_{IFR1}.$$

To verify this approach, simulations are carried out with $N_u = 30$. The results of simulation and model are given in Tab. 5.3 with maximum difference equal to 5.9%.

Table 5.3: Total cell data rate ($D_{T,IFR1}$) vs η (IFR reuse 1, bandwidth=10 MHz, opportunist).

η	$D_{T,IFR1}$ [Mbps]		Difference
	Fluid model	Simulation	
2.5	56.6	56.9	0.48%
2.6	62.8	61.6	1.95 %
2.7	68.5	66.5	3%
2.8	74	71.5	3.6%
3	84.5	80.3	5.2%
3.2	94.4	89.2	5.9%
3.3	99.3	93.8	5.8%

5.3.2 IFR with Reuse K

For IFR with reuse higher than one, analytical study is very similar to the previous one. The difference lies in the fact that only co-channel BS are considered in interference calculation and thus the half distance between base stations and BS density have to be modified. As a consequence, previous analysis results are still valid provided that R_c is replaced by $\sqrt{K}R_c$ and BS density is divided by K, i.e., ρ_{BS} is replaced by ρ_{BS}/K. Hence, using Eq. 5.2 and this new half distance between BS, SINR is given as:

$$\gamma(r) = \frac{r^{-\eta}(\eta - 2)}{2\pi \cdot \frac{\rho_{BS}}{K}(2\sqrt{K}R_c - r)^{2-\eta}}. \tag{5.13}$$

Using the same distance normalization as before (leading to the transformation of variable r to x) and after few manipulations, SINR can be written as:

$$\gamma_{IFRK}(x) = \frac{K\sqrt{3}}{\pi}(\eta - 2)(2\sqrt{K} - x)^{-2}(2\sqrt{K}/x - 1)^{\eta}. \tag{5.14}$$

Hence, spectral efficiency (in bps/Hz) for IFR reuse K can be given as:

$$C_{IFRK}(x) = \log_2[1 + \gamma_{IFRK}(x)]. \tag{5.15}$$

To validate the above approach, reuse 3 is considered as an example. Plot of SINR versus distance to BS for reuse 3 case, for both fluid model and simulation, is shown in Fig. 5.4. As expected SINR is higher than for reuse 1. However, bandwidth per cell equals one third the network bandwidth. Again, both analysis and simulation provide similar results. The fluid model is thus accurate not only for reuse 1 networks but also for higher reuse factors provided the parameters are adjusted.

As far as total cell data rate for three scheduling schemes is concerned, method used for IFR reuse 1 is still valid provided that $C_{IFR1}(x)$ is replaced by C_{IFR3} (Eq. 5.15) and cell bandwidth is divided by 3, in all calculations. Values of total cell data rate for fluid model and simulations are shown in Tab. 5.4, 5.5 and 5.6. In all cases, the difference between simulation and fluid model remains below 10% for η between 2.6 and 3.5.

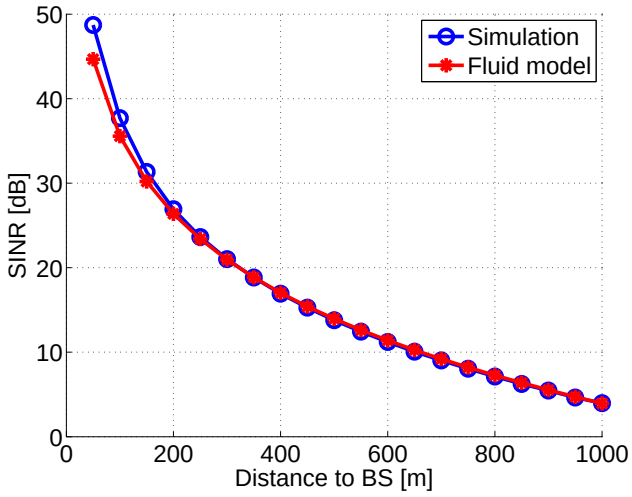

Figure 5.4: SINR vs distance to BS for IFR with reuse 3.

Table 5.4: Total cell data rate ($D_{T,IFR3}$) vs η (IFR reuse 3, BW=10/3 MHz, equal data rate).

η	$D_{T,IFR3}$ [Mbps]		**Difference**
	Fluid model	Simulation	
2.5	6.4	7.2	11.11%
2.6	7.55	7.95	5.03%
2.7	8.66	8.73	0.8%
2.8	9.74	9.55	1.99%
3	11.8	11.2	5.36%
3.1	12.8	12.0	6.67%
3.2	13.8	12.8	7.81%
3.5	16.7	15.2	9.87%

5.4 Fractional Frequency Reuse (FFR)

An example of FFR scenario is depicted in Fig. 5.5. As can be seen in the figure, cell space is divided into two regions, inner and outer. Inner region is a circular disk with radius $R_0 \leq R_c$ and the rest of the hexagon forms the outer region. Bandwidth is allocated to inner and outer in such a way that former incorporates frequency reuse 1 while the latter applies frequency reuse 3. As can be seen in Fig. 5.5, the network bandwidth W is equal to $W_0 + W_1 + W_2 + W_3$. It is also considered that $W_1 = W_2 = W_3$.

SINR versus distance with $R_0 = 0.7R_c$ for fluid model and simulation is given in Fig. 5.6. As expected FFR scheme improves radio quality at cell edge. Moreover, the results follow the previous positive trend, i.e., fluid model and simulations are in conformity.

Now we derive the expressions for total cell data rate assuming equal data rate, equal bandwidth and opportunist scheduling schemes. We also estimate the

Table 5.5: Total cell data rate ($D_{T,IFR3}$) vs η (IFR reuse 3, bandwidth=10/3 MHz, equal bandwidth).

η	$D_{T,IFR3}$ [Mbps]		Difference
	Fluid model	Simulation	
2.5	8.38	9.04	7.38%
2.6	9.63	9.91	2.81%
2.7	10.8	10.76	0.71%
2.8	12	11.7	3.04%
3	14.2	13.4	5.9%
3.1	15.3	14.4	6.55%
3.2	16.4	15.2	7.46%
3.5	19.4	17.8	8.8%

Table 5.6: Total cell data rate ($D_{T,IFR3}$) vs η (IFR reuse 3, bandwidth=10/3 MHz, opportunist).

η	$D_{T,IFR3}$ [Mbps]		Difference
	Fluid model	Simulation	
2.5	25.4	26	2.2%
2.6	27.8	28.0	0.7%
2.7	30	29.6	1.3%
2.8	32.2	31.5	2%
3	36.2	34.7	4.3%
3.1	38.2	36.6	4.4%
3.2	40.1	38.2	5.1%
3.5	45.7	43.4	5.4%

optimized inner region radius.

5.4.1 Equal Data Rate

To carry out total cell data rate, we first consider the inner circular region. Since for this region, frequency reuse is 1, the expression of SINR is given by Eq. 5.2 or equivalently by Eq. 5.3. Once again, it is considered that users are uniformly distributed in the cell space with $\rho_u = N_u/2\sqrt{3}R_c^2$. Since it is a circular region, the bandwidth of inner region is given as:

$$W_0 = \int_0^{R_0} W_u(r)\rho_u \, 2\pi r \, dr. \tag{5.16}$$

After replacing ρ_u by its value, transformation of variable r to x and using Eq. 5.5, we get

$$W_0 = \frac{\pi}{\sqrt{3}} D_u N_u \int_0^{R_0/R_c} \frac{x}{C_{IFR1}(x)} \, dx,$$

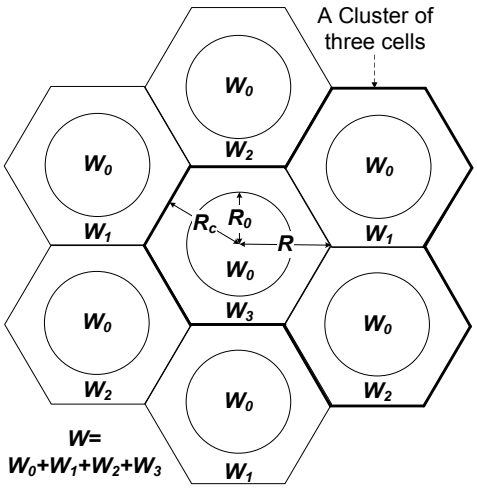

Figure 5.5: Fractional Frequency Reuse (FFR) case. Bandwidth W_0 is deployed with reuse 1 in the inner regions, while W_1, W_2 and W_3 are deployed with reuse 3 in outer regions.

where $C_{IFR1}(x)$ is given by Eq. 5.4. Let I_0 be the integral in the previous expression, so that $W_0 = \pi/\sqrt{3} I_0 D_u N_u$.

Let us now consider the outer area, which applies reuse 3. SINR for reuse 3 is given by Eq. 5.13 or equivalently by Eq. 5.14. In order to calculate the total bandwidth used in the outer region, double integral used in Eq. 5.6 is applied. With change of limits and replacing $W_u(r)$ by $W_{1,u}(r)$ we get:

$$W_1 = 12 \int_0^{\pi/6} \int_{R_0}^{R_c/\cos\theta} W_{1,u}(r) \rho_u \, r \, dr \, d\theta,$$

where $W_{1,u}(r)$, assuming equal data rate scheduling, is given as: $W_{1,u}(r) = D_u C_{IFR3}(r)$. After replacing ρ_u by its value and transformation of variable r to x, we get

$$W_1 = \frac{6}{\sqrt{3}} D_u N_u \int_0^{\pi/6} \int_{R_0/R_c}^{1/\cos\theta} \frac{x}{C_{IFR3}(x)} \, dx \, d\theta. \tag{5.17}$$

Let I_1 be the double integral in the previous expression, so that $W_1 = \frac{6}{\sqrt{3}} I_1 D_u N_u$.

Considering the fact that total network bandwidth is W with $W = W_0 + W_1 + W_2 + W_3$ and $W_1 = W_2 = W_3$ we can write: $W = W_0 + 3 \times W_1$. Finally using Eq. 5.16 and 5.17 and keeping in view that $D_T = D_u N_u$, we get expression of the total cell data rate $D_{T,FFR}$ for FFR case:

$$D_{T,FFR} = \frac{\sqrt{3} W}{\pi I_0 + 18 I_1}. \tag{5.18}$$

Total cell data rate calculation shows that fluid model and simulation differ by 5.6% with values of 13.2 Mbps and 12.5 Mbps respectively for 10 MHz of network bandwidth. Fig. 5.7 shows the total cell data rate as a function of the inner cell radius R_0. Both fluid model and simulations provide an optimum value of approximately 757 m.

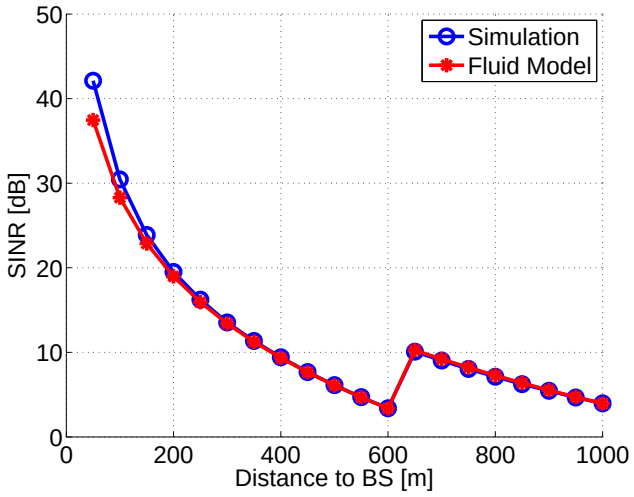

Figure 5.6: SINR vs distance to BS for FFR with $R_0 = 0.7R_c$.

5.4.2 Equal Bandwidth

To calculate cell data rate in this case, we adopt the same approach as was used in section 5.3.1.2 while considering $N_u W_u = W_0 + W_1$. By integrating the user data rate over inner circular region (using frequency reuse 1), total data rate of inner region is given as:

$$D_{T,Inner} = \frac{\pi(W_0 + W_1)}{\sqrt{3}} \int_0^{R_0/R_c} x C_{IFR1}(x)\, dx. \tag{5.19}$$

Similarly, assuming frequency reuse 3 for the outer region, total data rate of outer region is:

$$D_{T,Outer} = \frac{6(W_0 + W_1)}{\sqrt{3}} \int_0^{\pi/6} \int_{R_0/R_c}^{1/\cos\theta} x C_{IFR3}(x)\, dx\, d\theta, \tag{5.20}$$

and total cell data rate is the sum of inner and outer region data rates:

$$D_{T,FFR} = D_{T,Inner} + D_{T,Outer}. \tag{5.21}$$

Since this scheduling scheme assigns equal resources to all users (whether located in inner or outer region), the ratio of W_0 to W_1 should be proportional to number of users in two regions. But as we have assumed that users are uniformly distributed in cell space, this ratio should be equal to ratio of inner region area to outer region area:

$$\frac{W_1}{W_0} = \frac{2\sqrt{3}R_c^2}{\pi R_0} - 1, \tag{5.22}$$

and since $W_0 + 3W_1 = W$, it can be shown that:

$$W_1 = \frac{2\sqrt{3}R_c^2 - \pi R_0^2}{6\sqrt{3}R_c^2 - 2\pi R_0^2} W. \tag{5.23}$$

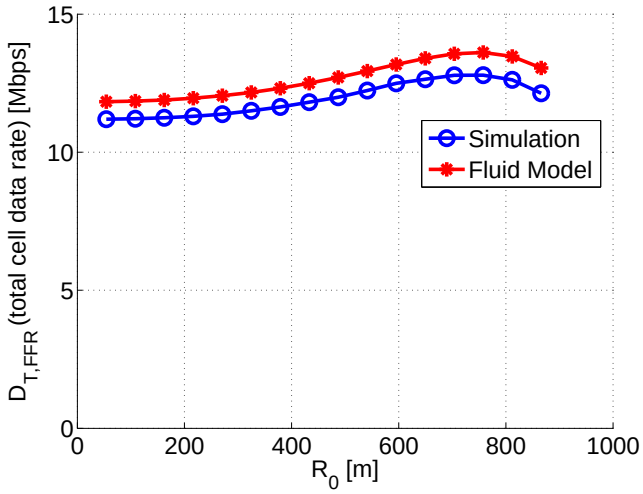

Figure 5.7: $D_{T,FFR}$ (total cell data rate) vs radius of inner region with equal data rate scheduling for FFR scheme. Maximum value occurs at $R_0 = 757\ m$ approx.

It can be made out from Eq. 5.23 that for every value of R_0, there is a specific value of W_1 and hence W_0. For different values of R_0, total cell data rate has been plotted in Fig. 5.8. It can be seen that maximum value of total cell data rate is for $R_0 = R_c$.

Tab. 5.2 and 5.5 have shown that IFR1 provides higher data rates than IFR3. In FFR, increasing R_0 and thus the bandwidth W_0 used with reuse 1, makes FFR closer to IFR1. On the contrary, decreasing R_0 makes FFR closer to IFR3. As a consequence, total cell data rate is maximum for the highest value of R_0.

5.4.3 Opportunist

For opportunist scheduling in FFR case, we assume that two users are simultaneously scheduled in a cell such that one user having the greatest SINR among inner region users and other one having the highest SINR among outer region users. If there is no user in any of the regions, bandwidth of that region goes unallocated. Following the methodology of section 5.3.1.3, for the inner region, PDF of the user's (nearest to the BS) distance, knowing there are $N_{u,i}$ users located in the inner region is given as:

$$p_{X,inner|N_{u,i}}(r) = \frac{2rN_{u,i}}{R_0^2}\left(1 - \frac{r^2}{R_0^2}\right)^{N_{u,i}-1},$$

or with substitution of r by x, the same PDF over small distance dx can be written as:

$$p_{X,inner|N_{u,i}}(x)\,dx = \frac{2xN_{u,i}}{(R_0/R_c)^2}\left(1 - \frac{x^2}{(R_0/R_c)^2}\right)^{N_{u,i}-1} dx.$$

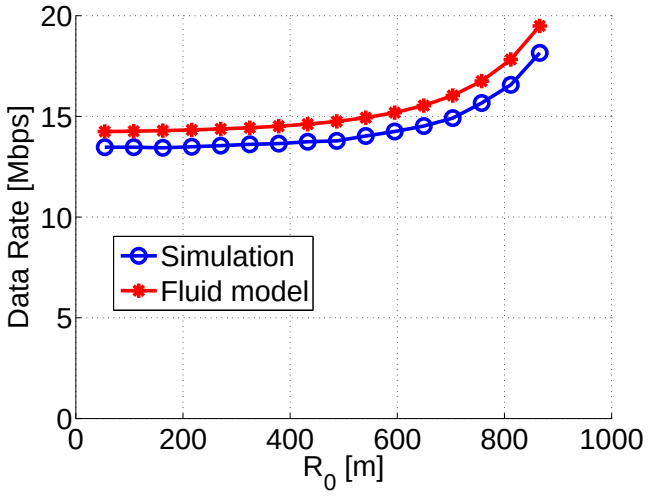

Figure 5.8: $D_{T,FFR}$ (total cell data rate) vs radius of inner region with equal bandwidth scheduling for FFR scheme. Maximum value occurs at $R_0 = R_c$.

Hence, the average spectral efficiency of inner region, given that there are $N_{u,i}$ located inside it, can be expressed by the following integral:

$$\bar{C}_{FFR,inner|N_{u,i}} = \int_0^{R_0/R_c} C_{IFR1}(x) p_{X,inner|N_{u,i}}(x)\, dx.$$

Similarly for the outer region, PDF of the user's (nearest to the BS) distance, knowing there are $N_{u,i}$ users located in the inner region is given as:

$$p_{X,outer|N_{u,i}}(r) = \frac{2\pi(N_u - N_{u,i})r}{2\sqrt{3}R_c^2 - \pi R_0^2}\left(1 - \frac{\pi r^2 - \pi R_0^2}{2\sqrt{3}R_c^2 - \pi R_0^2}\right)^{N_u - N_{u,i} - 1},$$

where $(N_u - N_{u,i})$ is the number of users in the outer region.

Once again with change of variable r to x, the PDF over small distance dx for outer region can be expressed as:

$$p_{X,outer|N_{u,i}}(x)\, dx = \frac{2\pi(N_u - N_{u,i})x}{2\sqrt{3} - \pi(R_0/R_c)^2}\left(1 - \frac{\pi x^2 - \pi(R_0/R_c)^2}{2\sqrt{3} - \pi(R_0/R_c)^2}\right)^{N_u - N_{u,i} - 1} dx,$$

and the average spectral efficiency for the outer region such that there are $N_{u,i}$ users in the inner region is given by following equation:

$$\bar{C}_{FFR,outer|N_{u,i}} = \int_{R_0/R_c}^{a} C_{IFR3}(x) p_{X,outer|N_{u,i}}(x)\, dx.$$

Note that in this latter equation, we approximate the hexagon by a disk of radius R_e. Finally, averaging the sum of data rates (of inner and outer regions) for all possible values of $N_{u,i}$ results in total cell data rate for FFR case:

$$D_{T,FFR} = \sum_{N_{u,i}=0}^{N_u} (W_0 \bar{C}_{FFR,inner|N_{u,i}} + W_1 \bar{C}_{FFR,outer|N_{u,i}}) P[N_{u,i}],$$

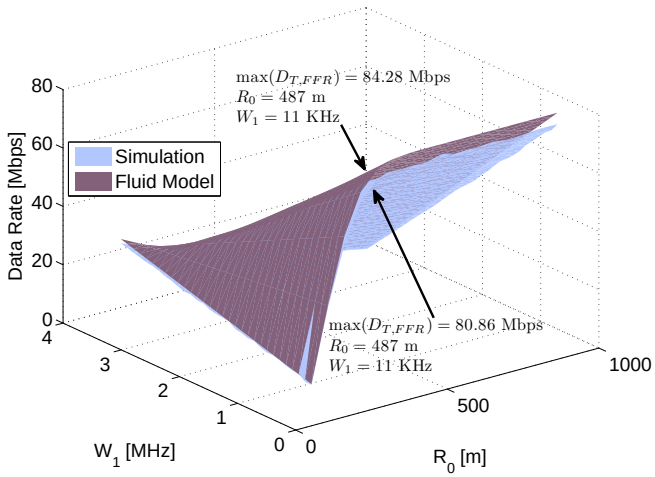

Figure 5.9: $D_{T,FFR}$ (total cell data rate) vs radius of inner region and vs bandwidth allocated in the outer region with opportunist scheduling for FFR scheme. Maximum value occurs at $R_0 = 487$ m and $W_1 = 11$ KHz.

where $P[N_{u,i}]$ is the probability that there are $N_{u,i}$ out of N_u users in the inner region:

$$P[N_{u,i}] = \left(\frac{\pi R_0^2}{2\sqrt{3}R_c^2}\right)^{N_{u,i}} \left(1 - \frac{\pi R_0^2}{2\sqrt{3}R_c^2}\right)^{N_u - N_{u,i}} \binom{N_u}{N_{u,i}}.$$

The total cell data rate (for FFR scheme) as a function of different values of W_1 and R_0 is shown in Fig. 5.9. Maximum value of total cell data rate can be observed for a value of $W_1 = 11$ KHz (i.e., one subcarrier) and $R_0 = 487$ m for both the simulation and fluid model. The maximum difference between simulation and analytical model results for all values of W_1 and R_0 is found to be 6.7%.

5.5 Two Level Power Control (TLPC)

In previous section, we discussed the concept of FFR in OFDMA and we have shown that SINR could be improved by using a reuse 3 pattern in cell outer regions. With FFR, it is however not possible to use full network bandwidth in a cell, which reduces the overall cell bandwidth.

To overcome this drawback, it is possible to adopt a reuse 1 pattern while using a Two Level Power Control (TLPC) mechanism to improve the radio quality in the outer region. The TLPC scheme is shown in Fig. 5.10. Total bandwidth in a cell (equal to network bandwidth) is divided into three equal parts: two parts allocated to inner region and one to the outer region. The output power per subcarrier in the inner region is P_i and that in the outer region is P_o. These two values of power are related as: $P_o = \delta P_i$, such that $\delta \geq 1$. The three spectrum parts W_1, W_2 and W_3 alternate from cell to cell in such a way that there is a pseudo-reuse 3 scheme in outer regions. Neighboring cells contribute to

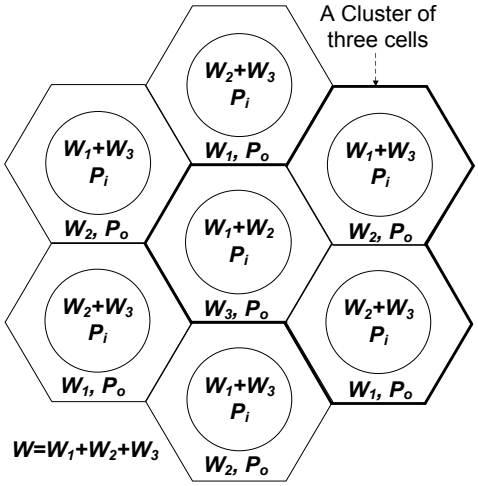

Figure 5.10: Two level power control case. Bandwidth W is partitioned into three equal parts, i.e., $W_1 = W_2 = W_3$.

interference in the outer region but with a reduced power P_i. As a consequence, the total network bandwidth is used in every cell but interference is expected to be reduced in outer regions.

Let us calculate SINR for inner and outer region of this two level power control network. For a user in the outer region (using e.g. W_3 in the center cell in Fig. 5.10), we divide the interference into two categories. One is from the cells using same subcarriers in the outer region and we represent it by I_{outer}. Other is from cells using same subcarriers in the inner region (neighboring cells) and is represented by I_{inner}. Then, SINR for a subcarrier in the outer region can be written as:

$$\frac{1}{\gamma_{TLPC,outer}} = \frac{I_{inner}}{P_o A r^{-\eta}} + \frac{I_{outer}}{P_o A r^{-\eta}}. \tag{5.24}$$

In order to find the values of I_{inner} and I_{outer}, consider that $\mathcal{B}_{outer}$ represents the set of BS causing I_{outer}. For a user u in outer region of a cell b, I_{outer} is given as:

$$I_{outer} = P_o A \sum_{j=1, j\in\mathcal{B}_{outer}}^{N_{BS}} r_{j,u}^{-\eta}. \tag{5.25}$$

As outer regions of BS in $\mathcal{B}_{outer}$ form together a reuse 3 scheme, the second term of right-hand side of Eq. 5.24 is simply $1/\gamma_{IFR3}$.

Adding up the interference from all network cells, I_{inner} can be written as:

$$I_{inner} = P_i A \sum_{j=1, j\neq b}^{N_{BS}} r_{j,u}^{-\eta} - P_i A \sum_{j=1, j\in\mathcal{B}_{outer}}^{N_{BS}} r_{j,u}^{-\eta}. \tag{5.26}$$

Thus, considering $\delta = P_o/P_i$:

$$\frac{I_{inner}}{P_o A r^{-\eta}} = \frac{1}{\delta}\frac{1}{\gamma_{IFR1}} - \frac{1}{\delta}\frac{1}{\gamma_{IFR3}}. \tag{5.27}$$

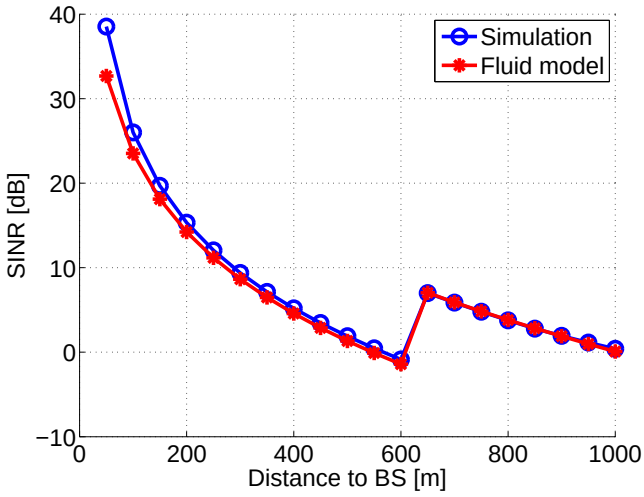

Figure 5.11: SINR vs distance to BS for TLPC scheme with $R_0 = 0.7R_c$ and $\delta = 5$.

Combining previous results, we can rewrite Eq. 5.24 as:

$$\frac{1}{\gamma_{TLPC,outer}} = \frac{1}{\delta}\frac{1}{\gamma_{IFR1}} + (1 - \frac{1}{\delta})\frac{1}{\gamma_{IFR3}}. \tag{5.28}$$

Now we find out SINR expression for inner region. Consider the central cell of Fig. 5.10, in which W_1 and W_2 are allocated to inner region and W_3 is used in the outer region. A user in inner region will be allocated a subcarrier that will either belong to W_1 or W_2. If we look at the bandwidth utilized in the six neighboring cells of center cell, we notice that out of six, three are transmitting on the same subcarrier with power P_o, while the other three with P_i. Hence, SINR for this inner region subcarrier can be approximated while considering that neighboring cells transmit with average power $(P_i + P_o)/2$.

$$\gamma_{TLPC,inner}(r) \approx \frac{P_i A r_{b,u}^{-\eta}}{\frac{P_o+P_i}{2} A \sum_{j=1,j\neq b}^{N_{BS}} r_{j,u}^{-\eta}} = \frac{2}{1+\delta}\gamma_{IFR1}. \tag{5.29}$$

Using the values of SINR for outer and inner regions, spectral efficiencies for two regions are given in Eq. 5.30 and 5.31.

$$C_{TLPC,inner} = \log_2(1 + \gamma_{TLPC,inner}), \tag{5.30}$$

$$C_{TLPC,outer} = \log_2(1 + \gamma_{TLPC,outer}). \tag{5.31}$$

To verify the above results, SINR vs distance to BS (with $R_0 = 0.7R_c$ and $\delta = 5$) is given in Fig. 5.11. As expected, radio quality is improved in outer region with TLPC compared to the IFR1 case in a similar way does the FFR. Let us now compare total cell data rates.

In order to calculate data rate for inner and outer regions for three scheduling schemes, we assume that in Fig. 5.10, $W_1 = W_2 = W_3$. We start with equal data rate scheduling scheme.

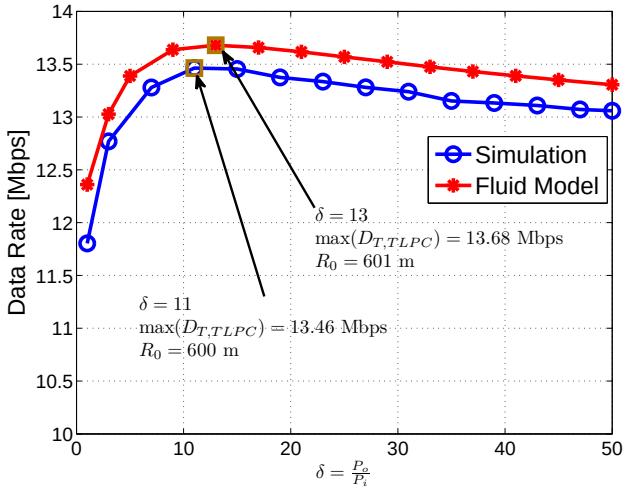

Figure 5.12: Total cell data rate vs different values of δ with equal data rate scheduling for TLPC scheme.

5.5.1 Equal Data Rate

Using the similar approach of section 5.4, we can write:

$$W_1 + W_2 = \frac{2W}{3} = \frac{\pi}{\sqrt{3}} D_{u,inner} N_u \int_0^{R_0/R_c} \frac{x dx}{C_{TLPC,inner}(x)},$$

and

$$W_3 = \frac{W}{3} = \frac{6}{\sqrt{3}} D_{u,outer} N_u \int_0^{\pi/6} \int_{R_0/R_c}^{1/\cos\theta} \frac{x}{C_{TLPC,outer}(x)} \, dx \, d\theta.$$

Using the above two equations, we can write the ratio between data per user for inner and outer regions as:

$$\frac{D_{u,inner}}{D_{u,outer}} = \frac{12}{\pi} \frac{\int_0^{\pi/6} \int_{R_0/R_c}^{1/\cos\theta} \frac{x}{C_{TLPC,outer}(x)} \, dx \, d\theta}{\int_0^{R_0/R_c} \frac{x}{C_{TLPC,inner}(x)} \, dx}.$$

Now, if we assume an equal data rate scheduler, $\frac{D_{u,inner}}{D_{u,outer}}$ should be equal to one. For a given value of δ, there exists a unique value of R_0 for which the above condition is satisfied. In Fig. 5.12, total cell data rate satisfying equal data rate scheme has been plotted for various values of δ. It is clear that for small values of δ, total cell data rate increases with increasing values of δ. The total cell data rate attains its maximum value of 13.68 Mbps for $\delta = 13.2$. Beyond $\delta = 13.2$ (or 11.2 dB), the total cell data rate starts decreasing. The corresponding values of R_0 for these total cell data rates are given in Fig. 5.13. The figure shows that R_0 is a decreasing function of δ. The value of R_0 corresponding to maximum value of cell data rate is approximately 600 m.

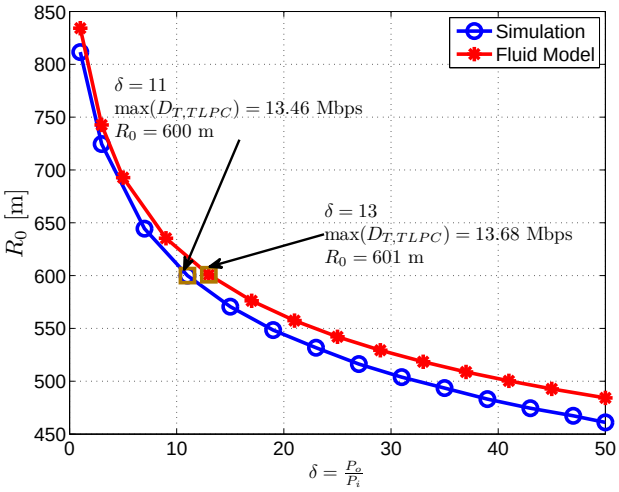

Figure 5.13: R_0 (radius of inner region that guarantees equal data rate among users) vs different values of δ for TLPC scheme.

5.5.2 Equal Bandwidth

With equal bandwidth allocation, the bandwidth of inner and outer regions should be proportional to areas of the two regions (cf. section 5.4.2) and since for TLPC schemes bandwidth of inner and outer regions are fixed, there exists a unique value of R_0 satisfying the two conditions.

$$\frac{W_3}{W_1 + W_2} = \frac{2\sqrt{3}R_c^2}{\pi R_0^2} - 1,$$

with $W_1 = W_2 = W_3 = W/3$,

$$R_0 = \frac{2}{\sqrt{\pi\sqrt{3}}} R_c.$$

Now the total data rate of inner region is given by Eq. 5.32:

$$D_{T,Inner} = \frac{\pi W}{\sqrt{3}} \int_0^{R_0/R_c} x C_{TLPC,inner}(x)\, dx. \tag{5.32}$$

Similarly total data rate for outer region is given as:

$$D_{T,Outer} = \frac{6W}{\sqrt{3}} \int_0^{\pi/6} \int_{R_0/R_c}^{1/\cos\theta} x C_{TLPC,outer}(x)\, dx\, d\theta. \tag{5.33}$$

Total cell data rate is the sum of total data rates of two regions:

$$D_{T,TLPC} = D_{T,Inner} + D_{T,Outer}. \tag{5.34}$$

A comparison of simulation and fluid model $D_{T,TLPC}$ values, as function of δ values, is shown in Fig. 5.14 which shows a close proximity between the two curves.

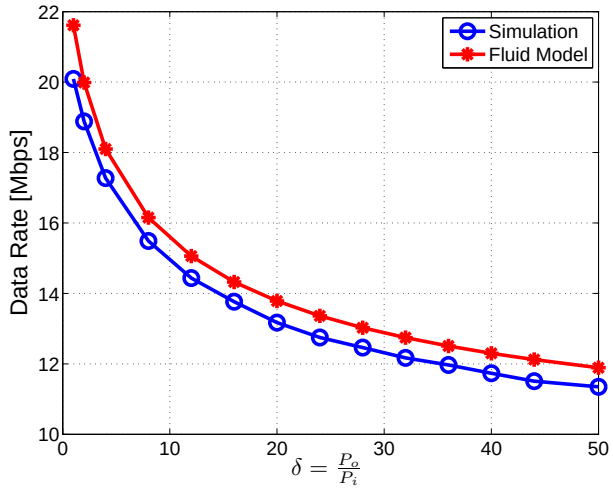

Figure 5.14: Total cell data rate vs different values of δ with equal bandwidth scheduling for TLPC scheme.

5.5.3 Opportunist

The computation of cell data rate is similar to the method used in section 5.4.3. However, in this case, inner bandwidth is $2W/3$, outer bandwidth is $W/3$ and average spectral efficiency for TLPC is used:

$$D_{T,TLPC} = \sum_{N_{u,i}=0}^{N_u} (\frac{2W}{3}\bar{C}_{TLPC,inner|N_{u,i}} + \frac{W}{3}\bar{C}_{TLPC,outer|N_{u,i}})P[N_{u,i}].$$

The results of simulation and fluid model are compared in Fig. 5.15. Total cell data rates are plotted as functions of R_0 and δ. The maximum cell data rate is found to be for $R_0 = 270$ m and $\delta = 1$ for both the simulation and fluid model. The maximum difference between the values of total cell data rates with simulation and fluid model is 7.23%.

5.6 Comparison of Reuse Schemes and Scheduling Policies

In previous sections, we have established through validation that analytical approach based on the fluid model can be used for IFR, FFR and TLPC schemes while considering three different scheduling types: equal data rate, equal bandwidth and opportunist. In this section, we present a comparison between these three reuse schemes and the three scheduling policies by applying fluid model.

If we look at Fig. 5.16, it can be deduced that IFR with reuse 3 shows the best performance in terms of SINR values. IFR reuse 1 is much lower than IFR reuse 3 in terms of radio quality. FFR exactly follows IFR reuse 1 curve until R_0 and IFR reuse 3 onwards. Compared to IFR reuse 1, TLPC improves SINR in outer region at the expense of a degraded radio quality in inner region.

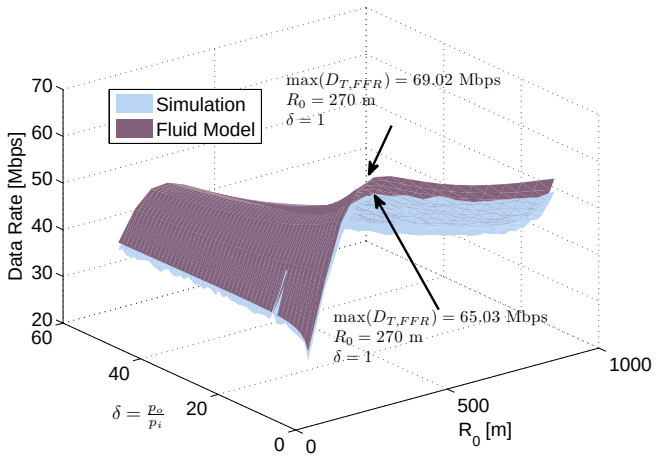

Figure 5.15: $D_{T,TLPC}$ (total cell data rate) vs radius of inner region and δ with opportunist scheduling for TLPC scheme. Maximum value occurs at $R_0 = 270$ m and $\delta = 1$.

Table 5.7: Total cell data rate (D_T) comparison of three reuse schemes and three scheduling policies with $\eta = 3$ and bandwidth=10 MHz.

Frequency Reuse Scheme	**D_T [Mbps]**		
	equal data rate	**equal bandwidth**	**opportunist ($N_u = 30$)**
FFR	13.61 ($R_0 = 757\ m$)	19.5 ($R_0 = R_c$)	84.28 ($W_1 = 11$ KHz, $R_0 = 487$ m)
TLPC	13.68 ($\delta = 13.2$, $R_0 = 600$ m)	21.6 ($\delta = 1$, $R_0 = 742$ m)	69.02 ($\delta = 1$, $R_0 = 270$ m)
IFR, Reuse 1	12.4	21.6	84.5
IFR, Reuse 3	11.8	14.2	36.2

We now compare total cell data rates for all frequency reuse schemes in the presence of three scheduling algorithms. Total cell data rates in FFR may depend upon value of R_0 and W_1. The same applies to TLPC w.r.t. parameters R_0 and δ. For these two schemes, maximum possible value of total cell data rate, based on optimal values of their parameters, has been considered in the comparison. These optimal values are presented aside with values of data rates (see Tab. 5.7).

The value of network bandwidth is 10 MHz. The number of users per cell N_u is considered to be thirty in all cases. Path-loss constant η is taken as three. Results of cell data rate are listed in Tab. 5.7.

With equal data rate, IFR3 touches the lowest performance although SINR values are greater. This is due to the fact that utilization of network bandwidth per cell is lower as compared to other schemes. TLPC has the maximum value with $\delta = 13.2$ and has a comparable performance w.r.t. FFR (with $R_0 = 757$ m). Hence, by applying TLPC and FFR schemes, we can diminish the problem of reduced radio quality (SINR) in the case of IFR1 in the border region of the cell. At the same time, bandwidth is more efficiently utilized than with IFR3. Due to

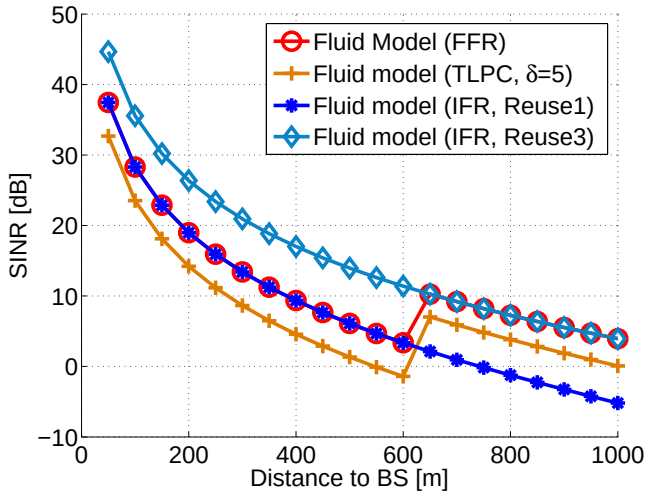

Figure 5.16: SINR vs distance to BS for three reuse schemes.

its simplicity, FFR could be preferred to TLPC with equal data rate scheduling.

An equal bandwidth scheduling aims at improving resource utilization (compared to equal data rate scheduling) while ensuring resource allocation to every user (on the contrary to opportunist scheduling). So, for all reuse schemes, total cell data rate is in between two other schemes. With equal bandwidth, IFR1 achieves the highest cell capacity because it benefits from the usage of total network bandwidth in every cell. Although SINR values are higher with IFR3, this scheme allocates only one third of the total network bandwidth to each cell, this explains again the lower achieved performance.

FFR and TLPC cannot do better than IFR1 and reach their maximum value for a set of parameters that makes them very close to IFR1. With FFR, setting $R_0 = R_c$ makes most of the bandwidth to be used with reuse 1. A higher radio quality at cell border is obtained at the price of a small reduction of the total cell data rate compared to IFR1. With TLPC, setting $\delta = 1$ reduces almost this scheme to IFR1.

Total cell data rate obtained with opportunist scheduling provides an upper bound (for a given number of users) on the cell performance at the price of fairness. Except in TLPC, only the best user is served and gets the whole bandwidth. IFR1 achieves once again the highest cell data rate. FFR tends towards IFR1 with very small bandwidth being allocated to the outer region. The choice of scheduling two users (one in the inner region, one in the outer) reduces the performance of TLPC compared to IFR1 since part of the bandwidth is allocated to a user a bit far from the BS.

Fig. 5.17, 5.18 and 5.19 show the total cell data rate as a function of the path-loss exponent for the three frequency reuse schemes and the three scheduling policies. It can be noticed that the hierarchy between frequency reuse schemes observed with $\eta = 3$ still holds for η between 2.6 and 3.6. For equal data rate scheduling, the advantage of TLPC over FFR is a bit more pronounced when η

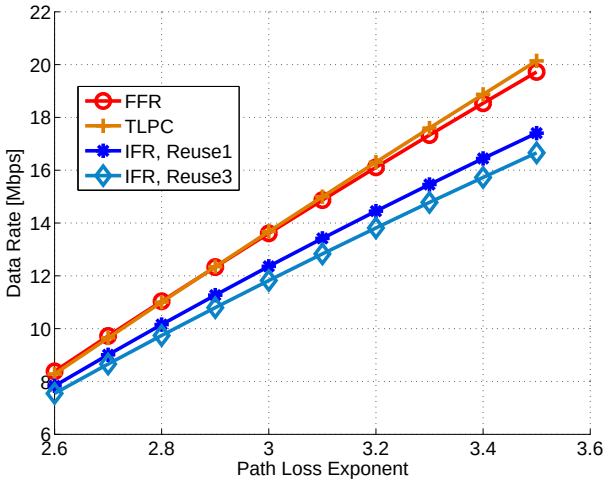

Figure 5.17: Data rate vs path-loss exponent with equal data rate scheduling for three reuse schemes.

increases. However, the main result is that in all cases, the total cell data rate increases linearly as a function of path-loss exponent.

5.7 Conclusions

In this chapter, we have presented an analytical approach, based on the fluid model, for analyzing OFDMA based networks. We have shown that our proposed technique is very flexible and can be used in different frequency reuse scenarios. We have introduced expressions of SINR and cell data rate for IFR, FFR and TLPC schemes and taking into account equal data rate, equal bandwidth and opportunist scheduling types. We have also validated our technique by comparing its results with those obtained from Monte Carlo simulations. Time required to obtain results with our analytical technique is however much shorter. We have shown that our proposed technique gives a fairly good performance for η values between 2.6 and 3.5 which is a range found in most of the practical scenarios. A comparison of the above three schemes is also provided. For each scheduling type, we have established the frequency reuse scheme which provides the maximum cell data rate.

After dealing with static analysis in radio coverage and capacity study, in the last part of the thesis, we take into account the dynamic system and discuss the traffic modeling issue. The analytical models for Best Effort (BE) traffic in a WiMAX system are presented in the next chapter. These models take into account different scheduling schemes and are validated through Monte Carlo simulations.

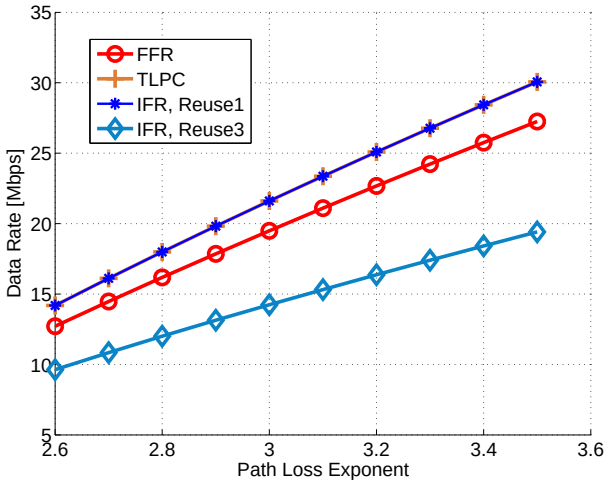

Figure 5.18: Data rate vs path-loss exponent with equal bandwidth scheduling for three reuse schemes.

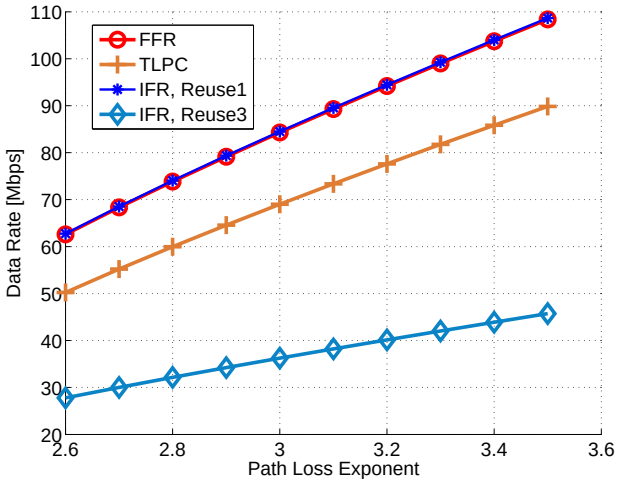

Figure 5.19: Data rate vs path-loss exponent with opportunist scheduling for three reuse schemes.

Chapter 6

Validation of Best Effort Traffic Models for WiMAX Networks

The work presented in previous chapters considered a static system. However, dynamics of a system complement the overall picture of dimensioning. Hence, in this chapter, we take into account a dynamic system which admits as an input the stationary probabilities of MCS from the static system. This analysis takes into account the nature of traffic and different QoS traffic classes of WiMAX.

The study in this chapter was carried out in collaboration with Laboratoire d'informatique de Paris 6 (LIP6). Our major contribution was validation and robustness study of analytical models for WiMAX Best Effort (BE) traffic presented in [19, 20, 21, 22]. Hence, in this thesis, we explain the validation and robustness analysis of these models for which a simulator was developed to carry out Monte Carlo simulations. To make a connection, key expressions of analytical models are briefly introduced in this thesis. These analytical models take into account mono/multi-profile Best Effort (BE) traffic where a profile is a set of parameters that represent a class of BE traffic. Four different scheduling schemes are also considered during the formulation of analytical models.

6.1 Introduction

WiMAX can accommodate various traffic types. For this purpose, different service categories have been introduced for WiMAX networks. For example, BE is a service category that could handle web traffic. A detailed account of simulation based BE traffic performance evaluation in WiMAX networks can be found in [71, 72]. Kim and Yeom in [71] have presented two bandwidth (resource) allocation schemes, keeping in view the bandwidth request mechanism, for BE traffic in WiMAX networks. They have also compared these two schemes with a scheme that works without bandwidth request mechanism. Authors of [72] have put forward a fair resource scheduling scheme for BE traffic and have analyzed the system performance with the help of simulations. In [73], authors have proposed a Weighted Proportional Fair (WPF) scheduling for BE traffic of WiMAX. Ana-

lytical expressions have been derived for different performance metrics. Authors have not compared their proposed scheme with any classical scheduling scheme (e.g., opportunist scheduling).

While considering the BE traffic, users may generate traffic of different profiles (characterized by the volume of data generated and reading time). Authors of [74] have studied the performance of multi-profile internet traffic for a WiMAX cell using packet level simulations. They have evaluated the throughput performance in a cell while considering the number of users, modulation schemes to be used by users and data rate required by users using System Level Simulation (SLS). In [75], a measurement based procedure has been adopted to evaluate the performance of fixed WiMAX network in presence of multi-profile best effort traffic. Niyato and Hossain [76] formulate the bandwidth allocation of multiple services with different QoS requirements by using linear programming. They also propose performance analysis, first at connection level, and then, at packet level. In the former case, variations of the radio channel are however not taken into account. In the latter case, the computation of performance measures rely on multidimensional Markovian model that requires numerical resolution.

BE traffic is characterized by its QoS parameters. One of these parameters is the maximum sustained traffic rate (MSTR). As defined in [26] (section 11.13.6), this is not the guaranteed rate but an upper bound. The procedure to implement this rate has been left open in the standard. Mean information rate (MIR), a notion similar to MSTR, has been introduced in [74]. Authors have studied the performance of multi-profile internet traffic in presence of different MIR values for a WiMAX cell. They have used packet level simulations to evaluate the cell throughput performance for different number of users while considering possibility of multiple modulation schemes.

In this chapter, we present analytical models (based on [19, 20, 21, 22]) for WiMAX BE traffic with considerations of mono/multi-profile traffic, different scheduling schemes and parameter MSTR. We first introduce analytical models for mono-profile BE traffic. Four scheduling schemes have been taken into account. Three of these scheduling schemes are the conventional ones and the fourth one has been devised to implement MSTR. The three conventional scheduling schemes are: throughput fairness, resource fairness and opportunist. The fourth one has been named as throttling policy. The extensions of these models for multi-profile traffic are also included in this chapter. The rest of the chapter has been arranged as follows.

In section 6.2, BE traffic model with mono-profile is discussed. A brief introduction of analytical models for conventional and throttling schemes is given. The validation part is discussed in detail. The multi-profile model is presented in section 6.3. Key aspects of multi-profile analytical model are given in the beginning of this section. The difference in validation study w.r.t. mono-profile have been highlighted. The last section 6.4 gives the conclusion of this chapter. To facilitate the reader, all figures showing simulation results have been shifted to the end of chapter.

6.2 Best Effort (BE) Mono-profile

In this section, a brief account of the mono-profile BE traffic model being proposed for WiMAX is given. To start with, few points are established.

- The population of MS in a cell is represented by N, that includes both active (in process of data download) and inactive (finished with a download till the next one starts) MS.
- Each mobile station (out of N) is assumed to generate an infinite length ON/OFF elastic traffic. An ON period corresponds to the download of an element (e.g., a web page). The ON periods are characterized by data volume (i.e., number of bits). The MS in ON period are called active and those in OFF period are inactive. Each ON period is followed by an OFF period (reading time) which is characterized by its duration.
- There are N_S slots in the downlink part of a WiMAX Time Division Duplex (TDD) frame.
- Based on its radio channel conditions, an active MS chooses one Modulation and Coding Scheme (MCS) out of K (such that $0 \leq k \leq K$) different possible ones. A slot can carry m_k bits with a MCS type k. Without loss of generality, MCS type 0 represents outage state i.e., channel conditions of MS are so bad that it is not able to receive/transmit any data. Hence we take $m_0 = 0$.
- A MS can switch its MCS after every frame i.e., channel may change after every frame.
- The number of MS, that can simultaneously be multiplexed into one TDD frame, is not limited. Hence, any connection demand will be accepted and no blocking can occur.
- There is also no limit on number of slots that a MS can be allocated in a TDD frame.

6.2.1 Markovian Model

The proposed analytical model for BE traffic of WiMAX is based on a Continuous Time Markov Chain (CTMC) made of $N + 1$ states. This CTMC is shown in Fig. 6.1.

Following are key attributes of the CTMC:

- A state n of this chain ($0 \leq n \leq N$) corresponds to the total number of active MS (i.e., MS that are in ON period) at a given instant .

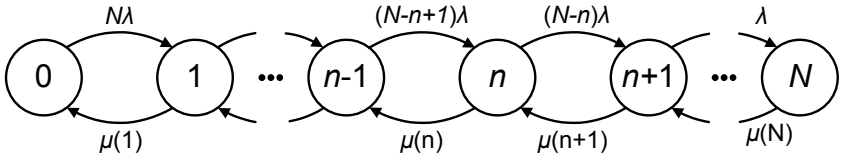

Figure 6.1: CTMC with departure rate depending upon active number of MS.

- A transition out of a generic state n to a state $n+1$ occurs when a mobile in OFF period ends its reading task and enters the ON period for data transfer. At any given instant this *arrival* transition is performed with a rate $(N-n)\lambda$, where λ is the rate corresponding to one MS ending its OFF period and is given as: $\lambda = 1/\bar{t}_{off}$. Here $\bar{t}_{off}$ represents the average OFF period.

- The departure from a state n to a state $n-1$ occurs when a mobile, in ON period, completes its transfer. If there are n active MS at a given time, this *departure* transition is performed with a rate $\mu(n)$. Since the MCS used by all active MS may not be the same, the ON period does not only depend upon the data volume to be downloaded but also the used MCS (out of $0 \leq k \leq K$). This departure rate is also scheduling method specific. Next we present the expressions for departure rate and performance parameters of conventional and throttling schemes.

6.2.2 Conventional Scheduling Schemes

Three conventional scheduling schemes (throughput fairness, resource fairness and opportunist) are considered for analytical modeling of BE traffic. The generic expression for departure rate for these three schemes is given as:

$$\mu(n) = \frac{\bar{m}(n) N_S}{\bar{x}_{on}\, T_F}, \tag{6.1}$$

where T_F is the duration of WiMAX TDD frame, $\bar{x}_{on}$ is the average volume of data in bits (e.g., size of a web page) and $\bar{m}(n)$ is the average number of bits per slot (average number of bits carried by every slot) when there are n active MS during a TDD frame. The value of $\bar{m}(n)$ depends upon probabilities of K different MCS represented by p_k (such that $0 \leq k \leq K$) and the scheduling scheme. Now we present the equations for average number of bits per slot for three conventional scheduling schemes. A brief introduction of each scheduling scheme has also been included.

6.2.2.1 Resource Fairness

For this type of scheduling policy, the scheduler equally shares the N_S slots among the active users that are not in outage during a TDD frame. The resultant data

to be downloaded by a MS during a TDD frame depends upon the MCS used by it. The average number of bits per slot for this scheduling scheme is given as:

$$\bar{m}(n) = \sum_{\substack{(j_0, j_1, ..., j_K) = (0,0,...,0)| \\ j_0 + j_1 + ... + j_K = n \\ j_0 \neq n}}^{(n,n,...,n)} \frac{n!}{n - j_0} \left(\sum_{k=1}^{K} m_k j_k \right) \left(\prod_{k=0}^{K} \frac{p_k^{j_k}}{j_k!} \right), \tag{6.2}$$

where j_k is the number of active MS using MCS_k and p_k is the steady state probability of the same MCS.

6.2.2.2 Throughput Fairness

With throughput fairness scheduling, slots are shared in a way that same instantaneous throughput is attained by all active users which are not in outage. Hence, MS using MCS with low bits per slot are assigned more slots as compared to the ones using a MCS with high bits per slot during a TDD frame. The resultant average number of bits per slot is given as:

$$\bar{m}(n) = \sum_{\substack{(j_0, j_1, ..., j_K) = (0,0,...,0)| \\ j_0 + j_1 + ... + j_K = n \\ j_0 \neq n}}^{(n,n,...,n)} \frac{(n - j_0)\, n! \prod_{k=0}^{K} \frac{p_k^{j_k}}{j_k!}}{\sum_{k=1}^{K} \frac{j_k}{m_k}}. \tag{6.3}$$

6.2.2.3 Opportunist

While considering the opportunist scheduling, all the slots are assigned to an active MS using the best MCS (with the highest bit rate per slot) among all active MS. If, however, more than one active MS are using the same best MCS, slots are equally partitioned among them. The average number of bits per slot for this scheduling policy is given as:

$$\bar{m}(n) = \sum_{i=1}^{K} \alpha_i(n) m_i, \tag{6.4}$$

where $\alpha_i(n)$ is the probability of having at least one active user (among n) using MCS_i and none using a MCS giving higher transmission rates (i.e. MCS_j with $j > i$). In fact, $\alpha_i(n)$ corresponds to the probability that the scheduler gives at a given time-step all the slots to MS that use MCS_i.

In order to calculate the $\alpha_i(n)$, we first express $p_{\leq i}(n)$, the probability that there are no mobiles using a MCS higher than MCS_i:

$$p_{\leq i}(n) = \left(1 - \sum_{j=i+1}^{K} p_j\right)^n. \tag{6.5}$$

Then, we calculate $p_{=i}(n)$, the probability that there is at least one mobile using MCS_i conditioned by the fact that there are no mobiles using a better MCS:

$$p_{=i}(n) = 1 - \left(1 - \frac{p_i}{\sum_{j=0}^{i} p_j}\right)^n. \tag{6.6}$$

Thus $\alpha_i(n)$ can be expressed as:

$$\alpha_i(n) = p_{=i}(n)\, p_{\leq i}(n). \tag{6.7}$$

6.2.2.4 Performance Parameters

There are three performance parameters for which formulae could be derived from the model. These parameters are: average instantaneous resource utilization (of TDD frame) $\bar{U}$, average number of an active user $\bar{Q}$ and average instantaneous user throughput during ON period $\bar{X}$. Same expressions for performance parameters are used for three scheduling schemes mentioned in section 6.2.2 by just using the associated expression for average number of bits per slot $\bar{m}(n)$ for each of the scheduling schemes.

In order to find the expressions for these parameters, stationary state probabilities of CTMC states are required. The steady state probability $\pi(n)$ is the probability that n mobile stations are active at any instant and is given by following equation.

$$\pi(n) = \frac{N!}{(N-n)!} \frac{\rho^n}{N_S^n \prod_{i=1}^{n} \bar{m}(i)} \pi(0), \tag{6.8}$$

where ρ is given by:

$$\rho = \frac{\bar{x}_{on}\, T_F}{\bar{t}_{off}}, \tag{6.9}$$

and $\pi(0)$ is given by Eq. 6.10 (as obtained through normalization):

$$\pi(0) = \frac{1}{1 + \sum_{n=1}^{N} \left(\prod_{i=1}^{n} \frac{(i-1)\,\lambda}{\mu(i)} \right)}. \tag{6.10}$$

Using these steady state probabilities, the expressions for three performance parameters can be obtained. Here we present these expressions in a sequential manner.

The average instantaneous resource utilization (of TDD frame) is give as:

$$\bar{U} = \sum_{n=1}^{N} \pi(n) \min\left(n \frac{\bar{x}_{on}}{N_S\, \bar{m}(n)}, 1 \right). \tag{6.11}$$

The average number of active MS is expressed as:

$$\bar{Q} = \sum_{n=1}^{N} n\,\pi(n). \tag{6.12}$$

In order to obtain the third performance parameter, average instantaneous user throughput during ON period, the mean number of departures (MS completing their transfer) per unit time is required which is represented by $\bar{X}_d$ and is given by the following equation:

$$\bar{X}_d = \sum_{n=1}^{N} \pi(n)\, N_S\, \mu(n). \tag{6.13}$$

Using Little's law, we can now derive the average duration $\bar{t}_{on}$ of an ON period (average duration of a transfer):

$$\bar{t}_{on} = \frac{\bar{Q}}{\bar{X}_d}. \tag{6.14}$$

Finally, the average instantaneous user throughput during ON period is given as:

$$\bar{X} = \frac{\bar{x}_{on}}{\bar{t}_{on}}. \tag{6.15}$$

6.2.3 Throttling Scheme

The implementation of MSTR is carried out using a scheduling policy called *throttling scheme* and has been proposed in [21]. In this scheduling policy, there is a limit on maximum achievable instantaneous user throughput and in a TDD frame, the user can be allocated only the number of slots required to guarantee its MSTR. We first present the expression for departure rate $\mu(n)$ for this scheduling scheme and then derive the performance parameters.

In order to find the departure rate $\mu(n)$, following points are to be kept in consideration:

- When a MS is in outage, it is unable to receive any data. In order to compensate for that, an increased instantaneous bit rate called Delivered Bit Rate (DBR) is introduced which is given as:

$$DBR = \frac{MSTR}{1 - p_0}.$$

- The number of slots per frame g_k required by a MS, using MCS_k, to attain its DBR is found as:

$$g_k = \frac{DBR\, T_F}{m_k},$$

given that $g_0 = 0$.

- The average number of slots per frame $\bar{g}$ required by a MS, using K different MCS, to realize its MSTR can thus be determined as:

$$\bar{g} = \sum_{k=1}^{K} p_k g_k.$$

Once $\bar{g}$ is obtained, the departure rate of throttling scheme is given as:

$$\mu(n) = \frac{N_S}{max\left(n\bar{g}, N_S\right)} n \frac{MSTR}{\bar{x}_{on}}. \tag{6.16}$$

In the next step, using this departure rate, we find the performance parameters for the throttling policy.

6.2.3.1 Performance Parameters

The steady state probability $\pi(n)$ can be obtained from death-and-birth process of Markov Chain as follows:

$$\pi(n) = \frac{N!}{(N-n)!} \frac{\rho^n}{n! \prod_{i=1}^{n} \frac{N_S}{max(i\bar{g}, N_S)}} \pi(0), \tag{6.17}$$

where $\rho = \frac{\bar{x}_{on}}{\bar{t}_{off} MSTR}$ and $\pi(0)$ is obtained through normalization.

The average number of active users can now be written as:

$$\bar{Q} = \sum_{n=1}^{N} n\, \pi(n). \tag{6.18}$$

In order to calculate average throughput $\bar{X}$, we use Little's law which says: $\bar{X} = \frac{\bar{x}_{on}}{\bar{t}_{on}}$, where $\bar{t}_{on} = \frac{\bar{Q}}{\bar{D}}$ with $\bar{D}$ representing the average number of departures per unit time. The expression of $\bar{Q}$ is give by Eq. 6.18 while $\bar{D}$ is given by the following expression:

$$\bar{D} = \sum_{n=1}^{N} \mu(n)\, \pi(n),$$

hence the average throughput can now be written as:

$$\bar{X} = \frac{\bar{x}_{on}}{\bar{t}_{on}} = \frac{\bar{x}_{on} \sum_{n=1}^{N} \mu(n)\, \pi(n)}{\sum_{n=1}^{N} n\, \pi(n)}. \tag{6.19}$$

6.2.4 Validation and Robustness Study

In this section we discuss the validation of the analytical model through extensive simulations. We also show its robustness when traffic and channel models are made more complex.

For this purpose, a simulator has been developed that implements an ON/OFF traffic generator and a wireless channel for each user, and a centralized scheduler that allocates radio resources, i.e., slots, to active users on a frame by frame basis. In a first phase, we validate the analytical model through simulations. In this validation study, the assumptions considered for analytical model are reproduced in the simulator. The assumptions are related to scheduling, traffic and channel models. This phase shows that describing the system by the number of active users is a sufficient approximation to obtain dimensioning parameters. It also validates the analytical expression of the average number of bits per slot $\bar{m}(n)$.

In the second phase, the robustness study, we relax the assumptions made for the analytical model by considering more realistic models embracing traffic and radio channel variations. Through the comparison with simulation results, we thus show how robust the analytical model reacts towards these relaxations.

We now detail the simulation models before presenting the simulations results for the validation and robustness studies.

6.2.4.1 Simulation Models

System Parameters: We consider a single WiMAX cell and study the downlink. Radio resources are thus made of time-frequency slots in the downlink TDD sub-frame. The number of slots depends on the system bandwidth, the frame duration, the downlink/uplink ratio, the subcarrier permutation (PUSC, FUSC, AMC), and the protocol overhead (preamble, FCH, maps).

System bandwidth is assumed to be 10 MHz. The duration of one TDD frame of WiMAX is considered to be 5 ms and the downlink/uplink ratio 2/3. For the sake of simplicity, we assume that the protocol overhead is of fixed length (2 symbols) although in reality it is a function of the number of scheduled users. These parameters lead to a number of data slots (excluding overhead) per TDD downlink sub-frame of $N_S = 450$.

Traffic Parameters: In the analytical model, an elastic ON/OFF traffic is considered. Mean values of ON data volume (main page and embedded objects) and OFF period (reading time), considered in validation study of both the conventional and throttling schemes are 3 Mbits and 3 s respectively. Throttling policy has one additional parameter, MSTR, whose value is taken as 512 Kbps for validation purposes. In robustness study of conventional scheduling schemes, behavior of model is analyzed for a higher and lower load (i.e., with ON data volume of 1 Mbits and 5 Mbits). On the other hand, for robustness study of throttling policy, MSTR is increased to 2048 Kbps.

In the validation study, we assume that the ON data volume and OFF period are exponentially distributed as it is the case in the analytical model assumptions. Although well adapted to reading period, the memoryless property does not always fit the reality for data traffic. This is the reason, for robustness study, ON data volume is characterized by truncated Pareto distribution. Recall that

Table 6.1: Traffic parameters.

Parameter	**Value**
Mean ON data volume $\bar{x}_{on}$	3 Mbits
Mean OFF duration $\bar{t}_{off}$	3 s
$MSTR$ for throttling scheme	512/2048 Kbps
Pareto parameter α	1.2
Pareto lower cutoff q	300 Mbits
Pareto higher cutoff q	3000 Mbits
Pareto parameter b for lower cutoff	712926 bits
Pareto parameter b for higher cutoff	611822 bits

Table 6.2: Channel parameters.

Channel state $\{0, ..., K\}$	**MCS and outage**	**Bits per slot** m_k
0	Outage	$m_0 = 0$
1	QPSK-1/2	$m_1 = 48$
2	QPSK-3/4	$m_2 = 72$
3	16QAM-1/2	$m_3 = 96$
4	16QAM-3/4	$m_4 = 144$

the mean value of the truncated Pareto distribution is given by:

$$\bar{x}_{on} = \frac{\alpha b}{\alpha - 1}\left[1 - (b/q)^{\alpha-1}\right], \tag{6.20}$$

where α is the shape parameter, b is the minimum value of pareto variable and q is the cutoff value for truncated pareto distribution. Two values of q are considered: lower and higher. These have been taken as hundred times and thousand times the mean value respectively. The mean value in both cases (higher and lower cutoff) is 3 Mbits for the sake of comparison with the exponential model. The value of $\alpha = 1.2$ has been adopted from [77]. The corresponding values of parameter b for higher and lower cutoff are calculated using relation (6.20). Traffic parameters are summarized in Tab. 6.1.

Channel Models: The number of bits per slot an MS is likely to receive depends on the chosen MCS, which in turn depends on its radio channel conditions. The choice of a MCS is based on SINR measurements and SINR thresholds. Wireless channel parameters are summarized in Tab. 6.2. Considered MCS (including outage) and their respective number of bits transmitted per slot are given.

A generic method for describing the channel between the BS and a MS is to model the transitions between MCS by a finite state Markov chain (FSMC). The chain is discrete time and transitions occurs every L frames, with $L\,T_F < \bar{t}_{coh}$ (the coherence time of the channel). For validation study, $L = 1$. Such a FSMC

Table 6.3: Stationary probabilities for three channel models.

Channel model	Memoryless	Average	Combined	
			50% MS (good)	50% MS (bad)
a	0	0.5	0.5	0.5
p_0	0.225	0.225	0.020	0.430
p_1	0.110	0.110	0.040	0.180
p_2	0.070	0.070	0.050	0.090
p_3	0.125	0.125	0.140	0.110
p_4	0.470	0.470	0.750	0.190

is fully characterized by its transition matrix $P_T = (p_{ij})_{0 \leq i,j \leq K}$. Note that an additional state (state 0) is introduced to take into account outage (SINR is below the minimum radio quality threshold). Stationary probabilities p_k provide the long term probabilities for a MS to receive data with MCS k.

Three models of wireless channel have been used in this validation and robustness study. These are the memoryless, average and combined. We discuss these models one by one with the respective scenario in which these are used.

- ***memoryless channel model:*** In the analytical study, channel model is assumed to be memoryless, i.e., MCS are independently drawn from frame to frame for each user, and the discrete distribution is given by the $(p_i)_{0 \leq i,j \leq K}$. This corresponds to the case where $p_{ij} = p_j$ for all i. This simple approach, referred as the *memoryless channel model*, is considered in the validation study, which exactly conforms to the assumptions of the analytical model. Let $P_T(0)$ be the transition matrix associated to the memoryless model.

In the robustness study, we introduce two additional channel models with memory. In these models, the MCS observed for a given MS in a frame depends on the MCS observed in the previous frame according to the FSMC presented above. The transition matrix is derived from the following equation:

$$P_T(a) = aI + (1-a)P_T(0) \qquad 0 \leq a \leq 1,$$

where I is the identity matrix and parameter a is a measure of the channel memory. A MS indeed maintains its MCS for a certain duration with mean $\bar{t}_{coh} = \frac{1}{(1-a)}\ frames$. With $a = 0$, the transition process becomes memoryless. On the other extreme, with $a = 1$, the transition process will have infinite memory and MS will never change its MCS. For simulations we have taken a equal to 0.5, so that the channel is constant during average 2 frames. This value is consistent with the coherence time given in [8] for 45 Km/h at 2.5 GHz. The two channels with memory are presented hereafter.

- ***average channel model:*** We call the case where all MS have the same channel model with memory ($a = 0.5$), the *average channel model*. Note

that the stationary probabilities of the average channel model are the same as those of the memoryless model.

- ***combined channel model:*** As the channel depends on the BS-MS (base station to mobile) link, it is possible to refine the previous approach by considering part of the MS to be under "bad" radio condition, and the rest in "good" one. Bad and good radio conditions are characterized by different stationary probabilities but have the same coherence time. In the so called *combined channel model*, half of the MS observe good radio condition, the other half confront bad one, and a is kept to 0.5 for both populations. The radio conditions are assigned to MS in the beginning of simulations and are not changed. For example, a MS assigned bad channel state in the beginning of simulation, will keep on changing its MCS with stationary probabilities of bad radio condition till the end of simulation.

Channel stationary probabilities for three channel models are given in Tab. 6.3. The stationary probabilities are found using the simulator discussed in chapter 2. The respective MCS stationary probabilities for good and bad radio conditions can be obtained for example by performing system level Monte Carlo simulations and recording channel statistics close (good radio condition) or far (bad radio condition) from the base-station. Stationary probabilities for memoryless and average models are obtained by averaging corresponding values of good and bad radio conditions' stationary probabilities.

In this chapter, for simplicity, we have considered only one set of stationary probability values (specific to a given frequency reuse scheme) for a given channel type. To obtain the results for different reuse types, it is sufficient to use the respective values of MCS probabilities given in chapter 2 and 3.

It is also to be noted that these MCS probabilities at the entrance of analytical model are related to all the MS (whether active or not) in a cell. The distribution of MCS probabilities of the active MS is different from it and will depend upon the employed scheduling scheme.

6.2.4.2 Pseudo-codes for Scheduling Schemes

The simulator implements the four scheduling schemes considered in this chapter, i.e., opportunist, fair in throughput, fair in slots and throttling. On a frame by frame basis, the scheduler allocates the downlink slots to the active users according to their radio conditions (their MCS) and to the scheduling policy. As already mentioned, the schedulers does not allocate resources to active users in outage. The way the number of slots allocated to each user is computed, is now detailed.

Conventional Scheduling Schemes: In a given frame, the number of slots allocated to active users should satisfy the following condition:

$$N_S = \sum_{k=0}^{K} N_S^{(k)} n^{(k)},$$

where $N_S^{(k)}$ is the number of slots allocated by the scheduler to a MS using MCS k and $n^{(k)}$ is the number of active MS using MCS k. Note that $N_S^{(k)}$ depends on the scheduling scheme and that the number of active users verifies $n = \sum_{k=0}^{K} n^{(k)}$. The way $N_S^{(k)}$ is chosen by the scheduler is detailed below in the scheduling pseudo-code.

Scheduling pseudo-code for conventional schemes

Let $\mathbf{K_F} \subset [0...K]$ be the set of MCS used by active MS in the considered frame.

▷ Opportunist

find $k_{max} = max(\mathbf{K_F})$

$N_S^{(k)} = \frac{N_S}{n^{(kmax)}}$ for $k = k_{max}$

$N_S^{(k)} = 0$ for all $k \neq k_{max}$

▷ Fairness in slot

$N_S^{(k)} = 0$ for $k = 0$

$N_S^{(k)} = \frac{N_S}{\sum_{k=0}^{K} n^{(k)}}$ for $k \neq 0$

▷ Fairness in throughput

if $k = 0$

$N_S^{(k)} = 0$

else

$N_S^{(k)} = \frac{N_S/m_k}{\sum_{k=1}^{K} \frac{n^{(k)}}{m_k}}$

end

Throttling Scheme: In order to offer DBR to all active MS in a frame, certain number of slots $N_S^{(F)}$ are required. If $N_S^{(F)} > N_S$, all active MS are degraded proportionally so that $N_S^{(F)} = N_S$. On the other hand, if $N_S^{(F)} < N_S$, $N_S - N_S^{(F)}$ slots go unused in a frame. The number of slots $N_S^{(u)}$ allocated to each active MS

in a frame is calculated according to pseudo-code given hereafter:

Scheduling pseudo-code for throttling scheme

Number of slots required by each active MS $N_S^{'(u)}$ in a frame to attain DBR is calculated implying following condition:

if $m_k^u \neq 0$

$$N_S^{'(u)} = \frac{min\left(x_{on}^{(u)}, DBR \times T_F\right)}{m_k^{(u)}}$$

else (i.e., if the MS is in outage)

$$N_S^{'(u)} = 0$$

end

where $x_{on}^{(u)}$ is the random value of ON data volume to be downloaded by MS u and $m_k^{(u)}$ is the bits per slot for mobile station u using MCS k during a TDD frame. The total number of required slots by n active users in a TDD frame can thus be calculated as:

$$N_S^{(F)} = \sum_{u=1}^{n} N_S^{'(u)}.$$

In order to find the degradation factor D, following procedure is employed:

if $N_S^{(F)} \leq N_S$

$$D = 1$$

else

$$D = \frac{N_S}{N_S^{(F)}}$$

end

Finally, the number of slots allocated to an active MS in a frame are:

$$N_S^{(u)} = D \times N_S^{'(u)}.$$

6.2.4.3 Simulator Description

We now discuss the key components of simulator used for validation of the model. The flow diagram depicting these components is shown in Fig. 6.2. Hereafter, we briefly describe each of these components one by one.

1. The *frame count* corresponds to number of TDD frames during which traffic statistics are recorded. In this step, frame count is initialized by setting its value to zero. It starts to augment once the boundary condition is satisfied which is the state when all the MS in the cell have completed download of their respective x_{on} atleast once. Here x_{on} is the random value of ON data volume generated based on type of distribution (i.e., Exponential or Pareto).

   It should, however, be noted that the frame count only refers to a part of total TDD frames traversed in a simulation. The total TDD frames in a simulation is the sum of the TDD frames passed to satisfy the boundary condition and the number of TDD frames during which traffic statistics are recorded.

2. In this step, random values of x_{on} and t_{off} for all MS in the cell are generated. The generation of t_{off} random value is carried out by considering exponential distribution while that of x_{on} random value is done by keeping in view either the exponential or pareto distribution (based on choice of simulation scenario).

   Minimum value is found from the t_{off} values of all MS and is subtracted from t_{off} values of all MS.

3. The users in download state are identified (i.e., whose $t_{off} > 0$).

4. For MS in download state MCS are randomly drawn using stationary probabilities of MCS and Bernoulli distribution. The values of stationary probability and coherence time depends upon the channel model which is an input in this step.

5. The scheduling of slots is accomplished based on choice of scheduling scheme (throughput fairness, resource fairness, opportunist or throttling). The pseudo-code for the scheduling schemes are given in section 6.2.4.2.

6. After the allocation of resources, the next step is to subtract the allocated bits from the data volume present in the buffer of the user in download state. The MS whose buffer goes empty are identified. OFF period of every MS (whether in download state or not) is decremented by one TDD frame duration (i.e., 5 ms).

7. The decision about whether the traffic statistics should be recorded or not is taken in this step. If the boundary condition is satisfied, the simulation passes on directly to step 9 otherwise it goes through step 8 and then onward to step 9.

8. In this step, three elements are registered for current TDD frame: bits allocated to MS in download state, number of users in download state and number of slots allocated out of total slots. Apart from this, the frame count is incremented by one.

9. If there are certain MS who have completed the download of their current x_{on} data volume, new random values of their next x_{on} and t_{off} are generated here. The inputs to this step are the same as are for step 2.

10. This step determines the end of simulation. If frame count has reached a preset value (e.g., the results in this report are obtained for 1 million frames), the simulation routes towards end otherwise it goes back to step 3.

11. If the end of simulation has been established in step 10, the output parameters (i.e., average instantaneous throughput per MS, average resource utilization and average number of active MS) are computed in this step.

6.2.5 Simulation Results

In this section, we present a comparison between the results obtained through the analytical model and scheduling simulator. The output parameters in consideration are $\pi(n)$, $\bar{U}$, $\bar{Q}$ and $\bar{X}$ (cf. section 6.2.2.4 and 6.2.3.1).

6.2.5.1 Validation Study

In this study, simulator takes into account the same traffic and channel assumptions as those of analytical model. However, in simulator MCS of users are determined on per frame basis and scheduling is carried out in real time, based on MCS at that instant. Analytical model on the other hand, considers stationary probabilities of MCS only. Distributions of ON data volume and OFF period are exponential and the memoryless channel model is considered.

Conventional Scheduling Schemes: Fig. 6.4, 6.5 and 6.6 show respectively the average channel utilization ($\bar{U}$), average number of active users ($\bar{Q}$) and the average instantaneous throughput per user ($\bar{X}$) for the three scheduling schemes. It is clear that simulation and analytical results show a good agreement: for both utilization and throughput, the maximum relative error stays below 6% and the average relative error is less than 1%. Note that analytical results have been obtained instantaneously whereas simulations have run for several days.

Fig. 6.7 further proves that the analytical model is a very good description of the system: stationary probabilities $\pi(n)$ obtained by either simulations or analysis are compared for a given total number $N = 50$ of MS. Again results show a perfect match between the two methods with an average relative error always below 9%. This means that not only average values of the output parameters can be evaluated but also higher moments with a high accuracy.

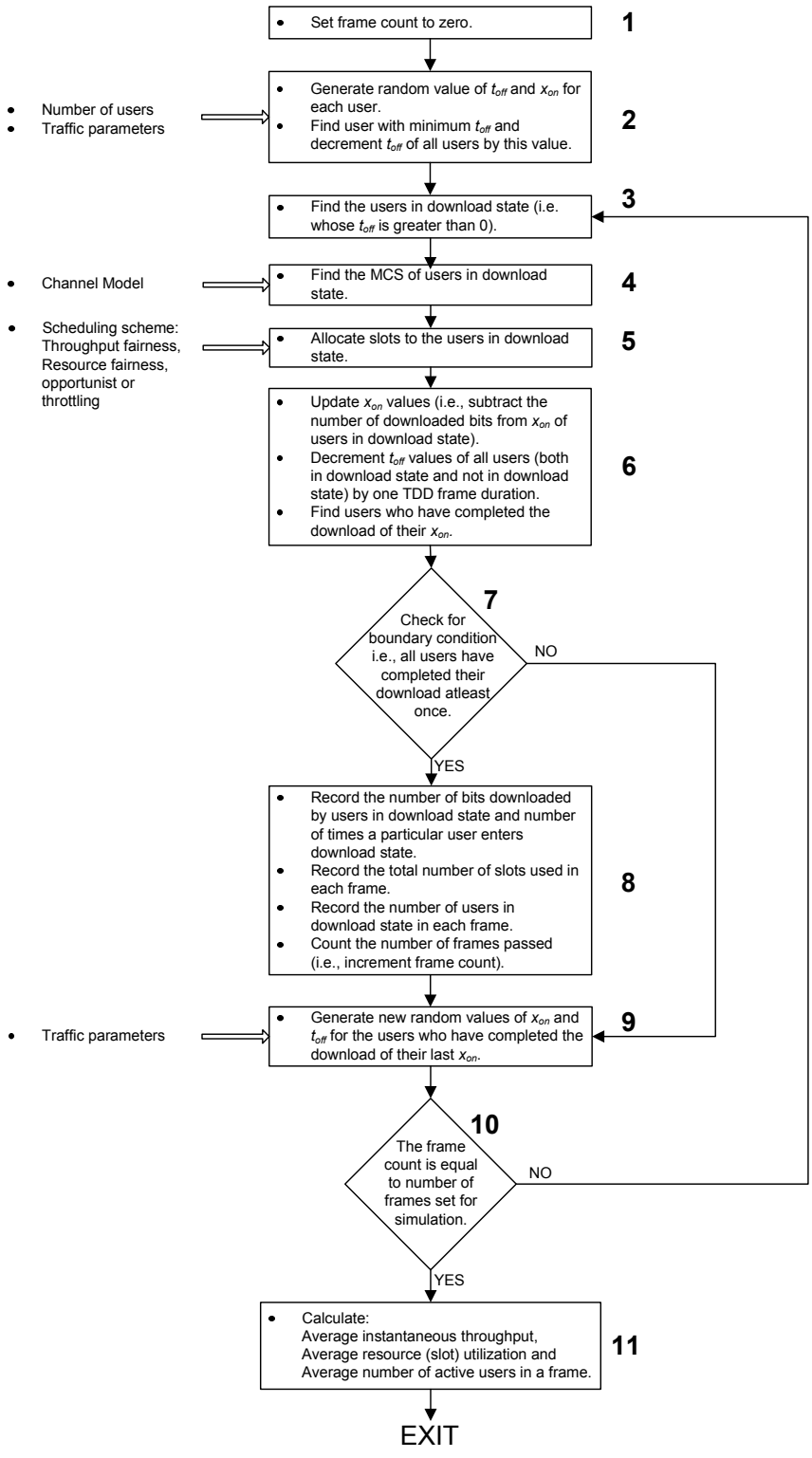

Figure 6.2: Flow diagram of simulator.

At last, Fig. 6.8 shows the validation for three different loads (1, 3 and 5 Mbps). The analytical model shows a comparable accuracy for all three load conditions with a maximum relative error of about 5%.

Throttling Scheme: The results of validation study for throttling scheme can be found in Fig. 6.9, 6.10, 6.11 and 6.12. The maximum difference between model and simulation results in all cases is found to be less than 2%.

6.2.5.2 Robustness Study

We now move to the robustness study, where assumptions concerning traffic and channel models made by the analysis are relaxed in simulations.

Conventional Scheduling Schemes: In order to check the robustness of analytical model towards distribution of ON data volumes, simulations are carried out for exponential and truncated pareto (with lower and higher cutoff). The results for this analysis are shown in Fig. 6.13. The average relative error between analytical and simulations results stays below 10% for all sets. It is clear that considering a truncated Pareto distribution has little influence on the design parameters. This is mainly due to the fact that the distribution is truncated and is thus not heavy tailed. But even with a high cutoff value, the exponential distribution provides a very good approximation.

Until now we have always considered the memoryless channel model. We now take into account two different channel models such that transitions among different MCS is characterized by a process with memory. The *average channel model* is a combination of good and bad channel states (corresponding to stationary probabilities of average combined given in Tab. 6.3).

For the *combined channel model*, MS are assigned both the good and bad channel states in simulations (corresponding to stationary probabilities of good and bad given in Tab. 6.3).

If we look at the plot of Fig. 6.14, it can be deduced that even for a complex wireless channel, the analytical model shows considerable robustness with an average relative error below 7%. We can thus deduce that for designing a WiMAX network, channel information is almost completely included in the stationary probabilities of the MCS.

Throttling Scheme: The results of robustness study for throttling scheme are given Fig. 6.15 and 6.16. These results follow the trend of those of conventional schemes.

6.3 Best Effort (BE) Multi-profile

The multi-profile BE traffic encapsulates different classes of BE users with each class specific to a certain traffic profile. In this section, an introduction of ana-

lytical models for conventional scheduling schemes and throttling scheme is given for multi-profile BE traffic. All assumptions made for mono-profile models still hold with addition of some new ones. Hereafter, these models are presented.

6.3.1 Conventional Scheduling Schemes

The assumptions specific to multi-profile traffic, while considering conventional scheduling schemes, are discussed below:

- The users are divided into R classes of traffic, each one having a specific profile. A profile is described by two parameters: size of ON period and duration of OFF period. These two parameters are supposed to be distributed exponentially. For a given class r, the average size of ON data volumes (in bits) and the average duration of OFF periods are denoted by $\bar{x}^r_{on}$ and $\bar{t}^r_{off}$ respectively. Hence, a traffic profile of a generic class r will be denoted by $(\bar{x}^r_{on}, \bar{t}^r_{off})$ in the following text.
- The total number of MS of class r is represented by N_r such that $N = \sum_{r=1}^{R} N_r$.

Now we pass on to brief description of traffic model by introducing the parameter ρ_r:

$$\rho_r = \frac{\bar{x}^r_{on}}{\bar{t}^r_{off}}. \tag{6.21}$$

It is assumed in the traffic model that all performance parameters depend upon these ρ parameters of different classes. In the next step, the profile of each class $(\bar{x}^r_{on}, \bar{t}^r_{off})$ is transformed into an equivalent profile such that $\frac{\bar{x}_{on}}{\bar{t'}^r_{off}} = \frac{\bar{x}^r_{on}}{\bar{t}^r_{off}}$. In this way all profiles have a common value of average ON data volume i.e. equal to $\bar{x}_{on}$. Their average OFF duration values, on the other hand, are not same i.e. equal to $\bar{t}^r_{off}$.

After this transformation of parameter values, the system can be described as a multi-class closed queuing network with two stations as shown in Fig. 6.3.

The station 1 is the Infinite Server (IS) station that models mobiles in OFF periods. As the name of station indicates, there are as many servers at this station as required. This station has class-dependent service rates $\lambda_r = 1/\bar{t'}^r_{off}$. The MS in download (i.e., active ones) are modeled by station 2 called Processor Sharing (PS) which is characterized by a class independent parameter $\mu(n)$ with n as the number of active MS. Since all MS served at station 2 have the same value of $\bar{x}_{on}$ (whatever their traffic class may be). The value of $\mu(n)$ is calculated in the same manner as was done for mono-profile BE traffic (refer Eq. 6.1).

After transformation of parameters, the closed queuing network shown in Fig. 6.3 can now be handled using extension of the BCMP theorem for stations with state-dependent rates [34]. Since this chapter is aimed at explaining the validation part, only key equations of the traffic model are presented. For clarity and ease of comprehension, only two class types of profiles $(\bar{x}^1_{on}, \bar{t}^1_{off})$ and $(\bar{x}^2_{on}, \bar{t}^2_{off})$ are used both in model equations and validation study.

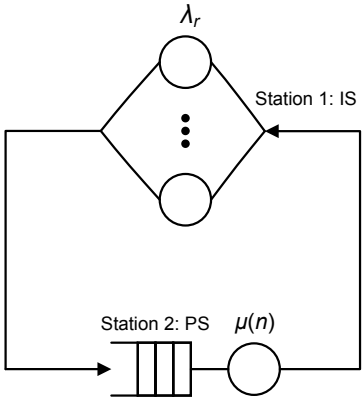

Figure 6.3: Closed-queuing network.

If N_1 and N_2 represent the total number of MS of class 1 and 2 respectively in the cell, the population vector can be written as: $\overrightarrow{N} = (N_1, N_2)$. We define a new vector $\overrightarrow{n}$ such that $\overrightarrow{n} = (\overrightarrow{n_1}, \overrightarrow{n_2})$, where $\overrightarrow{n_1}$ and $\overrightarrow{n_2}$ represent the MS population vectors at station 1 and 2 respectively. Here it should be noted that the small letter n, used in these vectors, should not be confused with the one used in section 6.2, where it represented the number of active users in the cell. The population vector at station i is given as: $\overrightarrow{n_i} = (n_{i1}, n_{i2})$. Here n_{i1} and n_{i2} represent the number of MS of class 1 and 2 respectively at station i. Since there are two stations and we have considered MS of two classes, we can write $N_1 = n_{11} + n_{21}$ and $N_2 = n_{12} + n_{22}$.

After defining the variables concerning population of MS, the steady-state probabilities can be expressed using extension of BCMP theorem as follows:

$$\pi(\overrightarrow{n}) = \pi(\overrightarrow{n_1}, \overrightarrow{n_2}) = \frac{1}{G} f_1(\overrightarrow{n_1}) f_2(\overrightarrow{n_2}), \tag{6.22}$$

where $f_1(\overrightarrow{n_1})$ and $f_2(\overrightarrow{n_2})$ are give as:

$$f_1(\overrightarrow{n_1}) = \frac{1}{n_{11}!\, n_{12}!} \frac{1}{(\lambda_1)^{n_{11}}\, (\lambda_2)^{n_{12}}}, \tag{6.23}$$

$$f_2(\overrightarrow{n_2}) = \frac{(n_{21} + n_{22})!}{n_{21}! n_{22}!} \frac{1}{\prod_{k=1}^{n_{21}+n_{22}} \mu(k)}, \tag{6.24}$$

and G is a normalization constant presented as:

$$G = \sum_{\overrightarrow{n_1}+\overrightarrow{n_2}=\overrightarrow{N}} f_1(\overrightarrow{n_1}) f_2(\overrightarrow{n_2}). \tag{6.25}$$

6.3.1.1 Performance Parameters

Three performance parameters: average instantaneous resource utilization (of DL TDD sub-frame) $\bar{U}$, average number of active mobile stations $\bar{Q}$ and average instantaneous user throughput during ON period $\bar{X}$, are considered for the analysis

of multi-profile traffic. These parameters are calculated using steady-state probabilities obtained through Eq. 6.22. The average number of class r customers departing from station 1 per unit time, represented by $\bar{D}_{1r}$, is equal to the average number of class r customers departing from station 2 per unit time $\bar{D}_{2r}$. We use a common notation D_r for both departure rates such that:

$$\bar{D}_r = \bar{D}_{2r} = \bar{D}_{1r} = \sum_{\overrightarrow{n_1}+\overrightarrow{n_2}=\overrightarrow{N}} \pi(\overrightarrow{n_1}, \overrightarrow{n_2}) n_{1r} \lambda_r. \tag{6.26}$$

The average number of class r mobile stations at station 2, i.e., which is the average number of class r active mobiles, is denoted by $\bar{Q}_r$ and is given by following equation:

$$\bar{Q}_r = \sum_{\overrightarrow{n_1}+\overrightarrow{n_2}=\overrightarrow{N}} n_{2r}\, \pi(\overrightarrow{n_1}, \overrightarrow{n_2}). \tag{6.27}$$

The average download duration of class r mobiles is the time spent by mobiles of class-r at station 2 and is obtained using Little's law as follows:

$$\bar{t}^r_{on} = \frac{\bar{Q}_r}{\bar{D}_r}. \tag{6.28}$$

Hence, the average throughput per user for class r is presented as:

$$\bar{X}_r = \frac{\bar{x}_{on}}{\bar{t}^r_{on}}. \tag{6.29}$$

Finally, the average resource utilization is given by equation:

$$\bar{U} = \sum_{\overrightarrow{n_1}+\overrightarrow{n_2}=\overrightarrow{N} | \overrightarrow{n_2} \neq (0,0)} \pi(\overrightarrow{n_1}, \overrightarrow{n_2})\ (1 - p_0^{n_{21}+n_{22}}), \tag{6.30}$$

where p_0 is the outage probability.

6.3.2 Throttling Scheme

As compared to the case of conventional scheduling schemes, traffic profile of a class in case of throttling scheme has one additional parameter i.e., MSTR. Thus a traffic profile for a class r is now represented as $(MSTR_r, \bar{x}^r_{on}, \bar{t}^r_{off})$. Parameter ρ for class r is given as:

$$\rho_r = \frac{\bar{x}^r_{on}}{\bar{t}^r_{off} MSTR_r}. \tag{6.31}$$

Next we transform each class r into an equivalent class whose ON period volume and $MSTR$ remain fixed and only OFF period changes i.e., $\frac{\bar{x}_{on}}{\bar{t'}^r_{off} MSTR} = \frac{\bar{x}^r_{on}}{\bar{t}^r_{off} MSTR_r}$. With this transformation, we can use the multi-class close queuing network (with two stations) of Fig. 6.3. The station IS has a class dependent service rates $\lambda_r = \frac{1}{\bar{t'}^r_{off}}$ while station PS has a class-independent service rate $\mu(n)$

depending upon the number of active mobile station n. Unlike for conventional schemes, the expression of mono-profile traffic to calculate $\mu(n)$ (Eq. 6.1) can not be directly used here. The equation to find $\mu(n)$ for station PS is written below:

$$\mu(n) = \frac{N_S}{max\left(\bar{g}(n), N_S\right)} n \frac{MSTR}{\bar{x}_{on}}, \tag{6.32}$$

where $MSTR$ and $\bar{x}_{on}$ pertain to equivalent class after transformation of profiles. Since active MS may belong to any class of traffic, the calculation of $\bar{g}$ is somewhat different from that of mono-profile case. For a class r, average number of slots required to reach its MSTR is:

$$\bar{g}_r = \sum_{k=1}^{K} p_{kr} \frac{DBR_r \; T_F}{m_k}, \tag{6.33}$$

where p_{kr} is the stationary probability for MS of class r using MCS k and $DBR_r = \frac{MSTR_r}{1-p_{0r}}$ (to compensate for loss because of outage).

In order to find $\bar{g}(n)$, the probability $\alpha_r(n)$ that an active MS belongs to class r, when there are n active MS, has to be calculated. Now if it is known that $n = N$, where $N = N_1 + N_2 + ... + N_R$, then $\alpha_r(n)$ can be written as:

$$\alpha_r(N) = \frac{N_r}{N},$$

and for $n = 1$, the probability $\alpha_r(1)$ can be approximated as:

$$\alpha_r(1) = \frac{N_r \rho_r}{\sum_{i=1}^{R} N_i \rho_i}.$$

After calculating the above two limiting values, we suppose that $\alpha_r(n)$ is a linear function of n such that:

$$\alpha_r(n) = a\, n + b,$$

where $a = \frac{\alpha_r(N) - \alpha_r(1)}{N-1}$ and $b = \frac{N\alpha_r(1) - \alpha_r(N)}{N-1}$. The equation for $\bar{g}(n)$ can now be expressed as:

$$\bar{g}(n) = \sum_{r=1}^{R} n\, \alpha_r(n) \bar{g}_r.$$

6.3.2.1 Performance Parameters

In this section, we find the expressions for performance parameters for which we require the steady-state probabilities. These probabilities can be found using the direct extension of the BCMP theorem for stations with state dependent rates (cf. section 6.3.1, Eq. 6.22, 6.23, 6.24 and 6.25). The average number of class r mobiles completing their download per unit time, can be written as:

$$\bar{D}_r = \sum_{\vec{n_1}+\vec{n_2}=\vec{N}} \mu_r(\vec{n_2})\, \pi(\vec{n_1}, \vec{n_2}), \tag{6.34}$$

where $\mu_r(\overrightarrow{n_2})$ is the departure rate of class r MS when there are $\overrightarrow{n_2}$ active MS and is given as:

$$\mu_r(\overrightarrow{n_2}) = \frac{N_S}{max\left(\bar{g}(\overrightarrow{n_2}), N_S\right)} n_{2r} \frac{MSTR_r}{\bar{x}^r_{on}} \quad \text{with} \quad \bar{g}(\overrightarrow{n_2}) = \sum_{r=1}^{R} n_{2r}\bar{g}_r. \tag{6.35}$$

The average number of active MS of class r active mobiles is given by Eq. 6.36.

$$\bar{Q}_r = \sum_{\overrightarrow{n_1}+\overrightarrow{n_2}=\overrightarrow{N}} n_{2r}\, \pi(\overrightarrow{n_1}, \overrightarrow{n_2}). \tag{6.36}$$

The average instantaneous throughput for class-r MS is written as:

$$\bar{X}_r = \frac{\bar{x}^r_{on}}{\bar{t}^r_{on}}, \tag{6.37}$$

where $\bar{t}^r_{on}$ is obtained through Little's law i.e., $\bar{t}^r_{on} = \frac{\bar{Q}_r}{\bar{D}_r}$ and values of $\bar{Q}_r$ and $\bar{D}_r$ can be found from Eq. 6.36 and 6.34 respectively.

At the end, parameter $\bar{U}$ is given by following equation:

$$\bar{U} = \sum_{\overrightarrow{n_1}+\overrightarrow{n_2}=\overrightarrow{N}} \frac{\bar{g}(\overrightarrow{n_2})}{max\left(\bar{g}(\overrightarrow{n_2}), N_S\right)} \pi(\overrightarrow{n_1}, \overrightarrow{n_2}). \tag{6.38}$$

6.3.3 Validation Study

To validate the analytical model, we now compare the results of the model with those of simulations. Robustness study results are not discussed here since they show the similar pattern as was found for mono-profile traffic.

6.3.3.1 Simulation Models

Now we present the system/traffic parameters and channel models used in simulations.

System Parameters: System parameters are the same as were considered for mono-profile validation study (cf. section 6.2.5).

Traffic Parameters: During a simulation cycle, total number of users, N, is partitioned among two classes (1 and 2), with equal number of users (i.e., $\frac{N}{2}$) in each class. Users in a class share the same traffic profile.

For conventional scheduling schemes, three different values of N (i.e., 4, 8 and 16) are taken into account. Simulations consist of twenty cycles. Traffic profile of class 1 users is kept constant during all simulation cycles. Traffic profile of class 2 users is changed from one simulation cycle to the other. Traffic parameters for conventional scheduling schemes are summarized in Tab. 6.4. Twenty different values of $\bar{x}^2_{on}$ result into twenty different multi-traffic profiles for a given number

Table 6.4: Traffic parameters for conventional scheduling schemes.

Parameter	**Value**
Number of users in the system N	4, 8 and 16
Mean ON data volume $\bar{x}_{on}^{1}$ (class 1)	1 Mbits
Mean ON data volume $\bar{x}_{on}^{2}$ (class 2)	$1, 2, ..., 20$ Mbits
Mean OFF duration $\bar{t}_{off}^{1}$ (class 1)	3 s
Mean OFF duration $\bar{t}_{off}^{2}$ (class 2)	3 s

Table 6.5: Traffic parameters for throttling scheme.

Parameter	**Multi-traffic**	
	Class 1	**Class 2**
$MSTR$ [Kbps]	1024	2048
$\bar{x}_{on}$ [Mbps]	3	3
$\bar{t}_{off}$ [s]	3	6

of total users in the system i.e., one multi-profile per simulation cycle. For all these multi-profiles, value of $\bar{x}_{on}^{1}$ is the same i.e., 1 Mbits. It is assumed that the mean ON data volume and OFF period are exponentially distributed as is the case in the analytical model.

In multi-traffic scenario with throttling scheme, we consider two different classes of traffic. Each class is characterized by particular values of MSTR, $\bar{x}_{on}$ and $\bar{t}_{off}$ (see Tab. 6.5). Simulations are carried out for varying number of total users.

Channel Models: In simulations, we have considered the *memoryless channel model* that was used in validation study of mono-profile model (cf. section 6.2.5). We also take the same values of stationary probabilities p_k (associated with MCS k) as were considered for mono-profile model. Furthermore, these values are same for users of different classes.

6.3.3.2 Pseudo-codes for Scheduling Schemes

Conventional Scheduling Schemes: The simulator allocates the resources to active users according to the throughput fairness policy whose pseudo-code is given hereafter:

Scheduling pseudo-code for throughput fairness scheduling

Let the number of active MS using MCS k and belonging to two classes be $n_1^{(k)}$ and $n_2^{(k)}$. If $N_S^{(k)}$ represents the number of slots allocated by the scheduler to a MS using MCS k, then its value is given by following expression:

$$N_S^{(k)} = \begin{cases} 0 & \text{if } k = 0; \\ \frac{N_S/m_k}{\sum_{k=1}^{K} \frac{n_1^{(k)}+n_2^{(k)}}{m_k}} & \text{if } k \neq 0. \end{cases}$$

Throttling Scheme: In order to offer DBR_r to all active MS of various classes in a frame, certain number of slots $N_S^{(F)}$ are required. If $N_S^{(F)} > N_S$, all active MS of every class are degraded proportionally so that $N_S^{(F)} = N_S$. On the other hand, if $N_S^{(F)} < N_S$, $N_S - N_S^{(F)}$ slots go unused in a frame. The number of slots $N_S^{(ur)}$ allocated to each active MS of any class r in a frame is calculated according to pseudo-code given hereafter.

Scheduling pseudo-code for throttling scheme

Number of slots $N_S^{'(ur)}$ required by each active MS of class r in a frame to attain DBR_r is calculated implying following condition:

if $m_k^u \neq 0$

$$N_S^{'(ur)} = \frac{min\left(x_{on}^{(ur)}, DBR \times T_F\right)}{m_k^{(ur)}}$$

else (i.e., if the MS is in outage)

$$N_S^{'(ur)} = 0$$

end

where $x_{on}^{(ur)}$ is the random value of ON data volume to be downloaded by MS u of class r. Similarly, $m_k^{(ur)}$ is the bits per slot for mobile station u of class r using MCS k during a TDD frame. For MS of R number of classes, total number of required slots by n (where $n = n1 + n2 + n3 + ... + nR$) active users in a TDD frame can thus be calculated as:

$$N_S^{(F)} = \sum_{ur=u1}^{uR} \sum_{u1=1}^{n1} N_S^{'(u1)}.$$

In order to find the degradation factor D, following procedure is employed:

if $N_S^{(F)} \leq N_S$

$D = 1$

else

$D = \frac{N_S}{N_S^{(F)}}$

end

Finally, the number of slots allocated to an active MS in a frame belonging to class r is given as:

$$N_S^{(u1)} = D \times N_S^{'(ur)}.$$

6.3.3.3 Simulator Description

The details of simulator are similar to the ones for mono-profile traffic (cf. section 6.2.4.3). All the steps of simulation are the same except, in every step, both traffic profiles are considered simultaneously.

6.3.4 Simulation Results

In this section, we present a comparison between the results obtained through the analytical model and scheduling simulator. Three output parameters, mean resource utilization, average throughput per user and average number of active users are examined.

Conventional Scheduling Schemes: The output parameters for conventional scheduling schemes are given in Fig. 6.17, 6.18 and 6.19. These parameters are plotted for twenty different multi-traffic profiles. The effect of increasing the

number of users in the system is also exhibited. It is evident from the curves depicted in the figures that the results of the analytical model are in well agreement with those of simulations. The difference between the two is less than 3% in most of the cases and less than 5% in the worst case.

If we study Fig. 6.18 in detail, it can be observed that $\bar{X}_1$ and $\bar{X}_2$ are not equal. We used a throughput fairness scheduling policy and the mobiles are not differentiated in any way in the PS queue, so it can be quickly made out that both throughputs should be the same which does not agree with the results of the figure. The difference between $\bar{X}_1$ and $\bar{X}_2$ is due to the fact that when a mobile belonging to class 1 enters the PS queue, its probability to find a given number of mobiles already present in the queue is different from the one of a mobile of class 2. As such, the mobiles of each class don't get the exact same amount of resource and hence result into different throughputs.

Another important result that can be extracted from the figures is the fact that the analytical model performs equally well under low, medium and high load traffic conditions. Finally the comparison results validate the key assumption of the analytical model, i.e., the fact that performance parameters only depend on the traffic profiles of the different classes through the aggregated parameters ρ_r given by relation 6.21. Indeed, if we consider the last points of all curves, it corresponds to a class 2 traffic profile of (20 Mbits, 3 s) in simulations, and transformed in the analytical model into an equivalent traffic (1 Mbits, 0.15 s).

Throttling Scheme: The output parameters for this scheme have been plotted in Fig. 6.20, 6.21 and 6.22. The results show that simulation and analytical model provide similar results not only for the overall system performance but also for each class (maximum difference is below 6%). As expected, users obtain their respective MSTR at low load and when load increases, they see their throughput proportionally degraded (Fig. 6.21).

6.4 Conclusion

In this chapter, we have detailed the validation of mono/multi-profile BE traffic models for WiMAX network. Results through simulation and analytical model are in good agreement. Apart from validation, we have also shown how robust the analytical model is w.r.t. changes in various assumptions. In robustness study, different traffic distributions, radio channel with memory and different load conditions were considered. For the case of traffic distributions, results were compared for exponential and pareto (low/high cut off) distributions. Radio channels with memory and with no memory were considered. Results were also good for low, medium and high traffic loads.

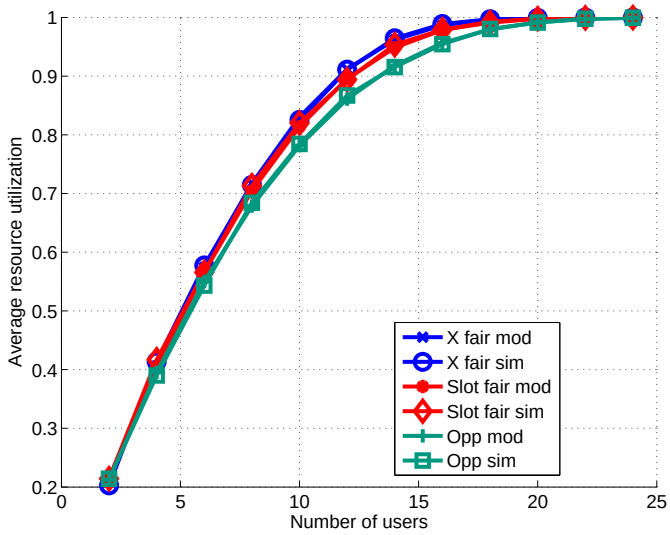

Figure 6.4: Average resource utilization for BE mono-profile with conventional scheduling schemes ($\bar{x}_{on} = 3$ Mbits and $\bar{t}_{off} = 3$ s).

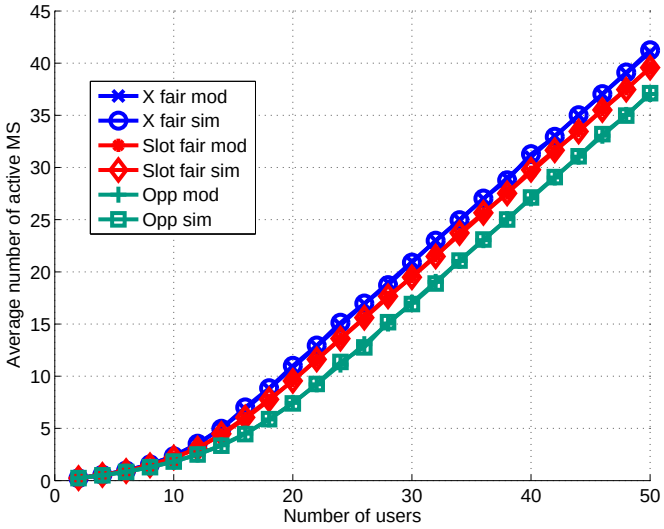

Figure 6.5: Average number of active MS for BE mono-profile with conventional scheduling schemes ($\bar{x}_{on} = 3$ Mbits and $\bar{t}_{off} = 3$ s).

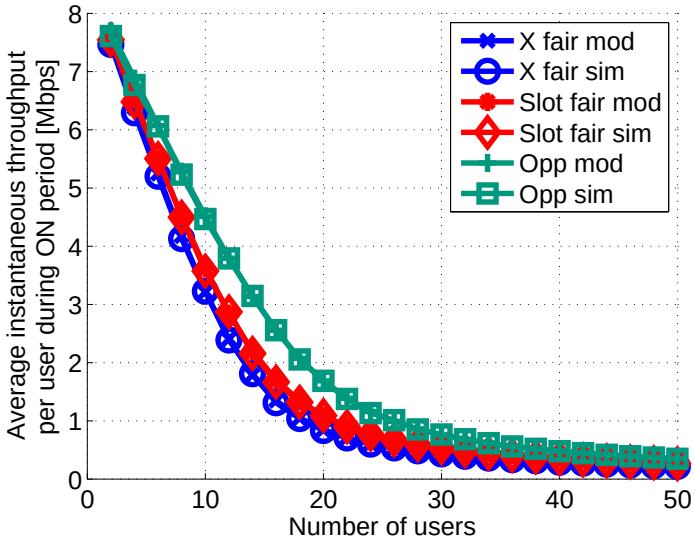

Figure 6.6: Average instantaneous user throughput for BE mono-profile with conventional scheduling schemes ($\bar{x}_{on} = 3$ Mbits and $\bar{t}_{off} = 3$ s).

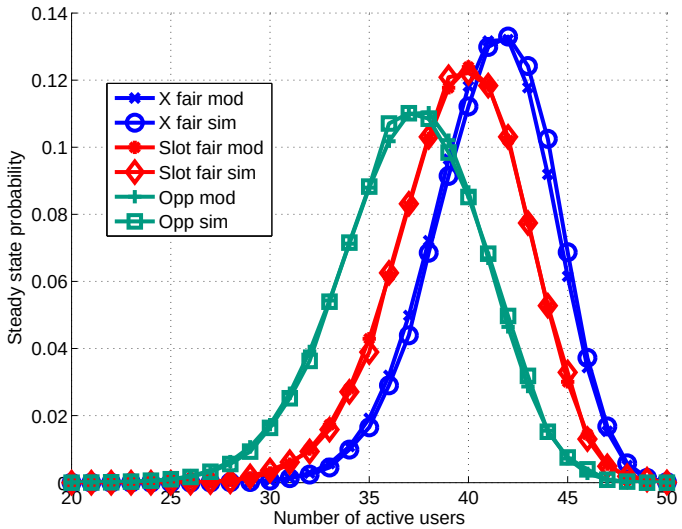

Figure 6.7: Steady state probabilities for BE mono-profile with conventional scheduling schemes for $N = 50$ ($\bar{x}_{on} = 3$ Mbits and $\bar{t}_{off} = 3$ s).

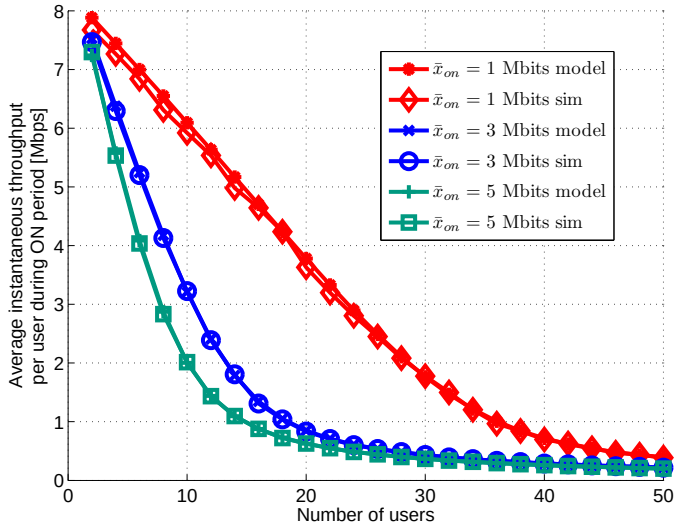

Figure 6.8: Average instantaneous user throughput for BE mono-profile with conventional scheduling schemes and different loads ($\bar{x}_{on}$ = 1, 3 and 5 Mbits; $\bar{t}_{off}$ = 3 s).

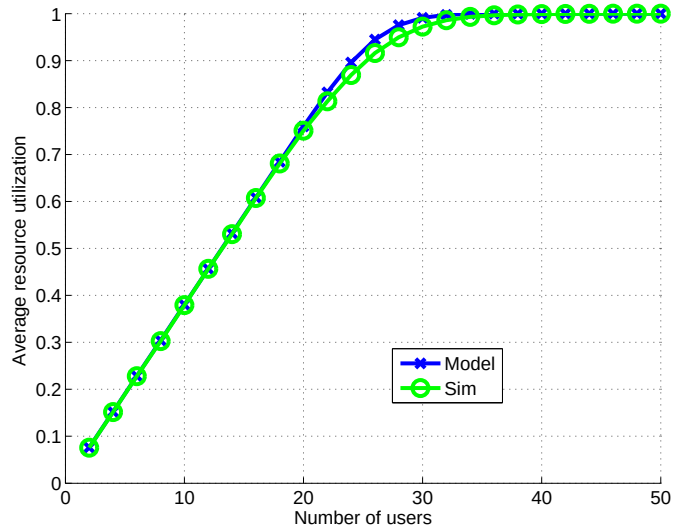

Figure 6.9: Average resource utilization for BE mono-profile with throttling scheme ($\bar{x}_{on}$ = 3 Mbits, $\bar{t}_{off}$ = 3 s and $MSTR$ = 512 Kbps).

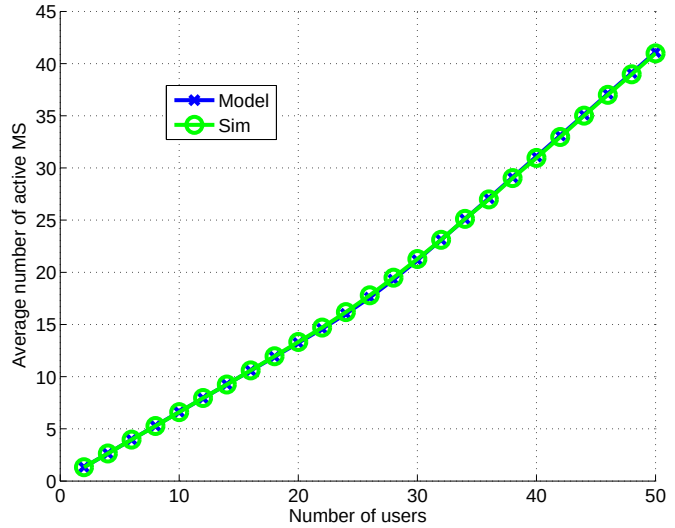

Figure 6.10: Average number of active MS for BE mono-profile with throttling scheme ($\bar{x}_{on} = 3$ Mbits, $\bar{t}_{off} = 3$ s and $MSTR = 512$ Kbps).

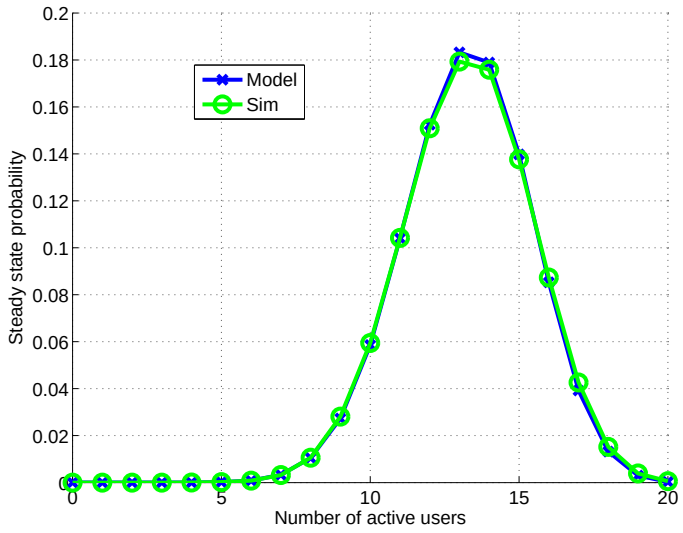

Figure 6.11: Steady state probabilities for BE mono-profile with throttling scheme for $N = 20$ ($\bar{x}_{on} = 3$ Mbits, $\bar{t}_{off} = 3$ s and $MSTR = 512$ Kbps).

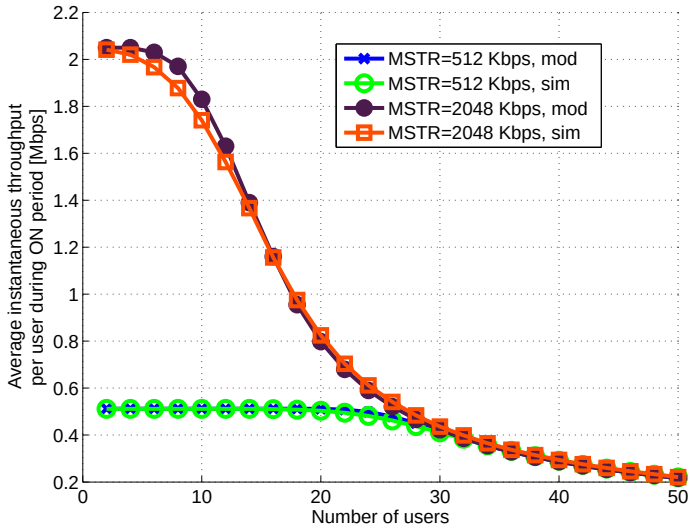

Figure 6.12: Average instantaneous user throughput for BE mono-profile with throttling scheme and different loads ($\bar{x}_{on} = 3$ Mbits and $\bar{t}_{off} = 3$ s; $MSTR = 512$ and 2048 Kbps).

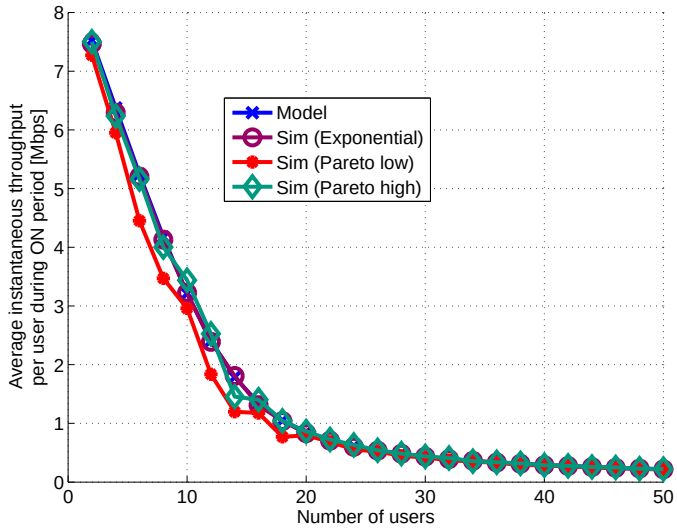

Figure 6.13: Average instantaneous user throughput for BE mono-profile with conventional scheduling schemes and different traffic distributions ($\bar{x}_{on} = 3$ Mbits and $\bar{t}_{off} = 3$ s).

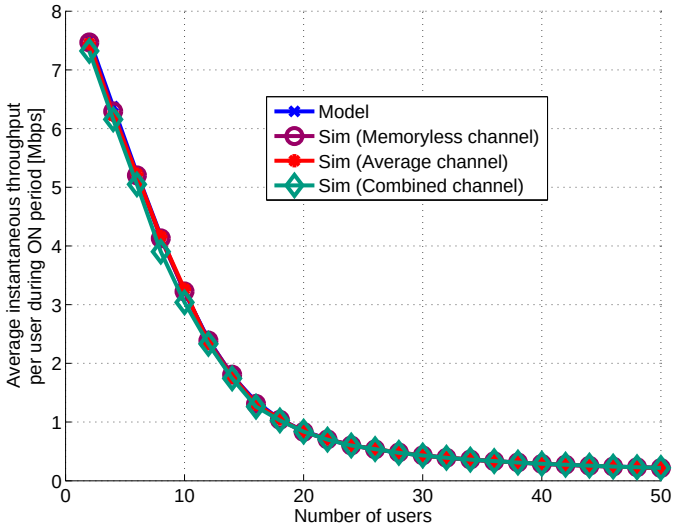

Figure 6.14: Average instantaneous user throughput for BE mono-profile with conventional scheduling schemes and different channel models ($\bar{x}_{on} = 3$ Mbits and $\bar{t}_{off} = 3$ s).

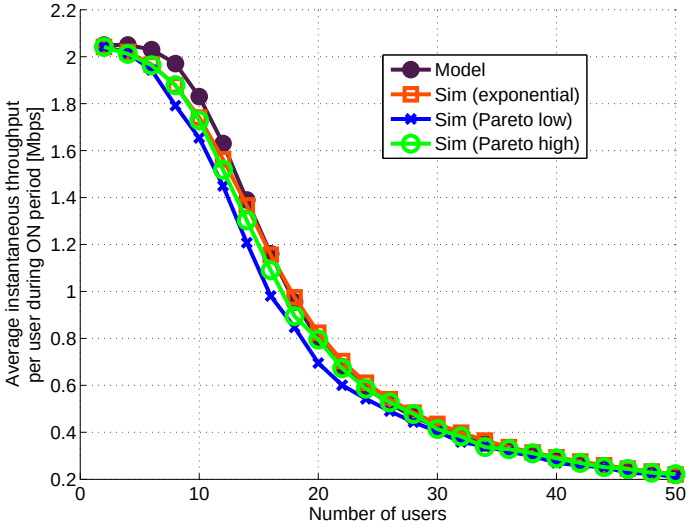

Figure 6.15: Average instantaneous user throughput for BE mono-profile with throttling scheme schemes and different traffic distributions ($\bar{x}_{on} = 3$ Mbits, $\bar{t}_{off} = 3$ s and $MSTR = 2048$ Kbps).

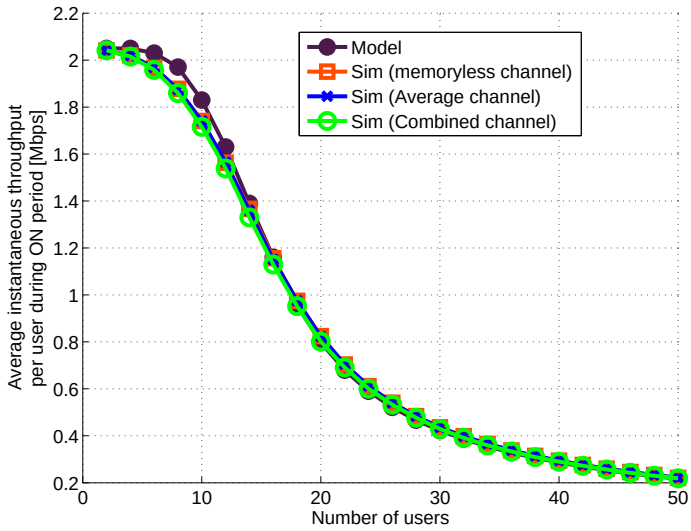

Figure 6.16: Average instantaneous user throughput for BE mono-profile with throttling scheme and different channel models ($\bar{x}_{on} = 3$ Mbits, $\bar{t}_{off} = 3$ s and $MSTR = 2048$ Kbps).

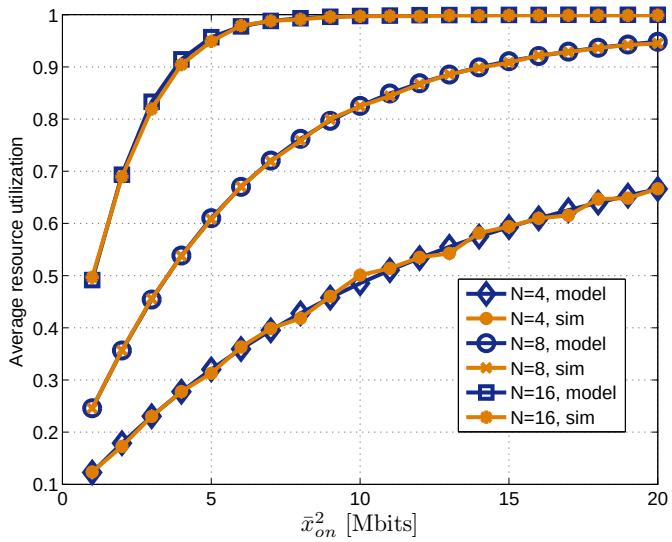

Figure 6.17: Average resource utilization for BE multi-profile with conventional scheduling schemes ($\bar{x}^1_{on} = 1$ Mbits and $\bar{t}^1_{off} = \bar{t}^2_{off} = 3$ s).

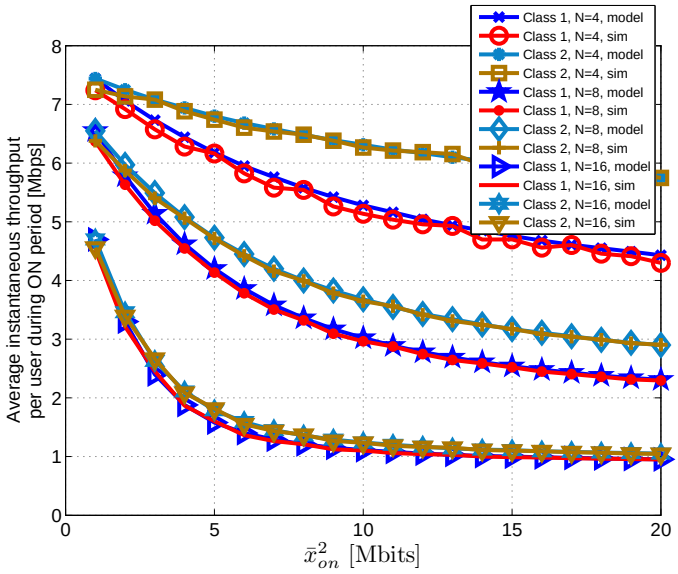

Figure 6.18: Average throughput per user during ON period for BE multi-profile with conventional scheduling schemes ($\bar{x}^1_{on} = 1$ Mbits and $\bar{t}^1_{off} = \bar{t}^2_{off} = 3$ s).

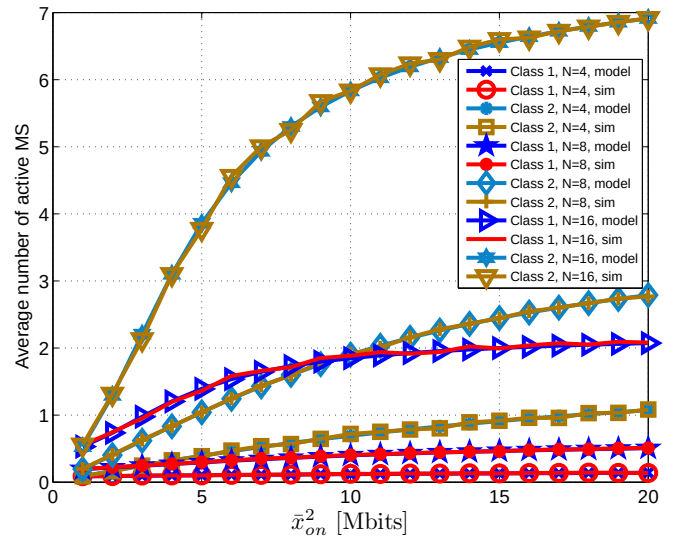

Figure 6.19: Average number of active users for BE multi-profile with conventional scheduling schemes ($\bar{x}^1_{on} = 1$ Mbits and $\bar{t}^1_{off} = \bar{t}^2_{off} = 3$ s).

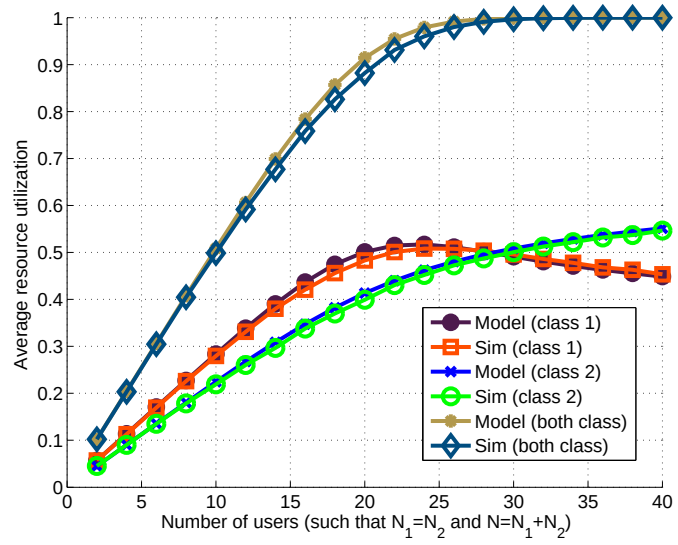

Figure 6.20: Average resource utilization for BE multi-profile with throttling scheme ($\bar{x}^1_{on} = \bar{x}^1_{on} = 3$ Mbits, $\bar{t}^1_{off} = 3$ s, $\bar{t}^2_{off} = 6$ s, $MSTR_1 = 1024$ Kbps and $MSTR_2 = 2048$ Kbps).

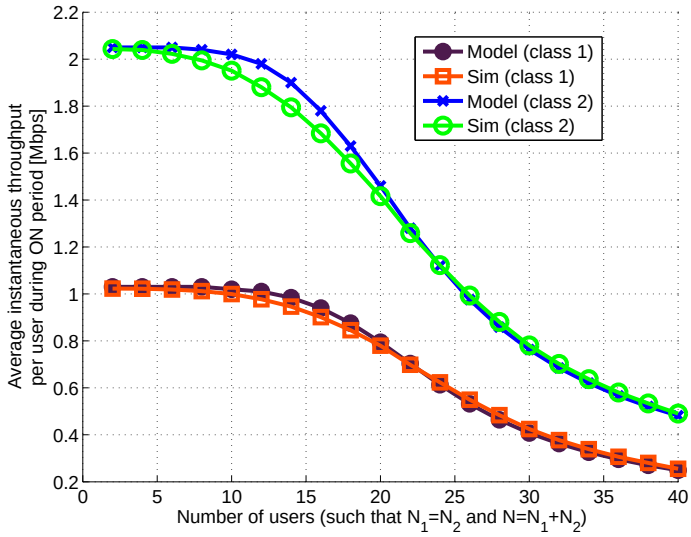

Figure 6.21: Average throughput per user during ON period for BE multi-profile with throttling scheme ($\bar{x}^1_{on} = \bar{x}^1_{on} = 3$ Mbits, $\bar{t}^1_{off} = 3$ s, $\bar{t}^2_{off} = 6$ s, $MSTR_1 = 1024$ Kbps and $MSTR_2 = 2048$ Kbps).

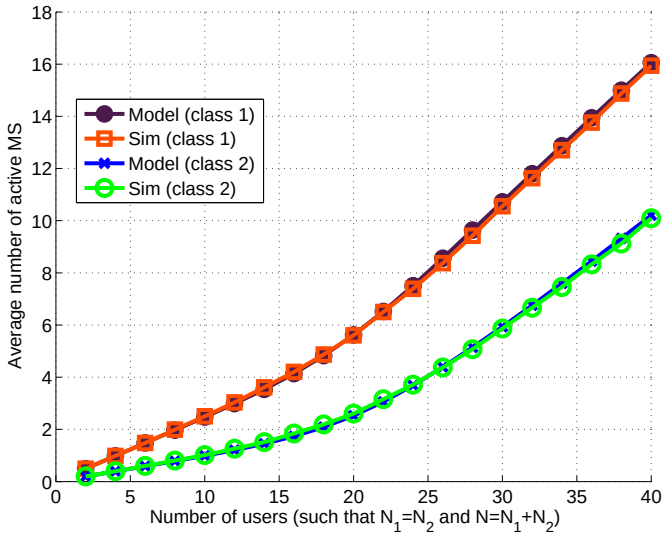

Figure 6.22: Average number of active users for BE multi-profile with throttling scheme ($\bar{x}^1_{on} = \bar{x}^1_{on} = 3$ Mbits, $\bar{t}^1_{off} = 3$ s, $\bar{t}^2_{off} = 6$ s, $MSTR_1 = 1024$ Kbps and $MSTR_2 = 2048$ Kbps).

Chapter 7

Conclusion and Future Work

In this chapter, we conclude the thesis report by presenting the brief outcome of different studies carried out during this thesis. We also discuss possible extensions as future work.

7.1 Conclusion

The performance targets set for OFDMA systems are quite promising. However, to achieve these targets, engineering tools are indispensable. In this thesis, we have presented a number of methods for OFDMA system engineering. These methods take into account both the static and dynamic systems. In the following, we briefly outline these methods.

We have developed a simulation based technique that made us possible to compare different frequency reuse schemes implying certain QoS parameters. It is shown that some frequency reuse schemes offering high throughput are faced with high outage. Hence, a compromise between the two is sought. We are able to show that without advanced features, OFDMA systems cannot employ aggressive frequency reuse because of considerable outage. Only reuse 3x3x3, characterized by 2% outage, is feasible in such a case. We also studied the change in performance with respect to different cell parameters (i.e., range and power) and could not notice significant variations.

By including the adaptive beamforming in the frequency comparison, it is concluded that more aggressive frequency reuse patterns (except reuse 1) than 3x3x3 provide more throughput with acceptable outage. Next we examined the possibility of achieving reuse 1. We were able to show that reuse 1 could be made feasible either by partial loading of subchannels (i.e., by using 80% of channels) or by exploiting the group structure of PUSC. Furthermore, we presented a comparison of three subcarrier permutation schemes (PUSC, FUSC and AMC) in case of reuse 1 and it was found that only beamforming per PUSC group could provide acceptable outage. AMC without BS coordination came up with more than 5% of outage.

It was pointed out in this report how important $SINR_{eff}$ statistics are and

that methods are desired to acquire these statistics efficiently. For this purpose, a semi-analytical method is proposed. As compared to methods based exclusively on Monte Carlo simulations, this method provides result with lesser time consumption with acceptable deviation of results.

More complex reuse schemes such as FFR vow to improve SINR for users near cell border by applying reuse 3 in the outer cell region and to benefit from aggressive frequency reuse by planning reuse 1 in the inner region. It provides a compromise between full reuse 1 and complete reuse 3 and exploits advantages of both. We have proposed an analytical method to calculate SINR for multiple reuse types including IFR, FFR and TLPC. We have also provided expressions for cell data rate by considering equal data rate, equal bandwidth and opportunist scheduling policies. It is demonstrated that optimum size of inner and outer regions for FFR and TLPC schemes depends upon the scheduling policy. The same is true for power ratio of inner/outer regions for TLPC and bandwidth division between inner/outer regions for FFR. We have also given a comparison between three frequency reuse schemes in terms of SINR values and data rates. We have also studied the effect of different path-loss values on our results.

As far as study of dynamic system is concerned, we have worked on validation and robustness study of analytical models developed for WiMAX systems. These models furnish the performance parameters that could be used in dimensioning process. Models take into account different scheduling policies and different classes of traffic. We have shown that models results obtained through model have little variation w.r.t. those of simulations. We have also concluded that the model provides acceptable results for different radio channels, traffic distributions and load conditions.

7.2 Future Work

There is a famous quote by Thorstein Veblen: *The outcome of any serious research can only be to make two questions grow where only one grew before.* With belief that our research work was serious, we propose possible extensions.

In case of static systems, we have studied the performance of adaptive beamforming for six frequency reuse patterns. We suggest the same analysis to be done with MIMO and compare the two. BS coordination techniques are important in context of AMC subcarrier permutation and should be worked upon. While we proposed a semi-analytical method to model $SINR_{eff}$ statistics, a complete analytical method (providing rapid results) is more desirable and should be sought. In analytical study of IFR, FFR and TLPC, we did not take into account the shadowing and fast fading phenomenon and hence would like to do so in future.

Our study of dynamic systems considered only elastic traffic. It would be valuable to include the real-time traffic into analytical models with this non-real time bursty traffic. It would provide a complete picture with respect to assignment of resource to two traffic types. Delay and jitter are not considered in the presented work and hence are to be accounted for. Adaptation of models

to LTE would also be a worthy task. In dynamic systems, we have considered one cell in the multi-cellular network. It will be beneficial to study the effect of interaction among network cells.

Appendix A

Details on Subcarrier Permutations

In this appendix, we explain the three subcarrier permuation types: FUSC DL, PUSC DL and AMC. These details are based on [26, 25]. For the purpose of explanation, 2048-FFT is kept as a reference. With 2048-FFT, used bandwidth is 20 MHz. Total number of subcarriers is 2048 (numbered as 0-2047). We shall refer this 0-2047 scale as 'absolute subcarrier index' in the proceeding text.

Before we start with the description of subcarrier permutation types, it would be valuable to establish definitions of few terms.

Subcarrier: An OFDM symbol is made up of subcarriers. There are three subcarrier types: data subcarriers (for data transmission), pilot subcarriers (for channel estimation purposes) and null subcarriers (for no transmission, guard bands, non-active subcarriers and the DC-subcarrier). Subcarrier spacing is 10.9375 kHz [8].

Subchannel: It is a set of subcarriers. In distributed subcarrier permutation mode (i.e., FUSC and PUSC), subcarriers of a subchannel are not contiguous. Their distribution is determined by a permutation formula given by Eq. 111 of [26]. In adjacent subcarrier mode, subchannels are constituted of contiguous subcarriers.

Slot: It is the minimum possible data allocation unit. It spans both the time domain (OFDM symbol) and frequency domain (subchannel). It is expressed as number of subchannels per number of symbols (see Fig. A.1).

Permutation zone: It consists of OFDMA symbols that use the same permutation scheme (i.e., PUSC, FUSC or AMC). According to [26] and [25], first zone in the DL subframe is essentially PUSC. The maximum number of downlink zones in one downlink subframe is eight. The maximum number of bursts to decode in one downlink subframe is sixty four. An example of different permutation zones (in DL and UP subframes) is given in Fig.A.2.

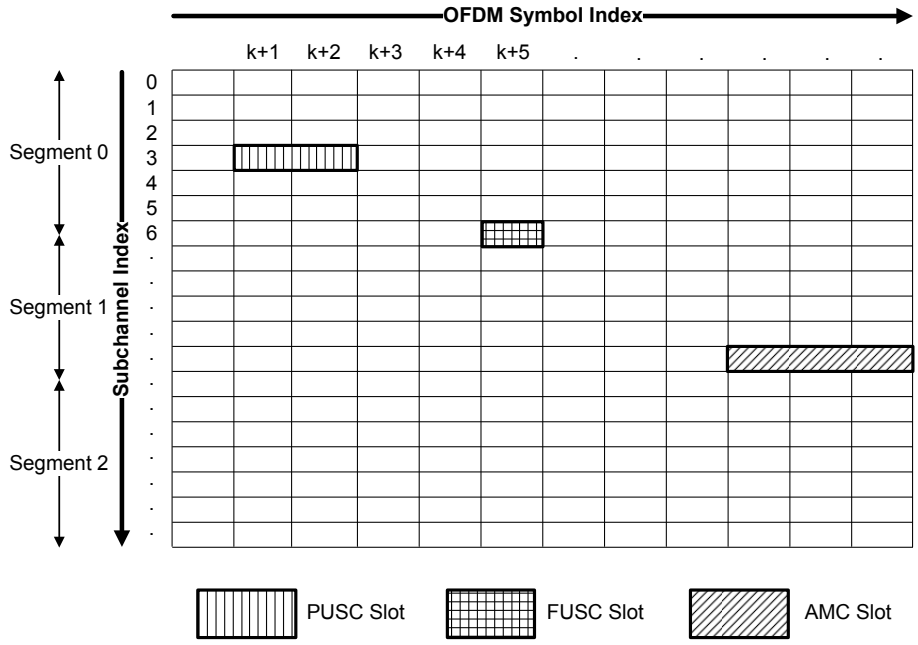

Figure A.1: OFDMA downlink sub-frame.

DC Subcarrier: In an OFDM or OFDMA signal, the subcarrier whose frequency is equal to the Radio Frequency (RF) center frequency of the station is called the DC subcarrier.

Perm_Base: It has been separately defined for DL and UL. In DL it is called DL_PermBase which is an integer ranging from 0 to 31 identifying the particular BS segment and is specified by MAC layer. It is set to preamble IDCell in the first zone and determined by the DL-MAP for other zones. For UL, there is a different integer called UL_PermBase which ranges from 0 to 69 and is assigned by a management entity.

A.1 Full Usage of Subchannels (FUSC)

With subcarrier permutation type FUSC, all of the subchannels are allocated to the transmitter. That is why it is called full usage of subchannel [25]. As already mentioned, it is used only in DL.

One slot of FUSC DL is one OFDM symbols by one subchannel (Fig. A.1), while one FUSC DL subchannel comprises of 48 data subcarriers. With 2048-FFT, there are 32 subchannels in total. Out of 2048, there are 173 left guard subcarriers, 172 right guard subcarriers, 1536 data subcarriers, 166 pilot subcarriers and one DC subcarrier. Out of 166, 24 pilot subcarriers are fixed and their positions (w.r.t. absolute subcarrier index) are specified in Tab. 311, page 531 of [26]. The rest 142 pilot subcarriers are variable and they change from one FUSC

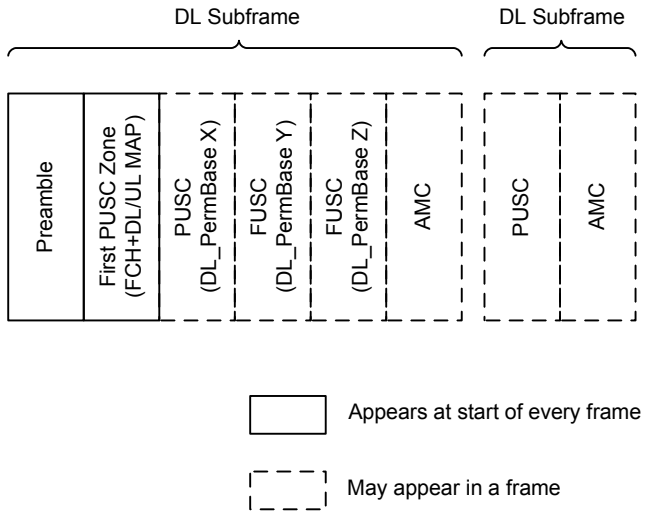

Figure A.2: Illustration of OFDMA frame with multiple zones (inspired from Fig. 219 of [26]).

symbol (starting from 0) to another. Their positions are given by the Eq. 110 of [25]:

$$\text{Pilot Locations} = \text{Variable Set\#}x \ + \ 6 \times (\text{FUSC Symbol Number} \mod 2),$$

where x is either 0 and 1. Half the variable pilot subcarriers (i.e., 71) belong to Variable Set#0 while other half belongs to Variable Set#1. The indices of pilot subcarriers in two Variable Sets are given in Tab. 311 (page 531 of [26]).

A.1.1 Subchannel Formation

Before subcarriers are assigned to subchannels, both fixed and variable pilot subcarriers are first separated. The rest of the subcarriers (data subcarriers) are combined in groups. Then permutation formula (Eq. 111 of [25]) is used to assign subcarriers to subchannels. As already mentioned, number of data subcarriers in every subchannel is the same, i.e., 48; however, number of subchannels is equal to the number of subcarriers in a group. With 2048-FFT, there are 32 subchannels in total.

During subcarrier distribution process, one subcarrier is picked up using the permutation formula from every group and is being allocated to a subchannel. The process is shown in Fig. A.3.

The Eq. 111 of [25] is rewritten here for reference:

$$subcarrier(k,s) = N_{subchannels} \times n_k + \{P_s[n_k \mod N_{subchannels}] + \text{DL\_PermBase}\} \mod N_{subchannels}$$

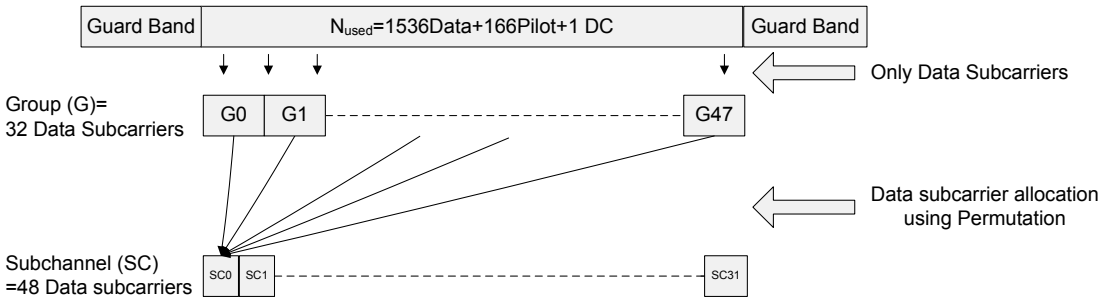

Figure A.3: Permutation process of FUSC DL (2048-FFT)

where

$subcarrier(k, s)$	is the index of subcarrier k among all available data subcarriers. With 2048-FFT, index of subcarrier ranges from 0-1535.
s	is the index number of a subchannel in a group, from the set $[0...N_{subchannels-1}]$.
$N_{subchannels}$	ranges from $0 - 32$.
n_k	$= (k + 13s) \mod N_{subcarrier}$.
k	is the subcarrier-in-subchannel index from the set $[0...N_{subcarrier} - 1]$. It ranges from $0 - 47$.
$N_{subcarrier}$	is always 48 for FUSC.
DL_PermBase	is already defined (cf. section-1.2.2.1).
$P_s[.]$	is the series obtained by rotating basic permutation sequence cyclically to the left s times (Tab. 311 [26]). $P_s[.]$= {3, 18, 2, 8, 16, 10, 11, 15, 26, 22, 6, 9, 27, 20, 25, 1, 29, 7, 21, 5, 28, 31, 23, 17, 4, 24, 0, 13, 12, 19, 14, 30}.

Following example explains the procedure:

Let $k = 46$, $s = 31$ and DL_PermBase =0

$n_k = (46 + 13 \times 31) \mod 48 = 17$

$$\begin{aligned} Subcarrier(46, 31) &= 32 \times 17 + \{P_{31}[17 \mod 32] + 0)\} \mod 32 \\ &= 544 + 29 \\ &= 573 \end{aligned}$$

Fig. A.4 shows 48 subcarriers of subchannel '0' of group zero plotted against absolute subcarrier index. It is clear from the figure that subcarriers of a sub-

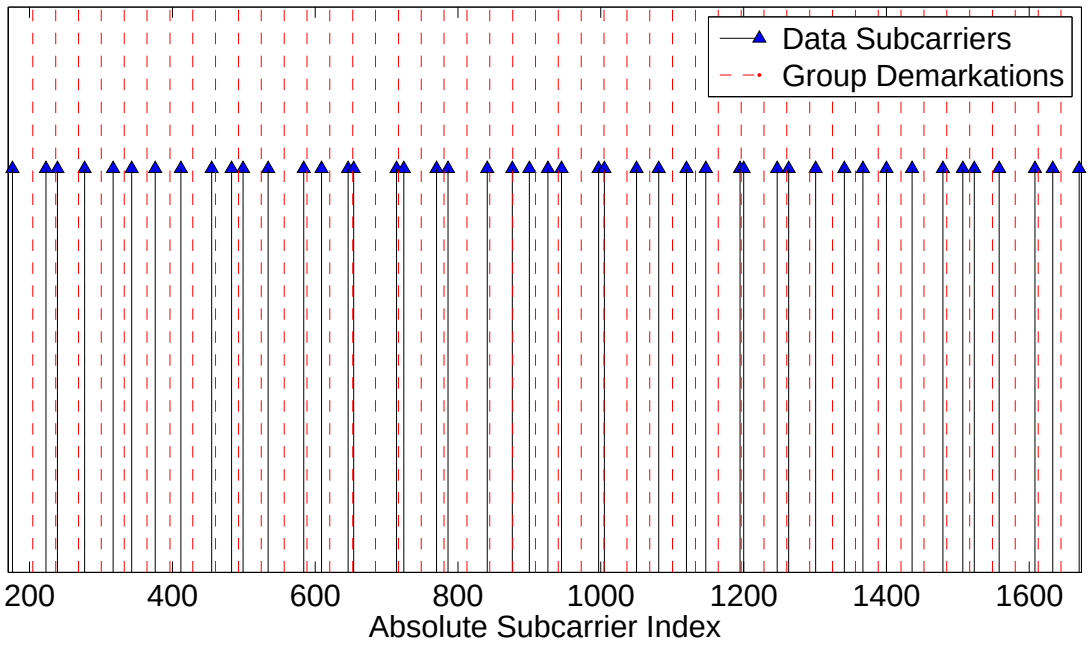

Figure A.4: Forty eight subcarriers of subchannel '0' and symbol '0' with $DL\_PermBase = 0$ for FUSC DL (2048-FFT)

channel are distributed throughout the available band (excluding guard bands). It can also be noticed that only one subcarrier is included from every group.

A.1.2 Partial Usage of Subchannels (PUSC)

In this type of subcarrier permutation, some of the subchannels are allocated to the transmitter. That is why, it is called partial usage of subchannel [25]. The subchannels allocated to one transmitter form a segment. Remaining subchannels are attributed to different segments. PUSC is used both in UL and DL but as mentioned earlier, here we shall explain only PUSC DL.

One slot of PUSC DL is two OFDM symbols by one subchannel (see Fig. A.1), while one PUSC DL subchannel is comprises 24 data subcarriers. Out of 2048, there are 184 left guard subcarriers, 183 right guard subcarriers, 1440 data subcarriers, 240 pilot subcarriers and one DC subcarrier. Few terms specific to PUSC DL followed by subchannel formation description are presented hereafter.

Segment: A set of available subchannels form a segment. It is a PUSC specific parameter. There can be three segments in a frame (see Fig. A.1).

Physical Cluster: It is a set of 14 adjacent subcarriers (12 data + 2 pilot). These clusters are contiguous in the frequency band (see Fig. A.5). There are total 120 physical clusters with 2048-FFT.

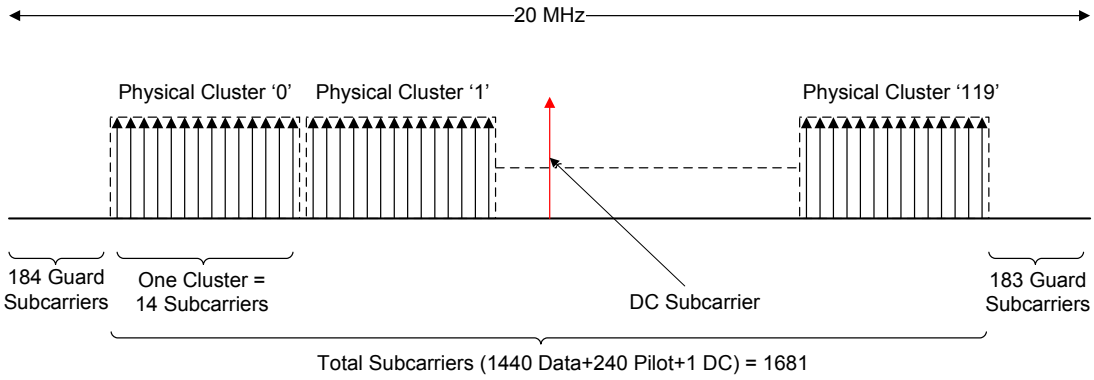

Figure A.5: Physical clusters in PUSC DL (2048-FFT).

Outer Permutation: It is the process by which physical clusters are renumbered according to a renumbering sequence to form logical clusters. This renumbering sequence is given in [25]. Two adjacent logical clusters are not contiguous in frequency domain.

Group (or Major Group): It is a set of logical clusters. Odd numbered groups contain half the number of logical clusters as compared to even numbered groups. These groups are commonly referred as major groups. There are six groups in total. With 2048-FFT, an odd group consists of 24 logical clusters while an even group comprises 16 logical clusters.

Inner Permutation: The process to form subchannels from the subcarrier of logical clusters of a group is called inner permutation.

For the purpose of inner permutation, the subcarriers of each group are indexed separately, i.e., every group will have subcarriers index starting from '0'. With 2048-FFT, even and odd groups will have subcarrier index 0-335 and 0-225 respectively. By applying inner permutation, '12' and '8' subchannels will respectively be formed from even and odd groups. Before subchannel formation, pilot subcarriers are identified and rest of the subcarriers are re-indexed i.e., 0-287 and 0-194 for even and odd groups respectively. These re-indexed numbers will be referred as group subcarrier index in subsequent sections.

A.1.3 Subchannel Formation

The permutation process to form subchannels is shown in Fig. A.6. The process is stepwise explained in the following text.

Step 1: All available subcarriers are partitioned as right guard band, data, DC, pilot and left guard band subcarriers. Each physical cluster is formed by grouping together 14 adjacent subcarriers. With 2048-FFT, there are total 120 physical clusters (numbered as 0-119). These clusters include all the data and pilot sub-

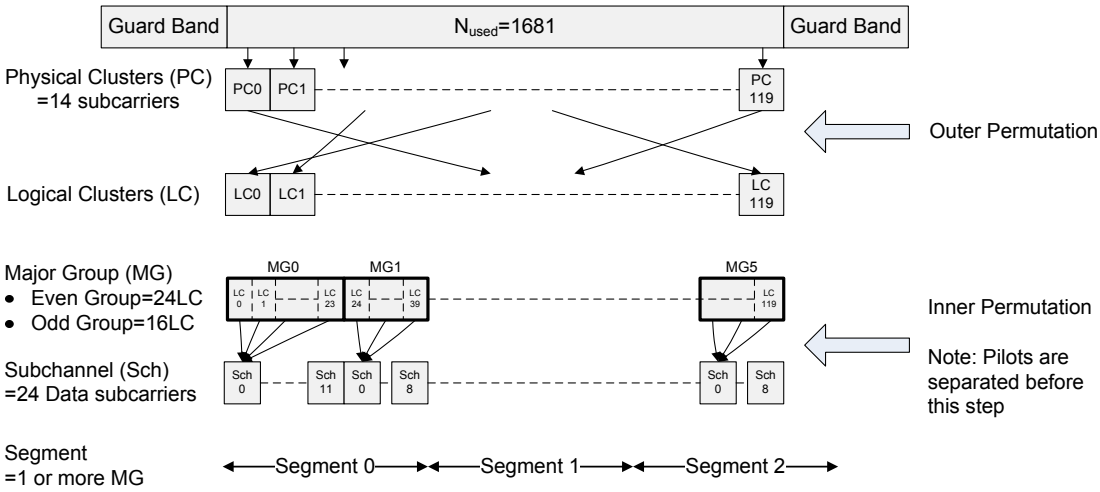

Figure A.6: Outer and inner permutations in PUSC DL.

carriers. Fig. A.5 explains this step.

Step 2: Logical clusters are formed by renumbering the Physical clusters obtained in step 1 using equation (referred from [26]) given below. This process is also called outer permutation.

$$\text{Logical Cluster} = \text{Renumbering Sequence(Physical Cluster)} + 13 \times \text{DL\_PermBase} \mod N_{clusters}$$

DL_PermBase in the first zone is set to zero for all the cells/segments. The renumbering sequence is given in [25].

Step 3: Logical clusters of step 2 are grouped together to form 6 major groups. These groups are numbered from 0 to 5. In case of 2048-FFT, even groups (0, 2 and 4) contain 24 logical clusters each, while odd groups (1, 3 and 5) have 16 logical clusters each.

In order to appreciate how this outer permutation achieves frequency diversity, plot in Fig. A.7 shows distribution of logical clusters of group '0' with respect to index of 120 physical clusters.

Step 4: Pilot positions are marked separately for odd and even OFDM symbol. These subcarriers will be separated from the rest before inner permutation is performed. For example, consider subcarriers of logical cluster '0' (With DL_PermBase= 0, it is the 6^{th} physical cluster). These subcarriers are numbered as 0-13 (Fig. A.8). Their positions w.r.t. the absolute subcarrier index $(0-2047)$ are 268-281. The pilot subcarriers for even symbols will be '4' and '8' ('272' and '276' w.r.t absolute subcarrier index). For odd OFDM symbols '0' and '12' ('268' and '280') will be pilot positions. The rest twelve subcarriers will be used as data

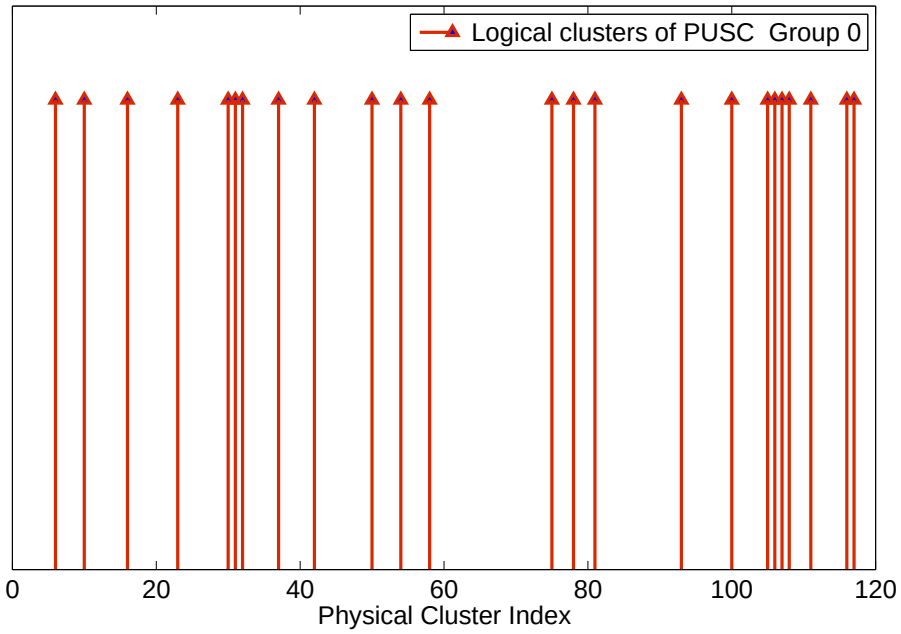

Figure A.7: Logical clusters of PUSC Group '0' versus physical cluster index (PUSC DL, 2048-FFT).

subcarriers in the inner permutation.

Step 5: Subcarriers of a group are assigned to subchannels using permutation formula given by Eq. 111 of [26]. It should be noted that this formula is explicitly applied to subcarriers of a group while in FUSC DL, it was applied to all data subcarriers. Subcarrier index obtained from this formula is the group subcarrier index (cf. description of inner permutation). The value of DL_PermBase used in subchannel formation is set as preamble IDcell for the first PUSC zone and can be set between (0-31) for the rest of the PUSC zones. Following example explains this step:

Let $k = 11$ (subcarrier-in-subchannel index), $s = 1$ (subchannel index in group), DL_PermBase= 0 and Group = 0

$$n_k = (11 + 13 \times 1)\ mod\ 24 = 0$$

$$\begin{aligned} Subcarrier(11, 1) &= 12 \times 0 + \{P_1[0 \bmod 12] + 0\} \bmod 12 \\ &= 0 + 9 \\ &= 9 \end{aligned}$$

This is the 9^{th} subcarrier of even group '0'. With all the above input parameters (for both the inner and outer permutations), it belongs to logical cluster '0' and physical cluster '6' (the one identified in step 4 also). Since the positions of pilot subcarriers are different for odd and even OFDM symbols, for even OFDM symbols, this will be the 278^{th} subcarrier (w.r.t. the absolute subcarrier index)

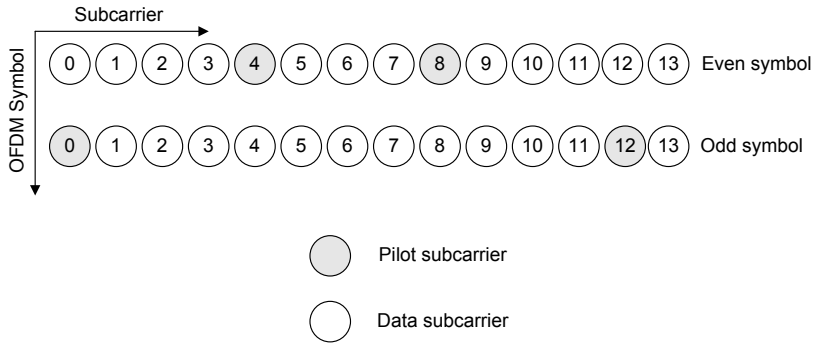

Figure A.8: PUSC DL slot.

and for odd OFDM symbols, this will be 277^{th} subcarrier (w.r.t. the absolute subcarrier index). In this way all subcarriers of a group are assigned to the subchannels.

We have already seen the effect of outer permutation on frequency diversity. To see the effect of both the inner and outer permutation at the same time, subcarriers of subchannel '0' (of group '0') are also plotted against the absolute subcarrier index (Fig. A.9).

A.2 AMC

The smallest unit in frequency domain for adjacent carrier permutation is called the bin. It is composed of 9 contiguous subcarriers. Out of 9, eight are data tones and one is pilot tone. The position of pilot tone inside the bin changes from one OFDM symbol to the other and the method is explained while discussing pilot allocations. A slot in AMC (or regular AMC) mode is two bins by three symbols. Although it has not been exclusively specified in [26, 25], but in consistent with nomenclature of PUSC and FUSC, we call the bins in a slot as subchannel. Hence, in AMC mode, there are two bins per subchannel.

A.2.1 Pilot Allocations and Data Mapping

Pilots are allocated first and separated from the data subcarriers. The indexing of pilot tones is done using equation given below [26]:

$$\text{Pilot Subcarrier Index} = 9k + 3m + 1$$

with

$$m = [\text{symbol index}] \mod 3,$$

where $k = 0, 1, 2....N_k$. The value of N_k (given in [26]) depends upon FFT size. Symbol index m is equal to zero for first symbol of an AMC zone. Once the pilots are allocated, data mapping to subcarriers is done in a sequential way.

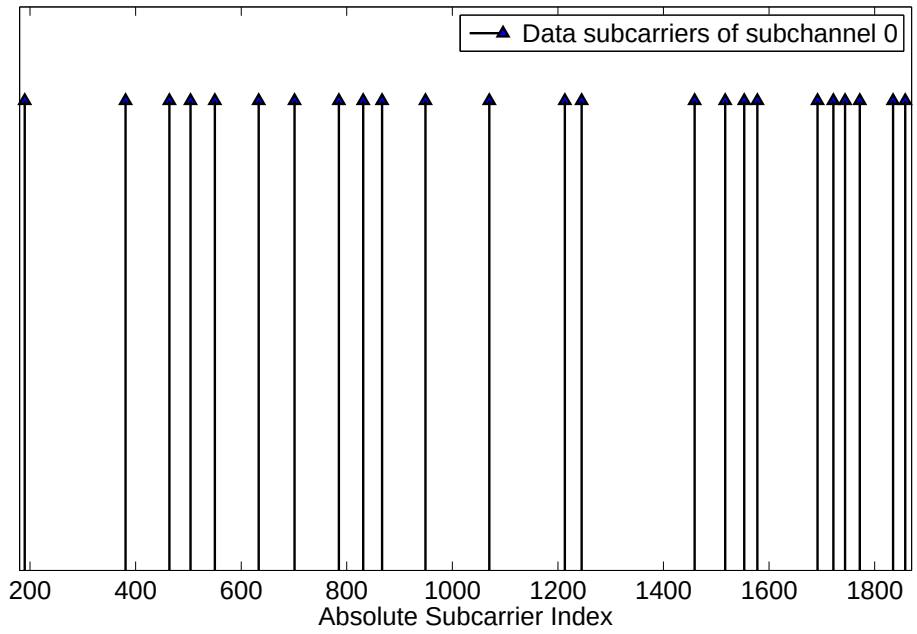

Figure A.9: Data Subcarriers of subchannel '0' and PUSC group '0' (first PUSC zone, DL_PermBase= 0 and odd symbol) plotted against absolute subcarrier index.

Appendix B

Remaining Results of Semi-analytical Method

In chapter 4, we presented results for only reuse type 3x3x3. In this appendix, we have given the results for five other reuse types: 1x1x1, 1x3x1, 1x3x3, 3x1x1 and 3x3x1. In addition, we have also included the results for reuse 1x3x1 with adaptive beamforming.

B.1 Reuse Type 1x1x1

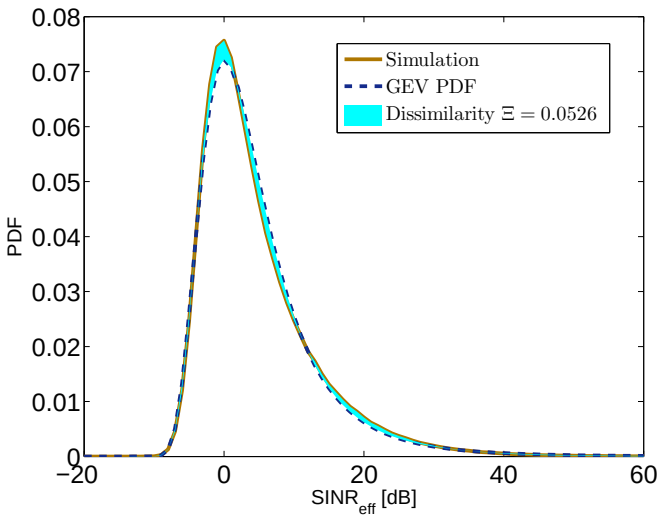

Figure B.1: $SINR_{eff}$ distribution through simulation and GEV parameters for $\sigma_{SH} = 9$ dB, $R = 1500$ m, $P_{Tx} = 43$ dBm and reuse 1x1x1.

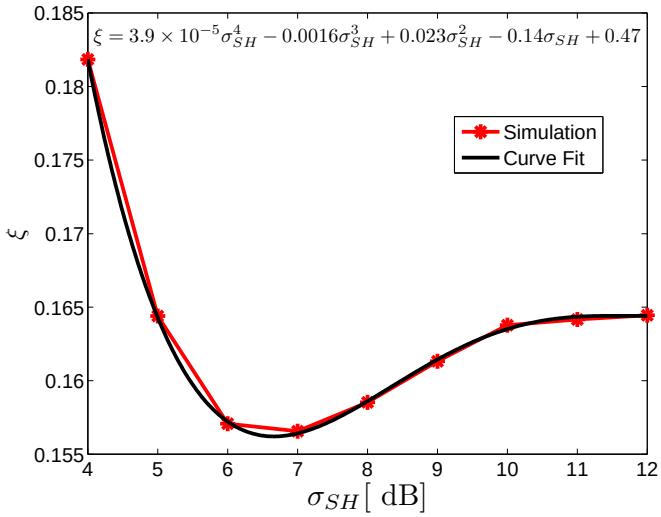

Figure B.2: Shape parameter ξ of GEV distribution vs σ_{SH} for $R = 1500$ m, $P_{Tx} = 43$ dBm and reuse 1x1x1.

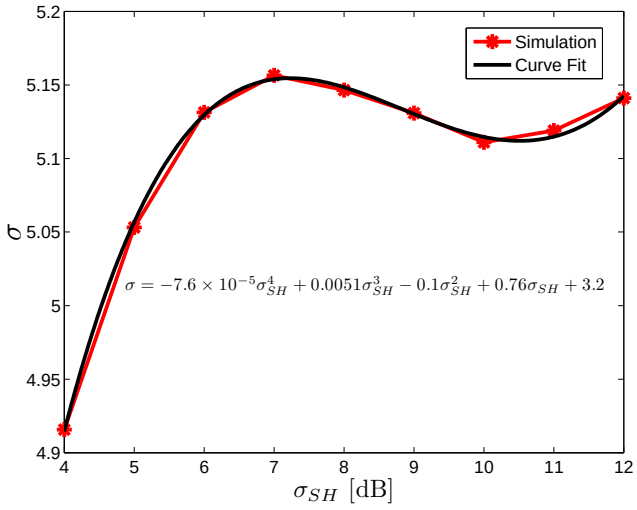

Figure B.3: Scale parameter σ of GEV distribution vs σ_{SH} for $R = 1500$ m, $P_{Tx} = 43$ dBm and reuse 1x1x1.

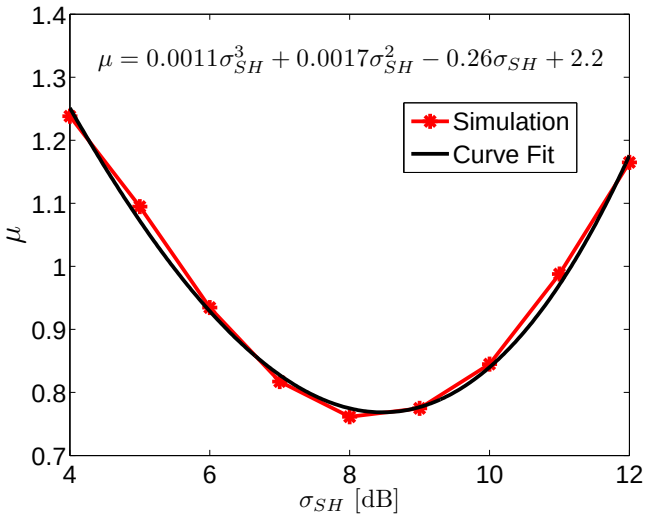

Figure B.4: Location parameter μ of GEV distribution vs σ_{SH} for $R = 1500$ m, $P_{Tx} = 43$ dBm and reuse 1x1x1.

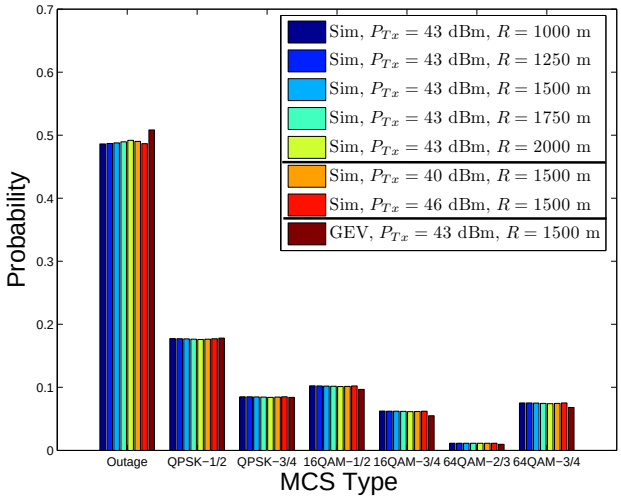

Figure B.5: MCS probabilities for $\sigma_{SH} = 7.5$ dB and reuse 1x1x1.

Table B.1: Comparison of results obtained through simulation and GEV parameters for $\sigma_{SH} = 7.5$ dB for reuse 1x1x1.

Simulation Configuration		**Dissimilarity Ξ**	**Percentage w.r.t max error**	**Throughput X [Mbps]**		**Percentage difference**
P_{Tx} [dBm]	**R** [m]			**Sim**	**GEV**	
43	1000	0.05	2.50	4.67	4.35	6.79
43	1250	0.05	2.50	4.66	4.35	6.65
43	1500	0.05	2.50	4.65	4.35	6.42
43	1750	0.05	2.53	4.64	4.35	6.08
43	2000	0.05	2.57	4.61	4.35	5.59
40	1500	0.05	2.54	4.63	4.35	5.95
46	1500	0.05	2.50	4.66	4.35	6.66

B.2 Reuse Type 1x3x1

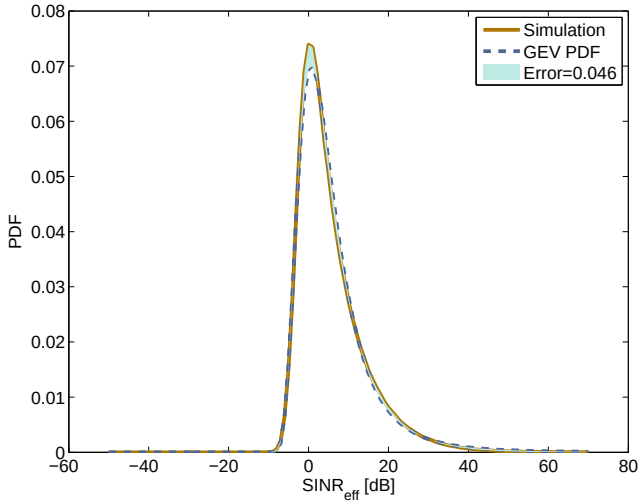

Figure B.6: $SINR_{eff}$ distribution through simulation and GEV parameters for $\sigma_{SH} = 9$ dB, $R = 1500$ m, $P_{Tx} = 43$ dBm and reuse 1x3x1.

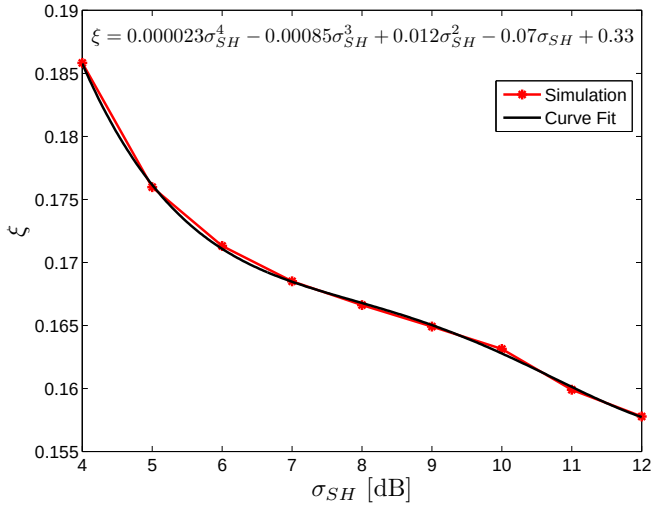

Figure B.7: Shape parameter ξ of GEV distribution vs σ_{SH} for $R = 1500$ m, $P_{Tx} = 43$ dBm and reuse 1x3x1.

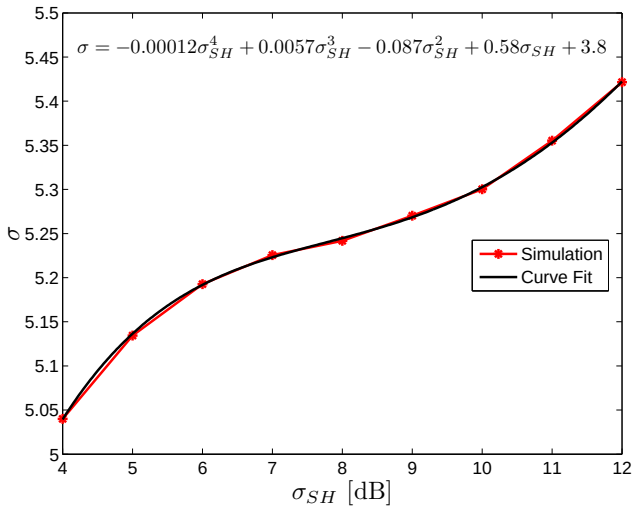

Figure B.8: Scale parameter σ of GEV distribution vs σ_{SH} for $R = 1500$ m, $P_{Tx} = 43$ dBm and reuse 1x3x1.

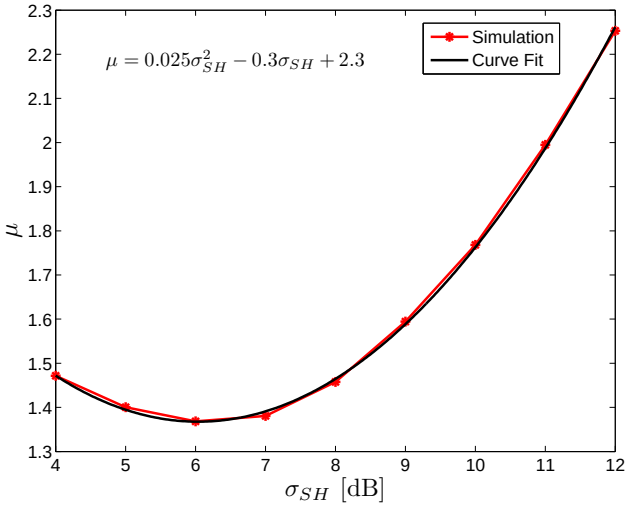

Figure B.9: Location parameter μ of GEV distribution vs σ_{SH} for $R = 1500$ m, $P_{Tx} = 43$ dBm and reuse 1x3x1.

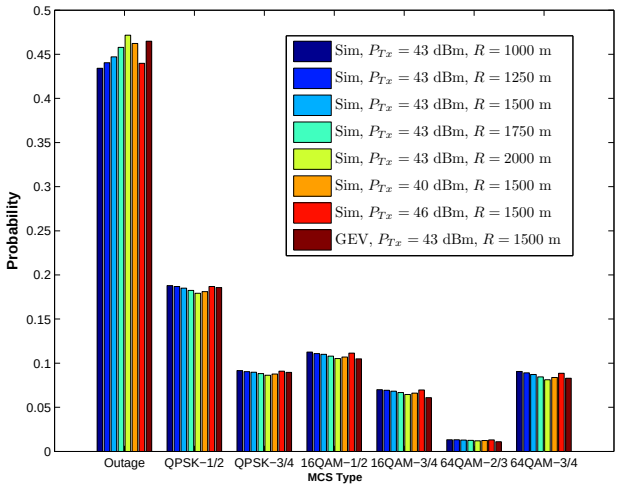

Figure B.10: MCS probabilities for $\sigma_{SH} = 7.5$ dB and reuse 1x3x1.

Table B.2: Comparison of results obtained through simulation and GEV parameters for $\sigma_{SH} = 7.5$ dB for reuse 1x3x1.

Simulation Configuration		**Dissimilarity Ξ**	**Percentage w.r.t max error**	**Throughput X [Mbps]**		**Percentage difference**
P_{Tx} [dBm]	**R** [m]			**Sim**	**GEV**	
43	1000	0.056	2.80	15.82	14.65	7.42
43	1250	0.054	2.70	15.62	14.65	6.23
43	1500	0.053	2.65	15.39	14.65	4.84
43	1750	0.064	3.20	15.04	14.65	2.62
43	2000	0.085	4.25	14.59	14.65	0.37
40	1500	0.071	3.55	14.92	14.65	1.80
46	1500	0.054	2.70	15.62	14.65	6.24

B.3 Reuse Type 1x3x3

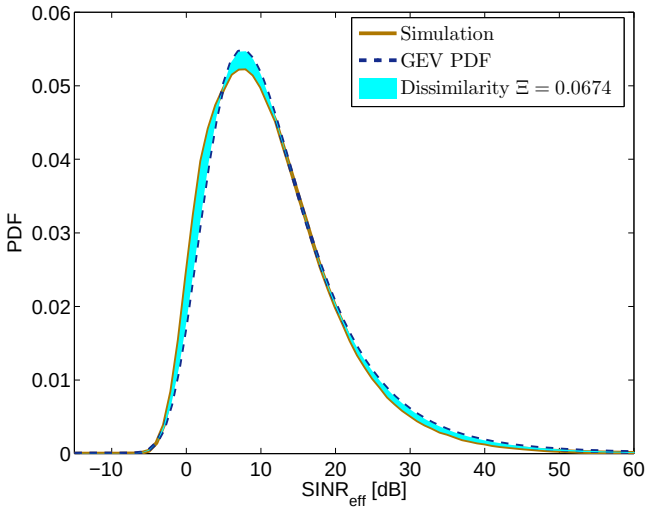

Figure B.11: $SINR_{eff}$ distribution through simulation and GEV parameters for $\sigma_{SH} = 9$ dB, $R = 1500$ m, $P_{Tx} = 43$ dBm and reuse 1x3x3.

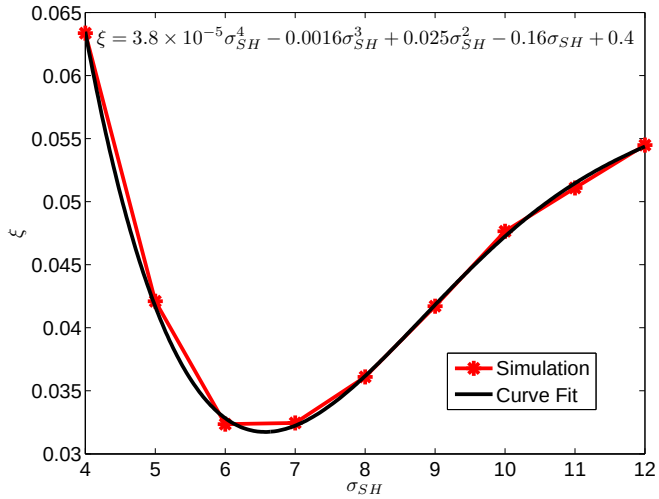

Figure B.12: Shape parameter ξ of GEV distribution vs σ_{SH} for $R = 1500$ m, $P_{Tx} = 43$ dBm and reuse 1x3x3.

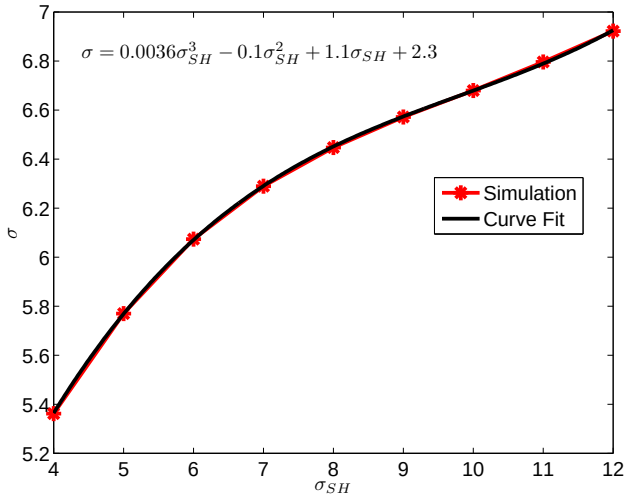

Figure B.13: Scale parameter σ of GEV distribution vs σ_{SH} for $R = 1500$ m, $P_{Tx} = 43$ dBm and reuse 1x3x3.

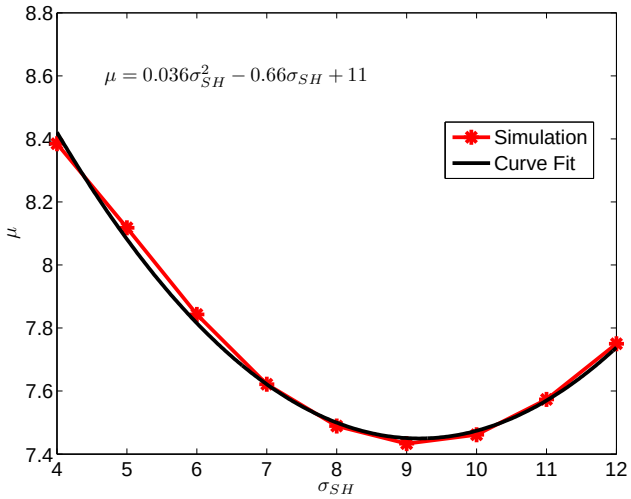

Figure B.14: Location parameter μ of GEV distribution vs σ_{SH} for $R = 1500$ m, $P_{Tx} = 43$ dBm and reuse 1x3x3.

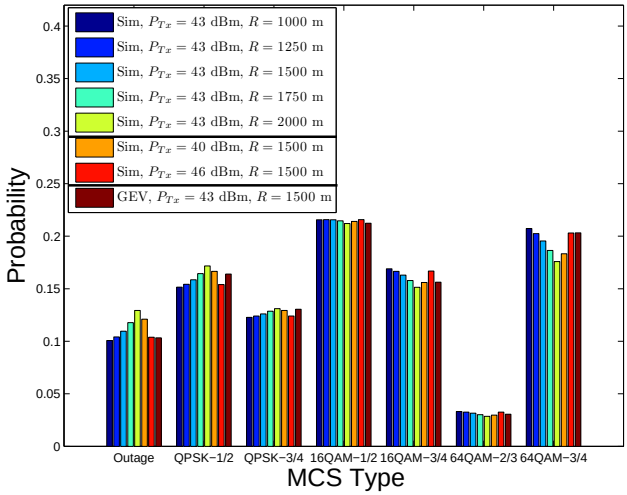

Figure B.15: MCS probabilities for $\sigma_{SH} = 7.5$ dB and reuse 1x3x3.

Table B.3: Comparison of results obtained through simulation and GEV parameters for $\sigma_{SH} = 7.5$ dB for reuse 1x3x3.

Simulation Configuration		**Dissimilarity Ξ**	**Percentage w.r.t max error**	**Throughput X [Mbps]**		**Percentage difference**
P_{Tx} [dBm]	**R** [m]			**Sim**	**GEV**	
43	1000	0.05	2.45	10.11	9.89	2.14
43	1250	0.05	2.48	9.99	9.89	1.04
43	1500	0.06	2.93	9.82	9.89	0.69
43	1750	0.09	4.26	9.59	9.89	3.14
43	2000	0.13	6.29	9.30	9.89	6.39
40	1500	0.10	4.82	9.51	9.89	4.05
46	1500	0.05	2.47	10.0	9.89	1.14

B.4 Reuse Type 3x1x1

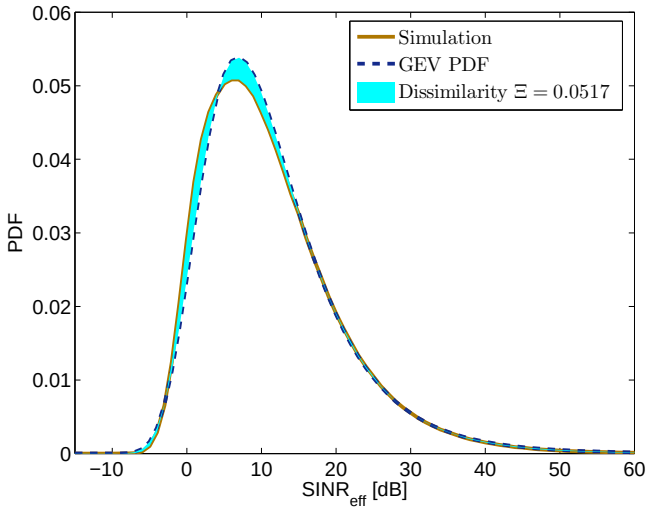

Figure B.16: $SINR_{eff}$ distribution through simulation and GEV parameters for $\sigma_{SH} = 9$ dB, $R = 1500$ m, $P_{Tx} = 43$ dBm and reuse 3x1x1.

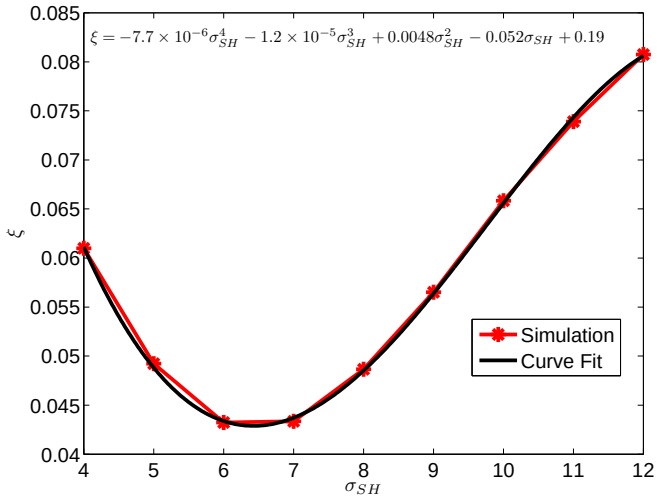

Figure B.17: Shape parameter ξ of GEV distribution vs σ_{SH} for $R = 1500$ m, $P_{Tx} = 43$ dBm and reuse 3x1x1.

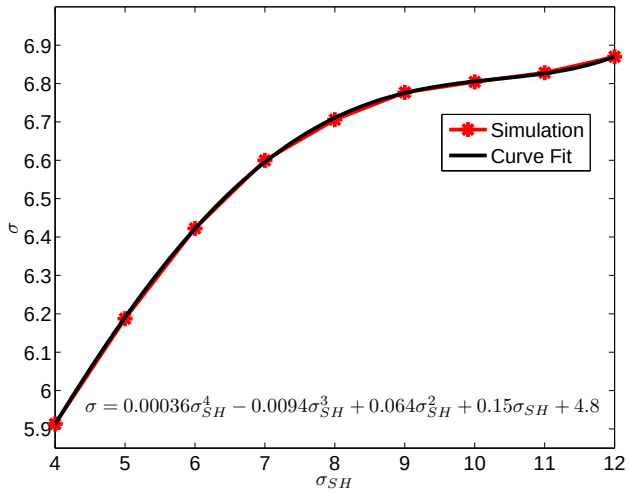

Figure B.18: Scale parameter σ of GEV distribution vs σ_{SH} for $R = 1500$ m, $P_{Tx} = 43$ dBm and reuse 3x1x1.

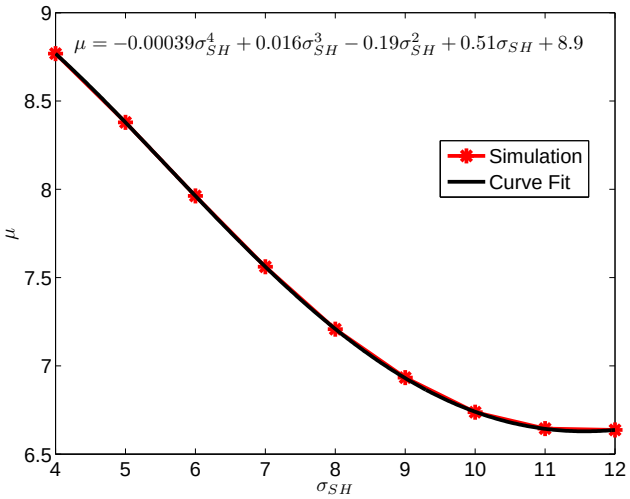

Figure B.19: Location parameter μ of GEV distribution vs σ_{SH} for $R = 1500$ m, $P_{Tx} = 43$ dBm and reuse 3x1x1.

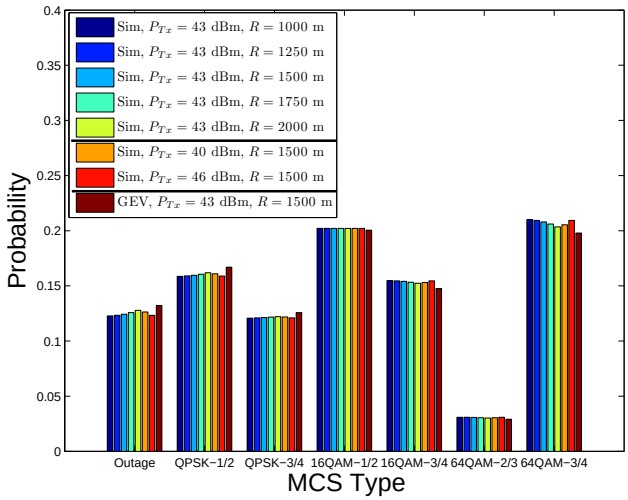

Figure B.20: MCS probabilities for $\sigma_{SH} = 7.5$ dB and reuse 3x1x1.

Table B.4: Comparison of results obtained through simulation and GEV parameters for $\sigma_{SH} = 7.5$ dB for reuse 3x1x1.

Simulation Configuration		**Dissimilarity Ξ**	**Percentage w.r.t max error**	**Throughput X [Mbps]**		**Percentage difference**
P_{Tx} [dBm]	**R** [m]			**Sim**	**GEV**	
43	1000	0.03	1.46	3.28	3.18	3.14
43	1250	0.03	1.47	3.27	3.18	2.96
43	1500	0.03	1.55	3.26	3.18	2.68
43	1750	0.03	1.71	3.25	3.18	2.25
43	2000	0.04	1.97	3.23	3.18	1.65
40	1500	0.04	1.78	3.24	3.18	2.08
46	1500	0.03	1.47	3.27	3.18	2.98

B.5 Reuse Type 3x3x1

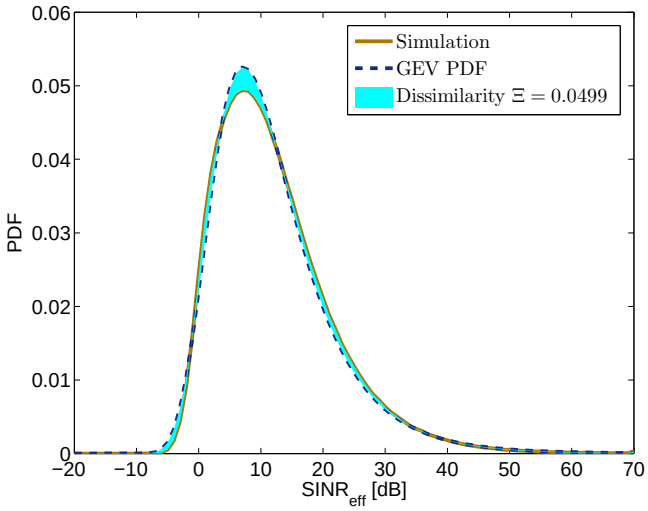

Figure B.21: $SINR_{eff}$ distribution through simulation and GEV parameters for $\sigma_{SH} = 9$ dB, $R = 1500$ m, $P_{Tx} = 43$ dBm and reuse 3x3x1.

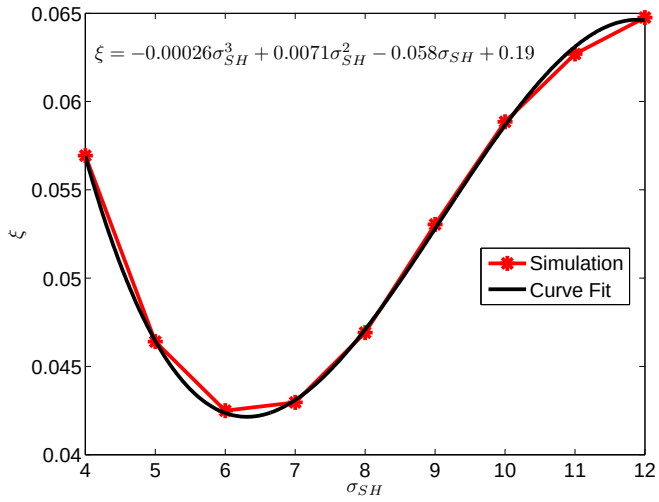

Figure B.22: Shape parameter ξ of GEV distribution vs σ_{SH} for $R = 1500$ m, $P_{Tx} = 43$ dBm and reuse 3x3x1.

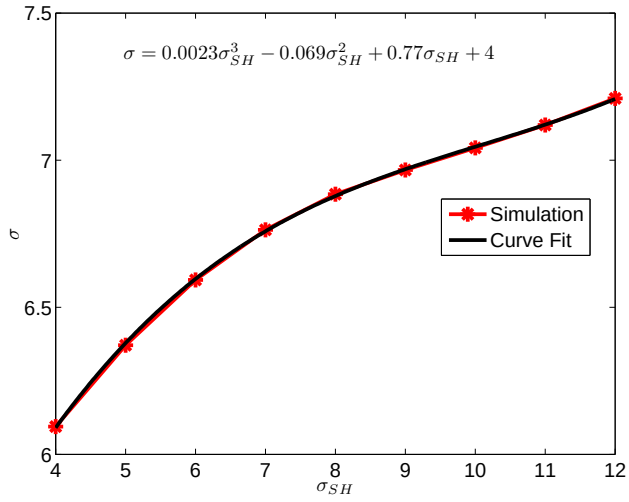

Figure B.23: Scale parameter σ of GEV distribution vs σ_{SH} for $R = 1500$ m, $P_{Tx} = 43$ dBm and reuse 3x3x1.

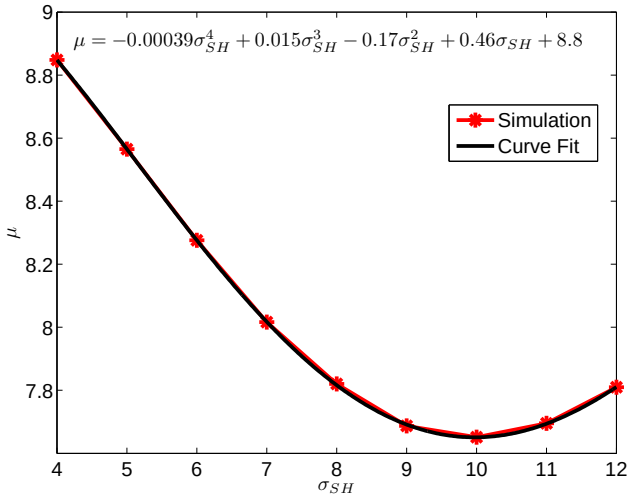

Figure B.24: Location parameter μ of GEV distribution vs σ_{SH} for $R = 1500$ m, $P_{Tx} = 43$ dBm and reuse 3x3x1.

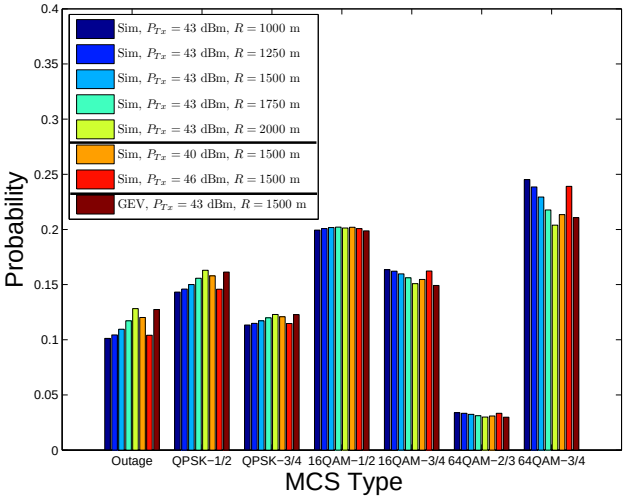

Figure B.25: MCS probabilities for $\sigma_{SH} = 7.5$ dB and reuse 3x3x1.

Table B.5: Comparison of results obtained through simulation and GEV parameters for $\sigma_{SH} = 7.5$ dB for reuse 3x3x1.

Simulation Configuration		**Dissimilarity Ξ**	**Percentage w.r.t max error**	**Throughput X [Mbps]**		**Percentage difference**
P_{Tx} [dBm]	**R** [m]			**Sim**	**GEV**	
43	1000	0.07	3.28	10.55	9.76	7.53
43	1250	0.05	2.62	10.42	9.76	6.41
43	1500	0.04	1.77	10.24	9.76	4.73
43	1750	0.03	1.42	9.99	9.76	2.34
43	2000	0.06	3.03	9.67	9.76	0.83
40	1500	0.04	1.80	9.90	9.76	1.46
46	1500	0.05	2.67	10.43	9.76	6.51

B.6 Reuse Type 1x3x1 with Beamforming

The simulator details for a beamforming capable WiMAX network can be found in section 3.3. The first scenario of PUSC has been considered.

Table B.6: Comparison of results obtained through simulation and GEV parameters for $\sigma_{SH} = 7.5$ dB for reuse 1x3x1 with beamforming.

Simulation Configuration		**Dissimilarity Ξ**	**Percentage w.r.t max error**	**Throughput X [Mbps]**		**Percentage difference**
P_{Tx} [dBm]	**R** [m]			**Sim**	**GEV**	
43	1000	0.23	11.60	25.38	27.66	9.00
43	1250	0.15	7.60	26.73	27.66	3.47
43	1500	0.04	2.01	28.81	27.66	4.00
43	1750	0.10	4.92	30.75	27.66	10.03
43	2000	0.19	9.31	32.31	27.66	14.39
40	1500	0.04	2.01	28.81	27.66	3.99
46	1500	0.04	2.01	28.82	27.66	4.00

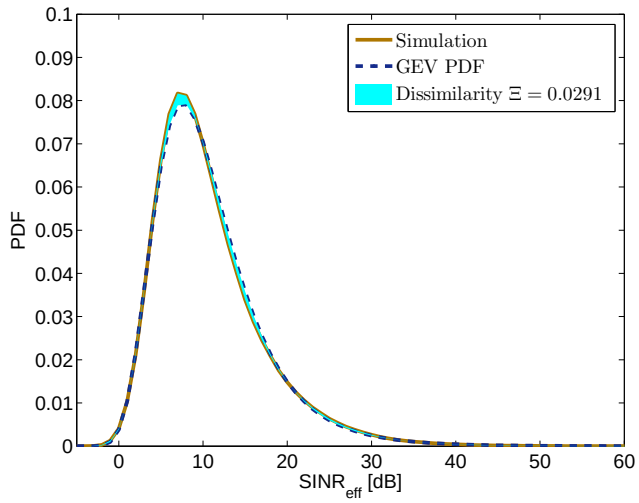

Figure B.26: $SINR_{eff}$ distribution through simulation and GEV parameters for $\sigma_{SH} = 9$ dB, $R = 1500$ m, $P_{Tx} = 43$ dBm and reuse 1x3x1 while taking into account beamforming.

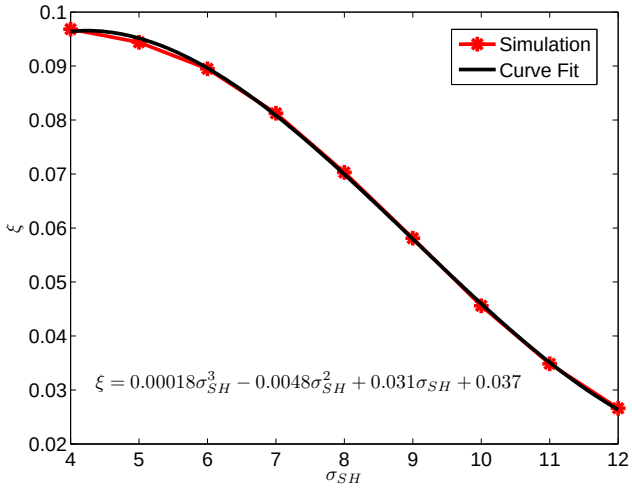

Figure B.27: Shape parameter ξ of GEV distribution vs σ_{SH} for $R = 1500$ m, $P_{Tx} = 43$ dBm and reuse 1x3x1 while taking into account beamforming.

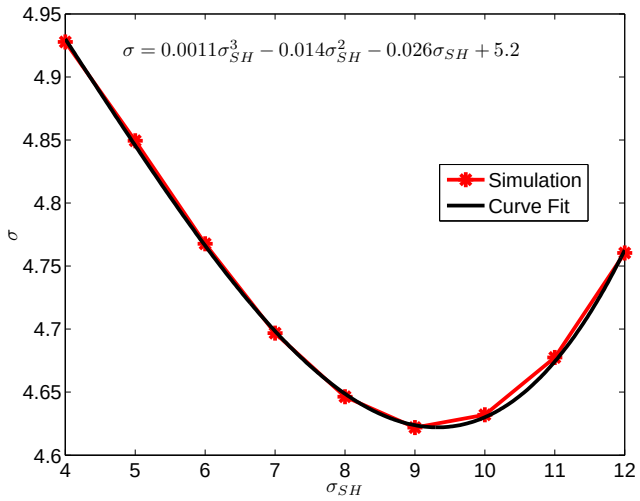

Figure B.28: Scale parameter σ of GEV distribution vs σ_{SH} for $R = 1500$ m, $P_{Tx} = 43$ dBm and reuse 1x3x1 while taking into account beamforming.

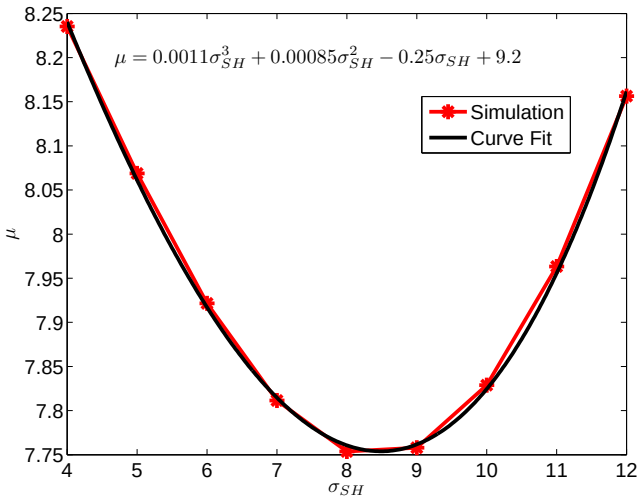

Figure B.29: Location parameter μ of GEV distribution vs σ_{SH} for $R = 1500$ m, $P_{Tx} = 43$ dBm and reuse 1x3x1 while taking into account beamforming.

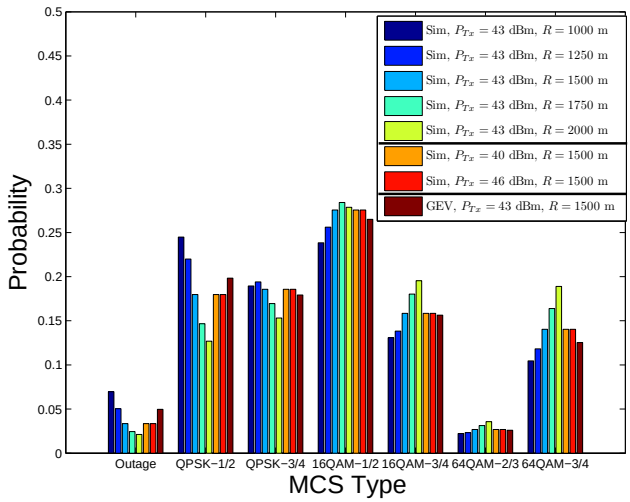

Figure B.30: MCS probabilities for $\sigma_{SH} = 7.5$ dB and reuse 1x3x1 while taking into account beamforming.

Appendix C

Fluid Model in OFDMA Networks

In this appendix, we recall the main results of the fluid model and derive the closed-form formula for SIR per subcarrier.

The key modeling step of the fluid model is replacing a given fixed finite number of BS by an equivalent continuum of transmitters which are spatially distributed in the network. This means that the transmitting power is now considered as a continuum field all over the network. In this context, the network is characterized by a user density ρ_u and a base station density ρ_{BS} [67]. We assume that users and BS are uniformly distributed in the network, so that ρ_u and ρ_{BS} are constant. We also assume that all base stations have the same output power per subcarrier P_{Tx}.

We focus on a given cell, a generic subcarrier and consider a round shaped network around this central cell with radius R_{nw}. The half distance between two base stations is R_c (see Fig. C.1 in case of reuse 1).

Let's consider a user u at a distance r_u from its serving base station b. Each elementary surface $zdzd\theta$ at a distance z from u contains $\rho_{BS}zdzd\theta$ base stations which contribute to $I_{ext,u}$. Their contribution to the external interference is thus $\rho_{BS}zdzd\theta P_{Tx}Az^{-\eta}$. We approximate the integration surface by a ring with center u, inner radius $2R_c - r_u$, and outer radius $R_{nw} - r_u$ (see Fig. C.2).

$$I_{ext,u} = \int_0^{2\pi} \int_{2R_c - r_u}^{R_{nw} - r_u} \rho_{BS} P_{Tx} A z^{-\eta} z dz d\theta$$

$$= \frac{2\pi \rho_{BS} P_{Tx} A}{\eta - 2} \left[(2R_c - r_u)^{2-\eta} - (R_{nw} - r_u)^{2-\eta} \right].$$

So, the SINR $\gamma_u \approx S_{b,u}/I_{ext,u} = P_{Tx} A r_u^{-\eta}/I_{ext,u}$ can be expressed by:

$$\gamma_u = \frac{r_u^{-\eta}(\eta - 2)}{2\pi \rho_{BS} \left[(2R_c - r_u)^{2-\eta} - (R_{nw} - r_u)^{2-\eta} \right]}.$$

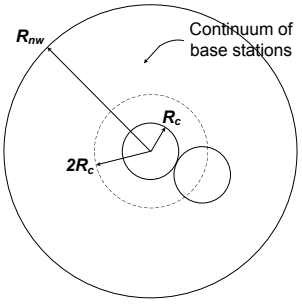

Figure C.1: Network and cell of interest in the fluid model; the distance between two BS is $2R_c$ and the network is made of a continuum of base stations.

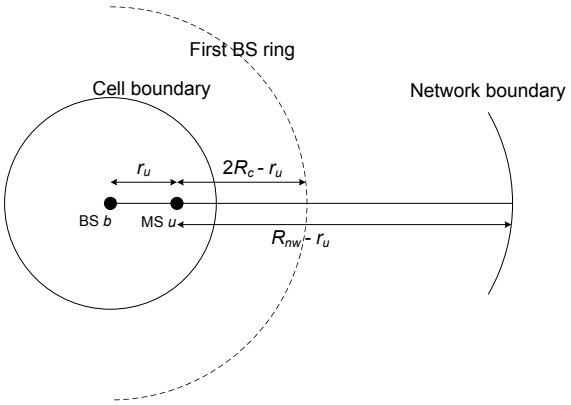

Figure C.2: Integration limits for interference computation.

Note that γ_u does not depend on the BS output power. This is due to the fact that we assumed an homogeneous network and so all base stations emit the same power on a given subcarrier. In this model, γ only depends on the distance r from the BS and can be defined for each location, so that we can write γ as a function of r i.e., $\gamma(r)$. If the network is large, i.e., R_{nw} is big as compared to R_c, γ_u can be further approximated by:

$$\gamma_u = \frac{r_u^{-\eta}(\eta - 2)}{2\pi\rho_{BS}(2R_c - r_u)^{2-\eta}}.$$

The fluid model and the traditional hexagonal model are two simplifications of the reality. None is a priori better than the other but the latter is widely used, especially for dimensioning purposes. That is the reason why comparisons are performed throughout chapter 5.

Reference [68] has shown that the considered network size can be finite and can be chosen to characterize each specific local network's environment. This model thus allows us to do the analysis adapted to each zone while taking into account considered zone's specific parameters. Moreover, it can be noticed that the fluid model can be used even for great distances between the base stations.

Bibliography

[1] I. Koffman and V. Roman, "Broadband Wireless Access Solutions Based on OFDM Access in IEEE 802.16," *IEEE Communications Magazine*, April 2002.

[2] F. Wang, A. Ghosh, C. Sankaran, P. J. Fleming, F. Hsieh, and S. J. Benes, "Mobile WiMAX Systems: Performance and Evolution," *IEEE Communications Magazine*, October 2008.

[3] J. G. Andrews, A. Ghosh, and R. Muhamed, *Fundamentals of WiMAX: Understanding Broadband Wireless Networking*. Prentice Hall, 2007.

[4] S.-E. Elayoubi, O. B. Haddada, and B. Fourestié, "Performance Evaluation of Frequency Planning Schemes in OFDMA-based Networks," *IEEE Transactions On Wireless Communications*, May 2008.

[5] T. Bonald and A. Proutiere, "Wireless Downlink Data Channels: User Performance and Cell Dimensioning," in *Proc. of ACM Mobicom*, September 2003.

[6] S. Borst, "User-Level Performance of Channel-Aware Scheduling Algorithms in Wireless Data Networks," in *Proc. of IEEE Infocom*, March/April 2003.

[7] S. Liu and J. Virtamo, "Performance Analysis of Wireless Data Systems with a Finite Population of Mobile Users," in *Proc. of 19th International Teletraffic Congress*, August/September 2005.

[8] K. Ramadas and R. Jain, "WiMAX System Evaluation Methodology," WiMAX Forum, Tech. Rep., January 2007.

[9] M. Maqbool, M. Coupechoux, and P. Godlewski, "Comparative Study of Reuse Patterns for WiMAX Cellular Networks," ENST (TELECOM ParisTech), Technical Report, April 2008. [Online]. Available: http://perso.telecom-paristech.fr/~coupecho/publis/rapportreuse08.pdf

[10] M. Maqbool, M. Coupechoux and P. Godlewski, "Comparison of Various Frequency Reuse Patterns for WiMAX Networks with Adaptive Beamforming," in *Proc. of IEEE VTC Spring*, May 2008. [Online]. Available: http://perso.telecom-paristech.fr/~coupecho/publis/vtc08spring1.pdf

[11] M. Maqbool, M. Coupechoux, and P. Godlewski, "Effect of Distributed Subcarrier Permutation on Adaptive Beamforming in WiMAX Networks," in *Proc. of IEEE VTC Fall*, September 2008. [Online]. Available: http://perso.telecom-paristech.fr/~coupecho/publis/vtcfall08.pdf

[12] M. Maqbool, M. Coupechoux, P. Godlewski, and V. Capdevielle, *"Achieving Frequency Reuse 1 in WiMAX Networks with Beamforming" book chapter in "WIMAX, New Developments"*, First ed. Intech, (to appear) 2009. [Online]. Available: http://perso.telecom-paristech.fr/~coupecho/publis/intechbook09.pdf

[13] M. Maqbool, M. Coupechoux, and P. Godlewski, "Reuse 1 in WiMAX Networks with Beamforming," in *Proc. of Wireless World Research Forum (WWRF), 22nd meeting*, May 2009. [Online]. Available: http://perso.telecom-paristech.fr/~coupecho/publis/wwrf09beam.pdf

[14] M. Maqbool, M. Coupechoux and P. Godlewski, "A Semi-analytical Method to Model Effective SINR Spatial Distribution in WiMAX Networks," in *Proc. of IEEE Sarnoff Symposium*, March 2009. [Online]. Available: http://perso.telecom-paristech.fr/~coupecho/publis/sarnoff09.pdf

[15] M. Maqbool, M. Coupechoux, and P. Godlewski, "A Semi-analytical Method to Model Spatial Distribution of Effective SINR in WiMAX Networks," TELECOM ParisTech, Technical Report, Draft Version, 2008. [Online]. Available: http://perso.telecom-paristech.fr/~coupecho/publis/rapportsemianalytic08.pdf

[16] M. Maqbool, M. Coupechoux, P. Godlewski, S. Doirieux, B. Baynat and V. Capdevielle, "Dimensioning Methodology for OFDMA Networks," in *Proc. of Wireless World Research Forum (WWRF), 22nd meeting*, May 2009. [Online]. Available: http://perso.telecom-paristech.fr/~coupecho/publis/wwrf09dim.pdf

[17] P. Godlewski, M. Maqbool, M. Coupechoux and J. M. Kelif, "Analytical Evaluation of Various Frequency Reuse Schemes in Cellular OFDMA Networks," in *Proc. of the 3rd International Conference on Performance Evaluation Methodologies and Tools*, October 2008. [Online]. Available: http://perso.telecom-paristech.fr/~coupecho/publis/valuetools08.pdf

[18] M. Maqbool, P. Godlewski, M. Coupechoux and J. M. Kelif, "Analytical Performance Evaluation of Various Frequency Reuse and Scheduling Schemes in Cellular OFDMA Networks," *Elsevier Performance Evaluation Journal*, (to appear) 2009. [Online]. Available: http://perso.telecom-paristech.fr/~coupecho/publis/peva09.pdf

[19] G. Nogueira, B. Baynat, M. Maqbool, and M. Coupechoux, *Book chapter in "WiMAX Networks Planning and Optimization"*, First ed. Auerbach

Publications, CRC Press, Taylor & Francis Group, 2008. [Online]. Available: http://perso.telecom-paristech.fr/~coupecho/publis/bookwimax08.pdf

[20] B. Baynat, S. Doirieux, G. Nogueira, M. Maqbool and M. Coupechoux, "An Efficient Analytical Model for WiMAX Networks with Multiple Traffic Profiles," in *Proc. of ACM/IET/ICST IWPAWN*, October 2008. [Online]. Available: http://perso.telecom-paristech.fr/~coupecho/publis/iwpawn08.pdf

[21] B. Baynat, S. Doirieux, G. Nogueira, M. Maqbool, and M. Coupechoux, "An Analytical Model for WiMAX Networks with Multiple Traffic Profiles and Throttling Policy," in *Proc. of WiOpt*, June 2009. [Online]. Available: http://perso.telecom-paristech.fr/~coupecho/publis/WiOpt09.pdf

[22] B. Baynat, G. Nogueira, M. Maqbool, and M. Coupechoux, "An Efficient Analytical Model for the Dimensioning of WiMAX Networks," in *Proc. of 8th IFIP-TC6 Networking Conference*, May 2009. [Online]. Available: http://perso.telecom-paristech.fr/~coupecho/publis/networking09.pdf

[23] G. Kulkarni, S. Adlakha, and M. Srivastava, "Subcarrier Allocation and Bit Loading Algorithms for OFDMA-Based Wireless Networks," *IEEE Transaction on Mobile Computing*, December 2005.

[24] H. Holma and A. Toshkala, *LTE for UMTS-OFDMA and SC-FDMA Based Radio Access*. John Wiley & Sons, Ltd, 2009.

[25] "IEEE Standard for Local and Metropolitan Area Networks - Part 16: Air Interface for Fixed Broadband Wireless Access Systems," 2004.

[26] "IEEE Standard for Local and Metropolitan Area Networks, Part 16: Air Interface for Fixed and Mobile Broadband Wireless Access Systems, Amendment 2: Physical and Medium Access Control Layers for Combined Fixed and Mobile Operation in Licensed Bands and Corrigendum 1," 2005.

[27] "Mobile WiMAX-Part II: A Comparative Analysis," WiMAX Forum, Tech. Rep., May 2006.

[28] L. Nuaymi, *WiMAX: Technology for Broadband Wireless Access*. Wiley, January 2007.

[29] "Mobile WiMAX-Part II: A Technical Overview and Performance Evaluation," WiMAX Forum, Tech. Rep., March 2006.

[30] C. Lengoumbi, P. Godlewski, and P. Martins, "Subchannelization Performance for the Downlink of a Multi-Cell OFDMA System," in *Proc. of IEEE WiMob*, January 2007.

[31] "WiMAX Forum Mobile System Profile 4 Release 1.0 Approved Specification. Wimax Forum," May 2007.

[32] D. Astély, E. Dahlman, P. Frenger, R. Ludwig, M. Meyer, S. Parkvall, P. Skillermark, and N. Wiberg, "A Future Radio-Access Framework," *IEEE Journal on Selected Areas in Communications*, March 2006.

[33] E. Dahlman, H. Ekström, A. Furuskär, Y. Jading, J. Karlsson, M. Lundevall, and S. Parkvall, "The 3G Long-Term Evolution Radio Interface Concepts and Performance Evaluation," in *Proc. of VTC Spring*, May 2006.

[34] F. Baskett, K. Chandy, R. Muntz, and F. Palacios, "Open Closed and Mixed Networks of Queues with Different Classes of Customers," *Journal of the Association of Computing Machinery*, April 1975.

[35] C. Tarhini and T. Chahed, "On Capacity of OFDMA-based IEEE802.16 WiMAX Including Adaptive Modulation and Coding (AMC) and Inter-cell Interference," in *Proc. of ICSNC*, October 2006.

[36] H. Jia, Z. Zhang, G. Yu, P. Cheng, and S. Li, "On the Performance of IEEE 802.16 OFDMA System under Different Frequency Reuse and Subcarrier Permutation Patterns," in *Proc. of IEEE ICC*, June 2007.

[37] F. Wang, A. Ghosh, C. Sankaran, and S. Benes, "WiMAX System Performance with Multiple Transmit and Multiple Receive Antennas," in *Proc. of IEEE VTC*, April 2007.

[38] C. F. Ball, E. Humburg, K. Ivanov and F. Treml, "Performance Analysis of IEEE802.16 Based Cellular MAN with OFDM-256 in Mobile Scenarios," in *Proc. of IEEE VTC Spring*, June 2005.

[39] C. F. Ball, E. Humburg, K. Ivanov, and F. Treml, "Comparison of IEEE802.16 WiMax Scenarios with Fixed and Mobile Subscribers in Tight Reuse," in *Proc. of EURASIP*, July 2005.

[40] L. Nuaymi and Z. Noun, "Simple Capacity Estimations in WiMAX/802.16 System," in *Proc. of PIMRC'06*, September 2006.

[41] R. Srinivasan, "Draft IEEE 802.16m Evaluation Methodology Document," IEEE 802.16 Broadband Wireless Access Working Group, Tech. Rep., August 2007.

[42] J. Proakis and M. Salehi, *Digital Communications*. McGraw-Hill, November 2007.

[43] D. Huo, "Clarification on the Wrap-Around Hexagon Network Structure," IEEE C802.20-05/15, IEEE 802.20 Working Group on Mobile Broadband Wireless Access, March 2005.

[44] J. Khun-Jush, "CDMA Uplink Power Control Methodology in SEAMCAT (VOICE ONLY)," STG(03)13 r1, SEAMCAT Technical Group, October 2003.

[45] J. W. Porter, J. F. Kepler, T. P. Krauss, F. W. Vook, T. K. Blankenship, V. Desai, A. Schooler, and J. Thomas, "An Experimental Adaptive Beamforming System for the IEEE 802.16e-2005 OFDMA Downlink," in *Proc. of IEEE Radio and Wireless Symposium*, January 2007.

[46] R. Pabst, J. Ellenbeck, M. Schinnenburg, and C. Hoymann, "System Level Performance of Cellular WiMAX IEEE 802.16 with SDMA-enhanced Medium Access," in *Proc. of IEEE WCNC*, March 2007.

[47] M. C. Necker, "Towards Frequency Reuse 1 Cellular FDM/TDM Systems," in *Proc. of ACM MSWiM*, October 2006.

[48] M. C. Necker, "Coordinated Fractional Frequency Reuse," in *Proc. of ACM MSWiM*, October 2007.

[49] D. S. Baum et al., "IST-2003-507581, D5.4 Final Report on Link and System Level Channel Models. WINNER," October 2005, https://www.ist-winner.org/DeliverableDocuments/D5.4.pdf.

[50] D. Tse and P. Viswanath, *Fundamentals of Wireless Communications*. Cambridge University Press, 2006.

[51] M. Zorzi, "On the Analytical Computation of the Interference Statistics with Applications to the Performance Evaluation of Mobile Radio Systems," *Trans. of IEEE on Communications*, January 1997.

[52] J. Cho and D. Hong, "Statistical Model of Downlink Interference for the Performance Evaluation of CDMA Systems," in *IEEE Communications Letters*, November 2002.

[53] A. Mäder and D. Staehle, *Interference Estimation for the HSDPA Service in Heterogeneous UMTS Networks*. Book Chapter in "Lecture Notes in Computer Science", Springer Publications, 2006.

[54] C. F. Ball, E. Humburg, K. Ivanov, and R. Müllner, "Rapid Estimation Method for Data Capacity and Spectrum Efficiency in Cellular Networks," in *Proc. of 14th IST Mobile and Wireless Communications Summit*, June 2005.

[55] M. Einhaus, O. Klein, B. Walke, and R. Halfmann, "MAC Level Performance Comparison of Distributed and Adjacent OFDMA Subchannels in IEEE 802.16," in *Proc. of European Wireless (EW)*, April 2007.

[56] Y.-J. Choi, C. S. Kim, and S. Bahk, "Flexible Design of Frequency Reuse Factor in OFDMA Cellular Networks," in *Proc. of IEEE ICC*, June 2006.

[57] J.-W. So, "Performance Analysis of VoIP Services in the IEEE 802.16e OFDMA System With Inband Signaling," *Trans. of IEEE on Vehicular Technology*, May 2008.

[58] S. K. Kim and C. G. Kang, "Throughput Analysis of Band AMC Scheme in Broadband Wireless OFDMA System," in *Proc. of IEEE WCNC*, April 2006.

[59] C. Monti, R. Giuliano, F. Mazzenga, and P. Loreti, "Interference Evaluation for a Cellular System Based on OFDMA," in *Proc. of Second International Mobile Multimedia*, September 2006.

[60] S.-E. Elayoubi, B. Fourestié, and X. Auffret, "On the Capacity of OFDMA 802.16 Systems," in *Proc. of IEEE ICC*, June 2006.

[61] S. Markose and A. Alentorn, "The Generalized Extreme Value (GEV) Distribution, Implied Tail Index and Option Pricing," University of Essex, Department of Economics, Economics Discussion Papers 594, 2005. [Online]. Available: http://ideas.repec.org/p/esx/essedp/594.html

[62] D. Sinha, H. Zhou and N.V. Shenoy, "Advances in Computation of the Maximum of a Set of Gaussian Random Variables," *Trans. of IEEE on Computer-Aided Design of Integrated Circuits and Systems*, August 2007.

[63] G. Liu, J. Zhu, F. Jiang, B. Zhou, Y. Wang, and P. Zhang, "Initial Performance Evaluation on TD-SCDMA Long Term Evolution System," in *Proc. of IEEE VTC Spring*, May 2006.

[64] M. C. Necker, "Local Interference Coordination in Cellular 802.16e Networks," in *Proc. of IEEE VTC Fall*, October 2007.

[65] C. He, F. Liu, H. Yang, C. Chen, H. Sun, W. May, and J. Zhang, "Co-channel Interference Mitigation in MIMO-OFDM System," in *Proc. of IEEE WiCom*, September 2007.

[66] C. Tarhini and T. Chahed, "On Capacity of OFDMA-based IEEE802.16 WiMAX Including Adaptive Modulation and Coding (AMC) and Inter-cell Interference," in *Proc. of IEEE Workshop on LANMAN*, June 2007.

[67] J.-M. Kelif and E. Altman, "Downlink Fluid Model of CDMA Networks," in *Proc. of IEEE VTC Spring*, May 2005.

[68] J.-M. Kelif, M. Coupechoux, and P. Godlewski, "Spatial Outage Probability for Cellular Networks," in *Proc. of IEEE GLOBECOM*, November 2007.

[69] J.-M. Kelif, M. Coupechoux, and P. Godlewski, "Effect of Shadowing on Outage Probability in Fluid Cellular Networks," in *Proc. of WiOpt*, April 2008.

[70] V. Erceg, L.J. Greenstein et. al, "An Empirically Based Path Loss Model for Wireless Channels in Suburban Environments," *IEEE Journal on Selected Areas in Communications*, July 1999.

[71] S. Kim and I. Yeom, "Performance Analysis of Best Effort Traffic in IEEE 802.16 Networks," *IEEE Transactions on Mobile Computing*, 2008.

[72] G. Leonardi, A. Bazzi, G. Pasolini, and O. Andrisano, "IEEE802.16e Best Effort Performance Investigation," in *Proc. of IEEE ICC*, June 2007.

[73] F. Hou, J. She, P.-H. Ho, and X. Shen, "Performance Analysis of Weighted Proportional Fairness Scheduling in IEEE 802.16 Networks," in *Proc. of IEEE ICC*, May 2008.

[74] D. Sivchenko, N. Bayer, B. Xu, V. Rakocevic, and J. Habermann, "Internet Traffic Performance in IEEE 802.16 Networks," in *Proc. of 12th European Wireless Conference*, April 2006.

[75] O. Grøndalen, P. Grønsund, T. Breivik, and P. Engelstad, "Fixed WiMAX Field Trial Measurements and Analyses," in *Proc. of 16th IST Mobile and Wireless Communication Summit*, July 2007.

[76] D. Niyato and E. Hossain, "A Queuing-theoretic and Optimization-based Model for Radio Resource Management in IEEE 802.16 Broadband Networks," *IEEE Transactions on Computers*, November 2006.

[77] A. Feldmann, A. C. Gilbert, P. Huang, and W. Willinger, "Dynamics of IP Traffic: A Study of the Role of Variability and the Impact of Control," *Computer Communication Review, a publication of ACM SIGCOMM*, October 1999.